FACULDADE DE CIÊNCIAS SOCIAIS E HUMANAS
UNIVERSIDADE NOVA DE LISBOA

3D Point Clouds in Urban Planning: Developing and Releasing High-end Methodologies based on LiDAR and UAV Data for the Extraction of Building Parameters

Carla Cristina Roque Rebelo

Tese de Doutoramento em Geografia e Planeamento Territorial. Especialização em Detecção Remota e Sistemas de Informação Geográfica

Janeiro, 2016

Tese apresentada para cumprimento dos requisitos necessários à obtenção do grau de Doutor em Geografia e Planeamento Territorial, Especialização em Detecção Remota e Sistemas de Informação Geográfica, realizada sob a orientação científica do Professor Doutor José António Tenedório e co-orientação Professor Doutor José Alberto Gonçalves.

ACKNOWLEDGMENTS

I would like to start by thanking my supervisor, Professor José Tenedório, for his support, encouragement, dedication and scientific vision that always inspired a constructive discussion at every stage of this research, and that was fundamental for the success of this work. I am also indebted for the trust, friendship, and understanding that he has always shown over these past few years, in all the good moments, but also in tough ones.

I am also very grateful to my co-supervisor, Professor José Alberto Gonçalves, for his support, availability and technical guidance at every stage of this project, and for sharing his knowledge and fostering the discussion, which was so important for this research.

I would like to thank all the people that have made this thesis possible: Professor Óscar Ferreira from the University of Algarve for providing me with LiDAR data; my friend, the engineer and topographer, Rita Batista, and the topographer José Batista for carrying out the topographic survey at Praia de Faro; and engineer João Marnoto from SINFIC for providing my with UAV data for Amadora and for his availability to perform a UAV flight over Praia de Faro. I am also indebted to him for having shared his knowledge and for all his support and friendship.

I would like to express my gratitude to the following people who have played an important role at this stage of my life.

To Professor João Catalão from the Faculty of Sciences of the University of Lisbon for providing me with information on Praia de Faro right at the beginning of this research.

To the e-GEO research centre that has recently been integrated into CICS.NOVA for its financial support for the acquisition of data, participation in national an international conferences, resources, and the possibility of using the facilities to carry out this work. In particular, I would like to thank Professor Maria José Nazaré Rocca (former e-GEO coordinator) and Professor Carlos Pereira da Silva, for his support as coordinator of the Geographic Modelling, Cities and Spatial Planning Group.

To the University of Algarve, for the financial support within the scope of the PROTEC programme that supports advanced training for lecturers at polytechnic higher education institutions.

To my colleagues at e-GEO: Bruno Neves, Teresa Santos, Sara Encarnação, Rossana Estanqueiro, Filipa Ramalhete, Sérgio Freire, and Ricardo Mendes. Special thanks to Raquel de Deus, of my class at university and a good friend, for her support and for having shared not only my frustrations but also the good moments.

To my friend António Rodrigues, a special friend, for the constant support, encouragement, and confidence. His suggestions, sometimes challenging, have ended up being very important for the course this project has taken. All the good moments shall not be forgotten.

To the company that has welcomed me, particularly to João Loução, Technical Manager, for the support he has given me in these past few months that enabled me to finish writing this thesis.

To my colleagues and friends at the University of Algarve, Sara Madeira, Ana Pinho, and Conceição Ribeiro. And special thanks to those with whom I shared an office – Carlos Sousa and Maria Celeste Gameiro – for the good environment that they have always fostered. To José Rodrigues, for the support and strength that he gave me to jumpstart this research.

To my colleagues Luis Crispim, Rui Dias, and Paulo Torrinha. Particularly to my friend and colleague, Rosa Oliveira, always available and always present. To Victor Ferreira and Jorge Gustavo for their help with open-source.

Last but not least, I would like to thank all my friends for their understanding over these past few years, particularly to my parents and my sisters for their support and their faith in me.

To my husband Sigismundo and my daughter Matilde, who have been the foundation for my balance and strength to accomplish this objective. This thesis would not have been possible without you.

3D POINT CLOUDS IN URBAN PLANNING: DEVELOPING AND RELEASING HIGH-END METHODOLOGIES BASED ON LIDAR AND UAV DATA FOR THE EXTRACTION OF BUILDING PARAMETERS

CARLA CRISTINA ROQUE REBELO

RESUMO

PALAVRAS-CHAVE: Plano Urbano, Nuvem de Pontos 3D, Modelação de Dados 3D, Altura Edifício, Volume, FOSS, 3DEBP

Os dados geográficos têm um papel determinante na formalização do plano urbano, enquanto instrumento de planeamento e documento normativo que define juridicamente as obrigações públicas e vincula os particulares, num determinado período temporal, no que respeita à disciplina urbanística de uma cidade ou de um aglomerado urbano, estabelecendo regras de uso e de ocupação do solo. O plano está associado a um processo, designado processo de planeamento; processo esse que é constituído por um conjunto de fases, dinâmicas e adaptativas, que se iniciam na sua elaboração e terminam na avaliação dos desvios entre o determinado no documento inicial e as metas e objectivos efectivamente atingidos. O plano, o processo e a praxis do planeamento exigem dados geográficos actualizados a cada instante, quer para as acções de monitorização quer para os momentos de avaliação.

Um dos aspectos cruciais do plano é a quantificação da volumetria do espaço edificado existente. Outro aspecto, também fundamental, é o da gestão dessa volumetria; quer da volumetria existente quer da volumetria adicional. O tema da volumetria dos espaços edificados tem constituído, aliás, um dos temas mais sensíveis quando se trata da densificação do espaço urbano existente ou do desenho de novos espaços urbanos de expansão. Considerando o quadro teórico apresentado, o tema central da tese trata da modelação de nuvens de pontos 3D obtidas por tecnologia LiDAR e por UAV, para as aplicações na elaboração do plano e no processo de planeamento urbano, designadamente quantificação dos parâmetros urbanísticos altura da fachada e volume dos edifícios.

A exploração do tema central da tese suporta-se em dois níveis: o nível da operacionalização e o nível da usabilidade. O nível da operacionalização concretiza dois objectivos: i) demonstração da relevância e da pertinência da extracção, medição e geovisualização 3D dos parâmetros urbanísticos baseadas na experimentação e implementação de técnicas de geoprocessamento; ii) demonstração da pertinência dos parâmetros urbanísticos extraídos considerando distintas morfologias urbanas. Para o nível da usabilidade definem-se igualmente dois objectivos: i) demonstração da usabilidade dos parâmetros urbanísticos extraídos avaliando o erro associado à extracção; ii) demonstração da usabilidade dos parâmetros urbanísticos extraídos para planeamento, em particular para o mapeamento dasimétrico de alta precisão.

Da investigação decorre uma solução metodológica. A solução metodológica nomeada *3D Extraction Building Parameters* (3DEBP) destina-se à extracção da área, da altura da fachada e do volume dos edifícios a partir de nuvens de pontos 3D. Esta solução foi criada tendo por base um conjunto de ferramentas FOSS: PostgreSQL/PostGIS, QGIS, GRASS e R-stats.

Foram realizados testes em duas áreas urbanas com morfologias distintas: Praia de Faro (morfologia irregular) e Amadora (morfologia regular). O teste sobre a área urbana da Praia de Faro utilizou uma nuvem de pontos LiDAR e uma outra extraída de levantamento realizado por UAV. O teste sobre um quarteirão urbano de Amadora foi realizado apenas sobre nuvem de pontos UAV. Os testes revelaram que a qualidade da informação extraída é dependente da morfologia urbana.

Nas conclusões discute-se a medição 3D com base em dados obtidos por tecnologia LiDAR e UAV, questiona-se a implementação de soluções FOSS para diferentes fases do processo de planeamento e defende-se a introdução intensiva da modelação 3D no plano urbano do futuro.

3D POINT CLOUDS IN URBAN PLANNING: DEVELOPING AND RELEASING HIGH-END METHODOLOGIES BASED ON LIDAR AND UAV DATA FOR THE EXTRACTION OF BUILDING PARAMETERS

CARLA CRISTINA ROQUE REBELO

ABSTRACT

KEYWORDS: Urban Plan, 3D Modelling, 3D Point Cloud, Building Height, Volume, FOSS, 3DEBP

Geographical data plays a major role in urban plan development, both as a planning instrument and as a normative document that legally defines public obligations and binds individuals, in a given period of time, regarding the urban aspect of a city or an urban conglomerate, and establishes standards for land use and land cover. The plan is associated with a process, called the planning process, which consists in a set of dynamic and adaptive phases that begin with its development and end with the evaluation of any discrepancies between the provisions of the original document and the accomplished goals and objectives. The plan, the process, and the planning praxis require up-to-date geographical data at all times, both for monitoring actions and for the evaluation phases.

One of the crucial aspects of the plan is the quantification of the existing building volume. Another fundamental aspect is managing that volume: both regarding the existing volume and any additional volumes. Actually, the building volume in built areas has been one of the most sensitive topics on the densification of existing urban spaces or the design of new growing urban areas.

Considering the existing theoretical framework, the central topic of this thesis focuses on 3D point cloud modelling obtained from LiDAR and UAV technologies, employed in the development of a plan and in the urban planning process, namely regarding two specific building parameters – building height and volume. The explanation of the central topic of this thesis is twofold: implementation and

usability. The implementation level has two goals: i) demonstrating the relevance and pertinence of the extraction, measurement, and 3D geovisualization of building parameters based on the experimentation and implementation of geoprocessing techniques; ii) demonstrating the pertinence of the extracted building parameters considering different urban morphologies. At the usability level, we defined two goals: i) demonstrating the usability of the extracted building parameters, evaluating the error associated with the extraction; ii) demonstrating the usability of these parameters for planning, particularly for high precision dasymetric mapping.

Based on our research, we propose a methodological solution termed. *3D Extraction Building Parameters* (3DEBP) and aimed at extracting areas, façade height, and building volumes from 3D point clouds. This solution was created with the following set of FOSS tools: PostgreSQL/PostGIS, GRASS, QGIS, and R-stats.

We performed several tests in two urban areas with different morphologies: Praia de Faro (irregular morphology) and Amadora (regular morphology). The former (Praia de Faro) used a LiDAR point cloud and another one extracted from a UAV survey, while the latter (urban neighbourhood of Amadora) only used a UAV point cloud. Both experiments reveal that the quality of the information extracted depends on urban morphology.

Finally, we discuss 3D measurement based on data obtained from LiDAR and UAV technology, raising questions on the implementation of FOSS solutions for different phases of the planning process, and arguing for the intensive introduction of 3D modelling for the future of urban planning.

Contents

List of Abbreviations

3DEBP	3D Extraction Building Parameters
AH	Historic Archive
AML	Lisbon Metropolitan Zone (Área Metropolitana de Lisboa)
ALS	Airborne Laser Scanning
BA	Building Area
BBA	Building Block Area
BBH	Building Block Height
BBV	Building Block Volume
BFH	Building Façade Height
BGRI	Geographic Base for Information Referencing (Base Geográfica de Referenciação de Informação)
BH	Building Height
BP	Building Parameter
BV	Building Volume
CCD	Charge Coupled Device
CIGeoE	Geospatial Information Centre Institute of the Army (Centro de Informação Geoespacial do Exército)
CIR	Colour-InfraRed
CLARA	CLustering LARge Applications
CMPMVS	Multi-View Reconstruction Software
CMVS	Clustering Views for Multi-view Stereo
DGOTDU	Direcção Geral de Ordenamento do Território e Desenvolvimento Urbano)
DGRF	General Directorate for Forestry Resources (Direcção Geral de Recursos Florestais)
DGT	Directorate General for the Territory (Direcção Geral do Território)
DSM	Digital Surface Model

DTM	Digital Terrain Model
EASA	European Aviation Safety Agency
EC	European Community
ESRI	Environmental Systems Research Institute
EuroSDR	European Spatial Data Research
FOSS	Free and Open Source Software
FP7	Framework Program
FSF	Free Software Foundation
GCP	Ground Control Points
GDAL	Geospatial Data Abstraction Library
GDBMS	Geographical Database Management System
GIS	Geographic Information Systems
GISDB	Geographic Information Systems Data Base
GPL	General Public License
GPS	Global Positioning System
GNSS	Global Navigation Satellite Systems
GNU GPL	General Public License
GRASS	Geographical Resources Analysis Support System
GSD	Ground Sampling Distance
GUI	Graphical user interface
ICP	Independent Check Point
IFOV	Instantaneous Field of View
IGC	Instituto Geográfico e Cadastral
IGeoE	Geographic Institute of the Army (Instituto Geográfico do Exército
IGP	Instituto Geográfico Português
IGN	Institut Géographique National (French mapping agency)
IGT	Territorial Management Instruments (Instrumentos de Gestão Territorial)
IMU	Inertial Measurement Unit
INSPIRE	Infrastructure for Spatial Information in Europe
LAS	LASer file format
LBPOTU	Spatial Planning and Urban Policy Framework (Lei de Bases da Política de Ordenamento do Território e Urbanismo)
LiDAR	Light Detection And Ranging
LGPL	Library General Public License
LoD	Level-of-Detail

MP	MegaPixel
NASA	National Aeronautics and Space Administration
NDSM	Normalized Digital Surface Model
OGC	Open Geospatial Consortium
OS	Open Source
PCGT	The Collaborative Platform for Territory Management (Plataforma Colaborativa de Gestão Territorial)
PDM	Master Plan (Plano Director Municipal)
PMVS	Patch-Based Multi-View Stereo Software
PNPOT	National Programme of Spatial Planning (Programa Nacional da Política de Ordenamento do Território)
PL/R	Procedural Language R
PLY	Polygon file format
POOC	Shoreline Spatial Plan (Plano de Ordenamento da Orla Costeira)
PRF	Pulse Rate Frequency
PROGIP	Computer Management Support Programme for Municipal Plans
PROSIG	Support Programme for the Creation of Local Nodes of SNIG
PROT	Regional Spatial Plans (Plano Regional de Ordenamento do Território)
RCM	Resolution of the Council of Ministers
REOT	Spatial Planning Status Reports (Relatório sobre o Estado do Ordenamento do Território)
RJIGT	Legal Framework for Territorial Management Instruments (Regime Jurídico dos Instrumentos de Gestão Territorial)
RGB	Red Green Blue
RMSE	Root-Mean-Square Error
RPAS	Remotely Piloted Aircraft System
SCE	Military Cartography Services (Serviços Geográficos do Exército)
SDI	Spatial Data Infrastructure
SfM	Structure-from-Motion
SGM	Semi-Global Matching
SNIT	National System for Territorial Information (Sistema Nacional de Informação Territorial)
SNR	Signal-to-Noise-Ratio
SQL	Standard Query Language

SSAIGT	Spatial Plans Automated Submission System (Sistema de submissão automática Informação Geográfica Territorial)
SRUP	Servitudes and Public Utility Restrictions
TEN	Tetrahedron Network
TIN	Triangulated Irregular Network
UAS	Unmanned Aerial System
UAV	Unmanned Aerial Vehicle
UOPG	Operating unit of planning and management (Unidade operativa de planeamento e gestão)
VE	Vertical Error
WFS	Web Feature Service
WGS84	World Geodetic System 1984
WMS	Web Map Service

Introduction

The Portuguese legislation on land use planning and urbanism has introduced new requirements for geographic information in these past few decades. Hence, the need for the integration of 3D geographical data acquisition technologies, accompanied by the development of advanced and dedicated methodologies, has become a relevant and priority research topic for urban planning.

One of these requirements related with the need for updated geographic information was introduced for the first time by the Legal Framework for Territorial Management Instruments (Regime Jurídico dos Instrumentos de Gestão Territorial – RJIGT) approved by Decree-Law No. 380/99, of 22nd September. This legal framework of the Territorial Management Instruments (Instrumentos de Gestão Territorial – IGT) promotes the analysis and characterization at different intervention scales of the territorial management instruments, including the urban scale, requiring the updating of geographic information and an evaluation report of the municipal plans every two years[1]. This report is required to assess whether there is any need to revise the plan. Consequently, at that time, geographical database updating for municipal plans was already a very important issue to monitor and evaluate those plans *in continuum*.

In this century, this Decree-Law was amended by Decree-Law No. 316/2007, of 19th September, and Decree-Law No. 46/2009, of 20th February, in order to simplify the procedures of the planning process by decentralizing them and increasing municipal responsibilities, while simultaneously clarifying concepts and intervention instruments. Moreover, the publication of two important Regulatory Decrees to support the planning process was approved on 29th May, 2009. One of these was Regulatory Decree No. 9/2009, which defined certain technical concepts in the fields of spatial planning and urbanism, such as building façade height, building volume

[1]Currently, this report must be drafted every four years, pursuant to article 189 of Decree-Law No. 80/2015, of 14th May.

and total volume, among others. The other one was Regulatory Decree No. 10/2009 that established the rules for mapping to be used in IGT, including the positional accuracy of topographic mapping to be used in the elaboration of IGT.

This legislation was the starting point for this research work, based not only on a vision of a geographic information updating, but also on the introduction of 3D data that can support an efficient system of indicators to monitor and evaluate plans.

In the meantime, a new legal framework – RJIGT – has recently been published by Decree-Law No. 80/2015 of 14th May, which constitutes a revision of Decree-Law No. 380/99 as a consequence of Law No. 31/2014 on the general bases for a public policy on soil, spatial planning, and urbanism[2].

The aim of this new Decree-Law is to launch a new concept and a new form of land management that is more coherent, consequential, and responsible, where the spatial effects of the economic and social dynamics are reinforced in the spatial planning. This revision of the IGT legal framework has brought to light four aspects that are crucial to the planning process: i) improving efficiency with the dematerialization of the elaboration and revision procedures in the planning process; ii) ensuring the 'democratization' of the plans by promoting the self-knowledge of all the stakeholders; iii) reinforcing the monitoring and evaluation phases of the territorial plans, whose mandatory underlying indicators should be included in the content of the plan; and iv) replacing the 10-year time frame for the revision of the plans with a 'dynamic time frame', which means that the revision of the plans has become more dependent on the results of the monitoring and assessment process.

Furthermore, Decree-Law No. 193/95, based on 2D mapping production rules, was replaced by Decree-Law No. 141/2014, of 19th September. This new law also integrates the usage and elaboration of maps regarding the territorial management instruments included in Regulatory Decree No. 10/2009 (which was revoked). This Decree-Law increases the need for topographic mapping updating for the elaboration/revision to one to three years depending on the type of municipal plan.

This new legislation reinforces the importance of technology in monitoring and evaluating the plans. Consequently, the research on the usability and pertinence of 3D data acquisition technologies for the planning process carried out in this thesis was strengthened by this new legislation. In other words, the recent legal

[2]Lei de bases gerais da política pública de solos de ordenamento do território e de urbanismo.

framework of RJIGT does not challenge the approach of this thesis, but reinforces its importance for the planning process.

Problematics and goals of the research

What role do the new data acquisition and modelling technologies play in the planning process?

The planning process for territorial management instruments is dynamic due to urban development. This dynamics is essentially reflected on the elaboration/revision, monitoring and evaluation, and public discussion phases and presents a challenge for the planning process, in so far as it requires modelling and constantly measuring urban areas.

Due to this dynamic character of the planning process, the new IGT legal framework privileges the monitoring and evaluation of the plans. Therefore, the monitoring of a plan requires continuously updated geographic information, which simultaneously allows a systematic supply of plan indicators.

One of the challenges of monitoring a plan as a management instrument is the urban scale, namely monitoring urban densification and land-use changes from *non aedificandi* to *aedificandi*. These issues require very simple measurements, such as building height and building footprint area for the estimation of built volumes. These volumes are in turn used for general strategic studies, such as solar radiation models to determine the energy potential of cities, noise models that are associated with a requirement of the law, urban wind field physical models, air pollution models, urban density models, and dasymetric mapping techniques for the reallocation and aggregation of semantic data according to a common geometry. All these models and other general urban analysis studies require building height for the identification of new buildings or changes in building height. The new legislation reinforces the monitoring of urban dynamics, which implies issues tied with measuring and modelling building volume.

Furthermore, 3D geovisualization has proven to have greater receptivity from the citizens and stakeholders when a plan is publicly discussed. Although, the construction of models still makes use of classical photogrammetry measurements, that is not enough insofar as the time and cost is substantially higher when compared with the time and cost of recent acquisition methods from point clouds and 3D modelling data.

Thus, in response to the initial question, the new data acquisition and modelling technologies play an important role in the planning process by the introduction of 3D data for 3D measuring, such as the acquisition of building height and volume that can supply a system of 3D indicators to monitor plans, and for 3D geovisualization at the public discussion phase.

The scope of this research is understanding how to extract building parameters from 3D point clouds obtained from Light Detection And Ranging (LiDAR) or Unmanned Aerial Vehicle (UAV) airborne systems to support the urban issues mentioned above. Therefore, the development of a semi-automatic methodology using Free and Open Source Software (FOSS) technologies that allow us to model and measure building parameters – area, height, volume, and total volume – shall be demonstrated. Furthermore, the evaluation of the building parameter errors is also an important task to support the level of usability of this data for urban planning.

The research objectives of this thesis are twofold:

At the operational level:

- demonstrating the relevance and pertinence of the extraction, 3D measurement, and 3D geovisualization of building parameters on the experimentation and implementation of these actions;
- demonstrating the pertinence of the building parameters extracted from distinct urban morphologies.

At the usability level:

- demonstrating the usability of the building parameters for the planning process through the evaluation of errors. The usability will be established by the definition of an error threshold for each building parameter that is acceptable for the monitoring or 3D geovisualization;
- demonstrating the usability of building parameters for urban planning issues, particularly for high precision dasymetric mapping techniques.

Conceptual structure of the thesis: point clouds modelling for urban planning

Conceptually, this research project should address a structure based on spatial data acquisition for 2D/3D modelling that aims to demonstrate and operationalize geographical data acquisition technologies for a plan and for the extraction of

building parameters at the urban scale, as the culmination of the response to the objectives proposed.

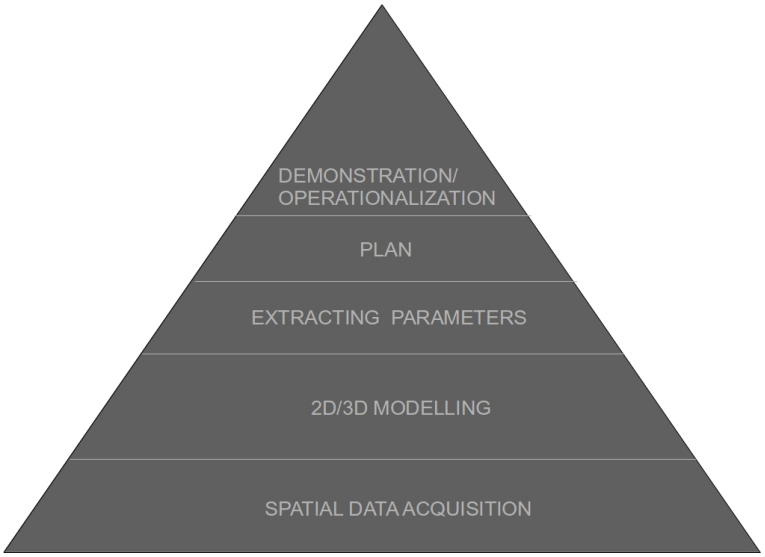

Synthesis of the methodology: from data to demonstration

The general methodology has a hierarchical structure. Each of the higher levels inherits the characteristics of the lower levels. The acquisition of spatial data forms the basis of this structure, as indeed it is the basis of all the operational projects related with the production of geographic information for urban and spatial planning: remote sensing surveying, Global Positioning System (GPS), photogrammetry, mapping, etc. It is, in fact, the most elementary stage in the geographic information production process for the planning process.

The 2D/3D modelling inherits the quality data obtained at the basis of this structure. In fact, data quality is at the base of this structure, which necessarily includes the evaluation of errors, depending on the technologies and acquisition processes. The knowledge of this error is absolutely essential to infer the quality of the models produced. That quality may be lower in the case of urban analysis for characterization purposes (a phase in which the most important aspect is an overview of the city or country) in the preparation of a plan. Anyway, one cannot work in the planning process without knowledge of the error and eventually the possibility of it spreading.

The quality of the measurement based on building parameters (extraction of parameters) inherits the two levels mentioned above and depends on the quality of the 2D/3D models produced, as well as on their usability for planning. Consequently, the ultimate goal is the internalization of the generated models into the plan.

If it is technically possible to quantify the error information and the effect of this error in the creation of the models, then we can state that this is demonstrated through its operationalization (higher level of the structure) in the planning process, either urban planning or spatial planning.

Structure of the thesis

The thesis is structured into four chapters as follows:

- *Chapter 1* the geo-information technologies are addressed by showing their importance for and evolution within the planning process over these past few decades in Portugal and their current trends for urban planning. The geo-information technologies applied in this thesis are described, namely the LiDAR system and low-cost UAV related with the acquisition of 3D point cloud data and the Free and Open Source technologies used to explore and modelling 3D point clouds.

  This chapter contributes to the acquisition of spatial data presented at the base of the methodological framework, which forms the knowledge basis for the beginning of this research.

- *Chapter 2* highlights the experimentation with and implementation of 3D point clouds for the extraction of building parameters – area, height, volume, and total volume – of single family dwellings.

  Two approaches are presented: (1) experimenting with a LiDAR point cloud for the extraction of building parameters, which includes the usage of an automatic methodology, the evaluation of building height, and characterization of the roofs extracted with semi-automatic methodologies; and (2) testing and comparing UAV and LiDAR point clouds for the extraction of building parameters using a FOSS methodology. It also includes a deep analysis of the errors registered in the estimation of building parameters – area, height, volume, and total volume – for each technology.

- *Chapter 3* addresses the low-cost UAV technology for the extraction of building parameters in an urban morphology composed of residential building blocks.

  Two approaches are presented: (1) the evaluation of building heights extracted from building block types; and (2) the demonstration of the pertinence and usability of the extracted building block volume parameter for high precision dasymetric mapping.

Chapters 2 and 3 are the core of this thesis: they contribute to the 2D/3D building parameters modelling and extracting within the methodological framework. Furthermore, the evaluation of the errors that was carried out in each chapter contributes to the demonstration of the pertinence and usability of the data extracted for the planning process.

- *Chapter 4* contains the discussion of the issues addressed in this research and summarizes the main conclusions of this thesis.

  This chapter highlights the following four issues: (1) it emphasizes the importance of 3D measurement for urban planning; (2) it summarizes the different approaches that we have tried out in this research and reviews the main results and their contributions to this research; (3) it contrasts the results obtained in this research with the new 3D paradigm in the planning process, based on relevance, pertinence, and usability; and (4) it provides future directions regarding the 3D measurement and 3D geovisualization for the planning process, including the optimization and improvement of the solution proposed in this thesis, and the future perspectives for 3D data in urban planning. This chapter contributes to the demonstration and operationalization within the methodological framework.

Chapter 1

Geo-Information Technologies for 3D Geographical Data: New issues for Urban Planning

Geo-information technologies are the main support of urban planning. They are the source of the spatial representation of strategies and instruments within the framework of plans and policies provided at local, regional, and national level.

Ranzinger & Gunther (1998, p.159) wrote 'For decades urban planning was done by drawing plans and building elaborate models from wood and pasteboard.' In the meantime, technology turned the drawing plan into one dimensional arrays of bytes with different formats. The digital age has changed the vision and the way urban planning is conducted. Nowadays, urban planning is facing a new age, which comprises a 'democratization' of three-dimensional geographical data acquisition technologies.

The progress in geo-information technologies over these last decades has solved the lack of data. The acquisition of geographical data in different formats and methods has been somewhat trivialized.

The aim of this chapter is to demonstrate the evolution of geo-information technologies in the planning process in Portugal. Furthermore, 3D point clouds acquired from LiDAR or UAV technologies shall be presented, which constitute a new challenge and vision of digital spatial representation for urban planning – *Could there be a new paradigm?*

We shall also discuss FOSS technologies that can be supported by these new costless technologies for urban planning in Portugal. *What is the vision of Portugal regarding FOSS technologies?*

1.1 *New developments in terms of geographical data for planning in Portugal*

Hall (2002, p.3) states that 'It is simply impossible to think of this type of planning without some spatial representation – without a map.' The planning process is based on a strategic framework that guides physical planning and is concerned with the regulation of the physical form of the urban area, the spatial arrangement of land uses, and the evaluation of proposed goals. All these issues are implemented through an ongoing and cyclic planning process for which geographical data are needed on several phases of the cyclic process.

The planning process[1] is a sequential process that comprises the following phases (Figure 1.1): *i)* ***making the plan***, which includes the elaboration, formalization and implementation of a plan, for which the acquisition of official and approved updated topographic mapping is crucial; *ii)* ***participation and public discussion*** that consists in the public presentation and discussion of the proposed plan through events in accordance with a previously published programme. The presence and participation of different stakeholders is required where the spatial representation is essential to facilitate and promote the communication among public stakeholders, decision-makers and technical experts. The visualization from printed mapping or a geovisualization from environment Geographic Information Systems (GIS) or Web-based GIS visualization platforms are essential for a better effectiveness of the public discussion; *iii)* ***monitoring and evaluation*** should be seen as process interlinked with the information collected in accordance with certain indicators. This is used to evaluate the success and effectiveness of the implemented plan. According to Batista e Silva (1998) monitoring is a systematic observation of a plan for the evaluation of the originally proposed goals for that plan in order to evaluate the need to revise or even restart the planning process. Subsequently, in order to build a system of indicators related with spatial variables, the geographical

[1] Among the planning process phases we have selected only those that are related to geographic information.

data is required to obtain results and for the assessment; *iv)* ***revising*** reflects the ongoing nature of the planning process and establishes the beginning of a new cyclic process, for which updated official topographic mapping is required.

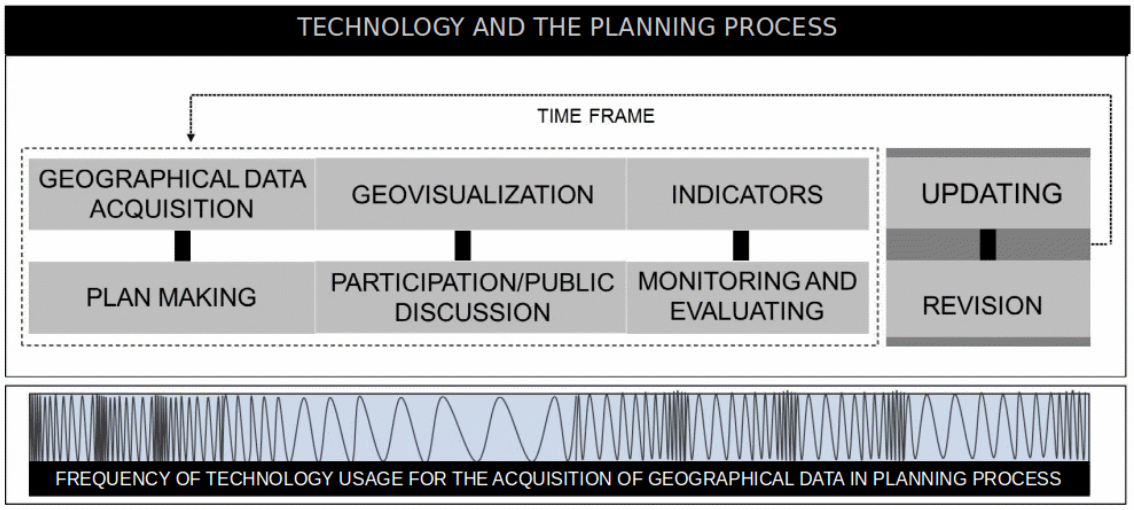

Figure 1.1: Frequency of updated mapping for the planning process

Geographical data is needed in all the phases of the planning process. Regarding the usage of geographical data in the planning process, there are two approaches: the first is the usage of official, updated, and approved topographic and imagery mapping under the law (Decree-Law No. 141/2014) that enables the positional accuracy required for the formalization of the plans; the second is the frequency of technology usage on time for the acquisition of geographical data in the planning process, which is higher in the plan-making and monitoring/evaluation phases, but lower in the public participation and revision phases (Figure 1.1). The scheme of Figure 1.1 assumes that the relationship between the pace of updating and the frequency of usage of geographical data is directly proportional in each phase. For instance, the time frame for the updating of geographical data in the plan-making and revision phases of a master plan (Plano Director Municipal – PDM) used to be 10 years, but now it depends on whether the evaluation[2] is appropriate and sustainable considering the frequency of usage.

For the elaboration/revision of municipal plans the current urban planning legislation also establishes a minimum criteria updating[3] for the topographic and imagery mapping usage: 3 years for master plans, 2 years for urban plans, and 1 year for detailed plans. The legislation also aims to standardize procedures and regulate

[2] Today, according to the new Decree-Law No. 80/2015, of 14th May, the time frame in any plan is variable depending on the needs for the evaluation of land use transformation.

[3] According to article 15-A of Decree-Law No. 141/2014, of 19th September.

the production and quality of regulatory cartography[4]. However, it is lacking in the use of geographical data in the monitoring and evaluation phases of the planning process. Moreover, in the relationship between the frequency of usage and updating of geographical data in the monitoring and evaluation phases there is a 'gap' or better still, map production is not able to provide an adequate support to these phases. In other words, the geographic information technologies currently implemented for the production of topographic maps do not maintain this relation.

How is it possible to monitor and evaluate indicators with ongoing updating mapping based on classical methods of map acquisition and production?

Can the new geographical data acquisition technologies address the existing 'gap' in terms of monitoring/evaluation? Can the frequency of usage in this phase be ensured by permanent updating?

These issues will be discussed later in this chapter. After that, we shall address the evolution of planning legislation together with geographic information technologies for the acquisition and production of topographic maps.

The topographic and imagery mapping used for urban planning in Portugal are produced by photogrammetric techniques. Photogrammetric techniques allow us to collect 2D/3D vector data from very high resolution stereo imagery acquired by an aerial camera system (large and medium format). Currently, the national entities in charge of the production of topographic maps in Portugal are the Geospatial Information Centre Institute of the Army[5](Centro de Informação Geoespacial do Exército – CIGeoE) for the 1/25000 scale and the Directorate General for the Territory[6] (Direcção Geral do Território - DGT) for a 1/10000 scale. These two entities are the official suppliers of this data. The production of large scale maps is also regulated by DGT and they can only be produced by companies that have the approval for that.

The topographic mapping production/updating can be summarized in four stages (Figure 1.2): 1) flight planning, where the technical flight parameters and specifications are proposed depending on the mapping scale; 2) acquisition of nearly

[4] Thematic mapping produced to support plans based on official and approved topographic and imagery mapping.

[5] This entity has had various names over time. Before its current name, it was called Geographic Institute of the Army (Instituto Geográfico do Exército – IGeoE).

[6] This entity was created in 2012 by a merger of Direcção Geral de Ordenamento do Território e Desenvolvimento Urbano (DGOTDU) and Instituto Geográfico Português (IGP).

vertical stereo aerial images[7] from a metric aerial camera; 3) application of photogrammetric procedures to the georeferencing block,[8] using tie points and Ground Control Points (GCPs), called aerial triangulation procedure; 4) photogrammetric procedures for the acquisition of vector data using 3D stereo vision or orthophotos[9] from the georeferenced block; 5) quality control procedures for mapping products, such as surveying GCPs to evaluate positional quality. The procedures used in each of these stages have changed with the development of technology over time in line with the legislation of land use planning and urbanism implemented in Portugal.

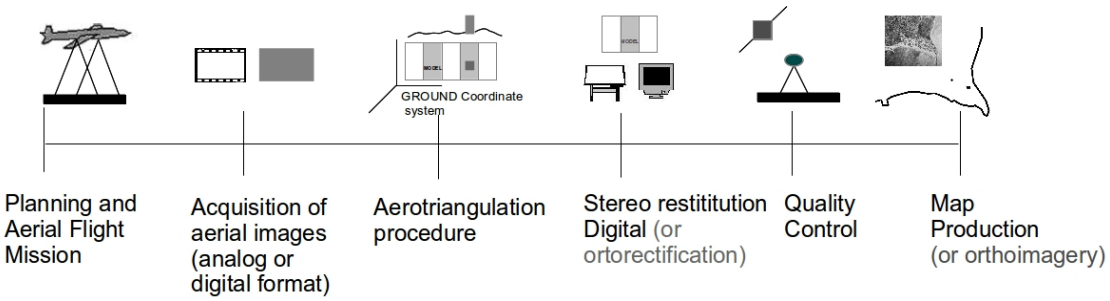

Figure 1.2: Workflow of mapping production procedures

In general, advances in mapping technologies have been integrated into planning processes over time, while the visualization and spatial representation of plans have also changed over the past forty years. The evolution of the legislation regarding land use planning and urbanism in Portugal and geographical data acquisition and visualization technologies over time comprises five periods: i) Analogue mapping for planning purposes in the late 1970s and in the 1980s; ii) Digital mapping in the 1990s; iii) Fully digital mapping and GIS in the 21st century; iv) Web-based 2D GIS and spatial platforms in the 21st century; and v) New paradigms for urban planning.

1.1.1 Analogue topographic mapping for planning purposes in the late 1970s and in the 1980s

Urban planning policies between 1975 and 1981 were defensive and reactive (Alves, 2007). The aim of these urban policies was to improve the quality of life for

[7] Vertical images imply that the tilt value should theorically be lower than 5° (position of optical axis related to nadir) and stereo means that images have an endlap minimum of about 60% (along flight) and sidelap of about 20% (between flight lines).

[8] A block is a set of photos, models and strips.

[9] Orthophotos are obtained from ortorectification process that consists in conversion of aerial images to an orthogonal projection, like a 'map' using a Digital Terrain Model (DTM) or a Digital Surface Model (DSM).

the population together with the preservation and protection of natural resources and heritage (Pereira, 2003). The first municipal plans appeared as 'local council' or 'structure plans' without a legal framework (ibidem). This experimental period in urban planning was based on the 'first law of assignments and competences of the municipalities' (Law No. 75/77, of 25th October), where the plan was referred to as a tool to support municipal management. Later, the legal framework for a 'master plan' was established by Decree-Law No. 208/82, of 26th May, and plan-making was regulated by Regulatory Decree No. 91/82, of 29th November. The master plan at this time was not mandatory and it was technically and formally complex and rigid (Alves, 2007). The plan was composed of the following mapping products: a contextual region map with the regional plan development, a map with the present situation that supported plan-making, and a map with the spatial representation of urban structure and the proposed zoning areas.

These mapping products were produced from analogue topographic maps M888 on a 1/25000 scale produced by the Military Cartography Services (Serviços Cartográficos do Exército – SCE[10]). The production of these topographic maps was obtained using the analytical stereo photogrammetry technique (Fernandes, 2002) and the aerial images were acquired by an analogue aerial camera based on 230 by 230 mm film. The stereo photogrammetry was based on the stereoscopic measurement principle, the so-called stereoscopic viewing[11], while the acquisition of geographical data was performed by a stereo restitution process (three-dimensional acquisition). The stereo restitution process was performed through two aerial photographs (called diapositives) with an overlap of about 60% (called stereo model) in the stereo plotting instrument for all the images of a block or strip. This manual process was performed with the analytical stereo-plotting instrument WILD A8, whose coordinates for the corresponding points in the stereo model were measured and recorded digitally using a computer system to calculate orientation. After the orientation of the stereo model had been accomplished, the operator traced the visible details identifiable in the stereo model in the computer where the display of elements acquired were shown on the drawing table. Thus, the mapping of streets, rivers and creeks, settlements and houses, vegetation boundaries, and altimetric elements (contours) is carried out on a digitizing table and recorded on magnetic tapes. More details about the production of topographic maps on a 1/25000 scale

[10] Currently the name is CIGeoE.

[11] Stereoscopic viewing means that it is possible to measure three-dimensional coordinates of one point using two (or more) images of the same object but taken from different positions.

in Portugal at this time can be found in Fernandes (2002).

Furthermore, at this time, the official cartography on a 1/10000 scale produced by the Portuguese Geographic and Cadastre Institute [12] (Instituto Geográfico e Cadastral – IGC.) was done in a similar way, but was not able to support plan-making because only 19 map sheets of Lisbon on a 1/10000 scale were available. In 1985, most of the municipalities only had print maps on a 1/25000 scale, and the plans were designed from this support. At the end of the 1980s computer-aided design started to be used by architects and engineers for the production of detailed plans (urban project) and urban plans based on the conversion of analogue maps to a digital format (raster). Subsequently, most municipalities started to work with computer aided design for urban studies, based on digital mapping obtained by the scanning of mapping documents (Matos et al., 1994).

During this time, the usage of analogue maps was a problem for the delimitation of land uses in a master plan, because of the lower accuracy in the definition of zoning areas due to instrument accuracy and human error (graphicism error) and distortions on the support (Campos & Silva, 1997).

At the end of the 1980s, there were only four effective master plans and three approved by Municipal Councils (Fernandes, 2001), mainly due to the 'absence of a planning culture' and the inexperience of the local administration to deal with the implementation of policies and plans (Pereira, 2003). Additionally, only thirty urban plans and 142 detailed plans were approved between 1985 and 1990 (Alves, 2007).

1.1.2 Digital mapping in the 1990s

Urban planning in the 1990s became a matter of utmost importance for the development of the territory because Portugal had joined the European Community (EC) in 1985 (Alves, 2007). The implementation of master plans became mandatory since the approval of community funding for projects required the existence of such an effective plan. This stage marked the first generation of master plans in Portugal with the definition of the legal framework for the municipal plans established in Decree-law No. 69/90, of 2nd March.

After the publication of this law the number of master plans did not in-

[12] Currently it is included in DGT as IGP.

crease as expected (Alves, 2007) because few technicians were able to respond to the amount of plans in the short time. On the other hand, there were technical mapping issues related to analogue topograhic mapping that were difficult to implement when designing the plans. Campos & Silva (1997) identify in the regulatory cartography two types of problems regarding the spatial representation of plans: *measurement* and *interpretation*. Both are mainly related with the scale of topographic mapping and with the use of topographic mapping in an analogue support. Some issues related with the elaboration of plans are summarized below:

- out-of-date official topographic mapping (some maps were over 20 years old) due to analytical photogrammetric methods and ground control procedures that were very time consuming. The delimitation of zoning areas was difficult without a real knowledge of the territory;
- incorrect handling of these mapping data by technicians, where the geographical data sometimes was acquired through the extended copies of mapping documents;
- topographic mapping was rarely scanned as a single document; what the base map used was a composition map of various scans. Sometimes several map sources on different scales were used to compose the base map (Matos et al., 1994);
- topographic mapping on a 1/25000 scale was not suitable for the spatial representation of land uses required for the elaboration of zoning master plans (planta de ordenamento), such as the delimitation of land uses and urban fringe;
- the use of digital maps obtained from analogue maps with distortions, where the overlap with other maps often presented deviations.

More details about the problems in the elaboration of mapping plans during this decade can be found in Campos & Silva (1997) and Matos et al. (1994).

Afterwards, the Portuguese government established two programmes in 1994 to solve these problems, whose main objective was to support the acquisition of geographical data by computer-aided design systems, ensuring the quality of analogue maps scanned and increasing plan-making and the evaluation of plans to 5 years: Computer Management Support Programme for Municipal Plans[13] (PROGIP) and

[13]Programa de apoio à Gestão Informatizada de Planos Municipais do Ordenamento do Ter-

Support Programme for the Creation of Local Nodes of SNIG (PROSIG). The difficulties in the implementation of these programmes can be seen in Matos et al. (1994).

Furthermore, around this time, the Portuguese government approved funding for the development of a new National Mapping Series on a 1/10000 scale by IGC[14] in order to support plan-making and revise municipal plans and special plans. Later, the ProCARTA programme was launched in 1994 to provide technical support to municipalities for the production of official digital mapping on a 1/10000 scale for five years, based on agreements signed between private companies and IGC. However, there were some difficulties in the implementation of this programme because the standards and procedures were not properly defined and companies did not possess the mapping technology needed for the management skills.

Following the growing trend in digital mapping usage, Decree-Law No. 193/95, of 28th July, was published to support plan-making. This law established the regulations for mapping production in Portugal, where the production and updating of official topographic mapping should be ensured by IGC(1/10000) and IGeoE (1/25000). Also, IGC should regulate and establish rules for the production of topographic mapping by private companies.

Urban planning policies in the second half of the 1990s were more proactive than reactive for the (re)qualification of urban areas was a priority (Alves, 2007) based on good practices for the usage of geographical data acquisition technologies. Later, at the end of the decade, the principles and objectives for territorial management and urbanism were established by the Spatial Planning and Urban Policy Framework (Lei de Bases da Política de Ordenamento do Território e Urbanismo – LBPOTU) approved by Law No. 48/98, of 11th August. Moreover, the legal framework for the IGT approved by Decree-Law No. 380/99, of 22nd September, promoted the characterization and analysis of the plans for territorial management at different levels of intervention.

According to the LBPOTU, three levels of plans were defined for IGT: a) at the national level, the National Programme of Spatial Planning (Programa Nacional da Política de Ordenamento do Território – PNPOT), sectorial plans and Special Spatial Plans (such as the Shoreline Spatial Plan – POOC); b) at the regional level, the Regional Spatial Plans; c) at the municipal level, the inter-municipal plan and

ritório.

[14]Currently, included in DGT.

municipal plans (Master Plan, Urban Plan, and Detailed Plan). This law introduced the monitoring and evaluation of the spatial planning policy in the planning process pursuant to article 28. Accordingly, the 'Spatial Planning Status Reports' (Relatório sobre o Estado do Ordenamento do Território – REOT) should be developed every two years by the Government (at the national level), Regional Boards (at the regional level), and Local Authorities (at the local level).

The RJIGT introduced significant changes in the planning process, particularly regarding plan-making, evaluation, and revision of municipal plans. Pursuant to article 98, an assessment report had to be submitted every two years to evaluate whether the plan needed to be revised. Furthermore, the revision of a master plan was mandatory after 10 years, and the municipal plans or special plans could only be updated after 3 years of formalization. This law integrated the monitoring stage into the planning process to support the evaluation.

During the 1990s, around 90% of the first generation of master plans had been published, the majority of which was approved between 1994 and 1995 (Pereira, 2003).

At the end of the 1990s, the topographic mapping production changed to digital photogrammetry, where all procedures of stereo restitution were made from digital photogrammetric workstations (softcopy photogrammetric systems). Softcopy photogrammetry involved replacing aerial photographs with digital ones. Subsequently, aerial imagery using conventional film-based cameras (large format diapositives) was scanned by a high-precision photogrammetric scanner. This photogrammetric scanner had specific basic requirements such as large format A3, a transparency unit for film material, high geometric and radiometric resolution, and high accuracy. This equipment was very expensive at the time, but it was a mandatory peripheral hardware to ensure the quality of map production.

Besides, photogrammetric procedures, including stereo restitution, became possible in a computer system based on algorithms developed from analytical photogrammetry. For instance, aerial triangulation became automatic based on stereo-matching techniques, where the tie points are automatically identified. This advance in photogrammetry allowed to georeference simultaneously every image in a block. The stereoviewing is accomplished artificially by displaying alternately a pair of images taken from different points of view with the active shutter-glasses method (Aber et al., 2010).

In Portugal, digital mapping was implemented at IGeoE in the second half of the decade with a photogrammetric workstation of *Image Station* from Intergraph and a *PhotoScan TD* photogrammetric scanner (Fernandes, 2002). In 1995, the first aerial flight with GPS was made in Portugal by the German company MAPS (Fernandes, 2002). This technology allowed for the reduction in the number of GCPs that were needed for the photogrammetric process.

The digital mapping technology reduced the time-consuming process of topographic map updating or production, since most procedures were automated. The production of digital maps on a 1/25000 scale (Figure 1.3) increased in the last five years of the 1990s, not only because of the improvements in terms of technology, but also because the needs of the CENSUS 2001 project resulted in the update of more than 80% of the councils.

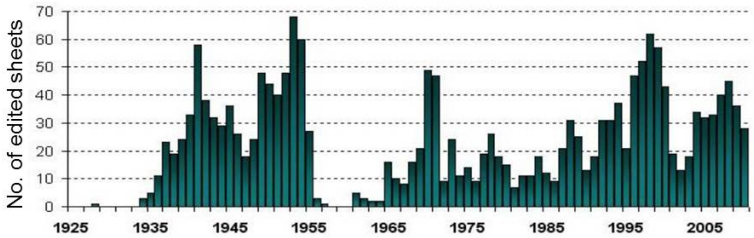

Figure 1.3: Updating of topographic 1/25000 mapping over time. Source: Gomes (2011).

In the last decade of the 20th century and the first decade of the 21st century, an average of 37 mapping sheets on a 1/25000 scale were produced per year (Gomes, 2011). However, map production has decreased in the past few years due to the lack of human resources.

1.1.3 Fully Digital Mapping and GIS in the 21st century

The spatial planning policy of the first decade of this century is characterized by the end of the 'First generation plans' and the beginning of the 'second generation plans' based on digital mapping and GIS technologies. The first generation master plans were completed in 2003 with the Góis master plan (Pereira, 2003).

According to Alves (2007), in 2004 only about 105 municipalities of a total of 278 had urban plans. This means that most municipalities grew without rules and regulations in built-up urban areas. DGT database at that time recorded the existence of 193 urban plans and 654 detailed plans. Regarding detailed plans, 8.4% of those were exclusively for the rehabilitation and regeneration of urban areas and

18.7% for industrial and service areas. Also, about 50% of the municipalities had the master plan under revision.

The revision of the master plans (2nd generation of plans) has been showing a greater dynamism as a result of several amendments to the legal framework of IGT. In this context, three important Regulatory Decrees that were approved on 29th May to complement plan-making stand out: Regulatory Decree No. 9/2009, which standardizes the technical concepts that would be used in spatial planning and urbanism; and Decree No. 11/2009 that defines the criteria for the classification and reclassification of land uses. However, Regulatory Decree No. 10/2009, which fixed the rules for the mapping that would be used for the elaboration and revision of the plans, was revoked in 2014. Part of its content was included in the new Decree-law No. 141/2014, of 19th September, on mapping production.

Recently, Decree-Law No. 193/95 was replaced by Decree-Law No. 141/2014 of 19th September, on 2D mapping production rules, which integrated part of the content of Regulatory Decree No. 10/2009. Furthermore, the new legal framework of the IGT was defined by Decree-Law No. 80/2015, of 14th May (see Appendix A), which takes into account the 'general basis for public policies on soils, land use, and urbanism' published (Law No. 31/2014, of 30th May). These new legislation has contributed to the stability, regulation, and standardization of the procedures involved in the planning process.

The spatial planning policy was marked by the approval of the strategic plan PNPOT with Decree-Law No. 58/2007, of 4th September and 6 Regional Spatial Plans (Planos Regionais do Ordenamento do Território – PROT)[15] were approved. These plans provide a benchmark for the revision of master plans, urban plans and detailed plans, and for the elaboration of special plans.

In this century, revision plans over have been conducted in a GIS environment, where all the thematic mapping is produced from official and approved topographic mapping[16] (on several scales: 1/2000, 1/5000, 1/10000, and 1/25000), which should be structured by the rules and technical specifications proposed by DGT.

These topographic maps produced by digital photogrammetric techniques remained, and the analogue and analytical stereo plotting instruments still used by

[15] Approved: Algarve PROT (2007), Oeste e Vale do Tejo PROT (2009), Alentejo PROT (2010), Centro PROT(2011), AML PROT (2008), and Norte PROT.

[16] According Decree-Law No. 141/2014 'Topographic mapping' represents the translation of base mapping ('cartografia de base') obtained from photogrammetric techniques.

some companies were replaced by digital photogrammetric workstations.

Photogrammetric workflow procedures (Figure 1.2) during this decade changed with the introduction of two technologies: the digital aerial camera and the direct georeferencing system. These two technologies allow us to obtain georeferenced aerial imagery in a digital format, eliminating the time consuming photogrammetric workflow scanning process. There was also an automation of the aerotriangulation process with direct georeferencing, including a reduction of GCPs required at this stage of the process.

Digital aerial cameras do not have a standard sensor format. They can be divided into large format, medium format, and small format systems. Most of these cameras have a rectangular image format, where the larger dimension is in the across-flight direction to reduce the number of required flight lines (Neumann, 2008). The image size of the large camera format is much higher, which also implies that less images are needed to cover the same area when compared with a medium format camera.

It is important to highlight that these advances in digital photogrammetry have turned the acquisition of 2D vector data and orthorectified imagery by a fully digital mapping production into a more time- and cost-effective process.

The first surveying flight with a digital aerial camera over Portuguese territory (which acquired 7056 images of 40% of the territory) was made at the end of 2004 using the large format camera Vexcel Ultracam[17] (Patrício, 2006). Moreover, two more aerial flights were made with this camera to cover the whole territory in 2005 and 2006. In 2007, the first large format airborne mapping system Intergraph/ZI DMC (Intergraph/ZI, now Hexagon Geosystems) was acquired by the Portuguese company Municipia. Today it is still the only digital aerial camera in the country.

Innovations in automated photogrammetry will be continued over the 21st century in terms of digital image processing algorithms and airborne digital cameras. Baltsavias (1999a, p. 89) stated that 'Research is mainly focusing on automation of feature extraction...' and the latest algorithms developed in photogrammetry have shown that this statement still holds true. Moreover, the contribution of computer vision to photogrammetry in these past few years was higher and it is expected

[17]This aerial flight resulted from an agreement between IGP and the General Directorate for Forestry Resources (Direcção Geral de Recursos Florestais - DGRF) for the production of very high resolution orthorectified imagery (50 cm).

to yield significant economic benefits to topographic map production in the future. According to Leberl et al. (2010), computer vision has produced various algorithmic innovations in multi-image matching and multi-image-based point cloud measurements.

Nowadays, the geographical data acquired by the digital photogrammetric stereo restitution is completely integrated into GIS environments, where the accuracy and semantic information of official geographical data is preserved. According to Tenedório et al. (2013), GIS have enabled the dematerialization of processes in urban planning.

GIS allow us to manage and structure 2D/3D vector data according to a data model in a geographical database. Consequently, technical standards for a master plan data model[18] (Normas Técnicas sobre o Modelo de Dados para o PDM) were developed and implemented in 2011. Their main objective was to establish norms and standards for the structuring of master plans in 2D geographical databases and for spatial digital representation. Furthermore, the master plan should include metadata information based on the INSPIRE[19] Directive. However, the Technical Standards for urban and detailed plans data model have not yet been developed.

All the functionalities of GIS (edition, spatial analyses, queries, multi-scale mapping) can support urban planning through the production of 2D mapping products more easily. Furthermore, the management of solutions, spatial analyses, and visualization of data in a GIS environment contributes to a better planning process, mainly in terms of decision-making, assessement, and elaboration of thematic maps.

During the first decade of the 21st century, GIS and computer-aided design systems were completely integrated and recognized by most municipalities as an important tool to support urban planning mapping. However, the revision of master plans in some municipalities was still performed by external officers, because the municipalities lacked skills, resources, and technical expertise in GIS. According to DGT (2013), at the end of 2013 there were 1508 IGT implemented and approved plans, which included: 122 national plans (1 PNPOT, 76 special plans,[20] and 45 sectorial plans), 6 PROT, and 1380 municipal plans (277 master plans, 248 urban plans, 853 detailed plans, and 2 inter-municipal plans).

[18]Required pursuant to paragraph 1 of Article 15-A. of Decree-Law No. 141/2015.

[19]Infrastructure for Spatial Information in Europe established by Directive 2007/2/EC of the European Parliament and of the Council of 14th March 2007.

[20]Including 9 POOCs.

1.1.4 Web-based 2D GIS and spatial platforms in the 21st century

In the past few years, the interaction between GIS data capabilities and communication technologies for the urban planning process have increased in Portugal, through the implementation of electronic platforms over the Internet. Some of the advantages of electronic platforms for the planning process are: a) encouraging transparency in plan-making for citizens; b) self-knowledge of the status of the planning process by all the stakeholders; c) increased effectiveness of plan-making, monitoring, and assessing; and d) plans can be consulted at all times.

Silva (2010, p.8) wrote that 'The growing access and use of information and communication technologies, especially the Internet (...) implied a democratization knowlegde on urban issues.' In Portugal the first steps towards the 'digital democratization of IGT information' began in article 147[21] of RJIGT, which states that all IGT should be available within the framework of the National System for Territorial Information (Sistema Nacional de Informação Territorial – SNIT). The SNIT was implemented in 2008 by DGT backed by web-based 2D GIS tecnhology and supported by Geomedia/Intergraph GIS tools. These web-services provided by SNIT as WMS (Web Map Service) and WFS (Web Feature Service) were based on Open Geospatial Consortium (OGC) specifications.

The SNIT is a modular platform managed by DGT (Alves & Simões, 2015). Presently, the SNIT has 3 main electronic platforms (Article 190 of Decree-Law No. 80/2015, of 14th May):

1. *Spatial Data Infrastructure SNIT* (SDI SNIT) supported by technology that follows INSPIRE rules, through which it is possible to consult an approved plan (revised, changed or first generation plan) and visualize the thematic mapping of a plan. The same spatial data structure is ensured for all master plans;
2. *Spatial Plans Automated Submission System* (Sistema de submissão automática Informação Geográfica Territorial – SSAIGT), where the plans can be submitted by public entities for publication in the Official Gazette and on SDI/SNIT. Currently, the geographic information of plans (georeferenced images, 2D vector data, and metadata) should be submitted according to the

[21] Decree-Law No. 380/99.

technical standards of the data model for master plans provided by DGT in 2011.

3. *The Collaborative Platform for Territory Management* (Plataforma Colaborativa de Gestão Territorial – PCGT) created in 2008 was designed to support, monitor, and assess ongoing programmes and plans, either by the responsible local authorities for its elaboration or revision, or by public entities and stakeholders that are also involved with the plan.

The SNIT has three more electronic platforms[22]: a) GeoEquip for public equipment (in progress); b) SRUP (Servitudes and Public Utility Restrictions); and c) AH (Historic Archive).

Currently, the following issues can be identified in the planning process: transparency, flexibility, standardization, and simplification. Transparency is given by the dissemination of plans using communication technologies, where citizens, stakeholders and public entities can more easily have access to the information regarding a plan. Plan-making and revision is more flexible, since the time frame for the revision of the plan is now defined by entities or plan-makers and should take into account the economic cycle. On the other hand, the standardization of plan-making is a mandatory issue based on spatial data infrastructure and digital spatial representation. The simplification of plan-making and revision processes should be achieved by the standardization of procedures and technical standards.

1.1.5 New paradigms for urban planning

Over time, the planning process followed the evolution of geographic information technologies, where the transition from the *physical planning process* (based on analogue mapping) to the *digital planning process* revolutionized planning procedures. The digital planning paradigm started with data acquisition technologies, followed by the computation of the planning process. In this case, the way plans are visualized and information is measured based on digital spatial representation (2D mapping).

Nowadays, new paradigms for the planning process in Portugal are eminent due to the reform of the RJIGT and advances in 3D data acquisition tech-

[22] All these platforms can be consulted in *www.dgterritorio.pt/sistemas_de_informacao/snit.*

nology, which will bring forward the *3D urban planning paradigm* and the *geo-democratization of planning*.

The first paradigm comprises 3D Measuring and 3D Geovisualization in the planning process. The second paradigm implies the 'democratization' of knowledge on urban issues (Silva, 2010) for different stakeholders, the civil society, and private sectors. Silva (2010) called this approach *e-planning* due to the extensive use of information and communication technologies in all phases of the urban planning process.

The *geo-democratization of planning* is now a reality in the planning process after the creation of the SNIT electronic platform and other electronic platforms such as shown in the previous subsection. In the future, these web technologies should be employed in all the stages of the planning process, given that the standardization of all the procedures is a priority for the spatial representation of urban plans and detailed plans. However, this *new culture of planning* with an *open planning* for everyone is an ongoig project.

How can 3D urban planning be a paradigm pursuant to the new legislation?

The vision of planning in Portugal is not '3D urban planning' yet, since the legislation relating to mapping and urban planning does not include the use of 3D data. On the other hand, it does not allow the usage of other mapping products in the planning process, unless offical and approved by DGT. However, the evaluation of sustainable planning policies required in the new legislation seems to have shifted from traditional 2D data to 3D data.

The new legal framework of the IGT requires a set of quantitative and qualitative indicators in the content of each plan to support the monitoring and evaluation of programmes and plans. On the other hand, the results obtained from that evaluation should be used to check whether the plans need to be revised or amended. For instance, the economic and financial sustainability evaluation of the transformation of land uses in urban areas, can require demographic indicators, levels of supply and demand of urban land indicators, and the total building volume density index.

The legislation also specified the following issues: *a)* the master plan should contain the specification of quantitative and qualitative indices, indicators and benchmarks, urban or planning, to be set in urban or detailed plans (Article 96). In particular, consolidated planned urban areas in a master plan shall also include indicators that define land uses and the total height of buildings or height of façades;

b) the urban plan should contain the indicators and urban parameters for each zoning defined in the master plan; and *c)* the detailed safeguard plan should contain, for instance, building height, building area and the number of stories, and, in the context of land registration, it must also contain building volume.

Some of the legislation requirements mentioned above demonstrate that the introduction of 3D measuring is an important issue to monitor and evaluate the plan because of the nature of some indicators that require 3D data, such as building height.

3D geovisualization is another crucial topic in 3D urban planning based in a generation of 3D models for the visualization of urban environments. Following Kolbe et al. (2005), these 3D models can be based on Level-of-Detail (LoD): (1) LoD0 raster visualization 2.5D; (2) LoD1 *Volumetric block model* in which the building is represented as a 'block' whose roof is not modelled; and (3) LoD2 *Volumetric envelope models* whose building roofs are detailed.

3D geovisualization using these 3D models in the participation/public discussion phase and also in the plan-making phase is essential to formalize the plan with greater effectiveness and efficiency. In the public discussion phase, it facilitates the visual communication and promotes the participation and interactivity between the civil community, stakeholders, and urban planners. Furthermore, it can contribute to the elaboration of a plan, such as the definition of zoning areas and the design of urban areas where hidden objects can be easily identified. Additionally, it also contributes to a visual impact assessment (Danese et al., 2009) in new development land uses or in areas planned for urban rehabilitation programmes, such as proportions and similarity with existing urban patterns (Danese et al., 2009).

The 3D urban planning paradigm reflects a new vision for the planning process. However, this paradigm cannot exist without appropriate 3D mapping technologies that can withstand constant updating of 3D data at a low cost. Nowadays, this is the major problem for the planning process that needs to continuously update its 2D geographical database, whose costs are much higher.

There have been many developments in terms of the ability to acquire faster and more accurate 3D data in a short amount of time due to advances in imaging or laser airborne sensor systems. Now, a high density 3D data can be obtained from two techniques: i) directly, from Airborne Laser Scanning (ALS) or ii) indirectly, from full stereo processing using dense stereo image matching. For instance, the recent

UAV systems can acquire 3D data (or 3D point clouds) in less than 24 hours at a low-cost. Although this information may seem not to ensure the necessary accuracy for the revision of the plans, its potential for the monitoring and evaluation and public participation phases can be shown. However, it is important to highlight that the intervention area of each plan can be an obstacle to the usage UAV technology, because this system was designed for aerial photogrammetric surveys over small areas.

1.2 *LiDAR point cloud*

The LiDAR system, also known as ALS, is an active remote sensing technology that provides its own lighting (no shadows in its basic signature) and records range measurements. This technology was introduced in the 1990s for surveying purposes (Hyyppä, 2011). It allows a quick and fully automatic collection of a georeferenced and dense 3D point cloud over a large area, unlike traditional surveying and traditional photogrammetry methods. The comparison between traditional methods of photogrammetry and ALS has been detailed in Baltsavias (1999a) and Ackermann (1999). More recently Leberl et al. (2010) compared the 3D point clouds obtained from novel automated photogrammetry and using the LiDAR system.

The advantages of LiDAR data in relation to very high spatial resolution images were recently addressed by Yan et al. (2015). The production of DSMs using the LiDAR system has advantages when compared with optical sensor systems in terms of data acquisition and type of objects recorded, such as: *i)* the acquisition of data in flight is independent from season and daytime; *ii)* the effects of relief displacement are reduced, and dominant shadowing in urban areas does not exist in LiDAR data (Yan et al., 2015); *iii)* enables the mapping of bare earth surfaces (or Digital Terrain Models) even in areas with dense vegetation or forest; and *iv)* detects all kinds of objects from an urban area, such as vegetated areas, trees, buildings, cars, ventilations ducts, antennas, power lines, and railings on rooftops.

The LiDAR point cloud enables: *a)* a high level of automation in the acquisition; *b)* a high level of detail (up to millions of points per square kilometres) which includes forest and vegetated areas; *c)* the acquisition of a large number of various forest and vegetation parameters (canopy height, canopy volume profile, tree height, above-ground and below-ground biomass and many others) (Mallet & Bretar, 2009

and Hyyppä, 2011); *d)* a high accuracy in the generation of 3D products, such as Digital Surface Models (DSMs), 3D building models and 3D city models for planning purposes, design, monitoring, and infrastructure maintenance.

The benefits of LiDAR have been proved in various urban studies that include the generation of 3D city models (Lafarge & Mallet, 2012; Kaartinen et al., 2005; Kada et al., 2009; Elberink & Vosselman, 2011), 3D building models (Zhou et al., 2004) and land cover classification (Yan et al., 2015).

An overview of airborne LiDAR systems is available in Baltsavias (1999c), Hyyppä (2011), and Yan et al. (2015). Additionally, a summary of some earlier and recent ALS systems can be seen in Toth (2009), Mallet & Bretar (2009) and Baltsavias (1999c). Toth (2009, p.148) noted '(...) that there are more than 250 airborne LiDAR systems used worldwide.' Now, most are produced by three major suppliers Optech, Hexagon (which includes Leica), and Riegl.

1.2.1 Components of LiDAR and operating principles

Most of the present generation of LiDAR sensors use the pulse principle (Wehr & Lohr, 1999) that measures the round-trip of short light pulses from the laser scanner to the point on the earth surface and returns to the receiver unit. Then, the distance between the LiDAR transmitter and the target [R] is given by $R = ct/2$, where t is the time between transmission and reception of the pulse and c is the speed of light.

The basic principle of LiDAR is to measure several thousand laser pulses per second emitted to the earth's surface at a high repetition frequency (PRF) by a laser ranging instrument. The position and orientation of each pulse that returns to the laser unit is also available from a direct georeferencing system. The direct georeferencing system (Figure 1.4) allows a 'real-time georeferencing' (Choi & Lee, 2013) through a positioning system based on GNSS (Global Navigation Satellite Systems) and an Inertial Measurement Unit (IMU) in the aircraft. The GNSS provides the position of the laser sensor (Xo,Yo,Zo) based on one or more GPS base stations and the IMU provides the sensor's attitude and heading angles (*roll* around x-axis, *pitch* around y-axis, and *yaw* around z-axis).

At the end of the LiDAR surveying flight, two data sets are available: a) six parameters of the direct georeferencing system (position and attitude) obtained from

three-dimensional coordinate transformation between the three reference frames, and b) the laser ranges with their respective scanning angles (Figure 1.4). These six parameters are used to georeference range measurements and the angular orientation of each laser pulse into a geodetic reference system (Lemmens, 2011). In other words, the 3D position of laser points (or backscattered pulses) is determined in WGS84 expressed by ellipsoidal geographic coordinates (ϕ, λ, h), where h is the elevation above reference ellipsoid. Subsequently, these laser points can be converted into a local coordinate system[23], which represents a map projection coordinates XY (easting, northing) and Z, which represents the elevation above the geoid (or orthometric height).

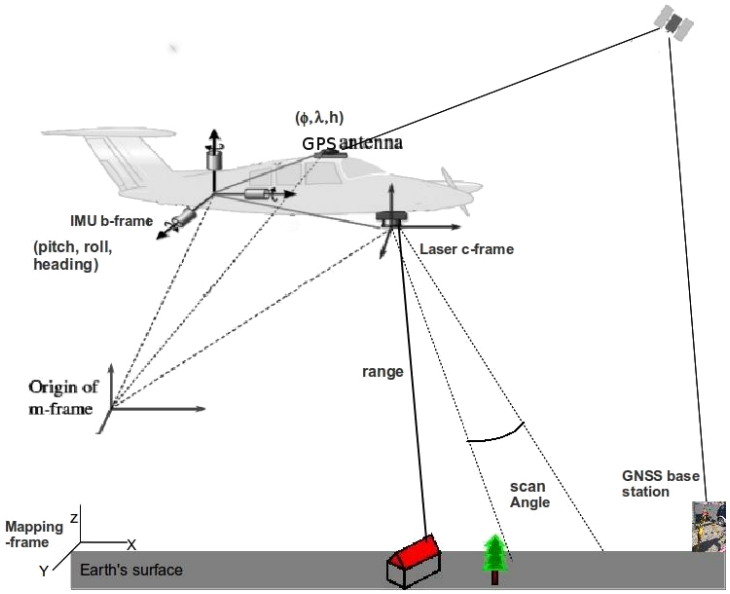

Figure 1.4: Schematic overview of the working of all components of an airborne LiDAR system.

According to Lindenberger (1993) in Wehr & Lohr (1999), the calibration data and mounting parameters should also be considered during this process. The calibration data is conducted by specific software developed by the same companies. According to Wehr & Lohr (1999), the calibration of 3D point clouds can be derived from: a) the relative orientation and position of the different flight-lines; and b) their absolute orientation and position with respect to an earth-fixed coordinate system.

The framework of direct georeferencing development shows various tests and reports that explain the operation of the system in image data of classical airborne systems (Bäumker & Heimes, 2001; Choi & Lee, 2013) and in laser scanning (Habib et al., 2006). Moreover, in the past few years some methodologies for direct ac-

[23]Generally, GCPs were used to calibrate the direct georeferencing system

quisition of 3D point cloud data in flight with a sub-decimetre accuracy have been developed (Skaloud et al., 2010).

1.2.2 Pulse laser characteristics

The knowledge of the basic characteristics and technical specifications of a LiDAR point cloud is essential for end users who intend to use this kind of data in specific applications. The point density per unit area of LiDAR point clouds is one of the most important parameters that end users should take into account in their studies, which depends on the specifications of the LiDAR system or on flight parameters. Yan et al. (2015) listed a set of representative case studies that used the ALS for urban land cover classification, providing laser scanning specifications used in each case study, such as system configuration and data resolution. The basic relations and formulas concerning ALS are detailed in Baltsavias (1999b).

An average point density value of a point cloud data is calculated by the number of points collected divided by their area (Sampath & Shan, 2007), which represents the number of 3D points per square metre. In Baltsavias (1999b), we can see an accurate expression to compute point density based on system specifications and LiDAR flight characteristics. These points are the returned laser pulses recorded by LiDAR during the flight (Figure 1.5).

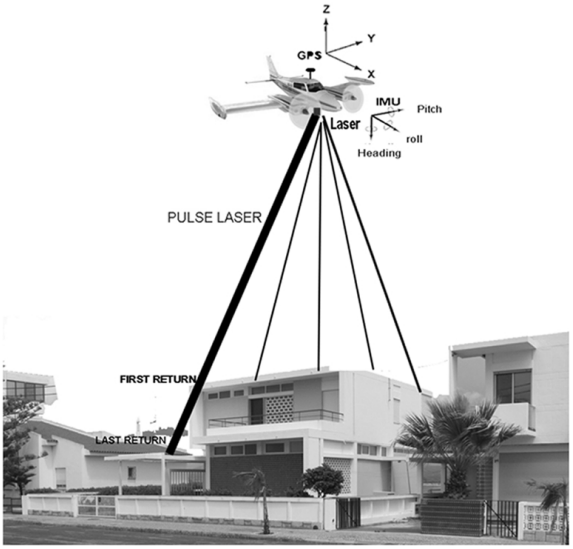

Figure 1.5: Data collection from ALS. Source: Tenedório et al. (2013).

Most LiDAR systems record discrete number of returns: they typically record first and last returns which correspond to the reception of the first echo return (first

object encountered) and the last echo of lower objects. For instance the laser beam hits a building edge where two echoes (or returns) can be generated (Figure 1.5).

Most recent systems are able to record multiple return (up to five) measurements for a single emitted pulse (Wehr & Lohr, 1999), where the signal is a fraction of the different objects reflected (Figure 1.6). This is a clear advantage of LiDAR when compared with image-based technologies (Forlani et al., 2006). Multiple pulses can occur on vegetated areas: a) in vegetation that is not very dense, the first echo belongs to the canopy top and the last pulse to the ground, and b) in forested areas, there are some gaps between branches and foliage where multiple echoes are recorded before the pulse hits the ground. In the last years of the last decade, LiDAR systems have significantly improved in terms of point density (number of points collected) and in terms of the widespread use of multiple returns (Toth, 2009).

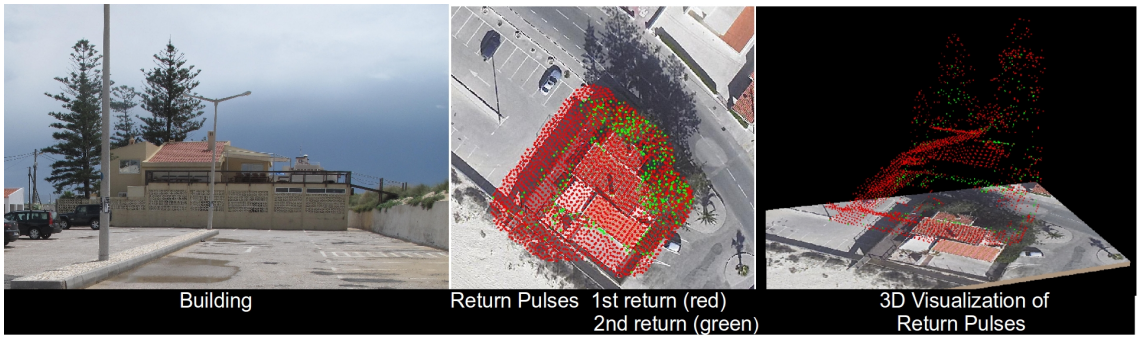

Figure 1.6: Return pulses recorded for a building surrounded by trees.

Zhang et al. (2006) have demonstrated that the last return measurements have a better overall performance in building identification methods for a study area that includes residential houses, complex buildings, individual trees, forest stands, parking lots, open ground, ponds, and roads. Zhang et al. (2006) also refer that multipath reflections (e.g. when a pulse hits glass walls or windows) in the first return result in incorrect low elevation measurements for the roof building, while the last return allows for an easier separation of ground and non-ground measurements and building measurements from trees due to its greater variability. Alexander et al. (2009) have shown that a high point density enables the highest overall accuracy of building type detection and it is useful for the identification of roofs. However, lower densities have proved to be more useful to identify roof morphology.

Point density (points/m^2) depends on LiDAR instantaneous field of view (IFOV) or footprint laser, pulse repetition rate (PRF), characteristics of the scan-

ner (scanning rate, scan configuration, and scanner calibration), and LiDAR flight parameters, such as height, speed, and number of flight lines (Carswell, 2011; Ackermann, 1999; and Baltsavias, 1999a). These parameters will be detailed later. For instance, a higher point density can be obtained from lower flight heights and a higher PRF value.

Topographic LiDAR systems usually use sensitive detectors in the laser scanning receiver unit, which operates in the near-infrared wavelengths at 1064 nm or 1550 nm to measure the properties of terrestrial targets. At these wavelengths, atmospheric conditions can slightly affect the pulse laser. The pulse energy is adapted for the wavelength value to ensure eye safety.

Since 2004, new ALS systems have appeared with the capacity to record additional and more detailed information about the physical properties of objects, digitizing the entire waveform of emitted pulse and the backscattered pulse (Figure 1.7), called full waveform (Mallet & Bretar, 2009). This means that in addition to X,Y,Z information on each point, it is now possible to record *intensity* and *pulse width* values (Mallet & Bretar, 2009). These two parameters provide information about the radiometry and geometry of the target, respectively.

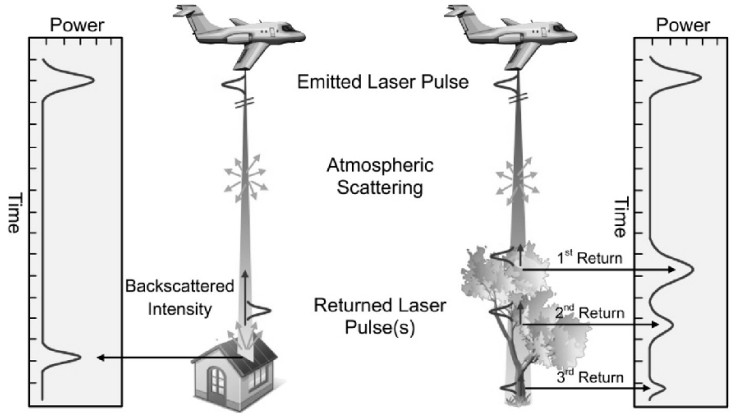

Figure 1.7: Laser pulses returned from building and trees and recorded signal strength. Source: Yan et al. (2015).

The peaks of backscattered laser energy that represents the intensity values of different targets allow us to identify different land cover types (Alexander et al., 2009). The intensity value in urban areas can help to filter out non-building urban objects, such as distinguishing roofs from trees (Lemmens, 2011 and Alexander et al., 2009). Additionally, it enables the determination of vertical surface structures such as roughness, height and shape of objects, canopy densities and height of trees, and

reflectivity (Lemmens, 2011).

Furthermore, the integration of multiple-pulses into air (MPiA) technology in 2007 allowed to fly at higher altitudes keeping the point density. The advantages of this technology were the reduction of acquisition time (and costs) and the reduction of the occlusion effect caused by relief variations. However, this technology can affect laser performance, since it is more difficult to preserve range measurement accuracy and adequate pulse energy at high pulse rates and at greater flying heights (Roth, 2011).

Relevant parameters for an end user

Footprint size

The footprint size parameter of LiDAR is a relevant parameter to record the details of the objects. It is the area illuminated by the laser on the ground (Wehr & Lohr, 1999), which is defined as a small footprint between 5-30 cm (Mather, 2004). The use of small footprints in topographic mapping for high resolution DSM is required for urban models (Mather, 2004), where the edge detection of buildings and other objects must be clearly identified with high sharpness (Lemmens, 2011) and for detailed local mapping of surface elevations (Mather, 2004). Lemmens (2011) also noted that the small footprint in tandem with high point density is essential for the 3D modelling of buildings.

Footprint size (Figure 1.8) depends on the IFOV of the laser, flight height, and scan angle from nadir (Mather, 2004).

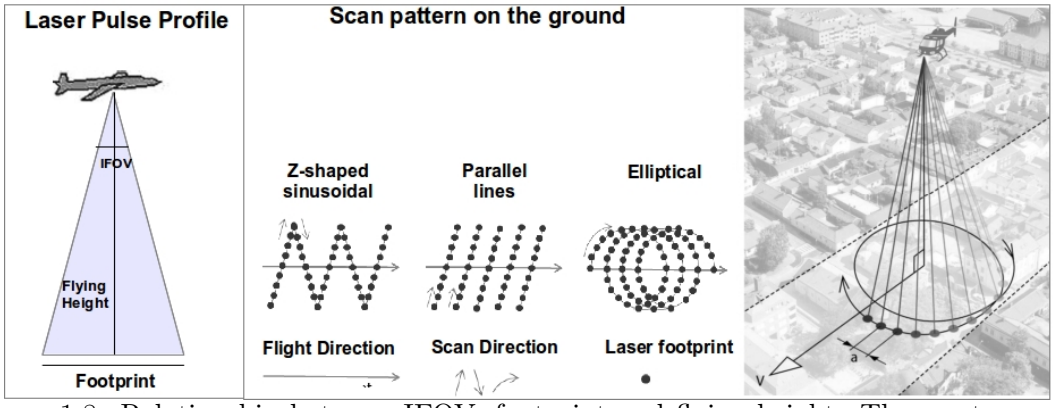

Figure 1.8: Relationship between IFOV, footprint and flying height. The most common scan patterns of ALS systems are represented in the centre, and on the right is the elliptical pattern.

For instance, if IFOV (also called beam divergence) is equal to 0.2 mrad, the footprint size is 0.2 m at a flying height of 1 km.

The footprint size varies linearly with the flying height, so if the flying height doubles, the footprint size will also double. More details about this relation can be seen in Baltsavias (1999b).

Pulse Repetition Frequency (PRF)

A large number of applications require a good number of points for the production of detailed 3D models. The number of pulses recorded (which represent points) by the LiDAR system is directly related to the pulse rate frequency (PRF). PRF is the number of pulses emitted per second. The evolution of PRF in the last 15 years in commercial LiDAR systems increased substantially from 50 kHz in 2001 up to 500 kHz (500,000 pulses per second) (Roth, 2011). The multiple laser systems have variable rates of up to 1000 kHz (Carswell, 2011). However, for most LiDAR systems (Leica, Riegl,Optech) the range varies between 100kHz and 200khz (Toth, 2009).

Laser scan pattern

LiDAR is recorded as an irregular point cloud, where the spatial distribution of 3D points depends on scan pattern, flight height, and flight speed (Lemmens, 2011 and Mather, 2004).

The scan pattern is the spatial arrangement of pulse returns that would be expected from a flat surface and depends on the mechanism used to direct pulses across the flight line. Advances in scan pattern control have increased point density and improved its distribution. The main ground scan patterns used (Figure 1.8) are Z-shaped sinusoidal, parallel lines, and elliptical. More recently multiple-output scanners have been used, as can be seen in Roth (2011), whose result is equivalent to having two fully synchronized LiDAR systems flying at the same time.

Most measurement points on the ground with a Palmer scanner (elliptical pattern) are scanned twice from different directions, where the ellipse of laser footprints translates with the movement of the airplane (Wehr & Lohr, 1999). The TopEye MKIIB is a system that integrates this type of scanner. These types of lasers have some advantages in urban areas, such as reducing the points occluded during the first pass, which acquires more details about the buildings. On the other hand, it provides a large number of wall hits when flying along the street in a city due to the conical scanning mechanism (Kaartinen et al., 2005). The use of these LiDAR point clouds with an elliptical pattern (Figure 1.8) was tested in the extraction of building parameters (see the case studies of Chapter 2).

1.2.3 Data handling and accuracy

The raw point cloud acquired from pre-processing after the flight is sorted and filtered. During this post-processing stage, the point cloud still needs manual editing with specific software to correct errors and fill in gaps between various flight lines. All these processes usually are not required for an end user, e.g. an urban planner, who only intends to obtain specific information.

However, filtering LiDAR point clouds is one of the most important steps that have to be applied by any end user by using proprietary software or implemented advanced tools for the extraction of specific information. A review of filtering algorithms and its applications to guide users to select the optimal method for a point cloud can be found in Meng et al. (2010) and Sithole & Vosselman (2004).

Filtering consists in removing the unnecessary points from a 3D point cloud. For instance the creation of a 3D building model requires the removal of points reflected from vegetation and bare ground.

Generally, LiDAR point cloud data is delivered in LASer file format (LAS)[24] following the American Society for Photogrammetry and Remote Sensing format standards. For instance, the LAS files used for the case study of Praia de Faro presented in Chapter 2 correspond approximately to 48 MB for a point density of about 6 pts/m^2. A LAS file includes at least the following information for each return: X-coordinate, Y-coordinate, elevation, return number, intensity, and scan angle.

The main factors that can affect the accuracy of 3D positioning in LiDAR point clouds are the accuracy of range (Baltsavias, 1999a) and the accuracy of parameters of GPS/IMU (position and orientation) of the laser beam (Baltsavias, 1999b and Leberl et al., 2010). Moreover, the accuracy of the point clouds depends on the accurate transformation of their coordinates from WGS84 to the local coordinate system (Baltsavias, 1999b).

Regarding the accuracy of this technology, Baltsavias (1999a) wrote that planimetric accuracy from ALS is 2-6 times less accurate than its vertical accuracy, while in traditional photogrammetry it is typically 1/3 more accurate. The altimetric accuracy is overcame below 10 cm (Mallet & Bretar, 2009; Hyyppä, 2011). The planimetric accuracy depends on flight height and LiDAR system characteristics,

[24] More information about LAS can be found in *http://www.asprs.org/Committee-General/LASer-LAS-File-Format-Exchange-Activities.html.*

which can vary between 20-80 cm (Hyyppä, 2011). However, Ahokas et al. (2003) say that planimetric accuracy can be below 40 cm even in forested areas.

1.2.4 Strengths and weaknesses of LiDAR point clouds for 3D modelling of buildings

One of the most usual applications of LiDAR point clouds in these past 10 years has been in 3D modelling of buildings. The potential of this data for 3D modelling of buildings has been demonstrated by various authors and projects, where its weaknesses are also shown. A good example of the evaluation of quality, accuracy, feasibility, and economic aspects of automatic building extraction based on LiDAR was performed by EuroSDR (European Spatial Data Research), whose report can be seen in Kaartinen & Hyyppä (2006). Additionally, the quality of 3D building models extracted from point clouds is detailed in Elberink & Vosselman (2011).

The 3D modelling of buildings that implies the extraction of building outlines[25], roof types, and building metric parameters (volume, height) has been tested by various authors. Some relevant considerations cited by them are summarized below to guide the users regarding the requirements and expectations for the usage of LiDAR point clouds in the reconstruction of 3D building models:

Building Outlines: *a)* Kaartinen et al. (2005) note we can expect much better accuracy concerning building outlines with the combination of TopEye laser data and digital aerial images acquired at the same time; *b)* the determination of building outline is affected by point density, the shadowing of trees and the complexity of the structure (Kaartinen et al., 2005); *c)* high point densities are suggested for the detection and outlining of buildings (Vosselman, 1999 and Hyyppä et al., 2015); *d)* the reconstruction and 3D modelling of buildings with sharp discontinuities can easily be obtained from a LiDAR DSM; *e)* the difficulties in extracting accurate building outlines for the generation of 3D building models were shown in Chen et al. (2011), Alexander et al. (2009) and Zeng et al. (2008); and *f)* the extraction of building edges with height discontinuity from LiDAR is difficult due to small footprint size compared with the average point spacing and unfavourable backscattering from illuminated targets (Sohn & Dowman, 2007).

[25]In this thesis, it is also called building roofs.

Roof types: *a)* Kaartinen et al. (2005) have demonstrated that the LiDAR point clouds are more suitable than photogrammetric techniques to derive building heights, and extract planar roof faces and roof ridges; *b)* Alexander et al. (2009) noted that the overall accuracy to detect roof types (flat and pitched) increases with increasing point densities; *c)* Zeng et al. (2008) extracted simple and regular roofs defined by two plans; *d)* lower point densities are better for the detection of roof morphology (Alexander et al., 2009); *e)* high point density allows us to detect correctly most of the planar faces of a roof, but small structures with different heights (such as dormers) near the edges of a roof are not easy to extract (Vosselman, 1999). Hyyppä et al. (2015) say that a rough extraction of building roof structures can be achieved with a point density between 1 and 40 pts/m^2; *f)* the level of difficulty in 3D reconstruction of roof face edges is strongly dependent on the type of edge (Vosselman, 1999); *g)* the gaps that appear in the point clouds are related with the poor reflectance properties of the roof surfaces due to water on flat roofs and dark slate roofs (Vosselman et al., 2005); and *i)* hip roof ridge lines and flat roof edges can be extracted with higher precision from LiDAR point clouds (Elberink & Vosselman, 2011).

Building height and volume: *a)* if the building models are used to compute volumes, Vosselman (1999) recommends the use of building outlines in the ground planes instead of roof edges extracted from point clouds; *b)* very high point densities are required to accurately obtain the height of jump edges (Vosselman et al., 2005).

Vosselman (1999) recommended the direct usage of LiDAR point clouds without the interpolation of this data in a regular grid, because it can avoid the usage of incorrect interpolated height values in the 3D modelling of buildings. Furthermore, the capacity and accuracy of the LiDAR system in the detection of trees and vegetation could be a disadvantage for the extraction of buildings, where the level of filtering of these points increases and is more complicated (Baltsavias, 1999b). Consequently, the building shapes are not regular because adjacent trees are difficult to remove. Meng et al. (2008) have developed a method based on building element structures using DSM LiDAR to detach the trees from the buildings.

LiDAR presents potential for the detection of buildings and modelling different roof types. However, the major difficulty is the extraction of accurate building outlines and length determination, whereas photogrammetric techniques are more suitable (Kaartinen et al., 2005). Most problems encountered in automatic reconstruction of building models '(...) often relate to either the characteristics of laser

scanners or the lack of (used) knowledge about the possible shapes of buildings' (Vosselman et al., 2005, p.182). Most problems mentioned above about 3D modelling can be solved with the combination of aerial images or ground plans with LiDAR data. Additionally, the development of interactive modelling environments to correct small errors and allow manual modelling using point clouds (Vosselman et al., 2005) can also improve the results.

1.3 *Very high resolution aerial imagery from UAV technology*

UAV technology is an alternative for low-cost aerial photogrammetric surveys over small areas, and consequently for the acquisition of low-cost 3D point clouds. In a broad sense, this technology is also known as Unmanned Aerial Systems (UAS), which identifies its major system components. Also, the term *drone* is generally applied to unmanned, powered, free-flying platforms (Aber et al., 2010), but usually it is not used in the context of mapping applications.

A UAV uses a passive sensing technology that provides the acquisition of very high resolution aerial images based on conventional photogrammetry principles, such as stereo aerial images coverage and the use of direct georeferencing systems. The main characteristics of this technology are its small size, its ligth weigth (usually < 4 kg), the fact that is remotely controlled on the ground (where the flight is programmed and supervised by a user or the user manually controls the flight) and it allows a faster acquisition of low-cost images. Besides, the flexibility of this technology is higher in terms of transport, since an autopilot airplane kit is quite mobile and can be taken to the survey area easily by car (Aber et al., 2010).

According to Everaerts (2008, p.120), 'A major obstacle so far to the introduction of UAVs for any purpose today is that they have not been integrated into the civil aviation authorities regulations.' This statement is still true, the carry systems for air traffic communication and air security regulations do not cover UAVs. For instance, in Portugal most UAV flights made for technology testing purposes were carried out without warrants. These flights have been made by classifying low altitude UAV systems as model aircrafts, which has caused some controversy in the country.

To try to solve this issue that has generated controversy in many European countries, the European Commission requested the European Aviation Safety Agency (EASA) to propose the creation of common rules for operating drones in Europe. The initial proposal was presented in September 2015 by the EASA and marked the beginning of a regulatory framework for UAVs. This document contained a set of safety rules (included in 33 proposals) for operating drones regardless of their weight. Some of the main proposals included in this document are (EASA, 2015): a) regulating commercial and non-commercial operations where the same drone might be used for both commercial and non-commercial activities; b) creating three subcategories (CAT) in the 'open category' [26] (low risk): CATA0 ***Toys*** and ***mini drones*** < 1 kg; CATA1 ***Very small drones*** < 4 kg; and CATA2 ***small drones*** < 25 kg; c) preventing unauthorized flights outside safe areas, where the drones can be pre-programmed not to fly out of specific areas (called *geo-fencing*).

These platforms can operate in conditions where traditional manned platforms cannot, due to cost, lack of flexibility or operational difficulties (Everaerts, 2008). The major differences between conventional airborne systems that use a large format camera and a UAV are summarized in Table 1.1.

The costs of aerial photogrammetric surveys in small areas with classical airborne systems are very high and the planning of flights is time-consuming, unlike UAVs. A UAV is more suitable in dangerous mission flights or inaccessible areas at low altitude, such as mountains, and earthquake and flood areas (Eisenbeiss, 2009). For instance it allows a faster evaluation and monitoring of the flooding or firing areas. In general, and compared with conventional airborne systems, UAVs have shorter flying times, but need more flight missions to cover a large area.

The most important aspect of this technology is also the high flexibility with which it allows to obtain very high resolution imagery for the acquisition of 3D data. The higher degree of automation in the acquisition of 3D data through advanced imagery processing, in contrast with the classical methods of digital photogrammetry (stereo restitution), enables the acquisition of 3D data even on site after the flight. Then, it becomes possible to check if there are any problems in the 3D data collected and prevent further trips to the site.

[26] 'Open' category means to ensure the safety through a minimum set of rules, operational limitations, industry standards, and the requirement to have certain functionalities (EASA, 2015).

Table 1.1: Characteristics of traditional aerial airborne and UAV plataforms (Source: Adapted from Everaerts, 2008).

Characteristics	**Conventional Airborne Systems**	**UAV (low-altitude)**
Coverage	local to regional (10-10000 km^2)	local up to 1 km^2 (approx. 5 cm pixel on ground)
Frequency Update Mapping	low or non-existing update programmes	Ad-hoc without programs in place
Flexibility	Integration of flight plans in air traffic; dependent on weather	Total, is dependent on weather, particulary wind conditions
Spatial Resolution	High to very-high (cm-dm)	Very high (mm-cm)
Positional Accuracy	High (methods for sub-pixel accuracy)	High (methods for sub-pixel accuracy)
Target Applications	Mapping, 3D city modelling, image acquisition	Crisis Management, Monitoring hazards, 3D modelling of buildings and objects
System Costs (approx.)	1 MEuros	15000-50000 Euros

The recent developments in computer vision for the purpose of image matching techniques have contributed to the high flexibility of photogrammetric workflow for the production of mapping products (such as orthophotos, DSMs and DTMs) and for the generation of high quality 3D point clouds very similar to a LiDAR 3D point cloud. This innovation in image matching allows us to deal with oblique aerial images usually acquired by UAV, which would be unacceptable in conventional photogrammetry procedures[27]. These issues have made this technology very attractive for urban applications. Various authors have demonstrated that image matching method using any airborne system can be an alternative to LiDAR such as Haala et al. (2010), Haala & Kada (2010), Leberl et al. (2010) and (Madden et al., 2015).

Unlike a LiDAR point cloud, the derivation of a UAV point cloud is not acquired directly, since it is strongly dependent on UAV imagery quality and stereo image matching processing. Therefore, the accuracy of a point cloud is highly dependent on these issues, particulary on Ground Sample Distance (GSD) or ground resolution of the input imagery (Küng et al., 2011; Strecha, 2011) and on a robust and automatic workflow that includes dense image matching (Küng et al., 2011).

The accuracy of elevation data included in a point cloud depends on image data quality, the complexity of object surfaces and of image matching techniques. Many authors have demonstrated the potential of this technology based on UAV/-Dense image matching through positional accuracy. The generation of an accurate

[27] The acquisition of 3D data in conventional photogrammetry requires nearly vertical aerial images - tilt $< 3°$.

3D point cloud at centimetre level has been easily demonstrated, such as the mapping products obtained from it (orthophotos and DSM). Haarbrink & Eisenbeiss (2008) and Manyoky et al. (2011) have demonstrated the generation of a 3D point cloud with horizontal and vertical accuracy of 2 cm and 4 cm, respectively. Similary, Madden et al. (2015) have demonstrated that UAV point clouds have a good accuracy to monitor natural and cultural resources, about 0.34 m horizontal and 0.30 m vertical. Leberl et al. (2010) have proved that it allows us to generate DSMs with an accuracy comparable to LiDAR and Küng et al. (2011) have shown that the accuracy of orthophotos obtained from this technology can range between 2 and 20 cm.

1.3.1 Components of UAVs and operating principles

UAV systems can be classified as 'low altitude UAV' or 'high altitude' (lower stratosphere, above 15 km) (Everaerts, 2008). However, here we shall only address low altitude UAVs as these are suited to small scale survey projects or mapping areas and whose characteristics have already been mentioned above.

A UAV system integrates a miniaturized direct georeferencing system and a small format digital camera, and both together allow for the acquisition of georeferenced aerial imagery. However, the direct georeferencing system (see Subsection 2.1.1) implemented in UAVs has some accuracy limitations, since the position and attitude parameters are less accurate. The framework for direct georeferencing on 'Ultra-Light UAV systems' can be seen in Chiang et al. (2012).

The digital camera has a 'typical camera size' (small). It also has a smaller IFOV when compared with digital photogrammetric cameras, which means more images to cover an area. On the other hand, the lower platform stability due to vibration could affect image quality with blurring (Lemmens, 2011). Additionally, various types of digital cameras can be used, such as RGB or CIR (false colour).

Generally, all the components of a UAV system are based on a modular assembly (Aber et al., 2010), and thus in case it is broken on the ground, it is easier and quicker to replace a damaged component or device. Usually, they do not carry systems for air traffic communication, but have communication links (wireless) between the receiver at the ground station software and the transmitter to command and control the mission flight.

Regarding the types of UAV platforms, they have different sizes and shapes and are similar to a model airplane that was modified to carry a camera and a GPS/IMU. The two major types of UAV aircrafts are fixed-wing and multi-rotors (Figure 1.9), whose shapes are similar to 'mini-aeroplanes' or 'mini-helicopter', respectively. Fixed-wing UAVs are more stable than multi-rotors and can carry a payload of up to a few kilograms depending on its wingspan (Lemmens, 2011). The multi-rotor systems include the quadcopter with 4 rotors or multicopters ($>$ 4 rotors). More details about these systems can be found in Welzheim (2015).

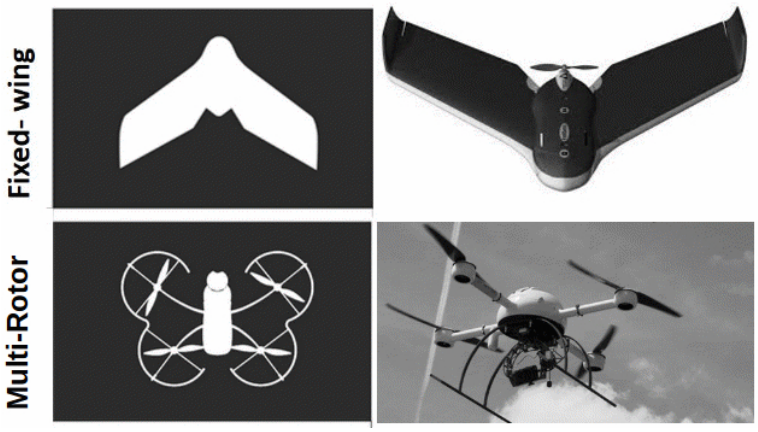

Figure 1.9: Low altitude UAV systems. Fixed-wing: eBee, SenseFly; Multi-rotors: an MD4-1000 quadcopter.

Operationally, the choice of the type of UAV essentially depends on the kind of intended applications, so we have to ask what the purpose of their usage is. Some of the operational characteristics of these systems are summarized in Table 1.2 which should be taken into account in the decision-making process.

Table 1.2: Characteristics of UAV system (Source: Sensefly, 2015)

Characteristics	**Fixed-wing**	**Multi-rotors**
Speed	High	Low
Max flying height (Welch et al., 1999)	300 m	150 m
Coverage	Large	Small
Take-off/Landing area	Large	Very small
Flight times and wind resistance	High	Low
Target Applications	Land surveying (rural), agriculture, GIS	reconnaissance of natural disasters, follow dynamic processes, surveying (urban)

For instance, in urban environments, a multi-rotor UAV can be better than a fixed-wing one, when the purpose is to fly along narrow streets and between higher

buildings. A fixed-wing system cannot hover or make tight turns, and requires a large take-off and landing area. However, if the objective is not to enter any urban environment but simply to acquire urban objects for modelling, a fixed-wing system can be appropriate. On the other hand, take-off and landing a mini-helicopter (few metres, about 20 m) could be the best solution in case there are no open spaces in the urban areas.

According to Lemmens (2011), there are other minimal criteria that the user should take into account, such as the cost; size and weight of payload; stability and vibration; human resources to launch and control the UAV; level of piloting skills; range; and safety. A fixed-wing UAV SenseFly system, such as a swinglet CAM, is one of the most lightweight systems (weighing around 500 grams), which enables the performance of a fast survey at low altitude over small urban areas without human intervention during the flight.

Operationality

In these systems, the range and altitude are reduced in comparison with classical airborne systems. These issues are important to enable the line-of-sight from pilot to the UAV and consequently a greater control of the equipment (Lemmens, 2011).

Unmanned platforms may operate in a fully autonomous flight or they can be controlled remotely by a user on the ground, therefore UAVs are also called 'Remotely Piloted Aircraft System' - RPAS (Mayr, 2013). In the first case, the visual contact with the UAV is made by a 'ground station software' where it is possible to monitor and control the flight planning programmed in real time, via continuous two-way wireless communication (Aber et al., 2010). Subsequently, during the flight, the user can see the trajectory and the location of the UAV and the image exposure stations are taken automatically along the predetermined flight lines into the into NASA WorldWind or Google Earth viewers. Moreover, it is possible to control the flight, namely correcting deviations from the flight lines or aborting the mission flight in safety. Most UAV systems have a security system: if the power battery is low or if it exceeds the threshold values for wind, the system itself aborts the mission.

Lemmens (2011) stated that UAV users should be experts in handling the remote control to avoid crashes, and that good flight preparations are also vital. For a successful mission flight, the user should take into account at least the wind,

overlapping of imagery, and altitude.

1.3.2 UAV point clouds: acquisition and processing

The acquisition of a 3D point cloud from UAV imagery has a sequential subset of steps based on an 'automatic photogrammetry workflow' (Figure 1.10) combining photogrammetry and computer vision. The acquisition of UAV imagery is the first step, which includes the flight planning and the UAV flight.

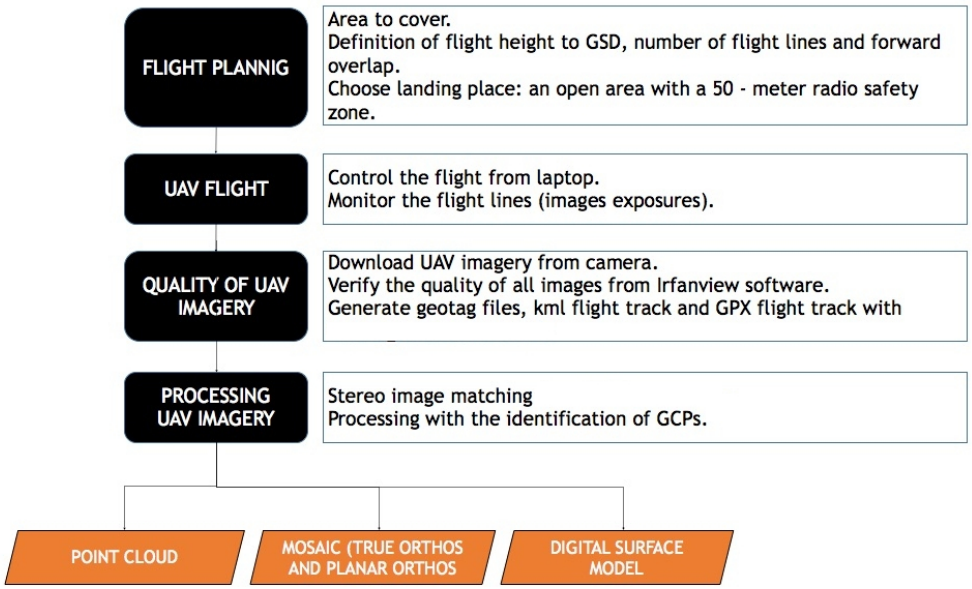

Figure 1.10: The workflow of UAV point cloud processing.

The UAV flight should be made in accordance with the project objectives of taking into account the 3D point density required for 3D modelling. The point cloud density is directly proportional to the GSD of the imagery. Therefore, this is one of the most relevant parameters in a flight mission. If the objective is to enable 3D modelling of buildings, then the GSD should be at least 5 cm for an average density at the order of 40-50 points/m^2.

The GSD is related with the size of each pixel element in ground units of imagery. The GSD for digital cameras is calculated as follows (Neumann, 2008):

$$GSD = \quad CCD \quad pixel \quad size \times (H/f) \tag{1.1}$$

where f is focal length of camera, H is flight height above ground, and *CCD (Charge Coupled Device) pixel size* depends on the CCD manufacturer, for instance, it can

vary approximately between 2 and 12 micron.

Generally, the GSD is defined during the flight planning and the flying height is a result of the GSD proposed. Additionally, the number of flight lines (direction and parallel distance of the flightlines) according to the area size and overlap parameters should be defined. For this task, the operator should take into account that a higher overlap of 80% to 90% along track and 60% across track is necessary to obtain higher density point cloud data. A higher overlapping in urban areas should be guaranteed in order to reduce the occlusion effect on stereo images.

The flight planning should be done by the user or automatically with software for an optimal plan. This flight plan is transferred to the on-board computer in the UAV via radio communication.

After the flight, a brief analysis of the quality of each image can be performed on site. Thus, this checking consists in the verification of shadows, clouds, image sharpness and other problems when registering pixel information. Sometimes it might be necessary to repeat the flight mission if the stereo image matching is not possible because of the bad quality of some stereo pairs of images.

According to the workflow (Figure 1.10), the next step is the automatic multi-stereo image matching processing to acquire a 3D point cloud. This processing is usually performed by an automatic workflow implemented in the software package that includes the computation of matching points from the oriented images and the 3D geometry reconstruction by aerial triangulation, through the use of six exterior orientation parameters, ω, φ and κ photogrammetric angles and object space coordinates of the exposure station of the camera (X_0, Y_0, Z_0) for each exposed image.

UAV georeferenced imagery can be fully automatically obtained without GCPs in a few minutes to check the quality of data. Approximate georeferencing is provided by the camera projection centres obtained by the navigation GPS receiver of the UAV. However, before the dense matching processing, it is convenient to identify GCPs within the stereo pairs, with a regular distribution along the imagery block, for increased geolocation accuracy of the 3D point cloud. Strecha (2011) showed that the horizontal accuracy of 2D mapping products obtained from UAV imagery varies between 0.05-0.2 m using GCPs and 2-8 m without GCPs.

The UAV technology and the dense matching processing of UAV imagery can obtain 2D/3D mapping products in a short time, such as a 3D point cloud,

orthomosaic and DSM. Usually, the UAV point cloud is delivered in a vector format which includes the X,Y,Z coordinates and RGB values. This type of data can easily contain 1 million points[28] (see case study of Chapter 2). It is important to stress that the manipulation and analysis of such large data sets is not possible in conventional GIS desktop software.

Dense stereo image matching

The basis of stereo image matching is to identify corresponding pixels (or tie points) on the left and right image of a stereo pair (or within the area of the stereo model) with a minimum forward overlap of at least 60% (prerequisite). In other words, it establishes the correlation between most pixels of stereo pairs. More recently, dense stereo image matching has allowed us to achieve a *dense 3D point cloud* with a density that is equivalent to the resolution of stereo models, i.e., there is an estimated 3D point for each corresponding pixel in the stereo model.

The emergence of digital imagery as the standard source has contributed to the development of stereo-matching algorithms. Furthermore, digital airborne camera systems have also contributed in these past 10 years to the improvement of stereo image matching towards dense stereo image matching. Two factors were essential to this development: a) better radiometric quality of images with the improvement of the signal-to-noise-ratio[29] (SNR) of the sensor; and b) cameras can now acquire stereo aerial imagery with high overlapping effortlessly, thus also enabling multiple overlapping stereo images.

The generation of 3D point clouds by image matching is dependent on radiometric image quality, which is influenced by many factors (season, solar elevation, weather conditions and sensor) (Rosnell et al., 2011). Among these factors, a sunny weather is the one that most affects the quality of the point cloud (Rosnell et al., 2011).

Multiple overlapping images (or multiple stereo pairs) increase the number of images per object point by changing the typical overlapping used in traditional photogrammetry. Haala & Rothermel (2012) refer that 'Overlaps of 80% along track and 60% cross track will result in at least 10 images per object point.' These multi-

[28]In practice, it represents about 400 MB size in a text file and approximately 200 MB size in the PLY format. PLY is also known as the Stanford Triangle format and allows the storage of 3D data, where the ascii header specifies the data by defining the elements, properties, data type, and description.

[29]SNR is the precision of the measured irradiance and it depends on the ratio of the received signal and its standard deviation (Jahne, 2004).

measurements for the same point in the aerial triangulation process increase the accuracy of a 3D point cloud.

According to Haala (2011), in dense urban areas multiple overlapping should be applied, especially to reduce occlusions in stereo aerial images due to relief displacement[30].

Nowadays, it is possible to obtain an accurate dense 3D point cloud from a *dense matching of multiple stereo aerial images* method. Haala (2011) shows the great potential of matching multiple overlapping images by using the Semi-Global Matching (SGM) algorithm developed by Hirschmüller (2008). This algorithm allows us to obtain one 3D point per each pixel in a stereo model through high computational performance. According to Hirschmüller (2011), it allows for robustness in radiometric differences and it offers a good compromise between accuracy and execution time. This algorithm was implemented by many researchers and companies, such as the solutions PIX4D, Leica Xpro SGM and StereoSGBM from the open source library OpenCV (Deuber et al., 2014). In lower textured areas of the images (roofs, walls or roads) the SGM offers better results for point cloud generation (PIX4D, 2013).

Various authors have demonstrated the potential of dense stereo image matching for the generation of 3D point clouds. Hirschmüller & Bucher (2010) have shown that DSMs of urban areas produced by SGM are more accurate and detailed than LiDAR DSM. Moreover, the dense matching of multiple stereo aerial images with SGM using UAV imagery was tested by Haala & Rothermel (2012) for the generation of DSMs. These authors have shown that a high point density can be achieved in low-textured areas.

3D point cloud from UAV

UAV point clouds are textured using RGB (Figure 3.4 in Chapter 3) or Color Infrared (Figure 2.8 in Chapter 2) spectral attributes from images, unlike LiDAR point clouds. Usually, UAV point clouds have an irregular and sparse distribution, which is very dependent on dense matching processing and also on imagery that reflects the characteristics of an overflown area.

The point density of a point cloud obtained from UAV imagery is strongly dependent on GSD, where the theoretical concept is *'one 3D point for each pixel that has been matched in a stereo model'*. However, this is not completely true

[30]Relief displacement corresponds to image displacements caused by topographic relief.

because dense image matching fails in some circumstances. It depends on characteristics related to area (urban, mountains, dense vegetation, etc..), the geometric complexity of the respective object surfaces and the capacity and performance of dense matching (or processing imagery algorithms), particulary in complex areas. The density of points can be reduced under dense vegetation, homogeneous or untextured surfaces (lower correlation), occlusions and shadow effects from man-made or natural objects[31] (a strong presence in urban areas) and radiometric changes due to changes in illumination. Generally, this results in gaps or sparse points in a point cloud (Figure 1.11). Furthermore, acquisition geometry can affect point density, i.e., highly tilted images can affect the overlapping between stereo pairs and consequently reduce point density.

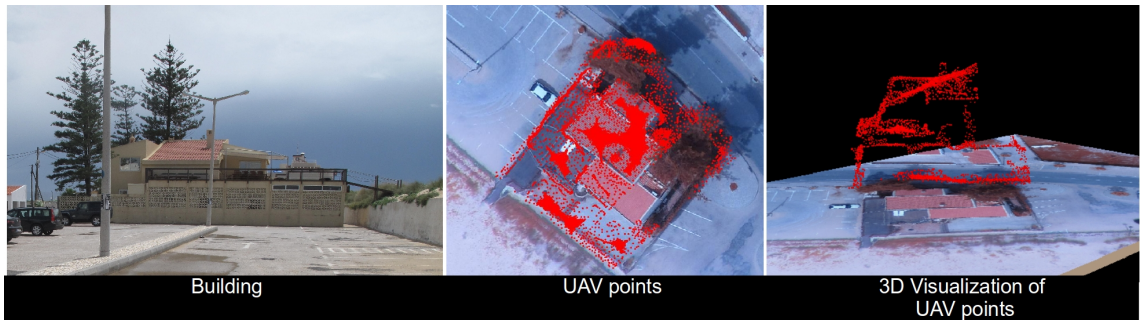

Figure 1.11: UAV points recorded for a building.

The accuracy, reliability, and density of elevation data as generated from automatic image matching is influenced by a number of factors. Important factors are the quality of the available image data and the sophistication of the used matching algorithms, but also the geometric complexity of the respective object surfaces. Furthermore, the point density is proportional to the number of pixels matched, which also depends on overlapping imagery and GSD. For instance (Figure 1.11), in vegetation areas (untextured areas) the number of matched features is lower.

Comparing LiDAR point clouds (Figure 1.6) with UAV point clouds (Figure 1.11), the latter have uneven density in this area, with very high point density clusters in the highest and steepest part of the roof and lower density in the areas occupied by trees. This image matching technique cannot obtain ground points on dense vegetation unlike LiDAR, which can do that successfully.

The development of UAV technology and SGM have allowed us to produce high-density 3D point clouds from multiple stereo images, where dozens of points per

[31] These effects are caused by variations in surface elevation.

square metre can be obtained (about 90 pts/m^2) with a vertical accuracy between 2 cm and 4 cm (Haala & Rothermel, 2012).

1.3.3 Strengths and weaknesses of UAV point clouds for the 3D modelling of buildings

The majority of the strengths and weaknesses of UAV and dense stereo image matching techniques were presented above. However, we should ask: *What are the strengths and weaknesses of this technique using directly a 3D point cloud for the extraction of buildings?* The generation of 3D building models and 3D city models at low cost is certainly a strength of this technology.

The generation of 3D building models (LoD1) for the extraction of building heights from this 3D data could be an advantage when compared with LiDAR, because the filtering process is easier, since less points need to be removed from the point clouds. In other words, stereo image matching is not successful in poorly textured surfaces which result in a lower point density, such as in vegetation areas (usually near buildings) or untextured surfaces (homogeneous surfaces, such as water and asphalt). Wefelscheid & Ronny (2011) have demonstrated the usage of this data in LoD1 building models.

However, the quality of stereo image matching on roof surfaces should be enabled for a higher and uniform point density. This is important for the extraction of accurate building roofs and building heights. In the extraction of building roofs from UAV point clouds there are some issues to take into account:

1. The detailed texture of the roof covering material can affect the quality of the 3D point cloud with gaps or lower point densities. The gaps can appear in tin roofs (Harwin & Lucieer, 2012) and flat black roofs (Rosnell et al., 2011). Therefore, lower point densities in flat roof cover has been shown in Rosnell et al. (2011).
2. Some untextured building surfaces could be an advantage, such as the image matching of 'white walls' (Küng et al., 2011).
3. The quality of stereo images can be influenced by weather conditions and consequently the quality of 3D point clouds obtained from them is influenced as well. According to Rosnell et al. (2011), the best point densities over homogeneous roof surfaces can be obtained from images collected under sunny

weather, except regarding the shadows of the buildings. However, if the images are collected under a cloudy sky, matching can fail to a large extent in these areas.

4. Küng et al. (2011) have shown the difficulties of stereo image matching process using PIX4D in two different buildings types for the generation of 3D models LoD1. These authors have demonstrated that: a) building roofs with a homogeneous texture can have 'floating points' (elevation errors); b) homogeneous texture in a cross gable roof (with various pitched plans) can have less floating points and a higher point density than a flat untextured roof; c) the roof edges of the buildings are well reconstructed; and d) 3D points on trees were often not computed.

In addition, there are some issues regarding the acquisition of UAV imagery:

1. A multi-rotor UAV carrying four combined cameras enables the acquisition of a large quantity of vertical images, which can ensure a better extraction of building roofs (Feifei et al., 2012).

2. The implementation of a UAV flight over urban areas with tall buildings is difficult, but beyond that, the effects of relief displacement are increased on images. This effect can affect the matching of 3D points that result in gaps. Qin (2014) recommends the usage of SGM in dense urban areas with tall buildings to generate a dense point cloud.

3. Manyoky et al. (2011) show that the acquisition of accurate UAV imagery position is limited by camera calibration, image quality, and the definition of the ground control points. Then, the estimation of building outlines should be enabled by these issues. Also, the high radiometric quality and multiple overlapping image matching is essential to city modelling (Toth, 2009).

4. GSD imagery between 8 and 15 cm is required for the interpretation of urban objects (Leberl et al., 2010). Such GSD imagery values or even lower are easy to obtain at a low cost from UAV.

5. Vallet et al. (2011) show a vertical accuracy in roofs within 10 cm under the smoothing effect near buildings. This smoothing effect results from image matching using PIX4D, which tends to smooth obstacles such as buildings, walls, and cars (Vallet et al., 2011).

It is important to note that the demonstration of this technology for 3D building models is recent and most studies are based on the extraction of buildings from DSM and not directly from point clouds.

1.4 *Free and Open Source Software (FOSS) to explore 3D point clouds*

A 3D point cloud requires tools for editing, exploring, analysing, and visualizing. In the case of a UAV point cloud, image matching photogrammetric tools are also needed for the generation of the point clouds. There are several commercial solutions to make all these operations, but most of these GIS or photogrammetric solutions are very expensive. On the other hand, they are 'black-box solutions', which limit the development and implementation of specific tools for the extraction of 3D information. The use of FOSS could be a potential solution for the usage of '3D data' in urban planning by local, regional and central government bodies in Portugal with the development and implementation of specific urban planning tools.

Espada (2010, p.1) has stated that 'After years of scepticism towards open source software, many of today's open source solutions are as good, if not better than proprietary software solutions.'

FOSS stands for 'Free' software and 'Open Source' (OS) software. Free software does not mean that it is free of cost, but it refers to the usage of software freedoms (Steiniger & Hay, 2009). These freedoms were established by the Free Software Foundation (FSF) (FSF, 2004 and GNU, 2013) from 0 to 3 and refer to:

(0) The freedom to run the program, for any purpose;
(1) The freedom to study the program and change it through the source code access, according to our needs;
(2) The freedom to redistribute copies of the program if you wish;
(3) The freedom to distribute copies of your modified versions to the public.

Additionally, there are software licenses that conform to these freedoms. This means that the code produced is open-source under the GNU General Public License (GNU GPL) and the GNU Lesser/Library General Public License (GNU LGPL). The GNU enables the modification and redistribution of software under the same license conditions (Steiniger & Hay, 2009).

One of the major benefits of FOSS tools is the dynamism of the development for teams and users within the applications, where there is a regular contribution and publication of source packages and tools to solve specific problems (Bivand et al., 2008).

How should we explore and visualize millions of 3D points using FOSS tools? How can development tools using open source for the extraction of 3D urban features from a point cloud fit within the monitoring and evaluation process?

These questions establish new challenges and a new vision in urban planning. A solid knowledge of the usage of FOSS tools is needed for the growth and improvement of urban planning processes, where the usage of 3D geographical data technologies can offer an added value. This means modelling large volumes of 3D data for the (semi)-automatic extraction of 3D geographical data or urban parameters under the development of robust methodologies and in optimized environments, that are user friendly and effective. Furthermore, the usage of 3D data through FOSS tools must be supported by full interoperability.

1.4.1 OS software within 3D point clouds

Today it seems very easy to produce 3D models with few technical and scientific skills regarding the issues that supported the technology. According to the specific functionalities of OS software, they can be classified into six categories (Table 1.3) within the usage for 3D point clouds.

Table 1.3: Categories of OS software useful to produce and explore 3D point clouds

Categories	**Description**	**OS Software**
UAV Imagery Tools	Computation of orientation parameters; Image matching process	Bundler, VisualSfM, Micmac, PMVS, CMPMVS
LiDAR tools	Specific tools to explore LiDAR information	BCAL, PCL
Desktop GIS	Editing, spatial analysis and visualization	GRASS, GvSIG,QGIS
Spatial database management system	Management and structured data; Data manipulation	PostgreSQL/PostGIS, SQlite/SpatiaLite
Geostatistical computing	Manipulation of statistical data, calculation and graphical display	R, GeoDa
Modelling and 3D Visualization	Creation of 3D models, modelling tools for 3D visualization and creation of textures	Meshlab, CloudCompare

The 'democratization' of technology and OS tools has advantages, but it is important to be careful in their usage, since it is important to ensure the quality of

mapping products.

OS Photogrammetric Solutions

The computer vision approach implemented in certain solutions has made it possible to obtain a point cloud from a set of images, but some open source photogrammetric solutions do not have the rigour and precision that is required for some applications (Deseilligny & Clery, 2012). For instance, some software packages will not provide the dense matching and precise aerotriangulation that are required for UAV imagery (Deseilligny & Clery, 2012) and that implies a combination of tools and various testing studies.

Some authors have tested UAV imagery in open source tools: Bundler-PMVS2 in Harwin & Lucieer (2012) and Dandois & Ellis (2010); comparisons between a method based on bundler SfM algorithms and the commercial solutions Photoscan and PIX4D web service in Turner et al. (2013); VisualSfM in Li-Chee-Ming & Armenakis (2014).

According to Wenzel et al. (2013) the algorithms for the acquisition of 3D point clouds can be integrated into two categories: 1) Processing imagery to obtain the orientation parameters of images (georeferenced images) followed by a bundle adjustment, such as Bundler, VisualSfM and Apero solutions; and 2) generation of 3D point cloud and surface reconstruction methods based on dense image matching techniques, such as PMVS, Micmac, CMPMVS and VisualSfM solutions. Below we have summarized some of the issues regarding these solutions.

Bundler

The *Bundler* software (Snavely et al., 2008) was developed during the Photo Tourism Project of the University of Washington in 2007. The *Bundler*[32] is based on the Structure-from-Motion (SfM) approach, which is an imaging technique to process unordered and redundant sampled images, which allows us to obtain a sparse point cloud. It allows us to obtain the orientation of images performing a least squares bundle adjustment on the matched features and a sparse point cloud from the 'Sparse Bundle Adjustment' package (Snavely, 2012).

PMVS

Patch-Based Multi-View Stereo Software (PMVS) is a multi-view stereo software that obtains orientation parameters from a set of stereo images (Furukawa &

[32]Available from *www.cs.cornell.edu/∼snavely/bundler/*

Ponce, 2010) and reconstructs 3D structures of an object or a scene. PMVS2 (new version) includes a dense multi-view stereo software to produce dense point clouds.

OSM - Bundler

Meanwhile an easy *OSM-Bundler* solution was created to obtain a dense point cloud that includes (Bartoš et al., 2014):

- Bundler – orientation parameters and reconstruction of sparse point clouds;
- PMVS2 – densification of point clouds (available from http://di.ens.fr/pmvs/);
- CMVS – splitting images into smaller clusters to improve the time processing of large sets of images (available from http://di.ens.fr/pmvs/).

This solution for UAV imagery holds a great potential in natural and man-made landscapes (Harwin & Lucieer, 2012). However, it is not a user-friendly interface.

VisualSfM

The VisualSfM application (Wu & et al., 2011) allows us to obtain a sparse point cloud based on bundle adjustment and a dense point cloud from running the PMVS/CMVS tools (Bartoš et al., 2014). VisualSfM is a GUI application, unlike OSM-bundler and has a good performance. According to Bartoš et al. (2014) it is the most suitable solution with reliable results when compared with OSM-bundler and other web-services solutions ('cloud-based' to get a point cloud, such as Microsoft Photosynth, Photosynth toolkit and Autodesk 123D Catch).

CMPMVS

CMPMVS (Jancosek & Padja, 2011) is an additional tool for the improvement of 3D reconstruction obtained from VisualSfM[33]. It allows more accurate results and reconstructs weak surfaces (e.g. untextured surfaces) better. In general, the workflow solution should be used after the 3D reconstruction obtained from VisualSfM, whose results for a 3D object or scene can be improved by CMPMVS.

APERO and Micmac

APERO and Micmac were developed by Institut Géographique National, (IGN, the French mapping agency), to compute 3D models from a set of stereo images (Deseilligny & Clery, 2012). APERO uses classical algorithm of bundle ad-

[33]Available from *http://ptak.felk.cvut.cz/sfmservice/websfm.pl?menu=cmpmvs*

justment to compute the orientation of images and Micmac performs an aerial image matching following 3D reconstruction from oriented images. Recently, APERO was implemented into the graphical user interface Micmac[34]. The limitations of Micmac are the complexity of its parameters and the fact that it is not fast enough for some applications (Micmac, 2013).

Meshlab

Meshlab is an application for the post-processing of 3D points, providing a set of tools for editing, cleaning, rendering, and producing meshes. Furthermore, it is very useful to support the 3D visualization of some solutions that do not have a graphical solution, such as OSM-Bundler.

In general, Meshlab is very suitable for 3D visualization of millions of 3D points, whose data format should be PLY, XYZ, and ASC (LAS files from LiDAR are not read [35]).

FOSS GIS, spatial database and statistical – *2.5D-FOSS-GISDB* solution

Nowadays, there are several GIS open source desktop packages with different goals, which are stable and reliable for many applications. On the other hand, they have a high interoperability, since it is possible to exchange data between them, thus facilitating the automation of processes.

A comparison between eight FOSS desktop GIS and proprietary GIS software (ESRI) regarding their main functionalities was conducted by Steiniger & Hay (2009). Also, Espada (2010) made a comparison between six FOSS desktop GIS.

FOSS tools for point clouds require a higher performance, which means a challenge with respect to data storage, processing, and manipulation. Consequently, the user must take this into account when choosing FOSS tools.

Below we detail potential tools to filter and structure 3D point clouds that are well supported by development teams. The (semi)-automatic extraction of 3D data for the generation of 3D building models requires a robust methodology preferably integrated into one solution.

Quantum GIS, Geographical Resources Analysis Support System (GRASS), R-stats, and PostgreSQL/PostGIS tools can establish a optimal and interoperable

[34] Available from *http://logiciels.ign.fr/?Micmac* site.
[35] For instance, a LiDAR point cloud in LAS format can be converted into PLY by GRASS GIS.

2.5D-FOSS-GISDB solution (Figure 1.12), i.e., a set of desktop GIS powered by a 2.5D geographic data base (containing 3D data).

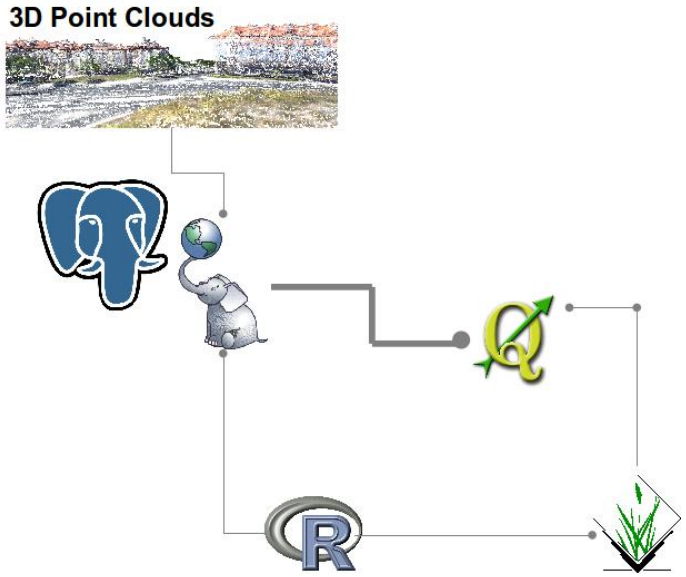

Figure 1.12: 2.5D-FOSS-GISDB solution for point clouds.

GRASS GIS

The GRASS is a free and open source GIS software released under the GNU General Public License (GNU GPL) (Neteler & Mitasova, 2008), which was implemented in the GIS community about 30 years ago by the US Army Corps of Engineers.

In GRASS GIS the data and projects are stored in a GISDBASE (often called grassdata) with their own structure. The GRASS environment is user friendly, but data structure and the way of working with data make it different from other desktop GIS. One of the advantages of GRASS is the interconection with other OS tools, such as QGIS, R-stats, GDAL/OGR libraries, PostgreSQL, and MySQL. This GIS solution can be found in Holl (2005) and Neteler & Mitasova (2008), which provides a good support to all the users that want to use it.

GRASS GIS is composed of a set of powerful tools for the generation of DSMs/DTMs products from 3D point clouds, including specific modules. Additionally, it also has a high performance for managing, processing (filtering and manipulation), analysing and visualizing point clouds. However, GRASS 7.0 is recommended for point clouds, because it has a high performance in terms of the time it takes processing operations when compared with version 6.X (Rebelo et al., 2013a).

GRASS has a set of specific tools developed to perform a fully automatic LiDAR data filtering and were tested by many authors: generation of DTM/DSM of an urban area (Brovelli, 2004; Sanchez & Brovelli, 2007); detection of buildings, ground and vegetation in comparison with TerraScan software (Brovelli & Lucca, 2011); performance and quality of algorithms for the generation of DSM/DTMs (Barazzetti & Brovelli, 2008; Brovelli et al., 2002). Also, these tools were tested with UAV data for the extraction of buildings (Rebelo et al., 2013a).

In the context of LiDAR filtering, some difficulties were recorded in the distinction between building and vegetation that is close to the buildings (Sanchez & Brovelli, 2007; Brovelli et al., 2002). However, in general, LiDAR data filtering has a good quality in urban scenarios and is on par with other proprietary tools (Brovelli, 2004; Brovelli & Lucca, 2011).

Quantum GIS (QGIS)

Quantum GIS was launched in 2002 and it is a user-friendly software for editing, analysing, and viewing. One of the major advantages for point clouds is the connection with the LAStools toolbox (for LiDAR) and PostgreSQL/PostGIS. Additionally, it is a 'light-weight' frontend for GRASS data (including GRASS GIS 7, 6X) (Espada, 2010), which facilitates the manipulation and editing of GRASS data.

QGIS is very useful to make spatial analyses and for a fast visualization of output data created inside a spatial geographical database PostgreSQL/PostGIS and output GRASS data. Moreover, now it includes 3D visualization, which makes it possible to create LoD1 building models in an easier way by using a *Qgis2threejs* plugin based on a web browser.

PostgreSQL/PostGIS

Scott (2007, p.109) stated that 'PostgreSQL is a strong open source database (...)'. The integration of PostGIS[36] as an extension of PostgreSQL[37] relational database results in the 'most powerful open source' spatial database solution for storing and analysing. PostGIS is a tool for spatial analysis that allows us to add several spatial data types and over 300 functions to PostgreSQL (Obe & Hsu, 2011).

PostgreSQL/PostGIS has earned much interest from researchers and compa-

[36] Available from *http://postgis.refractions.net*
[37] Available from *http://www.postgresql.org.*

nies due to the improvements it introduced in terms of the speed of spatial analysis operations with big data. In practice, the spatial analysis is performed by queries on a spatial database (the common *shapefiles* are replaced by tables), where each table (or layer) contains the geometry in one spatial column.

Furthermore, a set of methodological operations can be more easily scripted and automated using the procedural SQL language of PostgreSQL (PL/PgSQL) from a graphical interface, such as PgAdmin. Additionally, it can be included into procedural PL/R language which enables the integration of R statistical functions.

According to Espada (2010), database expertise and knowledge of Standard Query Language (SQL) is required for the design and maintenance of PostgreSQL databases, and these skills are much less demanding than the ones needed for Oracle or SQL Server.

The integration of 3D point clouds into a geographical database management system, such as PostgreSQL extended with PostGIS, is crucial for an efficient and faster handling of how to explore and perform spatial analyses with this data. The processing of point cloud datasets is difficult to achieve using desktop GIS technologies, except in GRASS GIS. However, the performance of GRASS is very low when compared with PostgreSQL/PostGIS[38]. The modification of PostGIS for the implementation of a 3D geographical database was investigated by Setan et al. (2006), where he proposed a PostGISPlus solution.

R statistical computing

R[39] is a free software environment for statistical computing, data analysis and graphics. It is also a flexible and powerful programming language. R has increased the number of contributed packages to handle and analyse spatial data in these past few years (Bivand et al., 2008).

Currently, R includes about 7550[40] source packages (which compares with 1200 in 2008). R provides a variety of spatial statistical functions in clustering, modelling, and graphical techniques. Additionally, there are many GIS packages that provide a 2.5D solution for viewing by draping thematic layers over a DSM (Bivand et al., 2008). Neteler & Mitasova (2008) have shown how open source GRASS GIS can be interfaced with R.

[38] Some issues regarding the usage of PostGIS for point clouds can be found in *http://smathermather.wordpress.com/category/postgis/pointcloud*

[39] R Development Core Team, 2008 available from http://www.r-project.org/about.html.

[40] *https://cran.r-project.org/web/packages*

Users can easily acquire and modify code available in R. The graphical display of results has made R a powerful tool for many applications.

1.4.2 The vision of FOSS tools in Portugal

The first initiative in FOSS tools in Portugal began in 2011 with the publication of the Resolution of the Council of Ministers (RCM) No. 46/2011, of 14th November. The RCM required the implementation of new software solutions for the rationalization of public administration. The RCM included the creation of a group committee on information and communication technologies to define guidelines for the institutions of the public administration. Subsequently, the Agency for Administrative Modernization created in 2008 developed a website[41] to support and strengthen FOSS policies in the public sector.

In the context of urban planning, there has been an evolution of FOSS tools in the past few years, but it still has not reached the level that was expected. Currently, the number of municipalities making use of open source GIS technology software is unknown. The lack of knowledge about the potential of these tools can be a reason, coupled with some resistance to change.

Presently, there is still some lack of interest in FOSS tools for the planning process and we have a good example of this with the standardization of the graphical representation of master plans. The symbology standards created for the revision of a plan that is mandatory do not have a model for FOSS, only for proprietary GIS software. Therefore, now the municipalities that switch to FOSS GIS technologies have a problem to solve. Since this standardization of plans indirectly requires the use of proprietary GIS tools, *what would be the motivation for FOSS usage, when the administration requires the opposite?*

The integration of FOSS tools into urban planning requires the creation of a solid team in Portugal with suitable skills and knowledge dedicated to the development of tools for urban planning. At the same time, this would make it possible to support the requirements of the legal framework and the migration of geographical databases to FOSS by municipalities would become a reality. Furthermore, the integration of new technologies for the acquisition of 3D data at low cost would easily be integrated into a 'fully low cost approach'.

[41] *www.softwarepublico.gov.pt/software-publico*

1.5 *Synthesis*

This section aims to summarize the following relevant aspects: *a)* the evolution of geo-information technologies within the legal framework of urban and spatial planning; *b)* 3D point clouds acquisition technologies, which include ALS and UAV; and *c)* present FOSS technologies that have enabled the processing of point clouds and can support the implementation of this data in urban planning.

a) *New developments of geographical data for planning in Portugal*

According to geo-information technologies, the developments of geographical data for planning in Portugal were marked by three main periods of time: analogue topographic mapping for planning in the late 1970s and in the 1980s; digital mapping in the 1990s; and fully digital mapping and GIS in the 21st century.

In the late 1970s and in the 1980s, topographic map production that supported planning was based on analytical photogrammetric techniques. During this time, the topographic map production process was very time consuming due to all the steps involved in the stereo restitution process. Thus, the elaboration of municipal plans was difficult due to the lack of topographic mapping, where only an unsuitable map on a 1/25000 scale for decision-making covered the whole country.

Digital mapping and a new legal framework for the planning process in the 1990s marked this period. The elaboration of plans became a priority for the implementation of policies in planning, where the plans were classified at a national, regional, and local level. The legislation for LBPOTU and the legal framework for the IGT were the two important legal issues implemented for planning.

Technology was marked by the conversion of analogue topographic mapping into digital mapping and by digital photogrammetric workstations. The implementation of the digital topographic mapping obtained from scanner systems brought many problems for the elaboration of plans due to the absence of technical guidelines to do it. Later, Decree-Law No. 193/95 was published to support and regulate mapping production in planning. Furthermore, the topographic mapping production began to be performed only in a computer system with all the peripherals needed for digital stereo restitution. However, the lack of updated topographic mapping remained a problem.

The fully digital mapping implemented in the last decade revolutionized the mapping production environment. The big technological geo-information innovation

was the replacing of analogue aerial cameras by digital aerial cameras combined with a direct georeferencing system. This aerial system made it possible to obtain direct georeferenced aerial images and to reduce the time and costs of mapping production. However, the updating time of topographic maps mainly for the planning process is still a problem due to its high costs.

At the same time, the changes that occurred last year on the legal framework of IGT have reinforced the importance of monitoring and evaluating plans as a mandatory issue to revise a plan. On the other hand, new levels were established to update oficial and approved topographic maps that should be used for the elaboration of each municipal plan. Furthermore, the accessibility level of the plans is 'democratized' through web platforms systems, where all the master plans must be submitted on a platform for approval based on standards for data structure and spatial representation.

Nowadays, the ALS or UAV technologies for the acquisition of 3D geographical data (Point Clouds) can establish two new paradigms: *3D urban planning paradigm* and *geo-democratization of planning*. The first paradigm for the new requirements of a RJIGT legal framework is present in the plan monitoring and evaluation phase, where the 3D data for measuring and computing quantitative indicators or indices is needed. Additionally, it establishes 3D geovisualization as a tool to support the decision-making process for the elaboration of plans and for public discussion. The second paradigm identifies the new web platform systems for urban planning that have recently been created in Portugal, allowing for the promotion of transparency in urban planning.

b) *LiDAR point cloud*

The LiDAR system is an active remote sensing technology that provides a faster collection of a georeferenced dense 3D point clouds over a large area. The main components of the LiDAR system is the laser scanning and the direct georeferencing system (GPS/IMU). The GPS/IMU allows a 'real time georeferencing' of thousands laser pulses per second emitted to the earth's surface by the LiDAR instrument.

The point density (points/m^2) of a LiDAR point cloud depends essentially on flight height (which defines the pulse footprint) and the particular characteristics of the laser scanner (beam divergence and effective measurement rate). Furthermore, the point cloud results from a discrete number of returns recorded. Typically, the 'first return' corresponds to the first objects encountered and the 'last returns' to

the last echo of lower objects. Therefore, the LiDAR point cloud contains the following information for each point: X,Y coordinates; elevation; return; backscattered intensity value of pulse laser energy.

The four major advantages of LiDAR over image-based techniques are: i) it always enables the mapping of bare earth surface even in areas with dense vegetation or forest; ii) shadow areas dominant in urban areas can be recorded by LiDAR data; iii) the acquisition of LiDAR data is independent from season and daytime; and iv) altimetric accuracy better than 10 cm. However, the weakness of this technology is the high cost when compared with other techniques for the acquisition of 3D data.

The usage of this data for the extraction of buildings requires a higher point density and the direct use of point cloud without any interpolation to raster is recommended. The major difficulties are the extraction of accurate building outlines and its length determination. Despite some difficulties in modelling complex buildings, LiDAR is a suitable technique for 3D modelling of buildings.

c) *Very high resolution aerial images from UAV technology*

The UAV (or UAS) technology is an (ultra)-lightweight (usually 500 gr to 4 kg) aerial photogrammetric system, which provides an alternative for low-cost aerial surveys over small urban areas. The UAV aircraft system is a small platform which integrates a small-format digital camera and a miniaturized direct georeferencing system (GPS/IMU). Low altitude UAVs are classified as fixed-wing (e.g. swinglet CAM of SenseFly) or as multi-rotor (e.g.quadoctopers).

Purpose flights are not yet integrated into civil aviation authorities. However, this situation will change soon now that the EASA has begun the process for the regulation of these mini-aircrafts in September 2015, publishing their first proposal.

The multiple overlapping of UAV imagery together with a dense multi-stereo image-matching allows us to achieve a dense 3D point cloud that is very similar to a LiDAR point cloud from very high resolution aerial images. Multiple overlapping UAV imagery means an overlap between 80% and 90% along flight direction and 60% between flight lines. On the other hand, dense multi-stereo image-matching is performed to estimate the 3D point coordinates for each pixel matched. This means that all the pixels of georeferenced multi-stereo pairs are matched followed by the 3D geometry reconstruction of matching points. The UAV point cloud produced by this technology has the following information for each point: X,Y coordinates; elevation; and RGB values.

However, UAV point cloud density is very dependent on GSD imagery, which is directly proportional. The radiometry and geometry quality of images and the characteristics of the area surveyed can also influence point cloud density. Therefore, density point is lower (sparse) or there are failures (gaps) in vegetation areas, untextured surfaces (dark surfaces, tiny roofs, etc..), shadows and occlusions (mainly in urban areas). The ability of dense stereo image matching to generate point clouds, particularly in these areas, is extremely important, and also for the accuracy of point cloud.

Some of the advantages of this system when compared with conventional digital airborne LiDAR and photogrammetric systems are: 1) low-cost system which is easier to buy; b) high flexibility, remotely controlled from the ground and easy to use; c) in less than 24 hours it is possible to perform a UAV flight and acquire a 3D point cloud from a small urban area; and d) it can achieve an accurate and dense point cloud point just like LiDAR.

The weaknesses of this technology is the limited flight time (battery life is usually between 30-60 min) and very high sensitivity to wind conditions. For the modelling of buildings the strengths are the lower points in vegetation near the buildings which facilitates the filtering. However, complex and untextured roofs and occlusions on the building roofs can result in a sparser point cloud and gaps, and both can cause difficulties to the modelling of roof shapes and result in a less accurate building outline.

d) *FOSS to explore 3D Point Clouds*

FOSS could be implemented as a potential solution for the usage of 3D data for urban planning, since it does not imply any costs with the maintenance of software licenses and it encourages the development of specific tools for the planning process. However, human resources with competencies and skills in FOSS tools and open source programming are needed.

Nowadays, there are FOSS tools for the acquisition of 3D point clouds which can be called 'OS photogrammetric solutions' and for spatial database analysis, manipulation and visualization called '*2.5D-FOSS-GISDB*' solution.

In the framework of *OS photogrammetric solutions*, these are classified into two categories: 1) Processing UAV imagery to obtain the orientation of images; and 2) Generating 3D point cloud and surface reconstruction methods. The first category includes Bundler, VisualSfM and Apero solutions, and the second category in-

cludes PMVS, Micmac, CMPMVS and VisualSfM solutions. These latter solutions are based on imaging technique SfM. A good solution within this photogrammetry framework is to combine 'VisualSfM, CMPMVS and Meshlab' or OSM-bundler (Bundler, PMVS and Meshlab).

The *2.5D-FOSS-GISDB* solution implies a set of desktop GIS powered by 2.5D geographic database (containing 3D data), which is composed of QGIS, GRASS, R-stats, and PostgreSQL/PostGIS software packages and can establish an optimal and interoperable solution. This solution is suitable for 3D point clouds and it allows: a) structuring a big volume of 3D data within a 2.5D geographic database PostgreSQL/PostGIS; b) filtering and performing a spatial and statistical analysis using GRASS GIS, R or PostGIS functions; and c) 2D/3D geovisualization from QGIS or GRASS. This solution can also be centred in QGIS, establishing a connection with GRASS and PostgreSQL/PostGIS, and R within PostgreSQL/PostGIS.

Furthermore, this solution allows us to develop new tools or automatic procedures within a 2.5D geographical postgreSQL/PostGIS database using the procedural SQL language of PostgreSQL (PL/PgSQL) and procedural language PL/R. All these issues can be very useful for the planning process as to the extraction of buildings parameters for monitoring and evaluating a plan.

The demand for FOSS tools has grown considerably in these past few years in Portugal. However, the vision on FOSS tools is still not sufficient for the implementation of a FOSS-based planning policy. The creation of a team of developers for urban planning is needed to support: a) the challenges required in the new IGT legal framework (such as the standardization of data models and the graphical representation of plans), and b) the introduction of 3D geographical data technologies in the planning process, such as geovisualization for public discussion, and computing indicators to the monitoring and evaluation phases.

In the next chapter, we shall demonstrate the usability of these geo-information technologies – UAV, LiDAR, and FOSS – for the extraction of building parameters in a small coastal urban area.

Chapter 2

Extraction of Building Parameters: A Case Study of a Coastal Urban Area – *Praia de Faro*

According to Baltsavias (1999a), ALS systems will replace photogrammetry in some applications and *open up new areas of applications* with more accurate cartographic products. Nevertheless, the junction of automated processing and ultra-light UAV imagery can produce results that are comparable to the ones obtained with traditional photogrammetric systems (Strecha, 2011).

The aim of this chapter is to demonstrate the usability of these two technologies, ALS or UAV, for urban applications, such as the measurement of building density parameters in urban area. The performance and accuracy of each of these technologies to extract building parameters will be tested and evaluated. The building parameters tested were building façade height, building area, and building volume. These parameters have the following definitions:

i) According to Decree-Law No. 9/2009, the *building façade height* parameter in Portugal corresponds to the vertical dimension and should be measured from the elevation of cornice, eaves (*beirado*) parapet wall, rooftop railings or gutters (*platibanda*) to the elevation of building base (also called 'elevation of the main entrance of the building' if it matches the ground level). However, taking into consideration that a building can have different façade heights according to its deployment on the

ground, only one façade side of the building was chosen to compute this parameter for this study. For this case study we assumed the upper elevation according to the eaves or parapet wall.

ii) the *building area* parameter is defined from the boundary of the building roof, which is equivalent to the building rooftop area. Usually, most building roofs are coincident with the ground area occupied by the building, such as shown below in Figure 2.1.

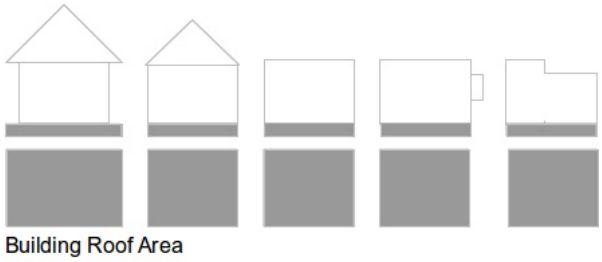

Figure 2.1: Building Roof Area

iii) According to Decree-Law No. 9/2009, the *building volume* (*volumetria do edificio*) in Portugal is the measure of the volume built above ground level, defined by the planes that contain the façades, rooftop, and ground level. In practice, the *building volume* can be calculated by multiplying building façade height by building roof area. Therefore, from the sum of building volumes it is possible to obtain the total volume parameter of a built-up area.

This chapter shall demonstrate the usability of 3D point clouds generated from ALS or UAV for the automatic or semi-automatic extraction of building parameters. This demonstration was performed based on the development of two different methodological approaches for a small study area, using only 3D point cloud data without any reference data.

The first methodological approach was the automatic extraction of building parameters from a LiDAR point cloud using the LiDAR Analyst for ArcGIS, which will be detailed in Section 2.2. In this case we explored a 'black box solution' from the end user's perspective. The second methodological approach (Section 2.3) was developed for a dedicated semi-automatic extraction of building parameters using FOSS technologies (2.5D-FOSS-GISDB), which we called 3DEBP solution. The latter approach was performed for UAV and LiDAR point clouds, which included the development of a Geographical Database Management System (GDBMS). Both methodological approaches were developed in two distinct stages: (1) building parameters extraction, and (2) evaluation of building parameters extracted using ac-

curate vector data.

Furthermore, the second methodology allowed us to compare the effectiveness and accuracy of two different technologies for the extraction of building parameters.

2.1 *Study area and data acquisition*

The study area – Praia de Faro – is an island-barrier bounded North by the Ria Formosa estuary and South by the sea, located in the Southern portuguese Coast of the Algarve region. The selected geographic area (Figure 2.2) has approximately 2.5 hectares, with a width of 100 m North to South and 250 m East to West along the principal and central street of the island. This open sandy beach is a built-up area with 19 buildings along the street. Most of these buildings are single-family dwellings with a maximum of two stories, although there is a building located Northeast of the study area with four stories (from the estuary side, from East to West, it is the fourth building).

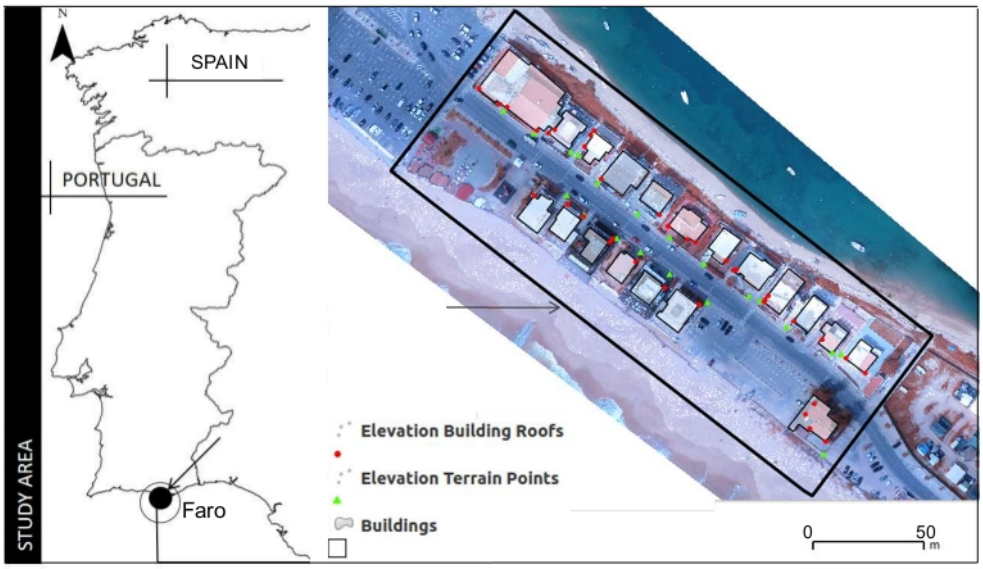

Figure 2.2: Study area: Praia de Faro.

The buildings represent a diversity of architectural styles and types, with irregular shapes. The roofs are either flat, multiple-level flat, pitched, and complex (with different slopes). The degree of dissimilarity between building shapes is high. This urban area is extremely complex and the building's typology is very heterogeneous (Table 2.1).

Table 2.1: Building code used in Sections 2.2 and 2.3.

Northern buildings			Southern buildings		
Code sect. 2.2	**Code sect. 2.3**	**Buildings**	**Code sect. 2.2**	**Code sect. 2.3**	**Buildings**
E1a,E1b	-		E10	ED10	
E2	ED1_2		-	-	-
E3	ED3		E11	ED11	
E4	ED4		E12	ED12	
E5	ED5		E13	ED13	
E6	ED6	 	E14	ED14	 
E7	ED7		E15	ED15	
E8	ED8		E19	ED19	
E9,E16	ED9_16		-	-	-
E18,E18a	ED18		-	-	-
E22	-		-	-	-

In Table 2.1, we can see the buildings of this study area and the algorithm used together with the methodologies that will be detailed in the following sections.

The challenge is the development of a methodology that is robust for the semi-automatic extraction of building parameters from this heterogeneous area using 3D point cloud data.

The 3D point cloud data of this study used for this demonstration have a difference of 4 years approximately between them. LiDAR point cloud data was provided in the framework of a project on the morphological impacts and coastal risks carried out by the University of Algarve. However, the UAV point cloud data was collected and processed for this particular study. More details about the point cloud data can be seen in Subsection 2.1.2. In addition to point cloud data it was necessary to collect accurate vector and raster data sources to support some specific studies along this work and for the evaluation of the results obtained.

2.1.1 Vector and raster reference data

The acquisition of reference building parameters – building area and building façade height – was performed from accurate 2D and 3D vector data, respectively. Subsequently, the reference building volume was computed from these two reference parameters. These reference building parameters were important to evaluate the building parameters estimated from each 3D point cloud.

The large-scale 2D vector data included accurate building outlines (Figure 2.2). This data was important to calculate the reference building area which allowed us to evaluate the area measurements extracted for each building. The 2D vector data was provided by *Sociedade POLIS Litoral Ria Formosa*. This information was acquired from traditional photogrammetric restitution with a horizontal accuracy below 40 cm. The 3D vector data included accurate elevation points of building roofs and terrain.In addition, 3D elevation points of roofs and ground were used to calculate the reference building façade height. The distribution of these 3D points selected from a subset can be seen in Figure 2.2. Furthermore, specific GCPs that have good visibility and definition on aerial images were also collected and used for the processing of UAV imagery.

Moreover, raster data was used along this work for the visual inspection of the building roofs extracted from 3D point cloud data. This data refers to true orthoimages[1] produced by aerial images collected from a digital airborne camera

[1]The true ortorectification process of aerial images take into account the elevation of all objects above ground - DSM.

used during a LiDAR flight and true orthomosaic produced from UAV imagery.

The characteristics of all reference data used in this study can be seen in Table 2.2.

Table 2.2: Description of reference data – vector and raster

Type of data	**Year**	**Data**	**Technical Acquisition**	**Data details**
3D vector data	2012	Elevation points of roofs	Leica TCR 705 Reflectorless Total Station	Corners and prominent points
		GCPs	Leica GPS900	Corners of causeway, crosswalk, and car parking
2D vector data	2002	Building outlines	Photogrammetric stereo restitution	Large-scale: 1:2000
		Road network	Photogrammetric stereo restitution	Large-scale: 1:2000
Raster data	2009	True-orthoimages	Source: Aerial images from the LiDAR flight with a Rollei AIC P20 (39 MP) camera and DSM	GSD: 9 cm
	2013	True-orthomosaic	Source: Aerial images from the UAV flight with CanonPowerShot ELPH300HS4.3 camera and DSM	GSD: 5 cm; Near-Infrared images (NIRGB)

All the elevation points (3D vector data points) were acquired from direct field measurement with ground surveying. The 3D topographic survey was first planned for the location of reference points in building roofs that are relevant for the determination of reference building façade height value (In Appendix B we can see a excerpt of this planning). Additionally, the ground points were defined near the buildings. The topographic equipment Leica Reflectorless total station used for surveying roof points can be seen in Figure 2.3c. This equipment has an angle accuracy measurement of 5".

Before the topographic surveying of 3D points a reference point network of control was established. These reference point network was important to support the survey of all the points planned in the study area. This local network was made in real time with a Leica GPS900 reference station and a real time rover setup (Figures 2.3a and 2.3b). Later, a topographic survey was conducted to obtain GCPs on specific locations for the processing of UAV imagery (Subsection 2.1.2.). This surveying included a subset of six points (Figure 2.7) selected from UAV imagery which have a good identification in various pairs of UAV images. These points were surveyed with Leica GPS900 with a cm-level accuracy of 3 cm on the ground.

Figure 2.3: Topographic survey equipment: a) Leica GPS900 reference station; b) Leica GPS900 rover;and c) Leica TCR 705 Reflectorless Total Station.

2.1.2 3D point clouds

LiDAR point cloud

The LiDAR point cloud was collected in November of 2009 at a flight height of 500 m above ground using an LiDAR system mounted on a helicopter. This LiDAR system has a airborne topographic laser scanner called TopEye MKIIB (Figure 2.4), which is fitted with an Applanix Rollei AIC 39 MegaPixel (MP) digital camera.

The laser scanner used by this system is the Palmer scanner which has an elliptical pattern. This type of scanner allowed us to collect a point cloud with higher point density, which can fully cover all vertical elements. However, for this study, the higher point density of the vertical elements may bring more difficulties for the extraction of building rooftop, which implies the development of effective tools to remove the points from all the building façades.

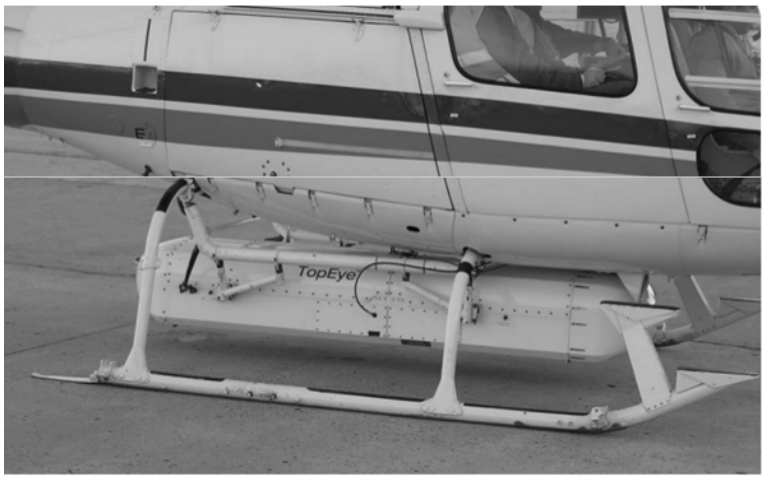

Figure 2.4: Airborne LiDAR system: TopEye MKIIB.

The range capture of the LiDAR flight recorded two returns per laser pulse (first and last returns). Each laser return results in a point data with X, Y and Z coordinates and the value of intensity for each point. The LiDAR point cloud of the study area has a density of about 6 points per square metre (this means that distance between points is less than one metre), and the last return points are about 5% of the first return points. Furthermore, the georeferencing of the point cloud was transformed from WGS84 to the local coordinate system (Hayford-Gauss Datum 73).

According to the flight planning report, the LiDAR point cloud that will be used along this study has a vertical accuracy of 10 cm. It is important to note that the LiDAR data was kindly provided by Micore project FP7 Framework of Algarve University, which was processed by the BLOM company that made the flight.

Later more details about this data will be provided in this section by a comparison with a UAV point cloud.

UAV point cloud

The UAV point cloud data was obtained from processing UAV imagery, which will be described later. The acquisition of UAV imagery data was performed on 12th April 2013 from a swinglet CAM produced by SenseFLY (Figure 2.5). This aerial system is remotely controlled from a laptop, weighs about 500 grams, and has an autonomy of approximately 30 minutes of flight time. It requires moderate wind that is not above 7 m/s.

The swinglet CAM (Figure 2.5) is equipped with a small digital camera (12 MP) and a small direct georeferencing system (GNSS and IMU). The sensor size is 6.2 x 4.7 mm and the focal length is 4.3 mm.

Figure 2.5: Airborne UAV system – swinglet CAM.

This small aerial system can achieve GSD between 2 and 40 cm at a flight

height of 50 to 1000 m, respectively (Bellavita et al., 2013).

Flight planning and UAV imagery processing

Planning the flight and processing UAV imagery was performed with the support of SINFIC. The acquisition of UAV point cloud data involves a subset of steps that were shown in Figure 1.6 of Chapter 1.

The first and second steps for the acquisition of UAV point cloud data is the flight planning and the execution of a UAV flight in the study area. This specific study area is not an easy area to fly in, because it is surrounded by the sea and the Ria Formosa estuary. On the other hand, this is an urban area near Faro airport. Therefore, the success of a UAV flight strongly depends on wind conditions, because it is very important to ensure the safety of the equipment and the civil society. However, if something went wrong during the mission, this equipment has a security system. In case of bad flight conditions or low battery, the system aborts the UAV mission and safely returns to the landing place.

The flight mission was planned in order to acquire stereo aerial images with a resolution between 3 and 5 cm and a higher overlap between aerial images. The landing place chosen is an open and safe area, which is 700 m from the aerial survey area. This operation included three flight missions, where two of them failed. The results of these missions can be seen in Table 2.3.

Table 2.3: UAV flight Missions

Mission	**Start time**	**GSD (cm)**	**Flight height (m)**	**Result of Mission**
1	11:10 PM	3	82	Failed the processing of UAV imagery.
2	3:15 PM	5	136	Success of flight and processing UAV imagery.
3	4:00 PM	4	109	Failed flight - UAV returned to the landing place because of lower battery.

During the UAV flight operation, the flight plan and the exposure of images were uploaded to the laptop on board the UAV and verifications were carried out. This allowed us to continually check the flight track, the coverage and the exposure of images. The checking of flight in real time allows to abort a mission if there are gaps along the coverage. Still, another advantage of this technology is the possibility

of roughly checking and processing UAV imagery immediately after the mission. Then, a rough analysis of the quality of each image can be done in situ. Thus, this checking consists in verifying shadows, clouds, image sharpness, and other problems in recording pixel data. Sometimes it is necessary to repeat the flight mission, if the stereo image matching is not possible because of the bad quality of some stereo pairs of images.

After the first flight mission, a rough processing of UAV imagery (without any GCP) was performed in a few minutes to check the quality of the flight data. At the end of the processing procedure some problems were identified in the point cloud data, such as the irregularity of points and most buildings were not covered by 3D points. Therefore, a second flight mission was planned at a flight height that was slighty larger to ensure the stereo matching success. During this operation, another mission flight was planned to obtain a smaller GSD for UAV imagery, but it failed.

The flight planning scheme of the successful mission is shown in Figure 2.6. Along the direction of the flight the forward overlap was about 80%, which enabled the location of one matching point in at least 5 stereo images. The lateral overlap (between flight lines) was about 60%. Also, the average distance between image exposures was 40 m and between flight lines it was 70 m (between flight lines 2 and 3) and 90 m (between flight lines 1 and 2)(Figure 2.6).

Figure 2.6: UAV flight scheme and actions performed in preparation for the flight.

The study area was covered by 47 aerial images (3000 by 4000 pixels each image). The operation along the three flight lines (Figure 2.6) was carried out successfully for a flight time of 10 min. The flight was performed with a wind speed below 10 km/h.

According the UAV point cloud processing workflow, the next step is performing the multi-stereo image matching processing. This processing was performed by an automatic workflow implemented into PIX4D software to obtain the 3D point cloud. However, the PIX4D that was used did not include the semi-global matching (SGM) algorithm. Before this processing stage a careful analysis of the quality of coverage of the UAV images was made, where only one image was deleted because of distortions.

The UAV imagery processing started with the measurement of six GCPs (Figures 2.7 and 2.10) for all stereo pairs of UAV images where they appeared. In this particular case, this meant identifying a GCP for about seven UAV images. This task is particulary important for the generation of more accurate point clouds, and orthophoto and DSM products. The processing time necessary to generate all these products was about 10 min.

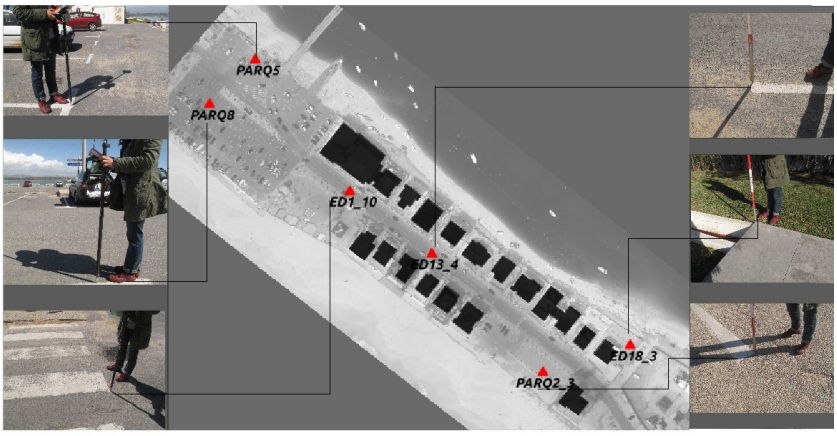

Figure 2.7: Ground Control Points used in UAV imagery processing.

The UAV point cloud produced (Figure 2.8) was georeferenced to the local coordinate system Hayford-Gauss-Datum 73 (according to the reference system of GCPs). At the end of this processing stage a quality report was produced (Appendix C), with details on the following: a) calibration of images for geotags, camera position, and overlap; b) bundle block adjustment; and c) geo-location for each GCP, which shows the residual errors X, Y and Z obtained along the measurement of GCPs on the images and the location of GCP measured for all pairs where these

appear.

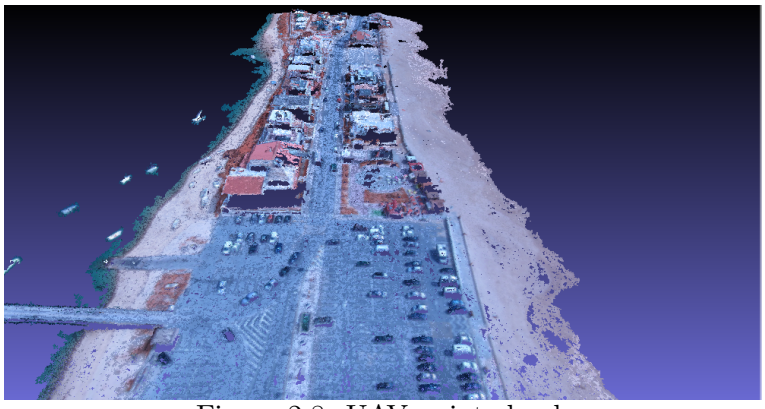

Figure 2.8: UAV point cloud.

For this small study area, the UAV flight and the processing of UAV imagery for the acquisition of a 3D point cloud, true orthomosaic and DSM were made in a few hours (less than 5h). More details on the software processing and the swinglet CAM system can be seen in Strecha (2011) and Vallet et al. (2011).

Comparison of point clouds – data and quality

A visual comparison between these two point clouds can be seen in Figure 2.9. The point density of the UAV point cloud of the study area is about ten times more than the LiDAR point density (Table 2.4). However, the distribution of 3D UAV points is extremely irregular, whereas LiDAR point clouds have a more regular grid.

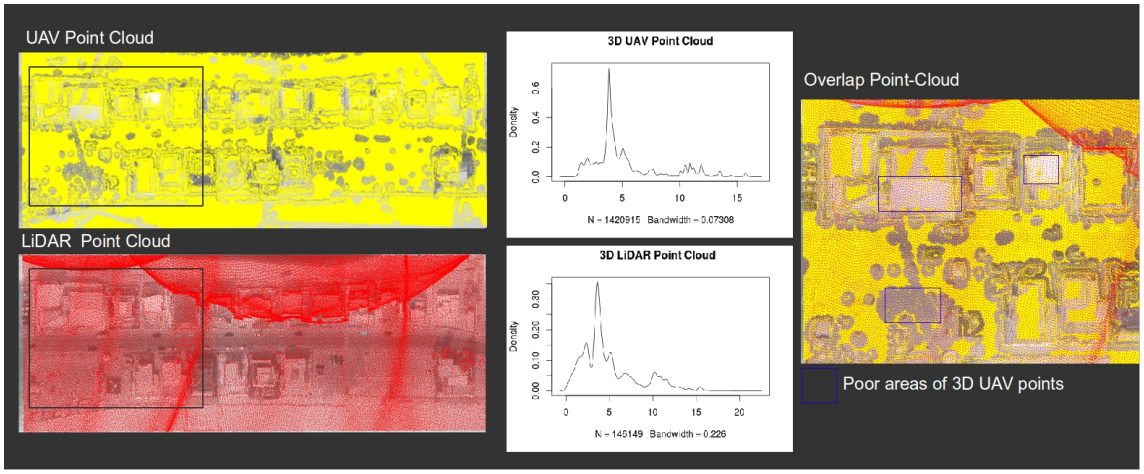

Figure 2.9: Comparison of density point clouds.

The UAV point cloud does not cover the total of the building rooftops. Conversely, the coverage of the LiDAR point cloud is uniform, where all the building

rooftops have 3D points. The elliptical coverage of LiDAR is visible by the highest density of points in the north section (Figure 2.9). In this area, point density reached 2-3 points per m^2. The overlap between these two point clouds (Figure 2.9) shows a poor point density for the UAV point cloud in the marked areas. This poor density may be caused by the processing parameters used for the acquisition of the point cloud or failures along the stereo pair overlapping of the images.

Additionally, the comparison between the density functions of the Z variable (Figure 2.9) shows that the UAV curve contains too many spurious data, because of the higher density of points. However, the LiDAR curve is slightly smoother. Most elevation values range between 3 and 5 m for both clouds. Table 2.4 summarizes the general characteristics of these two point clouds.

Table 2.4: Characteristics of 3D point clouds

Technology	Acquisition date	Number of points	Point density[1]/m^2	Elevation statistics (m)	Range elevations (m)
UAV	April 2013	1,420,915	61 pts/m^2	Zmean=5.14; Zmedian=4.08	Zmin=-0.21; Zmax=16.91
LiDAR	November 2009	146,149	6.3 pts/m^2	Zmean=4.92; Zmedian=3.83	Zmin=-0.03 Zmax=21.86;

[1] Average point density per square metre was estimated from the ratio between the number of points in the study area and total area.

The LiDAR system is more accurate for the detection of tree objects. Additionally, the range of elevation values recorded by LiDAR is larger than UAV data (Table 2.4). The peak values recorded from LiDAR correspond to a very tall cypress that is placed to the Southeast of the study area. The main factors that affect the density of a point cloud can be seen in Subsection 1.2.2.

These big data of millions of 3D points were stored on a management geographic database PostgreSQL/PostGIS. This issue will be an enormous advantage from the end user's perspective since it allows the acquisition and manipulation of building parameters from big data.

The positional quality of a point cloud is an important issue that should be ensured before the extraction of building parameters, such as high vertical accuracy. Whatever the methodology developed, if the point cloud has low vertical accuracy, then the accuracy of the building parameters extracted will be worse.

The evaluation of the positional vertical accuracy was made for each point cloud based on the selection of 37 Independent Check Points (ICPs) (Figure 2.10).

The requirements for the selection of ICPs were: i) enable that ICPs on the ground are present in both point clouds; and 2) they may not have been used in UAV imagery processing. The methodology adopted for this evaluation was the estimation of the Z coordinate for each ICP at the point cloud, using the Inverse Distance Weighted interpolation.

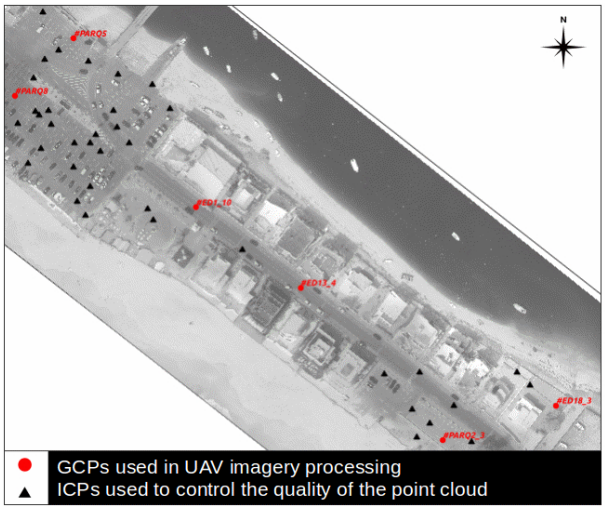

Figure 2.10: ICPs used for the evaluation of the vertical accuracy of each point cloud. The GCPs represented were not used in this process.

After the estimation of the Z coordinate in the point cloud, the vertical error $[e_z]$ is estimated from the difference between an accurate Z coordinate value (ICP) and a Z coordinate estimated by interpolation. The statistics of these vertical deviations were computed, such as the Root-Mean-Square Error (RMSE), average, standard deviation, minimum and maximum values (Table 2.5). All these statistics are indicators of the positional vertical accuracy of a point cloud.

The $RMSE_Z$ statistic is the square root of the average of the set of squared vertical errors, which is given by the following equation:

$$RMSE_z = \sqrt{\frac{(e_{z_1})^2 + ... + (e_{z_n})^2}{n}} \tag{2.1}$$

where n is the number of identical points selected in each point cloud.

Table 2.5: Positional quality of point clouds through the vertical errors of identical points

Point Cloud	$RMSE_z$ (cm)	Min e_z (cm)	Max e_z(cm)	Average e_z (cm)	Standard Deviation e_z(cm)
LiDAR	18.2	8.6	40.1	17.7	5.4
UAV	10.9	-19.4	22.2	1.09	10.8

Given the results displayed, there is evidence that the UAV point cloud is slightly better than the LiDAR point cloud (Table 2.5) based on the $RMSE_z$ value, but this difference is not relevant. Therefore, we should highlight that the LiDAR accuracy referred in the report was 10 cm. However, the processing and quality control of the LiDAR point cloud is unknown, namely the GCPs used for its calibration and the quality control method. Additionally, it is important to refer that the point clouds were not collected under the same conditions and around the same time. Therefore, it is possible to conclude that:

- These point clouds have positional quality for this study, because the average of vertical errors (10.9 cm and 17.7 cm) is acceptable for the estimation of building façade height parameter.
- The $RMSE_z$ values are lower than 20 cm. This level-accuracy affords us the necessary reliability to use this data for the extraction of building parameters.
- The UAV point cloud is sparser and more irregular than the LiDAR point cloud based on the standard deviation value, which means that the automatic extraction of building parameters can be more difficult from the UAV point cloud. It is more difficult to establish a methodology that is able to cover all the standard irregularities when removing points that do not belong to building rooftop and ground.

The following sections provide an overview of the usability of this data for the extraction of building parameters from different approaches. The objective is to look for answers through these approaches:

a) What type of tools are effective for the extraction of building parameters from the perspective of an urban planner: FOSS or proprietary tools?; *b) Is it possible to extract accurate building parameters solely from 3D point cloud data without accurate 2D/3D vector data acquired from stereo restitution?*; and *c) Is the 3D point cloud appropriate for the extraction of building parameters with an acceptable quality? If so, how can we integrate this data into urban planning?*

2.2 *Usability of LiDAR data for the extraction of building parameters*

The demonstration of the usage of 3D data from a LiDAR point cloud and

its potential shall be presented and discussed in this section. The main objective of this demonstration is to evaluate the level usability of a LiDAR Point Cloud in the following situations: *i)* automatic extraction of building height and roof outline for the generation of 3D building models with the ArcGIS LiDAR Analyst extension; *ii)* evaluation of LiDAR accuracy for the extraction of building parameters that involve the third dimension (building façade height and building volume) based on the development of a geoprocessing model; and *iii)* identification of the type of building rooftop from the pulse intensity of LiDAR, slope, point density, and elevation.

2.2.1 Evaluation of the automatic extraction of building parameters for the generation of 3D building models from a LiDAR point cloud: methodology and results

The automatic extraction of buildings from a LiDAR point cloud, using all return points (first and last return), can be performed following three steps: 1) interpolating from point cloud to raster DSM; 2) creating raster DTM from DSM; and 3) extracting building features based on DSM, DTM and Normalized Digital Surface Model (NDSM)[2] and a set of building parameters software.

The methodology developed for the building extraction was performed with the LIDAR Analyst. The flowchart of this automatic processing is shown in Figure 2.11. The methodology included two different approaches using a subset of parameters. In the first approach (Test 1) the buildings were extracted using the default parameters of the software. The second approach (Tests 2&3) was designed to improve the results of the first one by the introduction of two steps in the workflow: refining DSM and customizing a subset of extraction parameters.

The refining of DSM is an essential task in this workflow. When performing building extraction, it is necessary to ensure a good quality of the DTM extracted from DSM, because the difference between them (NDSM) will yield the height of the buildings. If the DSM or DTM are built without any filtering, it will be more difficult to extract accurate building roof lines. Afterwards, the refining process for obtaining DTM (tests 2&3) was carried out by editing the DSM, removing cars and other objects near the buildings.

[2]NDSM is the difference between DSM and DTM and it gives the heights of objects on a surface.

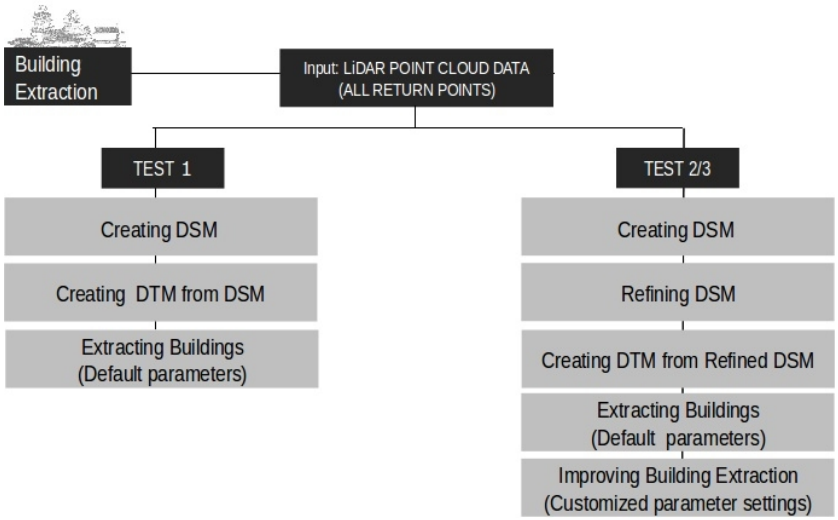

Figure 2.11: Methodological approach for building extraction based on a LiDAR point cloud. Adapted from Rebelo & Tenedório (2011a).

The next step (Figure 2.11) is the extraction of building roof lines using a set of building parameters, which can be manipulated with a combination of different parameter values. The building parameters are the minimum building height, area range, slope for building roof, texture variance trees to differentiate between trees and buildings, and smoothing tolerance that defines the maximum distance a point can move in relation to its neighbouring vertices. First, the parameters used to define the boundaries of the buildings were changed by the minimum and maximum slope values. Then, the best values for this range were repeated for different values of the texture variance parameter used in the extraction.

Table 2.6 shows three different combinations of parameter values within a set of several tests, whose results are illustrated in Figure 2.12. The selected tests (Table 2.6) defined two different approaches to extract building roofs: building blocks and isolated buildings or simply isolated buildings.

Table 2.6: Parameters defined for extracting building blocks and isolated buildings

Parameters	**Test 1**	**Test 2**	**Test 3**
Do not remove buildings with area between	30-35000m^2	30-35000m^2	30-35000m^2
Slope for building roofs (minimum-maximum)	15-40°	15-60°	40-80°
Texture variance trees	80%	80%	90%
Remove buildings lower height than	2 m	2 m	2 m
Smoothing tolerance	2.2 m	2.2 m	2.2 m

For the definition of these parameter values we need to have a knowledge of the building types and the characteristics of the study area. Moreover, the usage of orthoimages is important to visualize the building roofs and evaluate the results of the roof lines extracted automatically. On the other hand, the visualization of trees and vegetation on orthoimages can help to define the parameter value of texture variance trees.

The automatic extraction of building rooftops was based on the NDSM that is shown in Figures 2.12a and 2.12b. The overlapping of accurate building outlines and the NDSM (Figure 2.12c) shows that there are some residual differences along the boundaries of building rooftops.

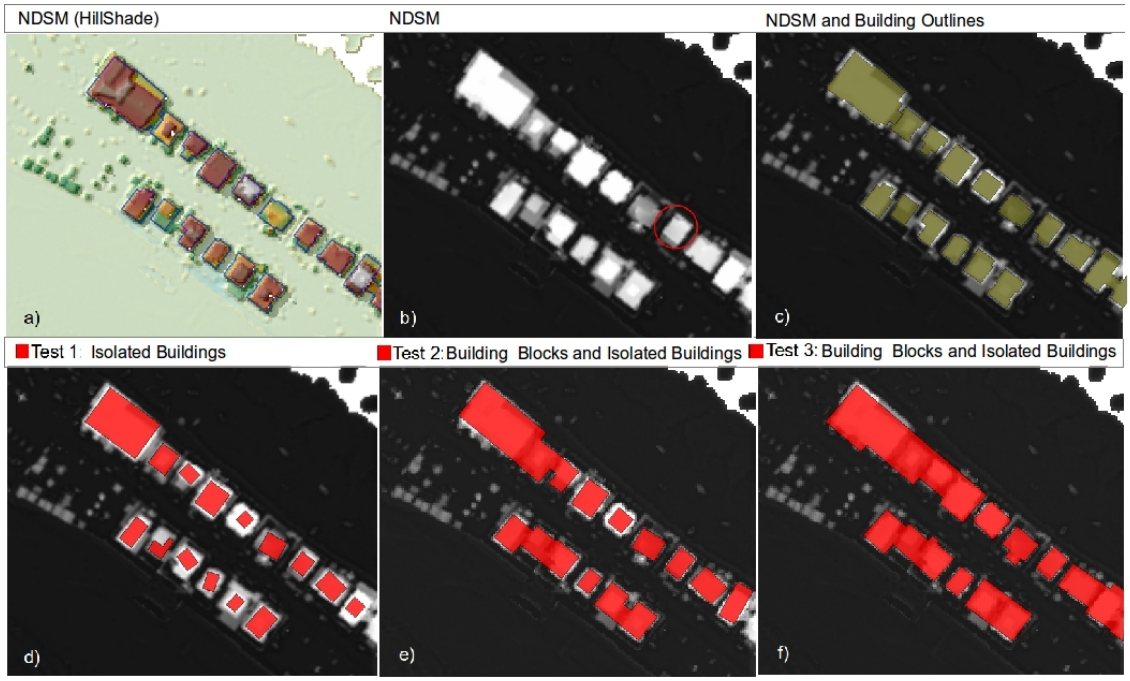

Figure 2.12: The source data used for the extraction of building roofs and the results acquired from different subset parameters. a) NDSM Hillshade; b) NDSM, where each pixel contains the height value of an object; c) NDSM with the overlap of accurate building outlines (reference data); d) Isolated building roofs extracted; e) Building blocks and isolated buildings extracted, where the NDSM was refined (Test 2); and f) Essentially, these are extracted building blocks, where the NDSM was refined (Test 3).

The first approach to the extraction of isolated buildings (15 buildings extracted) showed difficulties in the acquisition of accurate rooftop lines, because these did not match the highest elevation values visible in the NDSM (white shaded areas in Figure 2.12d). However, the change in the slope parameter range value made the extraction of building blocks (Figures 2.12e,f) possible, with better orientation and a roof outline that is more consistent with the NDSM.

This extraction process implies the acquisition of specific building attributes that are calculated simultaneously, such as average building height, minimum/maximum building height values, building area, and roof type. The total building area obtained from accurate building roofs[3] is 3213 m^2. The buildings extracted from tests 1 and 3 represent a total building area of 1986 m^2 and 4377 m^2, which is equivalent to a 38% and 36% percentage of error, respectively.

Furthermore, test 2 resulted in an estimated 3329 m^2 of total building area, with a percentage of error of about 3.6%. According to the presented results, test 2 has the best value for the total area of buildings, with an equivalent error of one building (-115 m^2).

It is possible to compare one single building (red circle in Figure 2.12b) acquired from stereo restitution (building outlines) and the automatic roof line extracted from point cloud, with a density of 12 points/m^2 in the building roof areas (Figure 2.13). For this building, the difference between the building height obtained by topographic survey (6.4 m) and the average building height extracted from LiDAR is of around 20 cm for test 1, -40 cm for test 2, and -50 cm for test 3. All these errors are acceptable because they are lower than the standard floor height. However, the building area extracted did not match the accurate building outline.

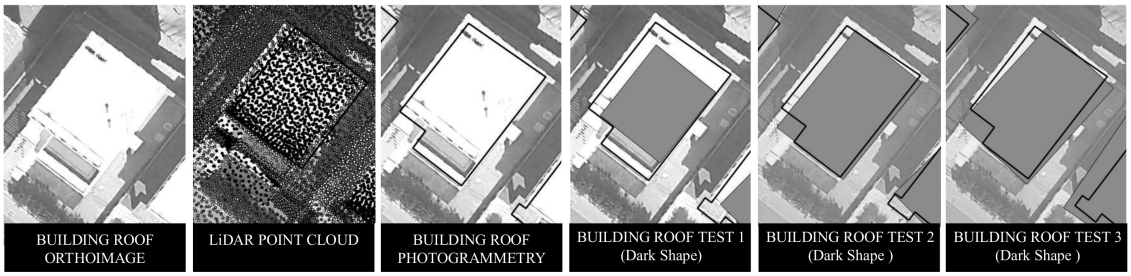

Figure 2.13: Comparison between building roofs extracted from stereorestitution and automatically by LiDAR data.

The generation of 3D building models without roof details, also called block model or LoD1 (according to Kolbe et al., 2005), can be easily done by extruding the footprint of each building roof to their average height (Figure 2.14).

On the other hand, we can visualize rooftops classified into three types: complex, simple/flat, and pitched (Figure 2.14). The roof of each building was classified differently according to parameters defined along the automatic extraction process. When the roof extracted was characterized by medium slopes, the roof was classified

[3]Building roofs extracted from stereo restitution.

as pitched and when the slope was low, the roof was classified as flat (Figure 2.14). The complex roof type is the result of higher slopes, such as the buildings blocks extracted from different roof-type buildings. If the building roof is not accurately extracted (or if it does not represent the 'real shape of the roof'), its classification by roof type or any other attribute can also be wrong. However, in all the tests the roof of the building represented in Figure 2.13 was well classified after the processing stage as simple/flat in accordance with the reality.

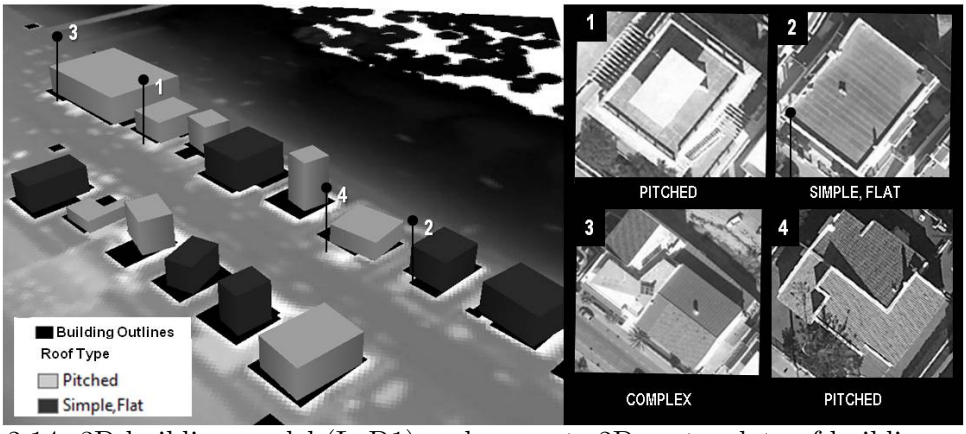

Figure 2.14: 3D building model (LoD1) and accurate 2D vector data of building outlines. The types of roofs extracted are shown, as well as the visualization of the classification of four buildings on the 3D modeL (adapted from Tenedório et al., 2013).

This demonstration shows that the automatic extraction of building parameters from LiDAR can be a great advantage for the generation of 3D block models of buildings, by extruding the building area parameter (building polygons) to building façade height values. However, the complexity and diversity of buildings with irregular sizes and heterogeneous surface structures caused difficulties in the extraction of building rooftops, therefore bringing up some difficulties in the generation of 3D building models exclusively from LiDAR data.

The LiDAR Analyst is not appropiated for this type of built-area, when there is high heterogeneity and complexity of building types, such as in Praia de Faro. The presence of this kind of complexity in an urban area makes it necessary to develop suitable methodologies for the extraction of building parameters (Section 2.3).

2.2.2 Evaluation of the LiDAR point cloud for the extraction of the building façade height parameter

The main objective of this section is to demonstrate the level of usability or

relevance of a LiDAR point cloud for the extraction of building height and building volume. Additionally, as mentioned in the previous section, we should evaluate the accuracy level that a LiDAR point cloud should achieve to ensure the acquisition of accurate building heights and thus be useful for urban planning. This demonstration was based on the development of a methodology to evaluate the accuracy of building height parameters extracted from a LiDAR point cloud. Firstly, we presented the methodology used for the estimation of building parameters. Secondly, we will compute and analyze the estimated vertical errors of building façade height estimated, as well as the total error of building volumes.

The methodology developed included a set of routine operations that have been automated and optimized, along geoprocessing models implemented in GIS and R statistical software environments. The reference data are also important for the development of this methodology, such as building outlines (2D-vector data) and accurate 3D points of the building rooftops (see Section 2.1). Therefore, the extraction of a 'set of LiDAR points' that defines the top of the building façade height (Figure 2.15) will be processed using the reference data.

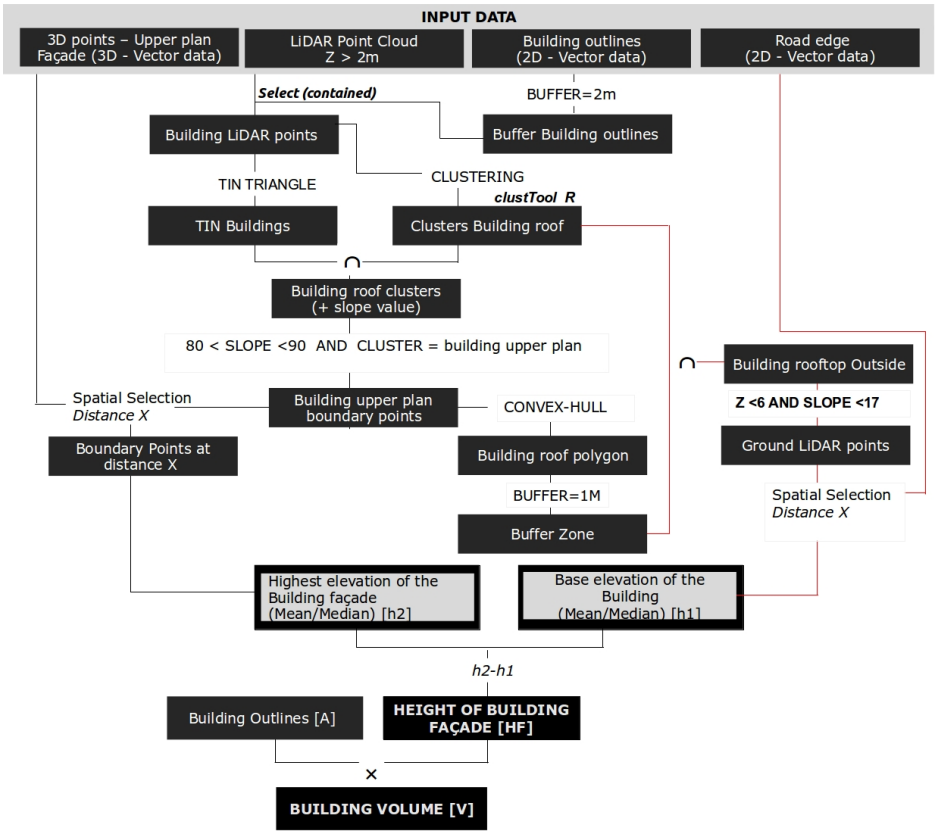

Figure 2.15: Flowchart for the extraction of building façade height and building volume from a LiDAR point cloud. The red lines in the workflow process correspond to the second part of the methodology.

The methodology for the extraction of building façade height was divided into three main parts (Figure 2.15): i) the extraction of the highest building façade elevation at the corner of the building; ii) the extraction of the building base elevation for the façade side that faces the public street; and iii) the end of this process is the computation of building façade height based on the difference between the highest elevation of the building façade and the base elevation of the building.

The first part was the extraction of *the highest elevation of the building façade*, near a cornice, parapet, rooftop railing or corner of the building façade (Figure 2.16).

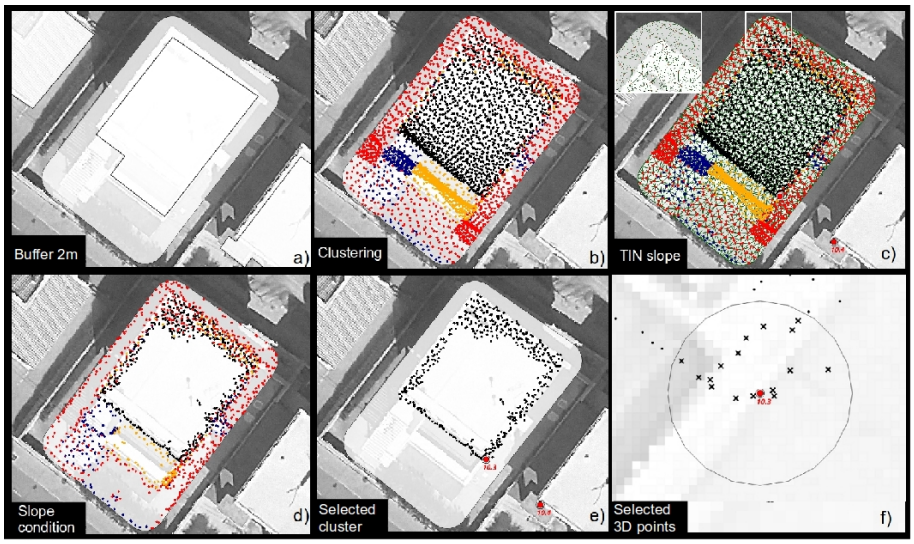

Figure 2.16: Results of first part of the geoprocessing model. a) Buffering the building outline; b) Clustering the LiDAR points of the building using elevation; c) TIN facets with slope values; d) Selected 3D points that are contained in the TIN facets within slope range values condition; e) Selected k-cluster; f) 3D points within 80 cm distance from the reference 3D point.

The following steps are followed at this stage (Figure 2.16): *i)* the selection of a set of LiDAR points contained within polygons which are generated by a buffer of 2-metre from accurate building outlines (see Figure 2.1) as shown in Figures 2.16a,b; *ii)* K-Means clustering (Hartigan & Wong, 1979) of LiDAR points (using clustTool library of R within ArcGIS) based on the elevation attribute. The objective was to delimitate the rooftops' upper plan that defines the building by k clusters. The number of k-clusters depends on the building roof type; *iii)* determining the boundary of LiDAR points which best defines the highest plan of each building roof by selecting the 'cluster and a range of slope values obtained from a Triangulated Irregular Network (TIN)' condition. The selection of clusters was based on a visual inspection. Next, the slope values were calculated from a TIN facet polygons gen-

erated by LiDAR points clustered. Finally, the cluster points that are contained in each TIN facet with a slope between 0° and 79° were removed; and *iv)* computing the average and median values of selected LiDAR points, which are within 80 cm of the reference 3D point of the rooftop (which defines the highest point of the building façade). In the case of certain buildings, we had to change this value to 40 cm to reject points that were incorrectly classified as rooftop.

The delimitation of all roof sections with different orthometric heights (Figures 2.16b,c) was achieved with clustering. However, the visual inspection was important to select the clusters that better represent each building rooftop. In Figure 2.16b the building is described by 4 clusters, but only the points that belong to cluster 2 (black points) are selected with a slope range between 80° and 90° (2.16d,e).

Subsequently, the extraction of *the base elevation building* was divided into the following four main steps (Figure 2.17): *i)* The boundary of each building rooftop was designed by the LiDAR points selected in the first stage, through the convex hull (Figure 2.17a). The term convex hull used by Park & Oh (2012) means 'the boundary of the minimal convex set containing a given non-empty finite set of points in the plane'; *ii)* The LiDAR points that are outside the convex hull polygon ('outside LiDAR points') within a buffer of 1 m from the boundary of the building polygon ('base building area') were selected (Figure 2.17b); *iii)* Afterwards, the 'LiDAR ground points' should be selected from 'outside LiDAR points' by a 'range elevation values and range slope values' condition. The condition was *the 3D points with an elevation lower than 6 m and contained in a TIN facet with a slope between 0° and 17°* (Figure 2.17c); and finally *iv)* computing the average and median values of 'LiDAR ground points' selected from the following spatial selection condition: 'LiDAR ground points' that belong to the base building area and are at X distance value from edge road.

The results of the second part of this methodology can be seen in Figure 2.17 for one building.

The LiDAR ground points selected at the end of this process (Figure 2.17d) were used to calculate a median elevation or the average value that represents the base elevation of the building. The end of this process is the computation of building façade height based on the difference between the highest elevation of the building façade and building base elevation. The building volume was also computed for each building from the area of building outlines and building façade height estimated from

LiDAR.

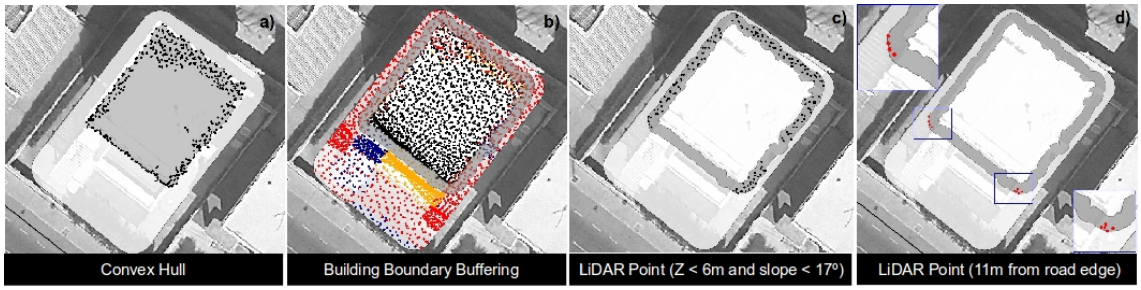

Figure 2.17: Results of the second part of the geoprocessing model - extraction of building base elevation. a) Building rooftop boundary from convex hull; b) One metre buffer from boundary of building rooftop; c) Lidar points outside the boundary; and d) LiDAR ground points selected for the estimation of building base elevation.

The building façade height parameter for the building (Figures 2.16 and 2.17) was estimated at 6.27 m (median value). The vertical error in the estimation of this parameter was only 10 cm in relation to the reference value of 6.47 m.

The evaluation of the building façade height parameter estimated for the 22 buildings of the study area was based on the difference between the reference building façade height and building façade height estimated from LiDAR, also called by vertical error. The following plots (Figure 2.18) show the vertical errors obtained for each building. The left plot shows the building façade height error achieved with median elevation values of building rooftop and base (Figure 2.18a), while the right plot is based on the average elevation values of the buildings.

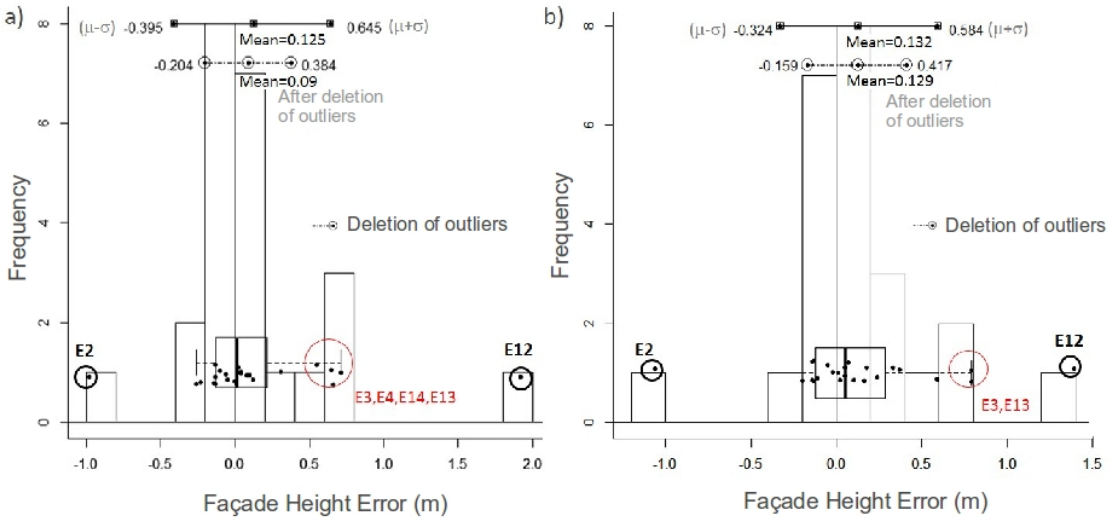

Figure 2.18: Distribution of building façade height errors by histograms, box and whisker plot. a) Median elevation of the selected LiDAR points; and b) Average elevation of the selected LiDAR points (adapted from Rebelo et al., 2012).

The variability of vertical error is higher for the 'average elevation values' plot on the right (0.38 m) than for 'median elevation values' plot (0.30 m) as shown in the interquartile range. Most vertical errors are lower than 0.2 m as can be seen on the histograms and boxes.

Therefore, both plots in Figure 2.18 identify two outliers E2 and E12 buildings (dark circle). For the right plot based on average measure the vertical errors were -1.06 m and 1.39 m, respectively (Figure 2.18b). On the other hand, for the same buildings, the vertical errors based on median measure were -0.98 m and 1.92 m (Figure 2.18a), respectively. These two vertical errors represented blunder errors. The E12 building suffered changes around its base (vegetation, grass or other elements), between 2009 and 2012 because there is a higher variability in 3D points measured by the GPS survey and the LiDAR flight. The vertical error of the E2 building resulted from an incorrect measurement of the base building elevation. The deletion of these two outliers in the first methodology (Figure 2.18a) means that approximately 73% of the vertical errors are within one standard deviation of the mean, but 4 new outliers (E3, E4, E14, E13) were identified. However, for the 'average building façade height' approximately 82% of the vertical errors are within one standard deviation of the mean, where 2 new outliers were identified (E3,E13).

The use of two different roof points for the same building was tested for two buildings – E13 and E14 (Figure 2.20). This was essential to understand how the selection of a particular type of point on the roof can influence the accuracy of the estimated building façade height. This point will be discussed in more detail later.

A statistical analysis was performed for the same sample in order to find whether there is any correlation between the magnitude of vertical error and: a) the rooftop point type (cornice, eave, parapet,...) chosen to estimate rooftop elevation; and b) the characteristics around the base of the building such as vegetation, trees, building elements or any other objects. Thus, two variables *building rooftop class* and *building base variation level* were designed for this particular analysis. The *building rooftop class* classifies the rooftop point into one of three classes: C1 - flat rooftop corner; C2 - rooftop railing or parapet wall; C3 - brick roof edge ('platibanda') or eaves. The *building base variation level* describes the level of variation around the base of the building that can affect the building base elevation value. Three classes were defined: G1 - 'clean area', without trees, vegetation or any other objects (lamps, stairs,..); G2 - vegetation or other built elements that can create higher gradients; and G3 - vegetation and other built elements.

The outliers of vertical errors revealed that the variability level in the extraction of this building parameter from a LiDAR point cloud is higher (Figure 2.19). According to each of the two variables – *building rooftop class* and *building base variation level* – the vertical errors obtained for the buildings E3, E4, E13 and E14 share some similarities: a) the building rooftop is type C2 (E13 and E14 have the same rooftop railing type; and E3 and E4 share the same parapet wall type); and b) the ground base of buildings E4 and E14 classified as G3 (vegetation and other built elements) contributed to an even greater vertical error.

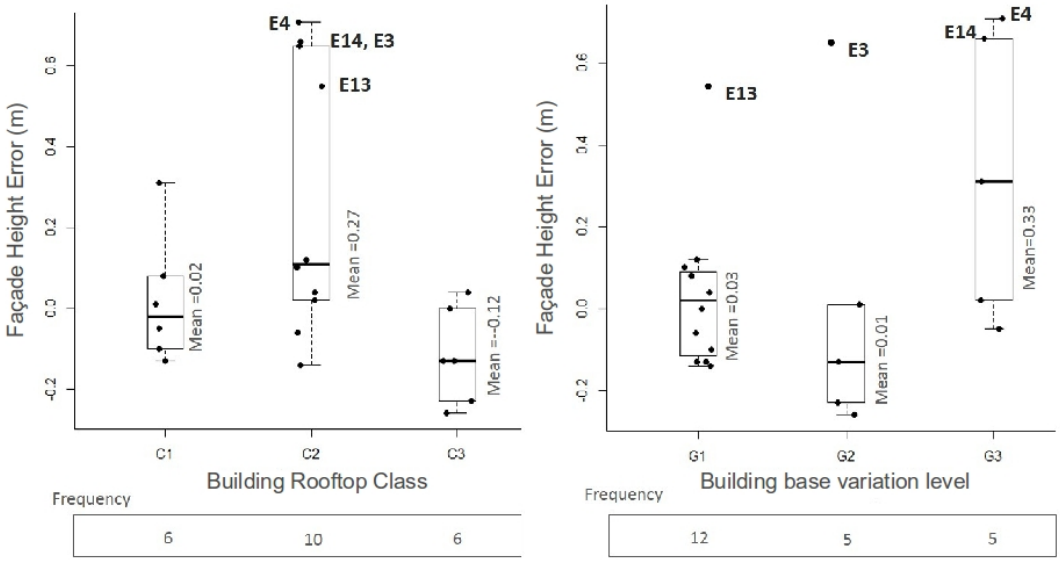

Figure 2.19: Distribution of building façade height errors (using median) by building rooftop class and building base variation level (adapted from Rebelo et al., 2012).

The vertical error variability is higher for the buildings that were classified as C2 and G3, whose interquartile range is 0.60 m and 0.64 m, respectively. This result shows that the conditions defined for filtering LiDAR points on building rooftops are not accurate for these type of roof points. It is difficult to remove 3D points that are located on the façade or other discontinuities along the building. Therefore, the vegetation detected and registered along the base of the building by the LiDAR point cloud is residual for these types of applications, and should be removed by an effective filtering.

Figure 2.20 depicts the behaviour of the vertical error for each combination of building type variables. This plot shows that: i) the highest vertical errors were registered for the combination G3.C2 (buildings E4, E14); ii) the maximum value of vertical error and the highest variability was obtained for type C2 buildings, whatever the level of building base variation; iii) the combination of G1.C1 and G1.C3

allowed us to estimate building façade height with greater accuracy and reliability; and iv) whatever the type of building rooftop, G3 highlights more variability.

For buildings E13 and E14, two building façade heights were estimated from different roof points (Figure 2.20). The vertical errors obtained for each of the two distinct points chosen on the roof of building E13 was 0.55 m on the roof railing and -0.14 m on the roof eave. Building E14 had a vertical error of 0.66 m for the point in roof railing, while for the point in the roof eave the vertical error was -0.05 m. This is an evidence that the selection of roof point type is important to acquire vertical accuracy for building façade height. On the other hand, there is low reliability in roof railing points for the extraction of this building parameter.

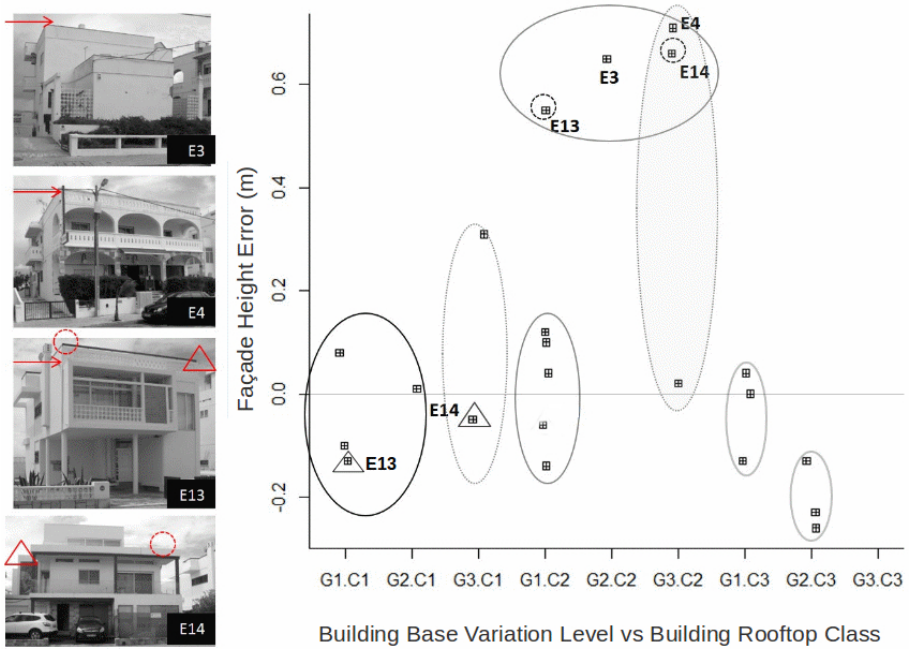

Figure 2.20: The behaviour of median building façade height errors by the combination of the two variables *building rooftop class* and *building base variation level* (adapted from Rebelo et al., 2012).

The 3D building model represented in Figure 2.21 shows the building façade height errors (based on the median measure) for each building. The two buildings E2 and E12 were removed, so they are not shown in that Figure, because they have been identified as blunders. On the other hand, the two buildings E13 and E14 are represented by an absolute vertical error value that is lower than 0.15 m in the roof points of the roof eave. This resulted in only two buildings whose vertical error was higher than 0.2 m (Figure 2.21), where the maximum building façade height error of 0.70 m was estimated for building E4. The magnitude of these errors obtained

was due to difficulties in the extraction of the points, because of the complexity of these building types.

Figure 2.21: Distribution of vertical errors for each building, where the two vertical errors identified as outliers were not represented (E2 and E12)(adapted from Tenedório et al., 2013)

The 3D building model (Figure 2.22) shows the volume of each building according to the number of stories. As we can see, the buildings with more vertical errors in terms of building façade height (Figure 2.22) were removed from the sample. The building façade height parameter estimated from LiDAR was used to calculate the total building volume.

What is the impact of these vertical errors in the estimation of total volume? The absolute total volume error estimated was 783 m^3 equivalent to 3% of the total reference building volume (calculated using the building façade height reference) for all the 22 buildings (about 20096 m^3).

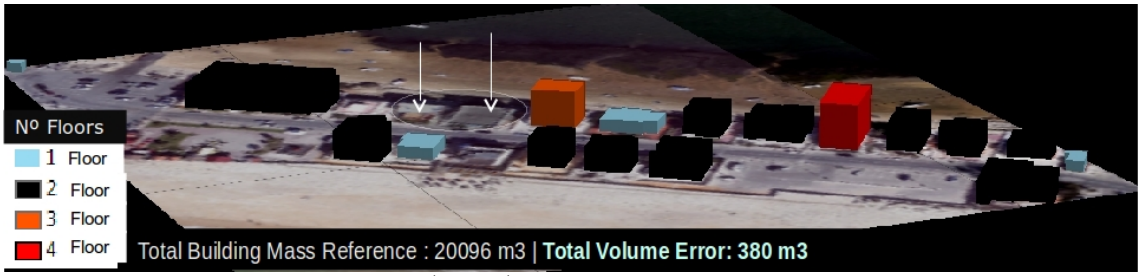

Figure 2.22: 3D building model (LoD1) that represents the distribution of buildings by the number of stories and the visual perception of the volume of each building (adapted from Tenedório et al., 2013).

However, for 18 buildings (Figure 2.22) with a vertical error below 20 cm, the absolute total volume error was 383 m^3, which is equivalent to 2% of the true total volume value or about 50% of E13 building volume.

2.2.3 Evaluation of LiDAR point clouds for the characterization of building roof types.

The classification of building roof types from a LiDAR point cloud was tested by various authors, such as Hofmann et al. (2009) who used cluster analysis, and Alexander et al. (2009), who used the slope parameter of the TIN polygons within the building footprints. The automatic identification of roof types and building materials using a LiDAR point cloud can be very useful for energy usage, but also to aid in fire fighting (Herold & Roberts, 2010).

The purpose of this subsection is to characterize roof types from a LiDAR point cloud using a clustering technique in a GIS environment. For this purpose, four variables are used, such as orthometric height and intensity of the laser pulse (included in LiDAR data), the point density and slope derived from DSM. The elements of a building rooftop will be assigned as sub-objects that belongs to a single object (object-roof) defined by the building rooftop boundary.

The methodology developed was integrated into GIS spatial analysis functions. The flowchart of this methodology is detailed in Figure 2.23.

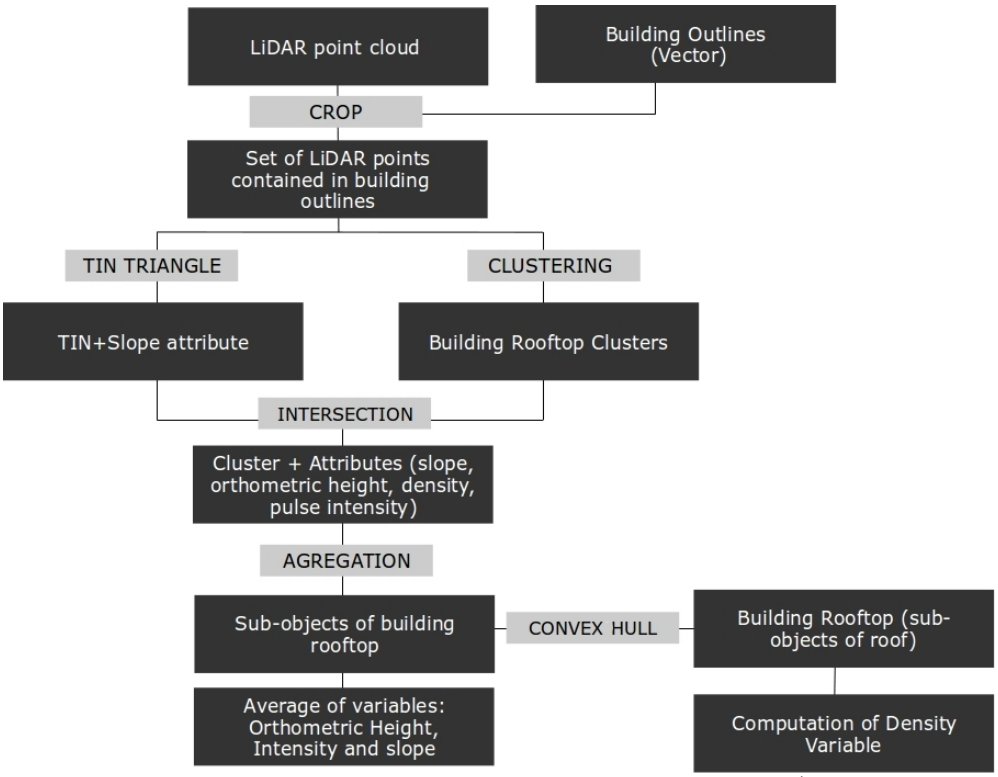

Figure 2.23: Flowchart of characterization roof type characterization (adapted from Rebelo & Tenedório, 2011b).

The main objective was obtaining an average value of sub-objects for each variable defined above. The sub-objects that will identify each element of the building roof were extracted by using the K-means Clustering Method (Hartigan & Wong, 1979) implemented in Rtools (toolbox for ArcGIS software).

The clustering was only performed for the LiDAR points that were contained within building outlines (object-roof). The clusters were obtained by using orthometric height variable, which allowed us to identify the different elements of the roof.

Afterwards, the average value of slope, height, and intensity were computed for each sub-object cluster within a building rooftop. Moreover, the point density value was computed on the ratio between the number of clustered LiDAR points and the area of the cluster.

The building rooftop's polygon was extracted from clustering by the convex hul algorithm implemented in ArcGIS software. This methodology was successfully applied to the flat roofs. The complex building rooftops (Figure 2.24a) were removed, because the clustering failed to successfully set the roof elements (Figure 2.24b).

Figure 2.24: The set of buildings removed. a) orthoimage and building outlines; b) Clusters of complex roof types.

Considering the bivariate Pearson correlation for the analysis of the relationship between the 4 variables stated above, the three following aspects can be mentioned (Table 2.7): a) indicates a slightly negative but non-significant correlation (Pearson $r = 0.34$) between intensity and orthometric height; b) weak

correlation (almost null) between the density of points per m^2/slope and between point density/intensity; c) moderate negative relationship (Pearson $r = -0.55$) between slope and intensity; and d) moderate positive correlation (Pearson $r = 0.47$) between point density and orthometric height.

Table 2.7: Statistical values of cluster sample obtained from LiDAR points

Variables	Average elevation	Average intensity	Average slope	Average point density
Average elevation	1	-0.34	0.37	**0.47**
Average intensity		1	**-0.55**	-0.24
Average slope			1	0.15
Average point density				1

Sample of clusters (sub-objects): 30; Confidence level: 95% to p=0.05.

Otherwise, if only similar clusters of building rooftops are selected (Figure 2.25) from a total of 30 extracted clusters (sub-objects), the negative correlation between slope and intensity variables increases to -0.77 for a small sample of 10 clusters.

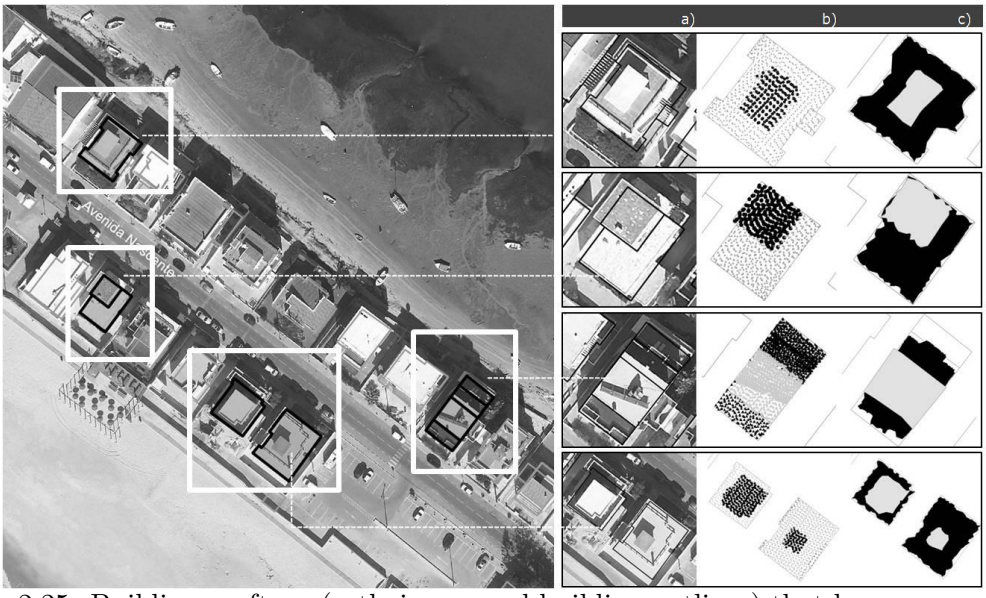

Figure 2.25: Building rooftops (orthoimage and building outlines) that have a correlation between intensity and slope: a) Orthoimage; b) Clusters; c) Building rooftops extracted from convex hull (adapted from Rebelo & Tenedório, 2011b).

The combination of the highest roof slopes (such as a terrace) and the highest

colour gradients resulting from the different materials used (red ceramics and white ceramics) will allow us to extract a set of building roof types pitched and contrasted by colour, material, or texture.

2.3 *Testing and comparing the usability of LiDAR and low cost UAV data for the extraction of building parameters using FOSS.*

The demonstration of the usability of a 3D point cloud for the extraction of building parameters without any other spatial reference data is the challenge proposed for this section. A higher level of automation in the acquisition of these building parameters using FOSS tools is also an objective of this demonstration, while simultaneously asserting the usability of this type of data in a 'low-cost environment'.

The usage of 3D point cloud data for the extraction of building parameters without reference data is the main objective of this case study. The need to obtain low-cost information about the territory with a higher degree of automation and updating has become a priority in this work. On the other hand, the combination of low-cost data with the development of a robust methodology based on FOSS tools is also a priority.

The methodology developed for UAV or LiDAR point clouds has three main stages (Table 2.8).

Table 2.8: Stages, tools, and data used in the methodology

Stages	**Data**	**Tools**
Extraction of the building elements (3D points): rooftop and ground	3D point cloud	R, GRASS and PostgreSQL/PostGIS
Computing building volume from building façade height and building area	Extracted 3D points and building boundary	PostgreSQL/PostGIS
Evaluation of building parameters	2D and 3D reference data	PostgreSQL/PostGIS

The first stage included the development of a semi-automatic methodology to

identify the relevant 3D points that better describe each building from a 'big volume of 3D data'. Part of this methodology implied the development of two algorithms in postgreSQL/PostGIS and R. The second stage included one algorithm to compute the volume of each building from 3D points extracted in first stage. Finally, the third stage consisted in the evaluation of all building parameters obtained from each point cloud data. In table 2.8 the data and tools used at each stage are detailed.

This methodological solution composed by the three main stages earlier mentioned was developed for this case study. We called it ***3D E**xtraction **B**uilding **P**arameters* – **3DEBP**, which will allow the extraction of building parameters using any 3D point cloud. The following subsections will describe each step of this 3DEBP solution.

2.3.1 Extraction of building elements from a 3D point cloud

The first part of the methodology developed for the extraction of building parameters from each point cloud was based on the following assumptions: i) extracting building parameters without accurate vector data, only a 3D point cloud should be used; and ii) using FOSS tools to implement a robust methodology for the acquisition of these parameters.

First, it is important to define which building parameters are involved in estimating building volume (Section 2.3.2) and then how to extract them from a 3D point cloud. The parameters are: i) building façade height, which is the difference between mean elevation of the top building boundary (these are approximately the points that define the eave or parapets of the rooftop) and the mean elevation of the ground near the building. The façade side of the building that faces the public street was chosen to compute this parameter; and ii) area, which is defined from the building façade height boundary, which is equivalent to the building roof area.

The methodology developed for each point cloud data included the following steps (Figure 2.26): i) selection of the set of points from point cloud that represents the building roofs. This filtering applied to the point cloud was performed by Clustering LARge Applications (CLARA) algorithm, which is implemented in the RCLUSTER library; ii) extraction of the building roof area was based on the generation of polygons from the points selected above, using the concave hull algorithm implemented in GRASS 7; these polygons represent the building roof area; and iii) selection of the set of points that represent top and ground building façade using

spatial analysis functions.

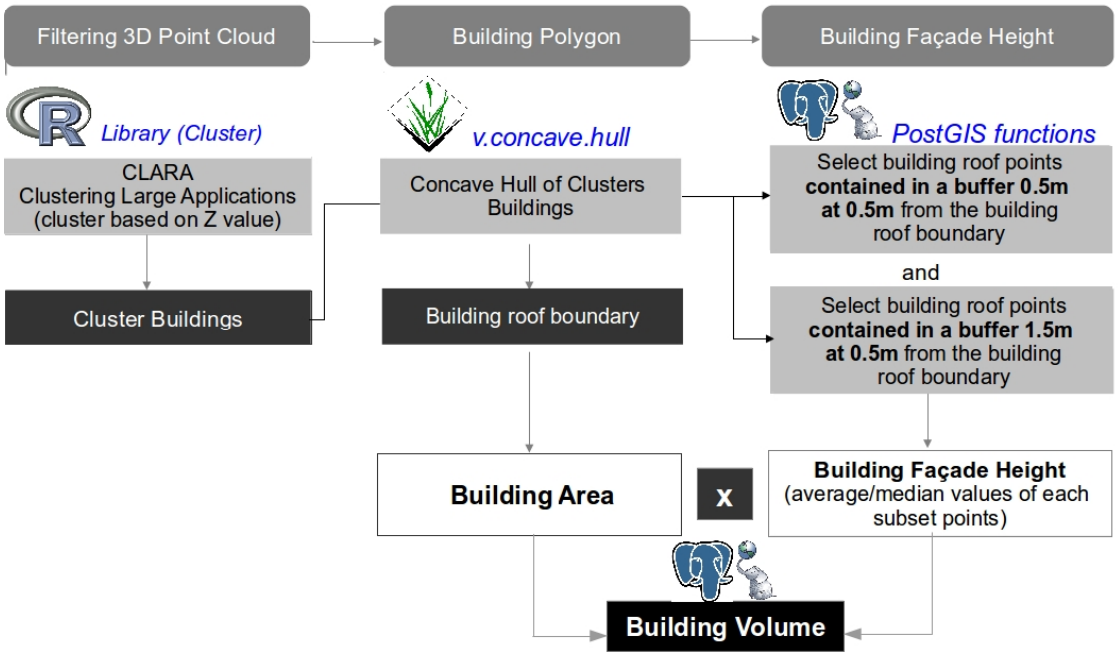

Figure 2.26: 3DEBP methodological approach for the extraction of building area, façade height, and volume from a 3D point cloud based on a FOSS solution (adapted from Rebelo et al., 2015).

All the steps above have been implemented in three algorithms for the automation of the methodology. The algorithms were developed using R programming language (CLARA algorithm) and SQL language in a GDBMS environment implemented using PostgreSQL/PostGIS for the steps i) and iii) mentioned above.

Point cloud clustering

Kaufman & Rousseeuw (1990, p.14) say that the clustering 'wants to form groups in such a way that objects in the same group are similar to each other, whereas objects in different groups are as dissimilar as possible'. Clustering in an object-oriented environment was the solution chosen to filter building points from 'big data'. However, the clustering algorithm should also be able to process big data. Among a variety of clustering algorithms implemented in the RCLUSTER library, the CLARA (RCLARA) algorithm is suitable for clustering large datasets as point cloud data.

The CLARA algorithm was especially developed to deal with large applications (Kaufman & Rousseeuw, 1986). This algorithm consists in a partitioning of a dataset into k-clusters (or k-groups) that show a high degree of similarity,

around k representative objects also called the *k-medoids* of the cluster (Kaufman & Rousseeuw, 1990). The requirements of a partition method are: a) each cluster must have at least one object; and b) each object must belong to exactly one cluster.

The use of CLARA for clustering the point cloud was carried out following two steps: a) a sample was drawn from the point cloud and clustered into k subsets, which also gives *k-medoids*; and 2) each object that did not belong to the sample was assigned to the nearest of the representative objects (also called *k-medoids*).

These two steps are based on the computation of the average distance between each object and its representative object, which represents a measure of the quality of the clustering. After all the s samples have been drawn and clustered, we selected the one for which the lowest average distance was obtained.

The dataset point cloud is represented by a matrix of millions of 3D points (objects), where each point is an object identified by three spatial variables (x, y, z) that belong to a spatial entity (buildings, ground, ...). The n-rows correspond to the objects (3D points) and the columns correspond to the spatial variables x, y and z.

$$n \textit{ objects of a point cloud} = \begin{matrix} \\ \\ x_{11} \\ x_{21} \\ \vdots \\ \vdots \\ x_{n1} \end{matrix} \begin{matrix} \textit{varx} \\ \\ x_{12} \\ x_{22} \\ \vdots \\ \vdots \\ x_{n2} \end{matrix} \begin{matrix} \textit{vary} \\ \\ x_{13} \\ x_{23} \\ \vdots \\ \vdots \\ x_{n3} \end{matrix} \begin{matrix} \textit{varz} \\ \\ \\ \\ \\ \\ \\ \end{matrix} \tag{2.2}$$

The methodological approach for this study is to cluster the point cloud into groups (k-clusters) that are similar: 'non-building points' and 'building points'. This clustering was performed using the spatial variable z, because it allows a rough identification of the ground and non-ground points. Then, the clustered point cloud will be represented by a vector $PC = \{x_{13}, x_{23}, x_{33}, ...x_{n3}\}$.

According to the nature of the objects present in the point cloud, the clustering process for each point cloud was performed for k (number of clusters) values between 2 (kmin) and 10 (kmax). This part of the clustering process was done by the following algorithm as shown in Listing 2.1 developed by Maechler (2015, p.15), which allows to generate the silhouette plots for each k-cluster that we will see later.

Listing 2.1: Clustering for k-clusters (kmin and kmax)

```
library (cluster)
kmin <- 2
kmax <-10
s <-100
c10 <- c("tomato", "forest green", "dark blue",
        "purple2", "goldenrod4","gray20","red",
        "yellow","blue","green")
for(k in kmin:kmax){
    plot(silhouette(clara(z, k=k, metric="euclidean", samples=s)),
    main = paste("k = ",k), do.n.k=FALSE,
          col = c10[1:k])
}
```

However, the s parameter[4] related to the number of samples used in the clustering process ranged between 10 (s) and 100 (smax) should be chosen. Listing 2.2[5] allowed us to verify the best s value, which is developed by Maechler (2015, p.15). Thus, if the results between the minimum and maximum s values are equal, then the minimum value s is enough for the clustering process (Listing 2.2).

Listing 2.2: Verification of clustering for s between 10 to 100

```
s <-10
smax<- 100
clx10 <- clara(z, k, samples=s)
cl.10 <- clara(z, k, samples=smax)
stopifnot(cl.10$clustering == clx10$clustering)
```

The evaluation of the clustering results obtained from the CLARA algorithm was performed by a graphical representation called *silhouettes*. The silhouette plots were obtained for each clustering process, which was implemented in R statistical software. The silhouettes are represented in a single diagram and each silhouette shows which objects lie well within one cluster (Kaufman & Rousseeuw, 1990). The silhouettes are very useful to analyse and compare the different clusterings obtained along this stage and it allowed us to choose the best result.

Each silhouette that represents all the clusters within a k-cluster processing allows us to choose the best clusters that represent the buildings. The best k-cluster should have an average similarity close to one.

[4] In this study the first value tested was $s = 10$.

[5] If the result was false, it implies that clustering results are the same for s and $smax$.

Following Kaufman & Rousseeuw (1990), two statistical measures were obtained at the end of the clustering process, where they are presented in each silhouette plot: a) **Average silhouette width of one cluster** s_i and b)**Average silhouette width for clustering** $\overline{s}k$. These two statistical measures summarize the quality of the results obtained for each clustering.

These two parameters are described below:

- **Average silhouette width of one cluster** s_i

  s(i) allows us to evaluate how well object i was matched with the cluster (Kaufman & Rousseeuw, 1990). s_i is given by the following equation:

$$s(i) = \frac{b(i) - a(i)}{max(a(i), b(i))}, -1 \leq s(i) \leq 1 \tag{2.3}$$

  where, $a(i)$ is the average dissimilarity of object i from all the other objects of a cluster A and $b(i)$ corresponds to the smallest value of $d(i, C)$ computed for all clusters $C \neq A$. $b(i)$ is given by the following equation

$$b(i) = min\, d(i, C), C \neq A \tag{2.4}$$

  where, $d(i, C)$ is the average dissimilarity of i from all objects of any cluster C different from cluster A.

  The interpretation of s_i is seen in Table 2.9 (Kaufman & Rousseeuw, 1990, p.85):

Table 2.9: Interpretation of s(i) values obtained for each cluster

s(i)	**Description**
close to 1	object i is 'well clustered' and has been assigned to an appropriate cluster.
close to 0	object i should lie between two clusters. This is an 'intermediate case', where it is not clear what cluster object i has been assigned.
close to -1	object i has been 'misclassified'. Probably object i was placed in the wrong cluster.

  Furthermore, the silhouette plot shows the average of s_i for all objects i that belong to a cluster called 'average silhouette width of one cluster'.

- **Average silhouette width of clustering $\overline{s}k$**

  The most difficult decision is to choose the 'most appropriate' value of k in a cluster analysis problem, because for the same problem there may be several solutions. The latter parameter which represents the average of s_i for $i = 1, 2, ...n$ is denoted by $\overline{s}k$. This parameter should be chosen as high as possible among a set of clustering results for the entire data set. According to Kaufman & Rousseeuw (1990, p.88) an approximation for the interpretation of 'average silhouette width' based on silhouette plot can be seen in Table 2.10 below:

Table 2.10: Interpretation of Average silhouette width for clustering (Kaufman & Rousseeuw, 1990, p.88)

$\overline{s}k$	**Interpretation of the clustering structure**
0.71-1.0	strong
0.51-0.7	reasonable
0.26-0.5	weak
< 0.25	not significant

The appropriate number of k-clusters for the point clouds of this case study ranged from 2 to 10. Subsequently, the algorithm was run between these values where the silhouette plots were also generated, as detailed in Listing 2.1. A visual analysis of the silhouette plots helps us to understand what the best k for clustering buildings is. Kaufman & Rousseeuw (1990, p.96) say '(...) we want the silhouettes to be as wide (or as dark) as possible.' The wider the representation of the silhouettes for a k-cluster, the larger the degree of similarity in that cluster shall be.

After computing the silhouette plot of a clustering into k-values ranging from 2 to 10, the next step is to choose the 'best' number of k for this dataset by meeting the following conditions: a) large average s_i values, as close to 1 as possible and without negative average s_i; b) highest value for average silhouette width [$\overline{s}k$]; and c) highest average $s(i)$ values for clusters that represent buildings.

The chart on the left in Figures 2.27, 2.28, and 2.29 shows the silhouettes for the best clustering results into k=2 clusters of the UAV point cloud data and k=10 clusters of each point cloud data (LiDAR or UAV). These silhouettes were chosen based on the criteria above. The silhouette contains on the rightmost columns the index of each cluster [j], the neighbour of each cluster [n_j] and an average silhouette width of each cluster [$ave_{i \in C_j s(i)}$]. The average silhouette width of clustering value

appears below the plot $[\overline{s}k]$. The silhouetes plotted allowed us to do an empirical analysis of the clustering structure.

In general, some clusters are more divided in case of higher k values. On the other hand, the size of the samples n depends on the number of clusters and it is given by $40 + 2k$ (Kaufman & Rousseeuw, 1990, p.145). Then for a clustering process defined as k=10 clusters (Figures 2.27 and 2.29) the size of the sample is 60. Lastly, the right images of these figures show the clusters of the 3D point cloud and the selection of clusters that only represent the buildings.

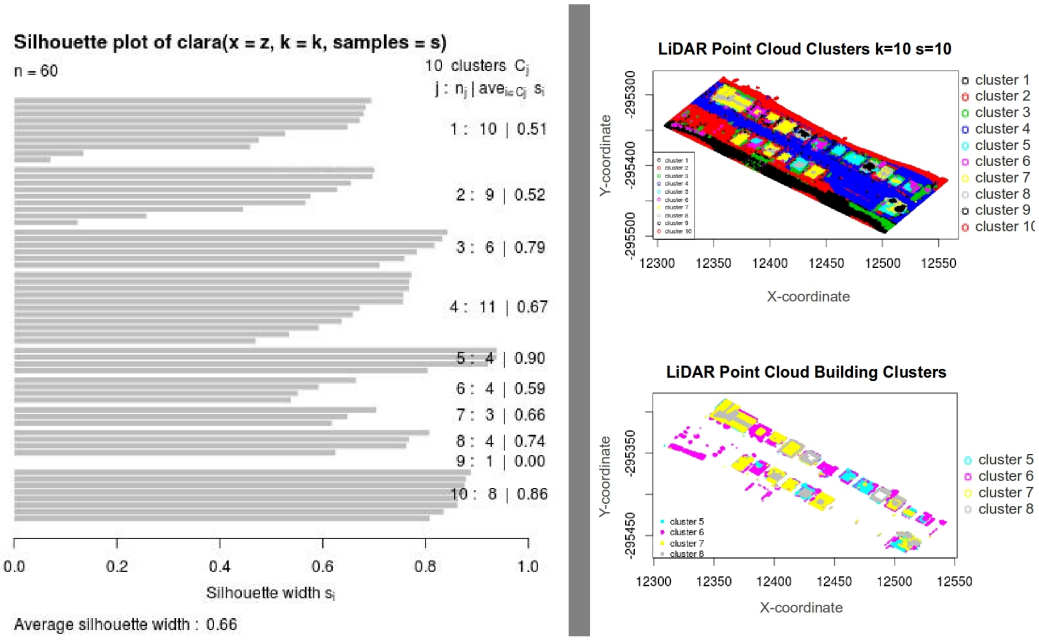

Figure 2.27: Silhouette plot for LiDAR point cloud clusters (k=10)

The LiDAR point clustering for k=10 clusters (Figure 2.27) obtained an average silhouette width of 0.66. For this sample, only 4 clusters represent the buildings, where the average s_i ranges between 0.59 to 0.90. These s_i values mean that these clusters are well clustered. However in cluster 7, there are some built structures that are not considered for this study, such street cafés.

After computing the silhouette plot for the UAV point cloud, we found that there were two appropriate number of k-clusters k=2 and k=10 for this data set. Both were used for the extraction of building heights to compare with the performance of slightly different clusterings. However, the clustering for k=2 seems better than k=10, because it identifies the objects that belong to the buildings and 'not buildings' with only 2 clusters.

The UAV point cloud silhouettes resulting from a number of clusters k=2

(Figure 2.28) have a strong clustering structure (0.82), where the clusters are more compact and clearly separated unlike k=10. The clustering structure for the UAV point cloud is worse for k=10 (0.59), where the clusters obtained from the UAV point cloud are more divided when compared with the number of clusters (Figure 2.29). Also, the clusters that represent buildings have narrower silhouettes.

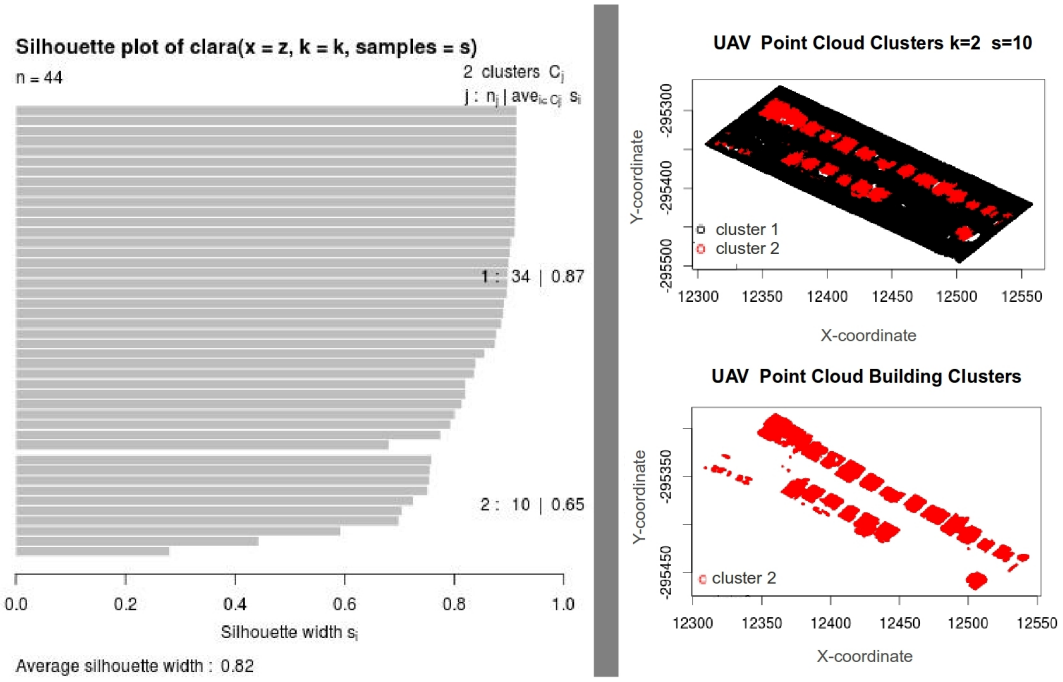

Figure 2.28: Silhouette plot for UAV point cloud clusters (k=2).

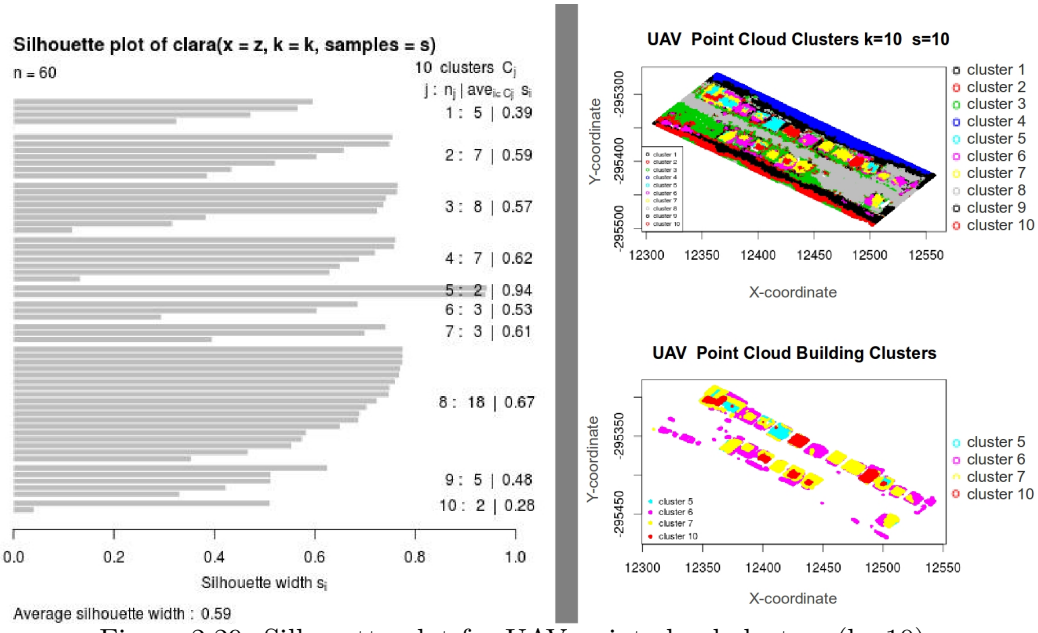

Figure 2.29: Silhouette plot for UAV point cloud clusters (k=10).

On the other hand, for the same number of clusters k=10, the clustering

structure for the UAV point cloud is slightly worse than the clustering structure of the LiDAR point cloud. This conclusion is obtained not only reading the average silhouette width clustering value, but also from the height of the represented silhouettes. The clustering of the UAV point cloud seems to divide some natural clusters in an artificial way, thus becoming narrower silhouettes.

The four UAV point cloud clusters (k=5,6,7,10) that represent the buildings are well clustered for k=10, because the minimum and maximum average s_i values range from 0.28 to 0.94 (Table 2.9). However, the structure of k-cluster 10 is weak (0.28) and could be artificial (Table 2.10). Table 2.11 summarizes the results obtained in the silhouette plots above, which shows the best k-clusters selected for each point cloud clustered representing the buildings. All these k-clusters have an average s_i greater than 0.2, which means that 3D points have been well classified within the cluster.

Table 2.11: Point cloud

Point cloud	k-cluster for entire data set,$\bar{s}k$ value	Classification of the clustering structure	Number of k-building clusters
LiDAR	0.66, k=10	reasonable	k=5,6,7,8
UAV	0.82, k=2	a strong	k=2
UAV	0.59, k=10	reasonable	k=5,6,7,10

All the clusters that represent buildings from each point cloud were selected for the next step of the methodology.

Extraction of building rooftops from point cloud clusters

The extraction of the building roof area was based on the generation of polygons by the points selected from clustering, using the *concave hull* algorithm implemented in GRASS 7.

The representation of building rooftop could be done by a convex hull from a dataset of points, where any segment line obtained from a pair of points is completely contained in the hull. According to Park & Oh (2012), the convex hull 'indicates the boundary of the minimal convex set containing a given non-empty finite set of points in the plane (or n-dimensional space)'. In practice, the vertices of the convex hull are points of a set of points and all the points of the subset are contained in the hull (Berg et al., 2008). However, the convex hull does not extract isolate buildings from a set of points with a distribution as presented in the previous section. Therefore,

the concave hull is a better choice to extract the shape of building rooftops from around vector points.

A more *concave hull* could be defined by a threshold value, which allows us to select the segment lines whose length is closer to the real shape of the building rooftop. Unlike the convex hull, for this type of geometry there may be a pair of points that are not contained in the hull.

This procedure was made by using the algorithm *v.concave.hull* implemented in GRASS 7. This algorithm creates a *concave hull* using Delaunay triangulation based on a subset of 3D vector points of a point cloud. This algorithm produces a TIN from the set of 3D vector points. Then, these triangular faces are converted into segment lines. Finally, part of the segment lines will be rejected if their length is above the threshold value defined by the user. This threshold value ranged between 0 and 10, where the lower values generate a more *concave hull* and for the higher value the hull will be convex (Figure 2.30).

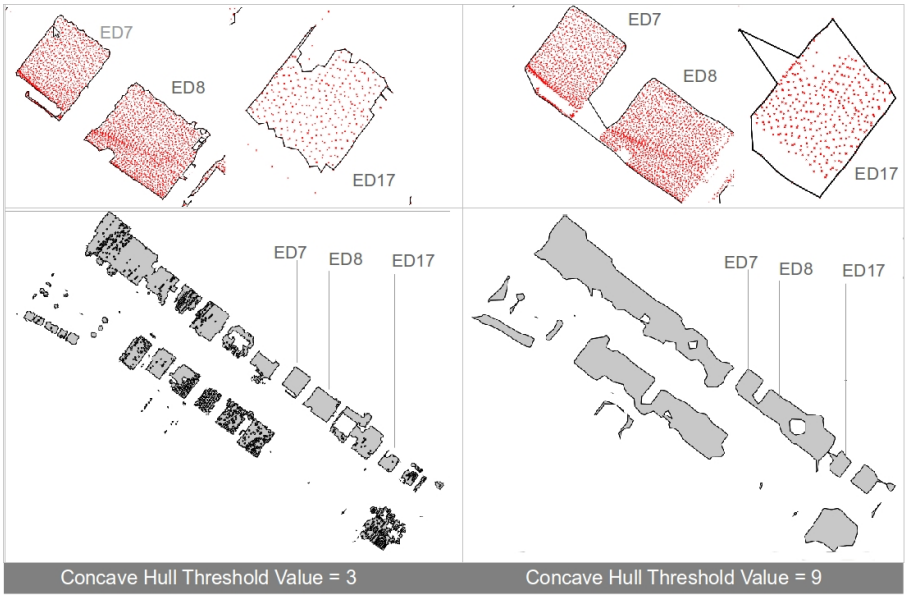

Figure 2.30: Extraction of building area by *concave hull* applying different threshold values.

This procedure is not automatic because the choice of the polygons that better represent the building rooftops requires a strong user interaction. The application of a threshold value for the *concave hull* that allows us to extract all the building rooftops is also not easy. Therefore, for the same set of points it was necessary to test various threshold values to extract the best shape for each building. Figure 2.30 shows different threshold values applied to the same subset of 3D points obtained from LiDAR point cloud clusters, whose lowest threshold value (3) allows

us to better extract the shape of the buildings.

Therefore, after the *concave hull*, it was necessary to remove small areas[6]. According to building typology the set of thresholds for this operation ranged between $10 - 30m^2$. This operation means that the polygons with an area between these range values are removed.

Figure 2.31 shows the results obtained for the clustering of the LiDAR point cloud, where most building rooftops are extracted by a threshold value of 3 for the *concave hull*. The extraction of building rooftops was also performed for the two other cluster samples of the UAV point cloud, based on the same methodology. For these cases, the threshold value for the *concave hull* was higher than the values used for LiDAR, which ranged between 8 and 9.

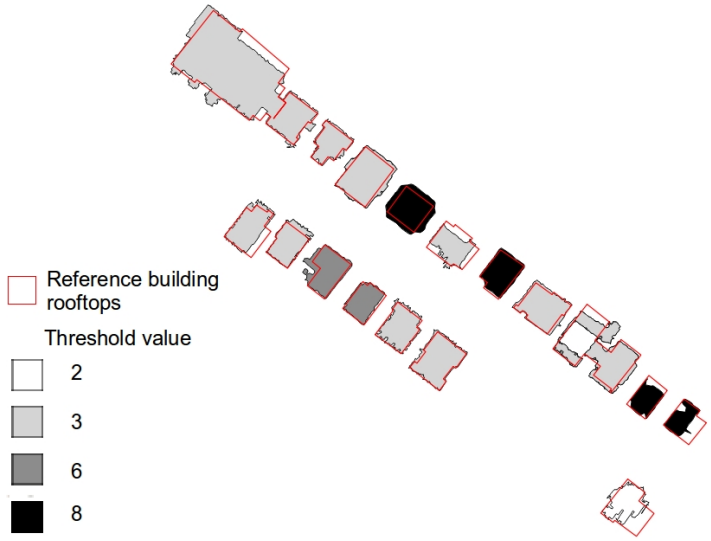

Figure 2.31: Extraction of building rooftop by *concave hull* based on different threshold values.

The extraction of vector building rooftops enables the computing of building area parameter. This parameter will be presented in the next subsection.

Extraction of 3D points that represent building rooftop edges and building base

The computing of building height was based on the selection of the set of points that represent the eave of the building rooftop and the ground base of the building, using a set of simple PostGIS spatial analysis functions. This procedure

[6] Small areas are removed using the algorithm *v.clean* of GRASS.

was done in a spatial database extender for a PostgreSQL/PostGIS database management system. The development of an algorithm in SQL using the PostGIS library (*http://postgis.net/*) that introduces spatial objects for PostgreSQL was carried out, called *building_top_base.sql*. The algorithm enables the automatic selection of a set of points in a few seconds. The various steps involved in this algorithm will be described in this section.

The algorithm *building_top_base.sql* was developed in two parts: a) the first part is based on the selection of rooftop edge points in order to estimate the building rooftop elevation; and b) the second part was the selection of ground points around one side of the building without any objects, such as trees and points of the façade. The side of the building we chose was along the public street. All these points were relevant to calculate ground base elevation.

The input data for the extraction of this set of points for each building was the set of points clustered from point cloud and the boundaries of building rooftops obtained from *concave hull*. The input data for the second part of the algorithm was the original point cloud and the public street buffer.

The construction of this algorithm was based on the following PostGIS[7] functions (Obe & Hsu, 2011):

- ST_Buffer() function: returns a buffer zone from taking any geometry, which radially expands its r distance units. All the points in this buffer zone are less than or equal to distance.

- ST_Union() function: spatial aggregate function, which groups all the records into a single geometry record.

- ST_Difference() function: returns a geometry that represents part of geometry A that does not intersect with geometry B.

- ST_Dump() function: this function is very useful to explode multi geometries into their component geometries. In this case-study, the multipolygons obtained from a specific operation will return the rows of geometry dump objects. The multipolygons will be converted into single polygons (one row for each polygon).

[7] Manual in *http://postgis.net/docs/*

- ST_Intersection() function: returns a geometry that represents the common area between two or more geometries.

- ST_Contains() function: represents the contains relationship, where if geometry A is within geometry B, then geometry B contains geometry A.

ST_Buffer, ST_Union, ST_Difference, ST_intersection, and ST_Dump functions were used to obtain two buffer zones as single polygons, where each one will represent the building rooftop edge and base ground. ST_contains was used to extract the 3D points that were contained in each of the two buffer zone.

The steps involved in *building_top_base.sql* each part of algorithm (see Appendix D) and the visualization of results acquired for one building of sample in each step can be seen in Figures 2.32 and 2.33. The basic underlying principle for the development of this methodology was to use a set of simple spatial analysis functions. The main PostGIS function spatial analysis used in this methodology was the spatial proximity ST_Buffer function.

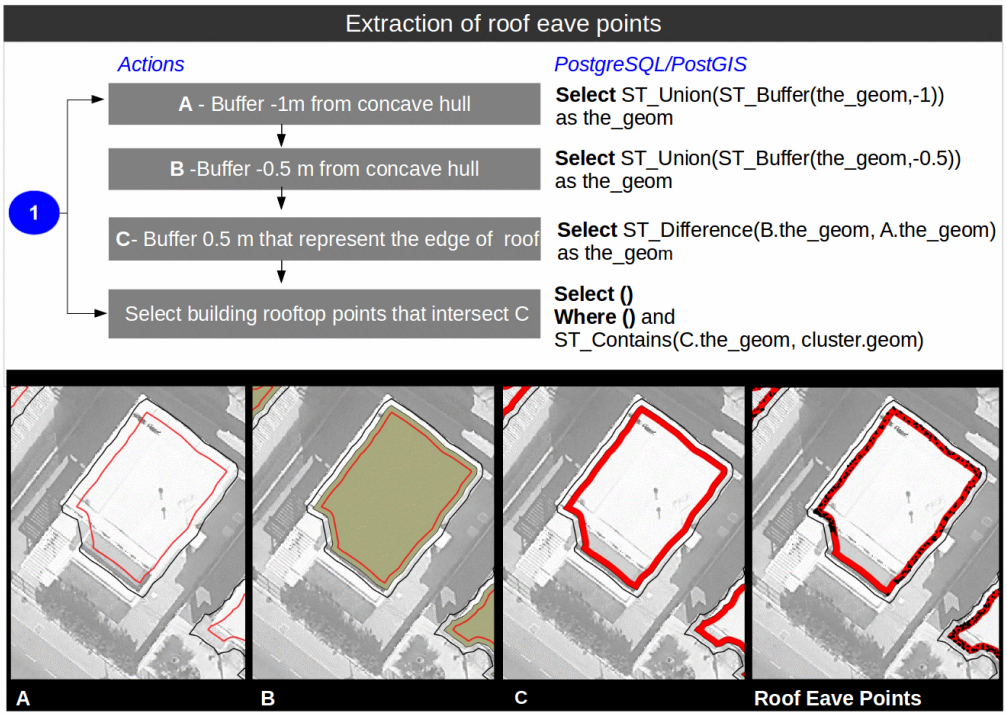

Figure 2.32: Extraction of roof edges from points.

The extraction of building rooftop edge zones was obtained from this function, that takes the boundary of building rooftop and radially expands it for a buffer of -0.5 m and for -1 m, where the difference between these buffers shall result in a

buffer zone of building rooftop edges. Afterwards, this simple polygon will be used to select the 3D points of the rooftop edges by the ST_Contains function. In Figure 2.32 we can see the 3D points selected for one building from a point cloud cluster, which define the roof eaves within a buffer of 0.5 m at 0.5 m from the boundary of the building rooftop. These points will be used later for the estimation of the average (or median) building rooftop elevation.

The sequence of all the PostGIS functions used for the extraction of 3D points that belong to building rooftop edges can be seen in Figure 2.32. According to this figure, part of the algorithm implemented in SQL with PostgreSQL/PostGIS functions used for this first task of the methodology is also presented in Listing 2.3.

Listing 2.3: Extraction of building roof eave 3D points

```
CREATE table A as
SELECT ST_union(ST_buffer(the_geom,-1)) as the_geom
 FROM building_rooftop;

CREATE table B as
SELECT ST_union(ST_buffer(the_geom,-0.5)) as the_geom
 FROM building_rooftop;

CREATE table C as
SELECT ST_Difference(B.the_geom, A.the_geom) as the_geom
 FROM A, B;

CREATE table result as
SELECT
     point_cloud_clustered.gid,C.gid *\gid is the primary key
     point_cloud_clustered.the_geom
 FROM  point_cloud_clustered, C
WHERE
     point_cloud_clustered.the_geom && C.the_geom
  AND
     ST_Contains(C.the_geom, point_cloud_clustered.the_geom);
```

The selection of 3D ground points on one side of the building was done by using the following steps presented in Figure 2.33 (see Appendix D). The selection of this set of 3D points was based on the location of the points within a 1.5 m buffer at 0.5 m from the building rooftop boundary, which intersects the public street buffer zone. This 0.5 m distance was established to reduce the wrong points that belongs to trees, building façade, balconies or other structures of the building.

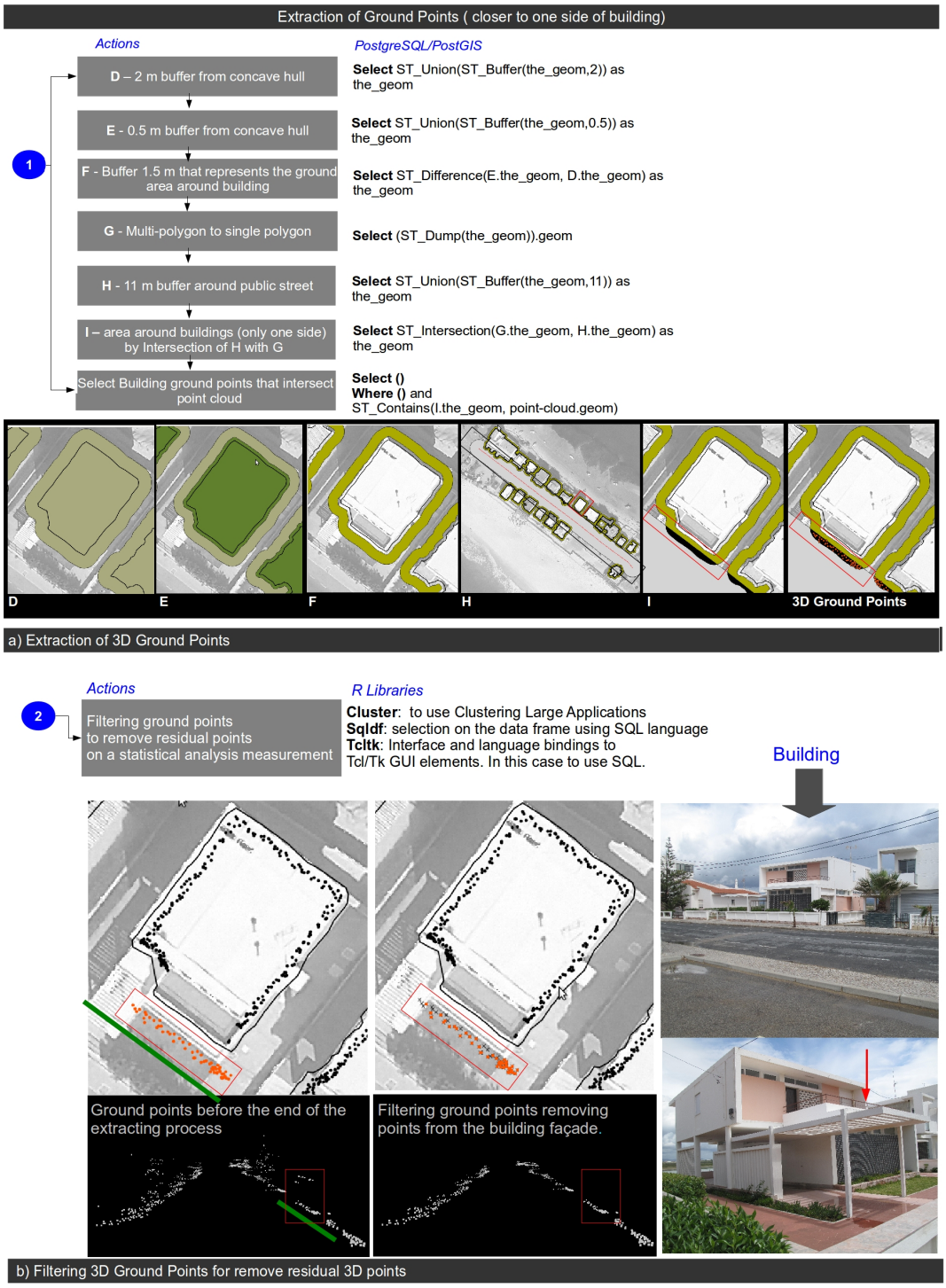

Figure 2.33: Extraction of ground points along one side of the building: a) The main steps of the first part of the methodology and the results for one building obtained in each step; b) Filtering 3D points extracted in the first part to remove 3D points of the balcony and building structure represented on the right side of the figure.

However, along this part of the methodology we had to develop another algorithm in R (Figure 2.33, step 2) to filter the extracted ground 3D points (see Appendix E). This filtering is intended to remove the 'wrong points' that do not

belong to the ground near the building. The filtering algorithm was adapted from the algorithm used in the clustering process. Then, this filtering was performed using CLARA from the cluster library based on the z variable of the point cloud. Depending on the number of spikes of empirical density functions for the variable z of the extracted points, the number of k-clusters were chosen by k_{ed} given by Equation 2.5:

$$k_{ed} = \text{n}^{\text{o}} \text{ of spikes kernel density curve} + 1 \tag{2.5}$$

Finally, the standard deviation measure $[\sigma_z]$ for the set of 3D points that belong to each cluster was analysed, where the clusters with $[\sigma_z]$ higher than one were removed. In the example above the k-cluster chosen to filter the set of clustered LiDAR points was k=2. The standard deviation value for k=2 was higher than 1 ($\sigma_z = 2.7$) and for k=1 it was $\sigma_z = 0.3$. Subsequently, the points that belonged to cluster k=2 were removed. The 3D view of these points can be seen in Figure 2.33, where the removed points belong to balconies and building structures.

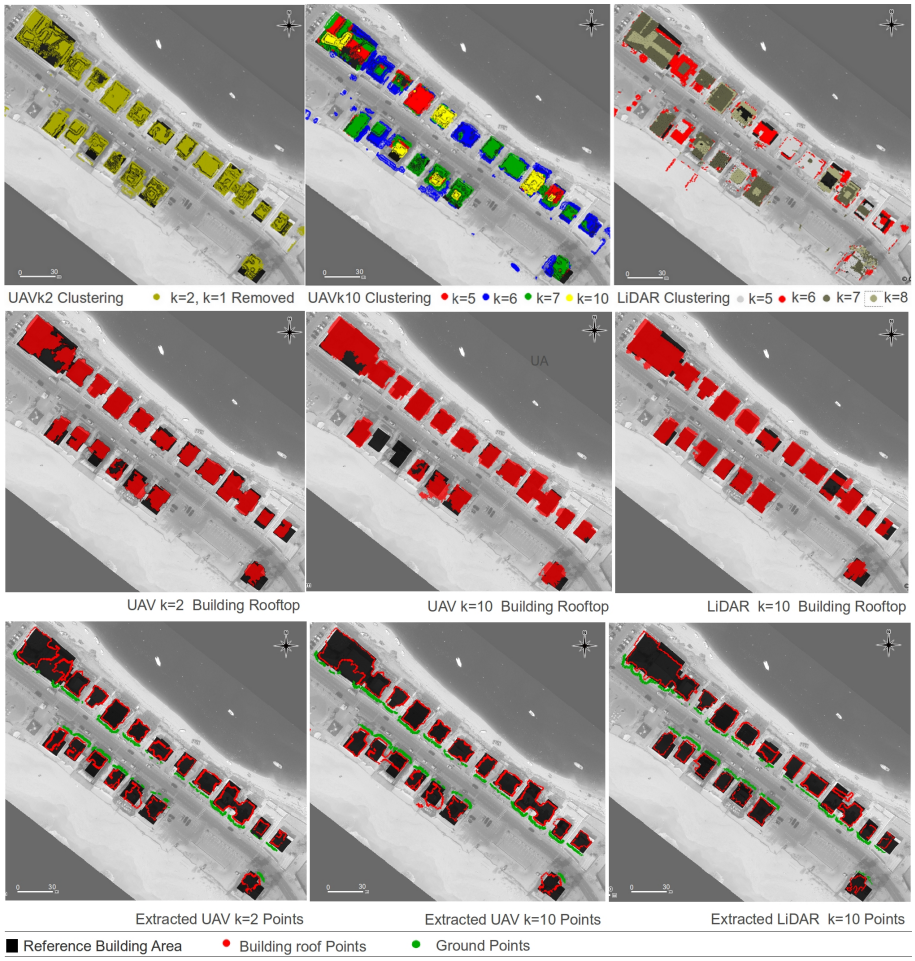

Figure 2.34: Results for the first stage of the methodology: clustering, *concave hull* and extraction of 3D points that represent each building (adapted from Rebelo et al., 2015).

All the building elements obtained from the clusted UAV point cloud and LiDAR point cloud can be seen in Figure 2.34. These elements are the 3D rooftop points, the boundary of the building rooftop (polygon), the 3D points of the roof edges, and the ground points of one side of the building.

The elements shown in Figure 2.34 were then used to calculate the building volume. The elevation mean (or median) of the set of extracted 3D points was used to calculate the building height parameter and the boundary of the building rooftop to calculate the building area parameter.

The next section will describe this process. However, there were two buildings that were not separately extracted from UAV point cloud to k=10 (UAVk10). These buildings were removed and therefore their building volume was not calculated.

2.3.2 Building volume and total volumetric parameters

The second stage of the 3DEBP mentioned at the beginning of this Section 2.3. (Table 2.8) reggarding the calculation of building volume was performed automatically. To compute this building parameter we developed a SQL algorithm *Building_vol* in a GDBMS environment using PostgreSQL/PostGIS.

The building volume parameter was obtained from the multiplication of the building façade height by the area of the building rooftop. The building façade height parameter was calculated from the statistical average (or median) values of the previously selected 3D points mentioned above (Figure 2.35).

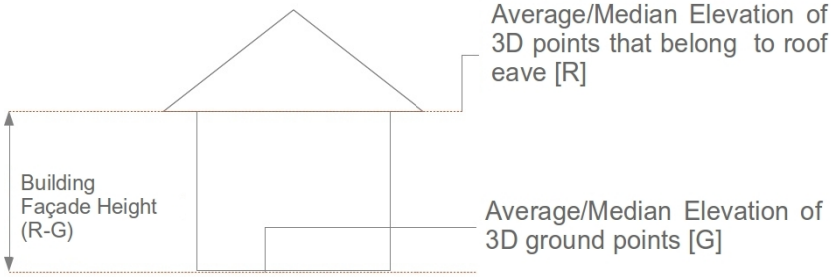

Figure 2.35: Building façade height parameter.

The high heterogeneity present in the typology of the buildings makes it difficult to decide which statistical measure is more suitable. Depending on the typology of a building we would expect to have a good knowledge on the use of the average and median measures for this type of applications. Hence, it is important

to test it in this study. Therefore, the methodology applied to calculate the building façade height took into account these median and average measures of the roof eave and base of the building.

An important implementation for the optimization of this step was the integration of R into PostGIS/PostgreSQL by PL/R – R procedural language. Part of the algorithm developed for the computation of average and median elevation of roof eave (or base the building) for each building is presented below in Listing 2.4. The *r_median* function PL/R implemented was developed by Conway (2012).

Listing 2.4: Compute average and median elevation of eave roof

```
CREATE or REPLACE function r_median(_float8)
 returns float as 'median(arg1)' language 'plr';

CREATE AGGREGATE median (
   sfunc = plr_array_accum,
   basetype = float8,
   stype = _float8,
   finalfunc = r_median
);

CREATE table "AVG_elevation_roof_points" as
  SELECT
          idbuilding,
          st_union(geom) as the_geom,
          count(*) as npoints_t,\* total of points
          sum(z) as sum_ztop
          median(z) as medianztop
     FROM "rooftop_points" group by idbuilding;

ALTER table  "AVG_elevation_roof_points"
   ADD column meanztop double precision;

UPDATE "AVG_elevation_roof_points"
   SET meanztop = sum_ztop/npoints_t;
```

The algorithm we developed (Listings 2.5 and 2.6) followed three main steps as can be seen in Figure 2.36: a) calculating the building area from the geometry previously extracted from the *concave hull* process (boundary of the building rooftop). The area (*areacloud*) was computed by using the PostGIS function ST_area; b) calculating the building façade height ($hfmeancloud$) from the difference between

average elevation (or median) of the roof eave (*meanztop*) and ground (*meanzpav*) as shown in Figure 2.35; and c) calculating the building volume from the parameters computed in a) and b) (Figure 2.35).

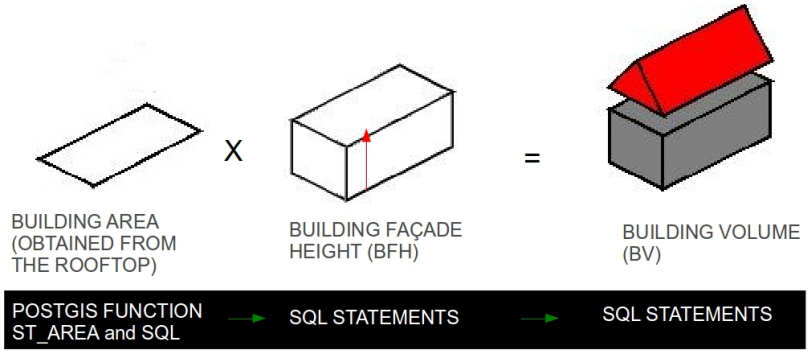

Figure 2.36: Parameters involved in the computation of building volume, which represent the three steps included in *Building_vol.sql* algorithm.

Part of the algorithm we developed that represents the figure above, can be seen in the following Listings 2.5 and 2.6.

Listing 2.5: Compute Building rooftop area (areacloud) and Building Façade Height (BFH) using average

```
--Compute the Building Area Parameter
CREATE table "area" as select *
    FROM out_concavehull;
ALTER table  "area"
    ADD column areacloud double precision;
UPDATE "area"
    SET areacloud=st_area(the_geom);

--Compute the average Building facade Height (BFH) from 3D points
--idbuilding: code of building; the_geom: Attribute of geometry
CREATE table "BFH" as select
idbuilding, the_geom, meanztop, meanzpav
 FROM "Building_Elements";

ALTER table "BFH"
    ADD column hfmeancloud double precision;
UPDATE "BFH"
    SET hfmeancloud= meanztop-meanzpav;
```

Listing 2.6 below shows the algorithm used to calculate the building volume and the total volume parameters. The latter is the sum of all the building volumes included in a bounded area.

Listing 2.6: Computing Building Volume (BV)

```
--Computing Building Volume (volmeancloud)
CREATE table "volume" as select
idbuilding, geom, areacloud, meanztop, meanzpav, hfmeancloud
  FROM "BFH_area";

ALTER table "volume"
    ADD column volmeancloud double precision;
UPDATE "volume"
    SET volmeancloud = hfmeancloud*areacloud;

--Compute Total Volume
SELECT sum(volmeancloud)
    FROM "volume";
```

This algorithm calculates the buildings volume and the total volume of all the buildings included in the study area within a few seconds. The building volume parameter was estimated for 19 buildings, where the code assigned to them is shown in Figure 2.37.

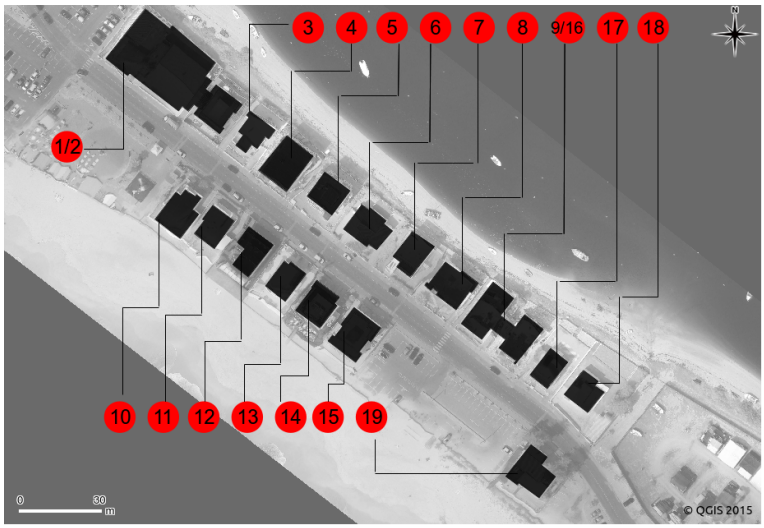

Figure 2.37: Buildings included in the case study with the adopted 'ED' code.

The building volumes computed from each set of extracted building elements are shown in Tables 2.12, 2.13 and 2.14.

Each table of results is based on specific point cloud clustering, where the building volume (BV) parameter was twice computed based on different statistical measures (average or median) of building façade height (BFH). The building parameters presented in these tables are rounded, where the building volume values

reported here resulted from an algorithm with more precise values.

The difference recorded between the average or median for the building façade height was less than 0.8 m, with the highest value obtained for building 3 (Table 2.12). On the other hand, the average of these difference values was 0.3 m. The building façade height parameter estimated ranged approximately between 4 m and 8 m. Furthermore, the differences in building volume calculated from both measures ranged approximately between 10 m^3 (buildings ED18 and ED7) and 333 m^3 (building ED1_2).

Table 2.12: Building Volume [BV] estimated from a LiDAR point cloud

Code	Area (m^2)	BFH_{ave} (m)	BV_{ave} (m^3)	BFH_{med} (m)	BV_{med} (m^3)
ED1_2	1001.146	**5.576**	**5583**	**5.910**	**5917**
ED3	126.088	**5.195**	655	**6.010**	758
ED4	256.813	7.488	1923	7.810	2006
ED5	204.733	6.374	1305	5.700	1167
ED6	116.147	4.186	486	3.860	448
ED7	147.377	**6.423**	**947**	**6.490**	**956**
ED8	198.620	6.317	1255	6.470	1285
ED9_16	308.251	6.504	2005	6.070	1871
ED10	158.464	6.561	1040	6.700	1062
ED11	138.611	4.280	593	3.770	523
ED12	178.366	6.397	1141	6.980	1245
ED13	115.155	6.576	757	6.840	788
ED14	155.774	6.543	1019	6.170	961
ED15	209.927	6.406	1345	6.570	1379
ED17	84.397	6.849	578	6.650	561
ED18	74.935	**4.923**	**369**	**5.050**	**378**
ED19	128.109	6.033	773	6.170	790
Maximum	1001.146	7.488	5583	7.810	5917
Minimum	74.935	4.186	369	3.770	378
Average	211.936	6.037	1281	6.072	1300
Total Volume m^3			**21773**		**22096**

According to Table 2.13, the results recorded for the k=2 UAV point cloud (UAVk2) are similar to LiDAR's, where the difference between building height estimated from median and average is approximately 0.35 m on average. This parameter approximately ranged between 3.5 m and 9.5 m. On the other hand, the differences in the building volume parameter ranged approximately between 2 m^3 (building ED11) and 840 m^3 (building ED9_16).

The results obtained for the k=10 UAV point cloud (UAVk10) using the median and average (Table 2.14) show more sensitivity in the estimation of building parameters, because the differences between them are greater than the other results

above. The difference between building height estimated from median and average is approximately 0.64 m on average. The differences in the building volume parameter ranged between 9.7 m^3 (building ED6) and 1015 m^3 (building ED9_16).

The range of building façade height estimated from UAVk10 is very similar to the results obtained for UAVk2.

Table 2.13: Building Volume [BV] estimated from a $k = 2$ UAV point cloud cluster

Code	Area (m^2)	BFH_{ave} (m)	BV_{ave} (m^3)	BFH_{med} (m)	BV_{med} (m^3)
ED1_2	814.114	5.470	4453	5.271	4291
ED3	154.085	6.646	1024	7.257	1118
ED4	248.319	7.078	1758	7.535	1871
ED5	159.265	9.449	1505	10.182	1622
ED6	138.727	3.647	506	3.509	487
ED7	129.201	6.176	798	6.330	818
ED8	192.586	6.230	1200	6.362	1225
ED9_16	385.950	**9.168**	**3538**	**11.346**	**4379**
ED10	148.585	6.615	983	6.718	998
ED11	136.879	**3.606**	**494**	**3.598**	**492**
ED12	113.101	8.651	978	9.307	1053
ED13	77.459	6.652	515	6.735	522
ED14	152.421	6.257	954	5.996	914
ED15	152.507	6.715	1024	6.628	1011
ED17	74.370	5.782	430	5.890	438
ED18	80.849	4.024	325	3.733	302
ED19	224.253	6.544	1467	6.567	1473
Maximum	814.114	9.449	4453	11.346	4379
Minimum	74.370	3.606	325	3.509	302
Average	198.981	6.395	1291	6.645	1354
Total Volume m^3			**21952**		**23013**

The total volume estimated from the LiDAR point cloud for the study area is approximately 22000 m^3 using median or average building height (Table 2.12). The difference recorded between these two values estimated is about 1.5% of the total volume estimated. However, for the UAV point clouds this difference is higher than LiDAR's, where for UAVk2 and UAVk10 it is about 5% and 10%, respectively. The application of average or median to the estimation of BFH seems to be more suitable for a LiDAR point cloud, where any measure (median or average) can be applied. In this case the difference for the estimated building heights (average values) was 3.4 cm and between the average volumes estimated it was 19 m^3. However, for the UAV point cloud, the scenario is different, because it was more sensitive to these measures, where the differences between them were higher. The average values between median and average building heights or building volumes were particularly different in the case of UAVk10.

Table 2.14: Building Volume [BV] estimated from $k = 10$ UAV point cloud cluster

Code	Area (m^2)	BFH_{ave} (m)	BV_{ave} (m^3)	BFH_{med} (m)	BV_{med} (m^3)
ED1_2	939.429	6.277	5896	6.930	6510
ED3	157.594	6.141	968	6.730	1061
ED4	249.351	7.008	1747	7.530	1878
ED5	161.844	9.530	1542	10.210	1652
ED6	189.744	**3.491**	**662**	**3.440**	**653**
ED7	143.414	5.818	834	6.460	926
ED8	200.223	6.115	1224	6.350	1271
ED9_16	428.560	**8.972**	**3845**	**11.340**	**4860**
ED10	198.783	5.853	1163	6.690	1330
ED13	79.778	6.559	523	6.720	536
ED14	186.406	4.344	810	3.820	712
ED15	155.695	6.583	1025	6.720	1046
ED17	123.410	4.300	531	3.540	437
ED18	122.088	4.275	522	3.940	481
ED19	178.308	5.502	981	6.550	1168
Maximum	939.429	9.530	5896	11.340	6510
Minimum	79.778	3.491	522	3.440	437
Average	234.308	6.051	1485	6.465	1635
Total Volume m^3			**22275**		**24521**

The average of building volumes estimated from LiDAR or UAVk2 was more similar. The 3D visualization of the buildings based on building parameters estimated from LiDAR and UAVk2 point clouds using average is shown in Figure 2.38.

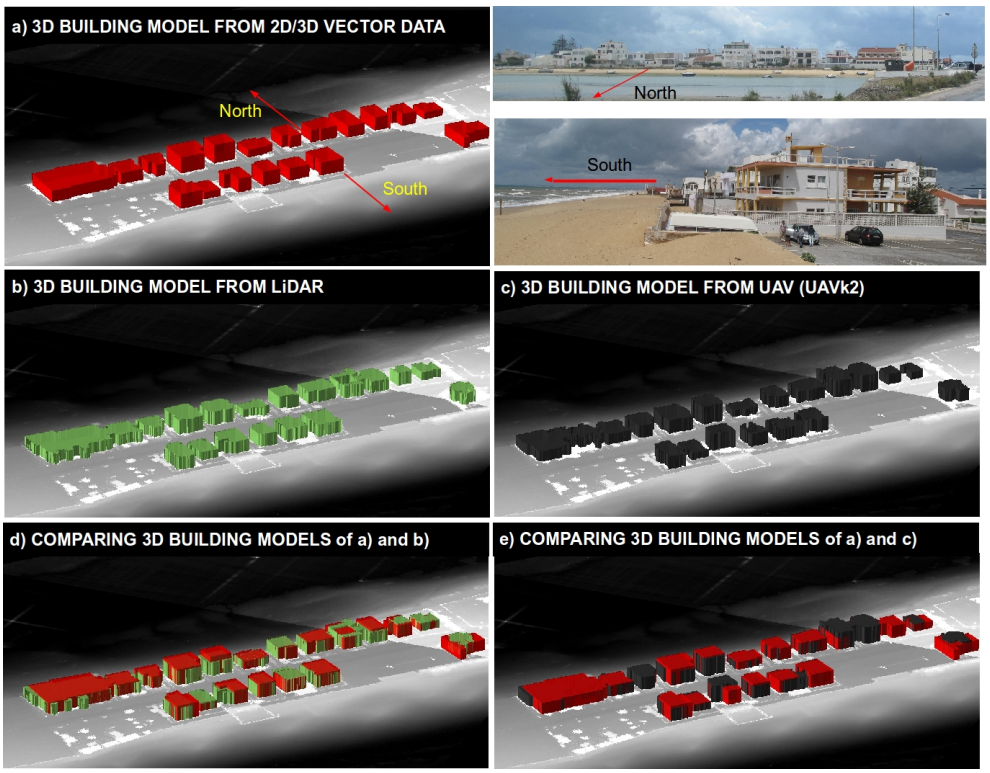

Figure 2.38: 3D visualization of buildings estimated from LiDAR or UAVk2 point clouds.

The application of this data extracted for the 3D visualization of the buildings can be very useful for an urban planner (Figure 2.38). The impact of the building parameter errors in the 3D visualization is irrelevant for the detection of a built-up area or for public discussion (Figure 2.38). This means that the buildings extracted from UAV or LiDAR are very similar to the reference 3D building models, especially if they are enhanced. In comparing UAV/LiDAR with the reference volumes it is possible to see that the 3D building model of UAV is more filled in red (reference color), which means that the volumes of these building models were mostly underestimated.

However, it is important to assess the quality of the building parameters estimated and presented in the tables above if we need another type of applications with this 3D visualization. The measurement of the magnitude of error for the building parameters estimated by the implemented 3DEBP solution will be disclosed in the next subsection. This issue is important to understand the level of usability of these estimated parameters for urban planning, such as 3D visualization.

2.3.3 Evaluation of the estimated building parameters

The building parameters estimated for this particular built-up area require an evaluation that allows to analyze : a) the magnitude of error for each building parameter estimated compared with other data that was acquired by traditional and more accurate methods, and b) the accuracy and performance of the 3DEBP methodology we have developed.

The magnitude of errors is mainly dependent on the characteristics of the buildings types. Furthermore, it is also dependent on the performance of the methodology in the extraction of building elements from heterogenous spatial distribution of data points for different types of buildings.

Among all the parameters, the extraction of the building area parameter with quality from any point cloud was the most difficult operation inside in the scope of this study. Along the extraction of the building area parameter we collected some polygons that did not represent the rooftop building boundary. One of the reasons for this is the fact that the original data does not cover the whole building rooftop. An example of this was the fact that the building rooftop of ED1_2 was not fully covered by UAV point cloud, such as shown in Figure 2.34 for clustering results.

Afterwards, we had to remove some of the extracted building rooftops using an empirical evaluation of the results. These empirical evaluation was based on visualizing and comparing the building rooftops extracted with the reference building rooftops. This procedure was very important to avoid the acceptance of buildings that had a lower error of the area with a boundary shape that did not correspond to the reality. A good example of this is the building ED14 (Figure 2.39).

The rejection of an extracted building rooftop was necessary for the buildings whose roof shape was very different from the building boundary reference. Three situations were identified in this rejection process: i) the shape of the building boundary as extracted from wrong 3D points that were included as the building rooftop, such as structures near the building that had the same elevation of the building rooftop; ii) difficulties in the clustering process, where it was not possible to select only points of building rooftop because of the complexity of the building type; and iii) the shape of the building roof had gaps because it was not fully covered by 3D points from original data. These gaps can be due to an inaccurate multi-stereo image matching processing of the aerial images or failures in overlapping imagery.

Some of the building roofs that were rejected in these conditions are identified in Figure 2.39. These buildings were not considered for the evaluation of building volume results.

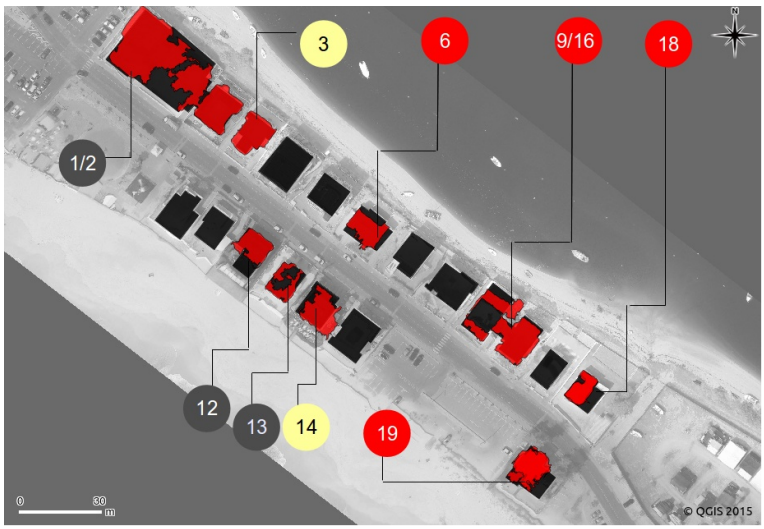

Figure 2.39: Building rooftops that were rejected because their shape did not represent their real shape. Yellow: situation i); Red: situation ii); and Grey: situation iii).

The evaluation of each estimated building parameter was performed within a GDBMS. This procedure was done automatically through an algorithm developed for this purpose. The first step of this evaluation was the computation of building

parameters for each building from reference data (Subsection 2.1.1). Then, the second step was to calculate the absolute building parameter errors for the building area and building façade height. Afterwards, the relative building volume error and the percentage of error for each estimated building volume was calculated.

The relative building parameter error [BP] is given by the following equation:

$$BP_{Relative\,Error} = \frac{|BP_{Ref} - BP_E|}{BP_{Ref}} \tag{2.6}$$

where BP_{Ref} and BP_E are the true building parameter value and estimated building parameter value, respectively. The difference between these two values is the absolute building parameter error. Then, the percentage of building parameter error is 100% times the relative building parameter error defined by:

$$BP\,Error(\%) = BP_{Relative\,Error} \times 100 \tag{2.7}$$

These two equations were implemented in the algorithm for the computation of errors for each building parameter.

Building Area

The computation of the absolute building area error was based on the difference between the buildings' footprints obtained by accurate photogrammetry techniques and the estimated building area.

The range of absolute building area errors obtained from each point cloud sample is shown in Figure 2.40. Building area values estimated from point clouds can be seen in Tables 2.12, 2.13, and 2.14.

The shapes of the extracted building roofs are more regular in the LiDAR point cloud. The number of building roofs extracted with more quality is slightly higher than the other samples (Figure 2.40). Seven buildings were rejected for UAVk2 and 6 buildings were rejected for UAVk10, unlike LiDAR (where only 4 buildings were rejected).

Table 2.15 shows the average absolute error, the minimum absolute error, the maximum absolute error and the standard deviation of absolute error for building area computed for each point cloud, but without the rejected buildings. The average

of absolute error for the building area parameter presents the lowest value of 20.6 m^2 for the LiDAR point cloud when compared with other point cloud samples. However, this difference is not significant.

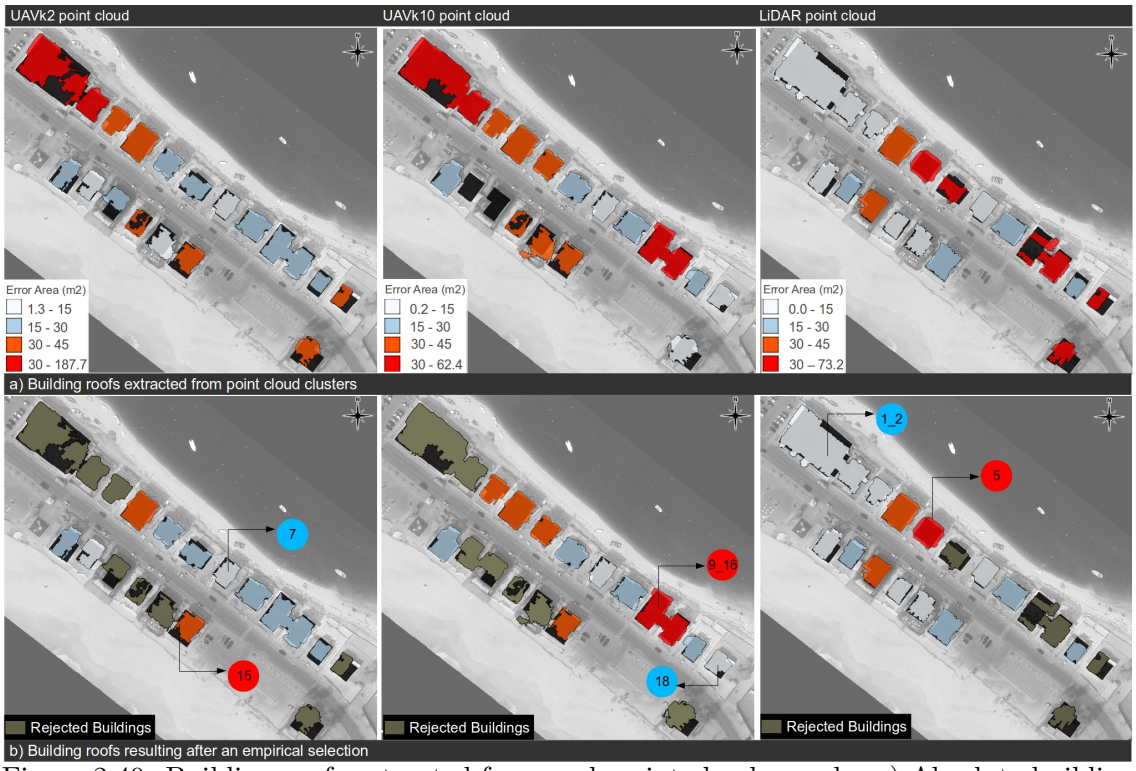

Figure 2.40: Building roofs extracted from each point cloud sample: a) Absolute building area errors; b) Building roofs rejected based on the shape of the reference building roof. The red circles are the maximum error and the blue circles are the minimum error. Note: The buildings are assigned without 'ED' to simplify the notation.

Furthermore, the table below shows that the errors obtained in the estimation of this parameter are very similar. However, for the UAVk2 point cloud, these errors are closely grouped, as indicated by the smaller standard deviation of their data, which possibly indicates more stability in the collection of the data. In comparison with Figure 2.40a, the range of values for absolute building area error is lower. The buildings with minimum and maximum errors presented in the table can be seen in Figure 2.40b.

Table 2.15: Statistical evaluation of absolute building area error obtained for each 3D point cloud without the rejected buildings.

DataSet	Average (m^2)	Maximum (m^2)	Minimum (m^2)	Standard Deviation (m^2)
LiDAR	20.6	73.2	0.7	19.9
UAVk2	23.3	39.4	6.2	10.6
UAVk10	27.6	58.4	0.3	15.9

Empirical density functions (Figure 2.41) for area estimates (without removing any buildings) show that generally all the point clouds approximate the reference distribution (empirical modes are similar).

Yet, regarding LiDAR data, it was not possible to distinguish small irregularities, hence the larger mode (Figure 2.41a). After the deletion of the buildings the curve for LiDAR shows a slightly better approximation to the reference values. On the other hand, UAVk2 captures the differences between buildings with too much detail (if we assume reference values as the 'true' values). Notwithstanding, the estimated curve for UAVk2 shows a better approximation of the true values when compared with the other graphs ('Before Rejecting Buildings'). However, for UAVk2 most building rooftop shapes were not correct as can be seen in Figure 2.41.

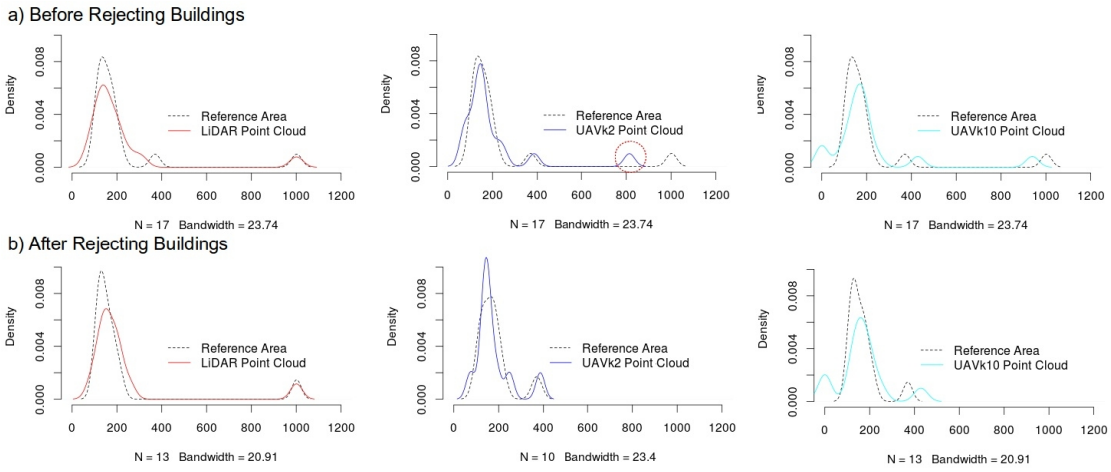

Figure 2.41: Empirical density functions for the reference building area vs. estimated buildings area: a) all the buildings are considered; and b) after removing the buildings.

The circle in Figure 2.41a before the buildings were rejected identifies the presence of an outlier, which represents the major error area (187.5m) obtained in the estimation of the building area from UAVk2, i.e. the problem mentioned previously for building ED1_2 identified in Figure 2.39. However, the 7 buildings removed for UAVk2 made the building straighter and overestimated in the large mode.

The extraction of the building area parameter is strongly dependent on the success of: a) the clustering in the selection of the 3D points that belong to the rooftop; b) the performance of *concave hull* in the design of the building rooftop; and c) the multi-stereo image matching processing of the aerial images for the acquisition of UAV point cloud; and d) suitable overlapping between aerial images in flight

direction and flight lines.

Building Façade Height

The building façade height parameter was evaluated for all the buildings. The evaluation of this parameter was based on absolute error. The absolute building height error, also called vertical error, was computed from the difference between the reference building façade height value measured by topographic surveying and the building façade height extracted from point cloud. The latter were detailed in Tables 2.12, 2.13, and 2.14 of Subsection 2.3.2.

The building façade height reference computed for this task was based on elevation points that were shown in Figure 2.1 of this chapter. The reference parameter value was computed from the elevation of rooftop (median/average elevation values) and the elevation of ground (median/average values) of each building. Then, the absolute building façade height error was computed from their average (or median) reference and estimated values.

The absolute building height errors obtained for each building are shown in Figures 2.42 and 2.43. The range of absolute building height error of each point cloud depends on the statistical measure used (median or average).

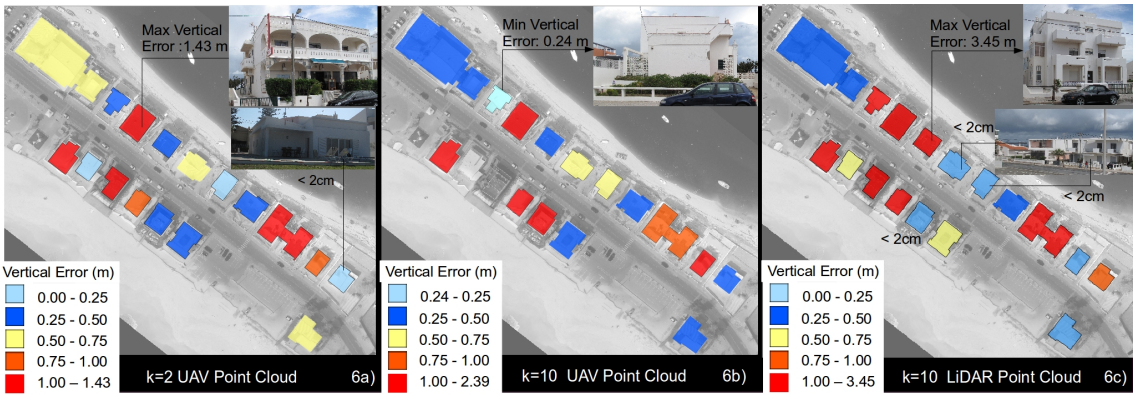

Figure 2.42: Absolute values of average building height errors.

The more complex building types have the highest vertical error, such as those shown for some examples in Figures 2.42 and 2.43. The value range of the vertical error for this parameter is higher for the median measure (Figure 2.43). The tallest building in this study area is building ED5 (9.8 m) and the shortest building is building ED11 (3.8 m). The UAV point cloud estimated building ED5 as the tallest of all, with a vertical error of +38 cm using the average. The LiDAR point

cloud sample estimated the building ED11 as the shortest by using the median, with a vertical error of -1.5 cm.

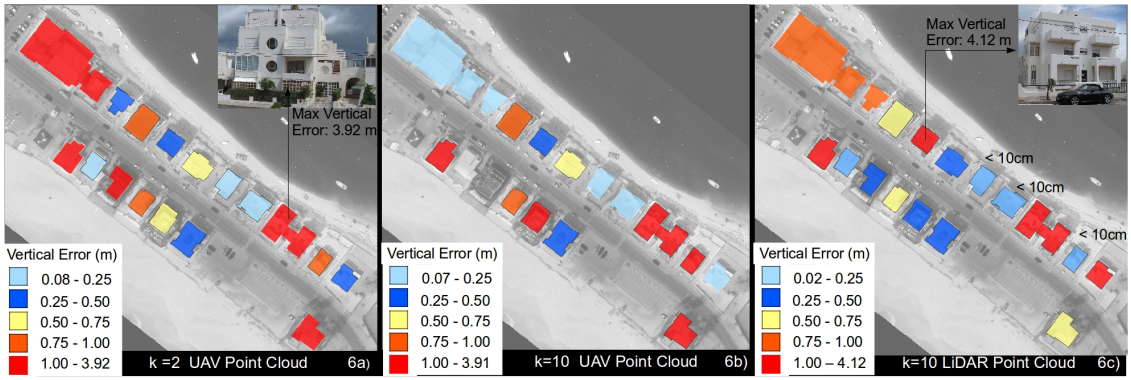

Figure 2.43: Absolute values of median building height errors.

In general, the vertical error for the buildings with a flat roof (see buildings ED7 and ED8 in Figures 2.42 and 2.43) was less than 25 cm (for LiDAR, it ranged between 2 cm and 10 cm). On the other hand, the vertical error for most buildings with a pitched and complex roof was above 50 cm.

The results achieved for this parameter show that the average measure is more reliable and stable to estimate this parameter from a UAV point cloud, but not from LiDAR data. However, the average building heights estimated from LiDAR registered vertical errors below 10 cm for 4 buildings. The estimation of median building heights from the LiDAR point cloud seems better than the usage of average, because only 4 buildings were extracted with a vertical error above 1 m, whereas for average there were 3 more buildings.

The synthesis of these results for each point cloud sample are presented in Table 2.16 using statistical measures. The table also shows that the vertical errors obtained in the estimation of this parameter are very similar. However, there is evidence that the UAV point cloud had the best results for the estimation of building height using the average measure. On the other hand, the results are slightly better for the median measure used in the LiDAR point cloud.

The maximum vertical errors of the building height parameter estimated from LiDAR (Table 2.16) were obtained for building ED5, with an error of 4.12 m and 3.45 m (Figures 2.42 and 2.43). The origin of this higher error was the 3D points of balconies, which were considered for the estimation of elevation at the top of the building.

Table 2.16: Building height error estimated from 3D point clouds

Measure of Building Height	Dataset	Average (m)	Median (m)	Maximum (m)	Minimum (m)	Standard Deviation (m)
Average	UAVk2	**0.61**	**0.51**	**1.43**	**0.01**	**0.43**
	UAVk10	0.90	0.59	2.40	0.24	0.75
	LiDAR	0.80	0.80	3.45	0.002	0.84
Median	UAVk2	0.89	0.68	3.92	0.08	0.92
	UAVk10	1.05	0.74	3.91	0.04	1.22
	LiDAR	**0.77**	**0.66**	**4.12**	**0.02**	**0.95**

Furthermore, the empirical density functions of each point cloud in the estimation of the building façade height parameter are very similar (Figure 2.44) as expected by the values shown in Table 2.16. Most values were overestimated by LiDAR and UAVk2. Once again, these plots confirm that the usage of the average measure for the UAV point cloud is better, since the estimated curve of UAV data is a slightly better approximation to their true values.

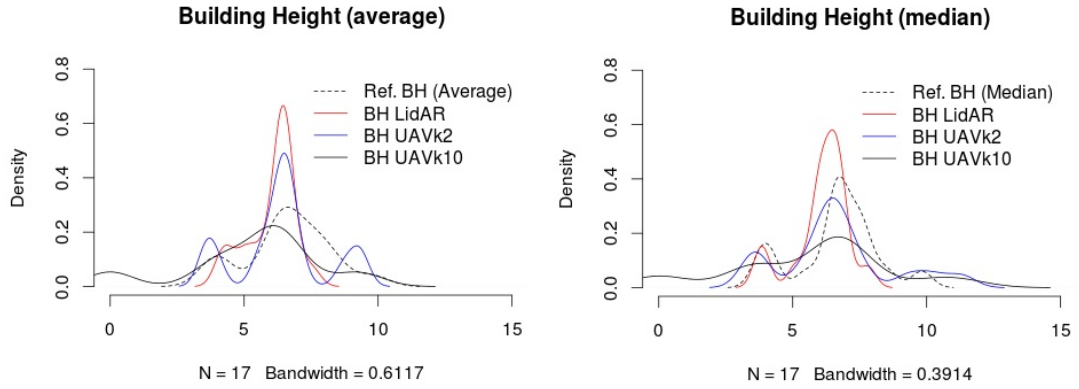

Figure 2.44: Empirical density functions: true building façade height curve and the building façade height estimated for all the point clouds based on average and median.

The comparison between estimated curves for LiDAR data in these plots shows that the curve of the median measure is slightly better adjusted to the reference curve between 3 m and 5 m, unlike the curve of the average measure.

Most building façade height (about 45% of the buildings) extracted from these sampling of point clouds was estimated with a vertical error below 0.5 m. On the other hand, for the best results of UAVk2 (average) and LiDAR (median) about 80% of vertical errors were below 1 m.

Furthermore, there is an evidence that the median and average measures used in the extraction of this building parameter are more appropriate for LiDAR and UAV, respectively.

Building Volume

The definition of building volume is established by the product of the two independent variables – building area and building height. The magnitude of the building volume error is dependent on the error obtained in the estimation of each variable.

The evaluation of each estimated building volume was based on absolute and relative errors. The absolute error is the difference between the values of reference building volume [V_{Ref}] and estimated building volume [V_E].

The relative building volume error is given by the ratio of absolute error and reference building volume, such as the following equation:

$$BV_{error}(\%) = \frac{V_{Ref} - V_E}{V_{Ref}} \times 100 \tag{2.8}$$

where V_{Ref} is the multiplication of the building area BA_{Ref} by building height BH_{Ref} obtained from more accurate techniques.

The estimation of building volume was carried out in two ways:

1. The estimated building volume was computed from the following parameter values: building area acquired by more accurate traditional techniques of 2D vector data acquisition (stereo restitution) noted by BA_{Ref}; and building height [BH_E] was estimated from point cloud data. Hence, Equation 2.9 can be written:

$$BV_{errorTypeI}(\%) = \frac{V_{Ref} - (BH_E \times BA_{Ref})}{V_{Ref}} \times 100 \tag{2.9}$$

2. The building volume estimated was computed from the building area [BA_E] and building height [BH_E] both estimated from point cloud data.

$$BV_{errorTypeII}(\%) = \frac{V_{Ref} - (BH_E \times BA_E)}{V_{Ref}} \times 100 \tag{2.10}$$

These results were obtained automatically based on values acquired from Listing 2.6 presented in Subsection 2.3.2, through the following algorithm (Listing 2.7) using the equations above.

Listing 2.7: Computing the relative building volume error using BH average (for BH median replace mean by median)

```
--INPUT: table "buildingsrefall" about reference data
         and table "volume" exposed in listing 3.6
--Join these tables by attribute idcode and idbuilding
  (code of building)

CREATE table error_volumes as
  SELECT volume.idbuilding, volume.geom,
         volume.areacloud , volume.hfmeancloud,
         volume.volmeancloud, buildingsrefall.refarea,
         buildingsrefall.hfrefmean,
         buildingsrefall.volrefmean
  FROM buildingsrefall, volume
  LEFT OUTER JOIN volume on
   buildingsrefall.idcode = volume.idbuilding;

ALTER table error_volumes
   ADD column (volrefmeancloud double precision,
               --BVerror (Type I)
               Error_BVtypeI_perc double precision,
               --BVerror (Type II)
               Error_BVtypeII_perc double precision);

UPDATE error_volumes
  SET volrefmeancloud = hfmeancloud*refarea,
      Error_BVtypeI_perc =((volrefmean-volrefmeancloud)
                                    /volrefmean)*100,
      Error_BVtypeII_perc =((volrefmean-volmeancloud)
                                     /volrefmean)*100;
```

The analysis performed for the building volume parameter was important to measure the level of usability of this type of 3D data in urban planning, without reference data (Equation 2.10) or simply using 3D data for the estimation of the building height parameter (Equation 2.9).

Then, we started by analysing the magnitude of the percentage of error for the estimated building volume. In order to do this, we conducted two analyses: one based on the reference building area and the other based on the building area extracted from the point cloud.

Building Volume (using only the 3D point cloud for the estimation of BH)

For this case the building volume estimated is dependent on the error of building height extracted from point cloud. According to average and median building height estimated, Figure 2.45 shows the relative building volume errors for each building.

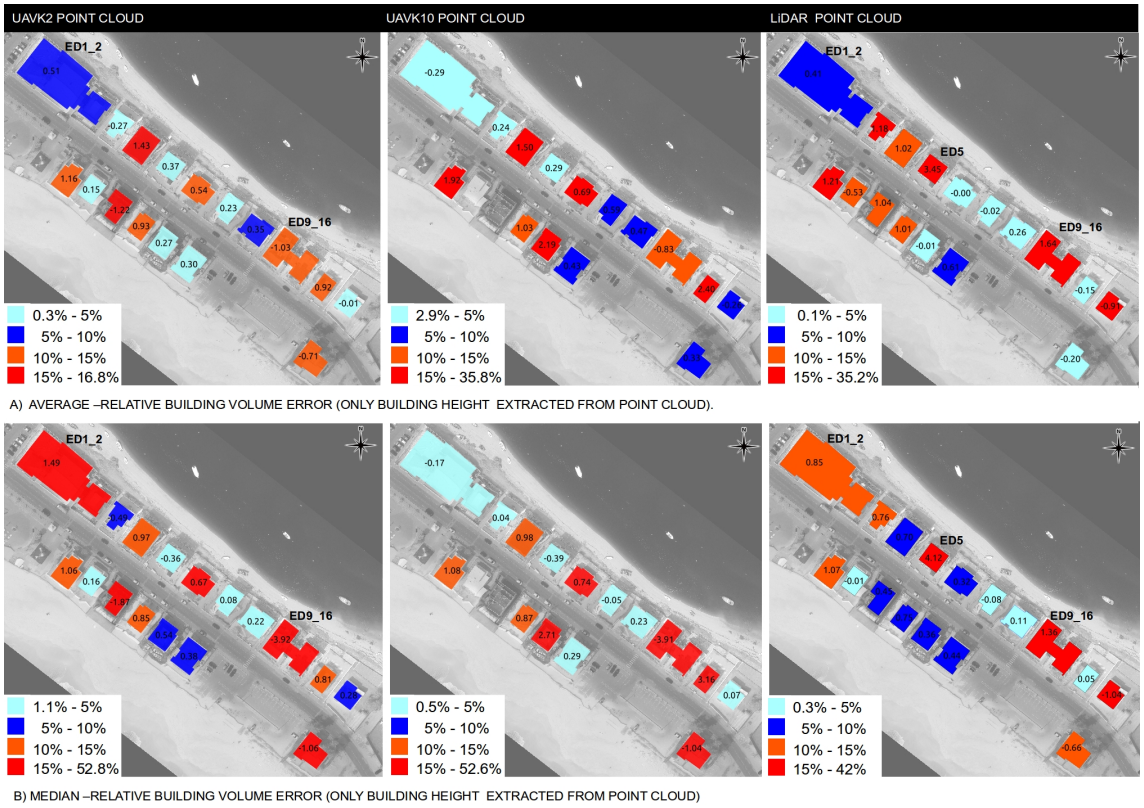

Figure 2.45: Relative building volume error obtained for the building volumes estimated from reference building area. The vertical error of the building height is also represented for each building.

The range of relative error is lower for the building volumes estimated from the average measure applied for BH. The best range of relative errors was obtained for the UAVk2 sample, which varies between 0.3% and 16.8%. Moreover, around 45% of the building volumes estimated from this point cloud have a relative error lower than 5%, unlike UAVk10 and LiDAR.

As the building height error increases, the higher will the error percentage for building volume (Figure 2.45) be. Then, the *Pearson* product-moment correlation coefficient (Table 2.17), r, for a confidence level of 95% was calculated for these two variables.

Table 2.17: Pearson correlation coefficient (r) for all the results presented in Figure 2.45

Errors	BV_{LiDAR}	BV_{UAVk2}	BV_{UAVk10}
$BH_{average}$	r= 0.93	r=0.95	r=0.98
BH_{median}	r= 0.94	r=0.98	r=0.99

For instance, the Pearson correlation between the absolute building height error and the percentage of building volume error is very high because there appears to be a positive relationship between them. Therefore, the Pearson correlation value is slightly higher for the building height estimated with the median statistical measure (Table 2.17).

Comparing the building façade height errors with the building volume errors computed with reference area (Figure 2.45) we can identify four situations behind this correlation: a) a vertical error in the estimation of building height up to 7 cm implies an error in volume under 1%; b) a vertical error up to 50 cm means an error in volume under 8% (Figure 2.46); and c) a vertical error up to 1 m implies an error in building volume under 15%; and d) a vertical error between 1-2 m results in an error of building volume that ranges between 15% and 25%.

Figure 2.46: Volume of buildings 7 and 8 with the representation of BH error (also called vertical error).

Additionally, the errors obtained in the estimation of BV are similar using average or median building height (Table 2.18). The statistical values obtained from

UAV are better for average BH based on the evaluation of average and standard deviation statistical error.

The building volume estimated from LiDAR is slighty better if the building height is estimated from the median measure, because around 60% of the buildings have a relative error that is lower than 10%, whose average of percentage error was 10.8% (Table 2.18). On the other hand, more than 20% of the buildings have an error under 10%, unlike the average measure used for building height (Figure 2.45). However, this point cloud has more estimated building volume (2 more buildings) with a relative error lower than 5% for average BH.

Table 2.18: Statistical measures of Relative Building Volume error (%) obtained for the building volumes estimated from reference building area

BV Parameter	**point cloud**	**Average**	**Median**	**Min**	**Max**	**Standard Deviation**
BH(average)	UAVk2	**8.8**	8.6	0.3	**16.8**	5.4
$*BA_{Ref}$	UAVk10	**13.2**	9.2	2.9	**35.8**	10.6
	LiDAR	11.2	11.9	0.05	35.1	9.55
BH(median)	UAVk2	13.2	11.2	1.2	52.7	12.3
$*BA_{Ref}$	UAVk10	15.5	11.4	0.5	52.6	17.5
	LiDAR	**10.8**	8.2	0.4	**41.9**	10.4

Nevertheless, UAVk2 (BH average) has the best results of all the samples, whose average of error is the lowest when compared with the other samples and the maximum error is about 17%.

The maximum error for all the UAVk2 (or UAVk10) samples in the estimation of building volume was about 53% for the same building (ED9_16). The maximum errors from LiDAR correspond to the estimated volume of building ED5, which also had the maximum error for building height.

In Figure 2.47, we can see the behaviour of building volumes estimated from the UAVk2 and LiDAR point clouds based on reference area. The LiDAR plots below prove that the building volumes estimated from median BH (Figure 2.47b) have a better approximation to the reference values in comparison with average BH (Figure 2.47a).

The circles in Figures 2.47a and 2.47b identify two peaks that represent the outliers in the estimation of volume of the complex buildings ED1_2 and ED9_16, respectively. Furthermore, the plot in Figure 2.47c proves that the estimated curve for UAVk2 has a slightly better approximation to the true values using the average

measure for BH. The circle in Figure 2.47d identifies the presence of two outliers, which represent two of the major errors obtained in the estimation of the building volume from the UAV point cloud. These two outliers represent buildings ED1_2 and ED9_16 (Figure 2.45), whose percentage error is significantly lower when we use the average measure for BH (Figures 2.47a and 2.47c).

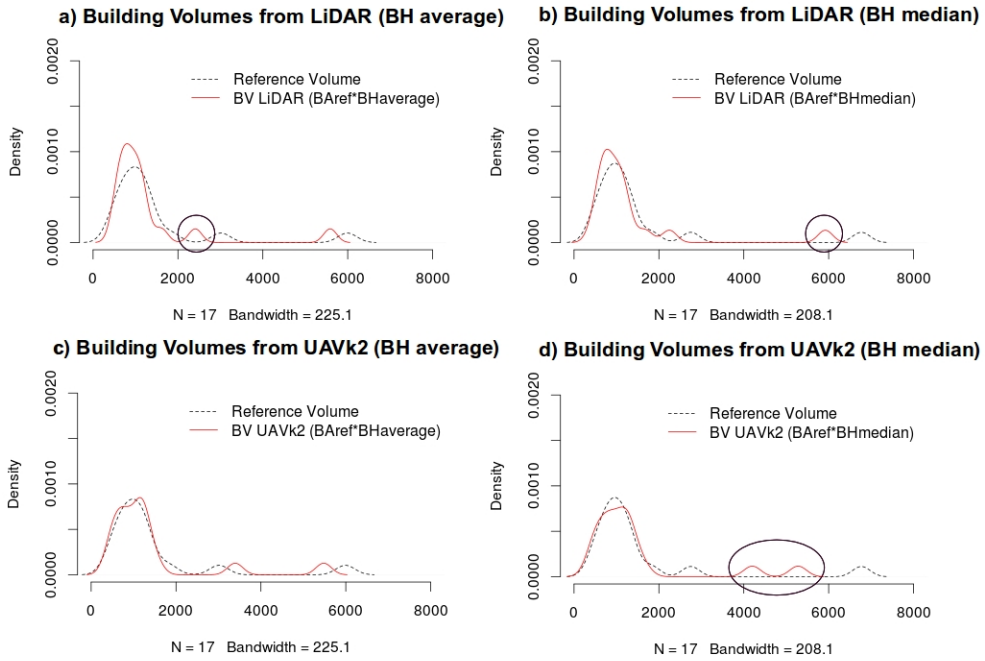

Figure 2.47: Empirical density functions of building volume estimated from each LiDAR and UAVk2 point clouds (with reference area) and reference building volume.

The usage of average building height can be better for estimation of the volume for complex buildings than the median building height, as can be demonstrated for all the results of building ED1_2 (Figure 2.45). Next, we will analyse the building volume estimated only from 3D point clouds.

Building Volume (using only 3D point clouds for BA and BH)

The building volume estimated in this context depends on the accurate level of building height and area parameters extracted from a 3D point cloud. According to the building areas accepted above, the relative building volume errors obtained for each building are shown in Figure 2.48. The magnitude of relative errors was higher than the previous case (Figure 2.45), because the accurate level of the building area was lower.

The usage of median or average building height has less impact on building volume error, because the building volume also depends on the building area error (Figure 2.48). The UAVk2 point cloud for 40% of the estimated building volume has a percentage of error under 10% for both measures adopted in the estimation of building height. Additionally, for the UAVk10 there was also around 45% of the building volume that have had a percentage of error under 10%. However, the results obtained for these clouds were worse for the building volumes estimated from median BH, where over 20% (UAVk2) and 9% (UAVk10) of the building volume had an error of 20% more than the building volume estimated from average BH.

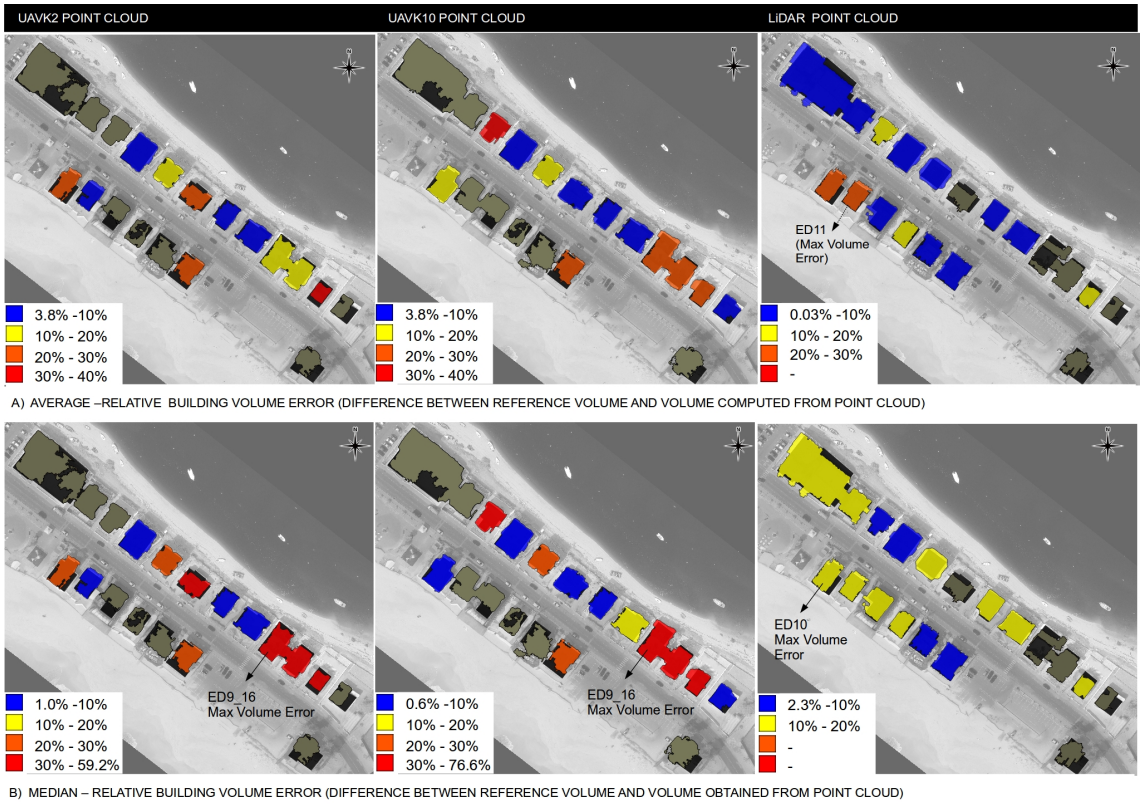

Figure 2.48: Relative Building Volume errors acquired for the building volumes estimated only from point clouds. The grey buildings illustrated were not considered.

The results of the LiDAR point cloud were slightly better, since the maximum value of relative error for building volumes estimated from average and median building height was under 30% and 20%, respectively.

In Figure 2.48a), the building volume estimated from LiDAR data had a relative error of under 10% for about 62% of buildings, unlike the building volume of Figure 2.48b) (about 31%). However, the errors were under 20% for every building volume estimated by using median BH.

According to Table 2.19, the best statistical measurements achieved for the estimation of building volumes from UAV point clouds were achieved with the average of building height parameter.

Table 2.19: Statistical measures of Relative Building's Volume error (%) obtained for building volumes estimated from point clouds.

BV Parameter	**Point Cloud**	**Average**	**Median**	**Min**	**Max**	**Standard Deviation**
BH(average)	UAVk2	**17.2**	16.9	3.9	**38.3**	11.7
*BA	UAVk10	**15.1**	11.9	3.8	**32.4**	10.6
	LiDAR	**10.2**	8.7	0.03	28.1	8.4
BH(median)	UAVk2	22.2	24.7	2.3	59.2	17.8
*BA	UAVk10	20.9	10.1	0.6	76.7	23.0
	LiDAR	**11.1**	11.3	2.3	**19.7**	5.7

Nevertheless, the average of relative errors (Table 2.19) achieved for UAVk2 building volume (17.2%) were about twice the average value obtained for the case of BV_type I (Table 2.18). The magnitude of this error is mainly due to the difficulty of estimating accurate values for the building area, where for this assessment around 40% of all the buildings were previously removed. Additionally, it is important to highlight that the range of relative building volume errors from UAVk2 in relation to the previous case greatly increased to twice as much (Table 2.18). The best range of relative error was given from the LiDAR point cloud, between 2.3% and 19.7% (using median for BH).

Moreover, the magnitude of errors achieved for this data is similar to the values registered for the building volumes estimated with reference building area (Table 2.18). This mean that the magnitude of building area error achieved from this point cloud (Table 2.15) has a low impact on the estimation of building volume. On the other hand, this can mean that the errors obtained regarding building area were statistically compensated by the building façade height errors. For example, the building volume of building ED5 was estimated with an error of under 10% (Figure 2.48a), because the large building area error of -73.2 m^2 was compensated by the large building height error of 3.45 m (Figures 2.40 and 2.42).

However, the empirical density functions (Figure 2.49) can better help in the interpretation of these results. The estimated UAVk2 curve for building volume has a slightly better approximation to the exact building volume values using the average measure for BH (Figure 2.49a). The building volume estimated from LiDAR

using the average BH seems to have a better approximation to the exact building volumes than the usage of median BH (Figures 2.49c,d).

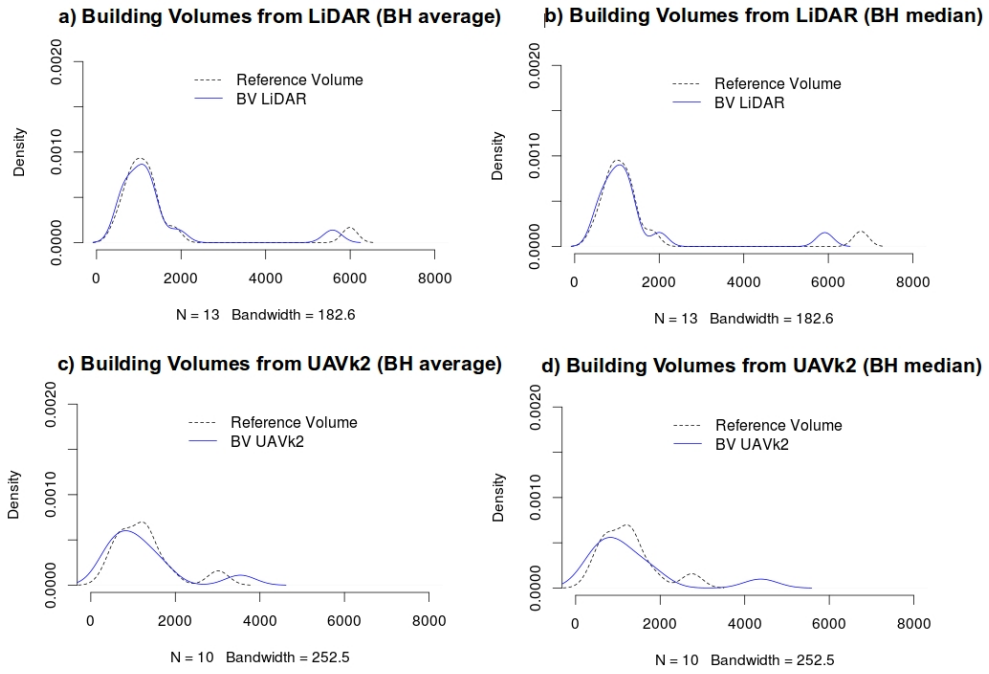

Figure 2.49: Empirical density functions of building volume estimated from each LiDAR and UAVk2 point clouds and reference building volume.

Every building volume estimated from a 3D point cloud depends on the magnitude of the building area and building façade height errors. In addition, building volume error was the result of a statistical compensation between the building area and the building façade height errors. Therefore, we may ask: *What is the best point cloud sample for the estimation of this parameter?*. This is a tough question, because of the nature of this parameter, where the compensation of errors could not be controlled from each variable involved.

Hence, lower errors in terms of volume do not mean good quality in extracted buildings. In other words, lower building volume errors do not imply that the extracted building volume is closer to a correct shape and height. The best solution is to evaluate separately the quality of the building parameters involved in its calculation.

Total Volume

The total volume (T_{vol}) parameter is the sum of all building volumes for a

delimited zone, given by the following equation:

$$Tvol = \sum_{i=1}^{N} BV_i, \tag{2.11}$$

where N is the number of buildings included in the delimited area.

The total volume obtained from the building volumes estimated will be evaluated to ascertain the error level of built-up volumes estimated from this data.

Table 2.20 shows the exact and estimated total volume values, the error obtained from the difference between the true and estimated values, and the percentage error in the estimation of this parameter. These values are presented for the total volume computed with exact building area (reference) or with building area estimated from point clouds. In this table, only the best results achieved for the samples above are shown. The relative total volume error of the other samples can be seen in Appendix F.

Table 2.20: Relative total volume error of building volume computed from BA (BAref-exact value; or BA estimated) and BH estimated from point cloud.

Type of BV	**Point Cloud**	**Tvol Reference** m^3	**Tvol Estimated** m^3	**Tvol Error** m_3	**Relative Tvol error %**
BHave*BAref	UAVk2	23953	23099	854	3.6
BHave*BAref	UAVk10	22426	21218	1208	5.4
BHmed*BAref	LiDAR	24453	22027	2426	9.9
BHave*BA	UAVk2	12685	12235	451	3.6
BHave*BA	UAVk10	12617	13127	-510	4.0
BHave*BA	LiDAR	18666	18140	526	2.8

The percentage of error achieved in the total volume represents the percentage of volume error in the total reference volume. The percentage of error for total volume ranged between 2.8% and 9.9%.

The values obtained for UAVk10 or LiDAR point clouds are higher with the usage of a more accurate building area than with an estimated building area. The reason for that is because the errors in terms of building height were compensated by the large errors obtained for the building area. However, the sample of UAVk2 shows more consistence, where the relative error is 3.6% for both results. This means that the compensation between errors was irrelevant for the total volume estimated

by UAVk2.

Most total volumes estimated were underestimated, unlike the total volume of BV type II estimated from UAVk10 (-510 m^3). This total volume error is distributed along each building and it is not distributed evenly, it depends on building type.

The buildings represented in Figure 2.50 give us a measure of the visual impact of these volume errors in each building, where the sum is the total volume error.

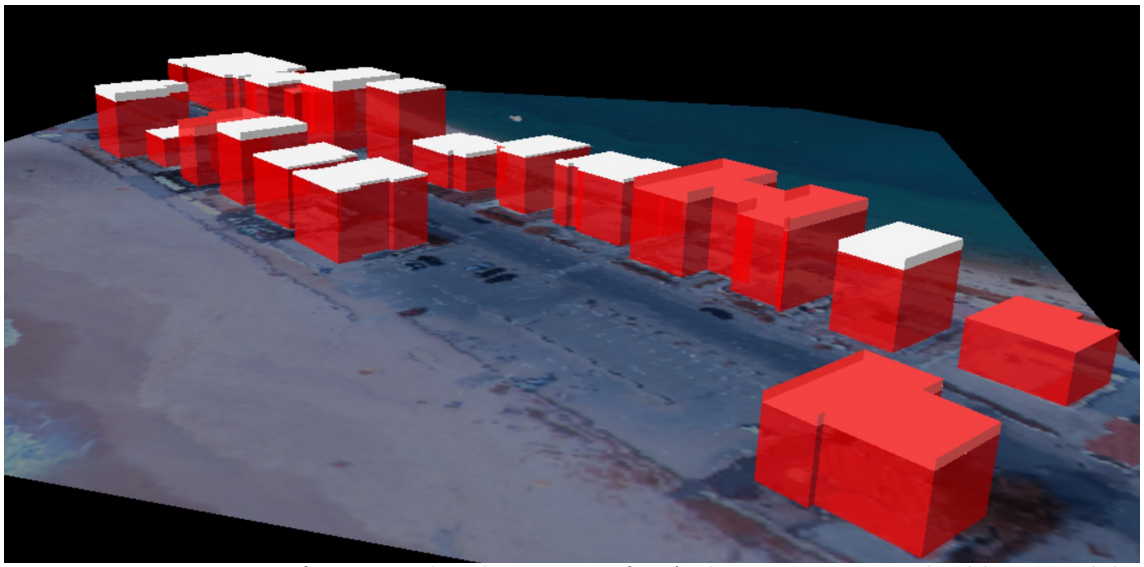

Figure 2.50: Impact of average height errors of UAVk2 on exact 3D building models. Reference building volume is represented in red. The resulting 3D UAVk2 building model is also represented by differences in height (white).

After this analysis on the magnitude of errors for all the building parameters, we had to evaluate the usability of these parameters for urban planning. The next section will discuss these results from the point view of an urban planner.

2.4 *Usability of LiDAR and UAV for urban planning*

Currently, the concept of smart cities is being thoroughly discussed. This concept has been progressively introduced in the speech about cities and, albeit lightly, in the strategic urban planning practice. This concept involves six dimensions: smart economy, smart mobility, smart environment, smart people, smart living, and smart governance. The concept has attained such popularity that nowa-

days cities are ranked based on the status of the aforementioned dimensions. The concept and the practice of the smart cities idea includes the notion of efficiency derived from the intelligent usage of information and communication technologies.

In this context, acquisition, processing and geographic information management technologies play an important role on the following levels: in terms of the quantitative and qualitative analysis of the city, regarding the characterization of the physical urban components (buildings, roads, blocks, infrastructures, etc.), and diagnosing and monitoring the physical indicators that have contributed to the promotion of a sustainable city. One of the classic problems regarding city management is the rigorous implementation of the objectives and measures established by the plan (a plan which is understood as a formal process of city creation and management). In spite of the existence of urban planning, informal urban construction is quite common – just as the densification beyond the boundaries foreseen in the plan is also common. In this context, 3D modelling of urban data, namely data obtained by LiDAR or UAV technologies shows the required accuracy both to estimate the volume of constructed mass for urban analysis and to present planning proposals that can later be offered for public discussion; as well as to monitor informal changes that can be witnessed in the city (Tenedório et al., 2013, p.218).

The methodology employed for the measurement and representation of 3D urban buildings was evaluated above for a sample of buildings in an urban coastal area. The study area is part of the Shoreline Spatial Plan (POOC - Plano de Ordenamento da Orla Costeira) between *Vilamoura* and *Vila Real de Santo António* in the South of Portugal with a total extension of 75 km (RCM No.103/2005, 27th of May). The Praia de Faro is located about 10 km from Vilamoura (West of Praia de Faro). The POOC plan covers a land strip with a maximum width of 500 m from the coastline.

The objective of this POOC is the **requalification, valorisation and protection** of this coastal area. Therefore, it intends to homogenise criteria of classification and identification for the coastal land, taking into account some particular aspects: a) the balance between shoreline and the occupation along the coastal strip; b) the protection and valorisation of sensitive areas; and c) the coordination of criteria with the existing Master Plans. Moreover, this POOC intends to: a) harmonize the future urban occupations, tourism and equipment with natural and cultural values, the landscape and the level of risk, establishing specific safeguard measures; b) rectify severe territorial dysfunctions, such as the construction in vul-

nerable and degraded areas on land of public water domain and adjacent areas; c) requalify degraded areas by the demolition of buildings and implementing renaturalization actions for habitats; and d) implement a set of measures and actions that will support a sustainable and integrated coastline management model.

In this context the coastal urban area of Praia de Faro was included as an operating unit of planning and management (Unidade operativa de planeamento e gestão) in Article 80 of the RCM No.103/2005. The UOPG is a territorial unit that can integrate more than one spatial class and it is isolated from the remaining coastline. The aim of this UOPG, also called UOPG III, can be seen in Article 83, of the RCM No. 103/2005, of 27th May, is to provide guidelines for the requalification and valorisation of Praia de Faro. The aim of this intervention in Praia de Faro is: i) carrying out a requalification project in the public water domain (*Domínio público hídrico*); and ii) drafting a design plan for the area, which is not in the public water domain.

However, the study area of Praia de Faro considered in this chapter is part of the intervention area of the design plan that is not in the scope of the public water domain and whose built environment will be restructured. The part of legislation RCM No. 103/2005, of 27th May, can be seen in Appendix G.

The UOPG contains a set of actions within a program that require an updating of the buildings that exist in the built-up area. The LiDAR and UAV data may be useful to the fast execution of some actions, since the large-scale 1:2000 digital mapping produced in 2002 by accurate methods is outdated. The LiDAR and UAV data can provide the updating of the built-up area through orthophotos and 3D point clouds for the resolution of some actions included in the UOPG (Article 83 (2) of RCM No.103/2005, of 27th May). As described below, it can be used to:

- elaborate a cost-benefit analysis that considers the removal of the existing buildings in the area that is not in the public water domain as an alternative to the protection solutions for the buildings located in the risk range. The identification of the built-up area by the methodology presented is enough for the execution of this analysis, where all the buildings of the area can be extracted from point clouds. On the other hand, we can estimate approximately the total volume of buildings that must be removed to estimate the total demolition or rehabilitation costs;
- relocate the permanent private owners that are located in the public water

domain to the area that is not in the public water domain. The extraction of building height from point clouds allows us to estimate approximately the number of stories and therefore the number of residents in each building to help relocating private owners;

- demolish and remove buildings placed in the public water domain. For this the UAV or LiDAR point clouds provide useful data for the identification of these buildings;
- plan pedestrian access along the built-up area to be restructured. As indicated above, we can identify this built-up area with 3D point clouds;
- renaturalize degraded areas and areas that will not be occupied. All the areas that are not built-up can be recognized from UAV or LiDAR data.

The usability of 3D point clouds for the extraction of building parameters in an urban area as heterogeneous as Praia de Faro was demonstrated by the methodologies proposed over this chapter. In this particular area, each building looks like a case study. Now, it is possible to answer the questions posed at the beginning of this chapter.

a) What type of tools are effective for the extraction of building parameters from the perspective of an urban planner: FOSS or proprietary tools?

Both – proprietary or FOSS tools – pose the same problems for the extraction of a regular and correct shape of the roofs. The difficulties in extracting building area and building façade height depend on roof type complexity, which make the application of tools for point cloud filtering much harder.

Depending on the complexity of the urban area, we might have to manipulate and implement other methods and adjust tools for the specific problems. This is only possible with FOSS tools. The LiDAR Analyst is limited to the LiDAR point clouds and it is a 'black box' for the extraction of building parameters. On the other hand, the manipulation and visualization of 3D point clouds with billions of 3D points for this type of applications is not possible with a usual GIS desktop, unlike GRASS (FOSS).

FOSS tools are a good solution for an urban planner that wants to identify buildings in an urban area or to manipulate data for the extraction of parameters. Thus, the financial implications are also a strong reason to use FOSS tools.

b) Is it possible to extract accurate building parameters solely from 3D point

cloud data without accurate 2D/3D vector data acquired from stereo restitution?

3D point clouds allow us to extract accurate building façade heights without accurate 2D/3D vector data (provided by photogrammetry or topographic survey). The challenge is the extraction of accurate building area from point clouds of very heterogeneous urban areas, where most buildings have a higher diversity and complex roof types.

The building volume parameter can be strongly affected by the quality of the extracted building area, which is more difficult to extract. Therefore, the usage of accurate building outlines obtained from stereo restitution for some complex roofs could be necessary to estimate this parameter.

However, there is strong evidence that 3D points acquired from UAV or LiDAR systems can be enough for the estimation of building parameters with an effective methodology and without accurate 2D/3D vector data.

c) *Is the 3D point cloud appropriate for the extraction of building parameters with an acceptable quality? If so, how can we integrate this data into urban planning?*

Both 3D point clouds have high vertical accuracy at the cm-level that allows us to extract accurate building parameters for urban planning.

This data for the generation of 3D building models - LoD1 - is enough for a public discussion of a detailed plan. Additionally, the delimitation of built-up areas or the block buildings of Praia de Faro from this data might be useful to guide the urban planner and the architects on the requalification of that area. Finally, for the monitoring of an urban area the accuracy level of building parameters is enough, since changes can be detected below one story.

The difficulty is to implement a methodology that enables a higher positional accuracy at the level of a detailed plan. However, further analysis is needed regarding the usability and relevance of the data for a wider building sample, where the improvement of the methodologies presented can be fully automated for a wider range of roof types.

2.5 *Synthesis*

This section summarized the main conclusions resulting from the methodologies developed for the extraction of building parameters in Praia de Faro using 3D

point clouds – UAV and LiDAR. They can be summarized as follows:

a) *On the evaluation of automatic extraction of building parameters for the generation of 3D building models from a LiDAR point cloud*

This first approach to the usage of LiDAR data in urban areas has revealed potential use for the delimitation of built-up areas or building blocks in an urban area. The individualized shapes of the building rooftops are difficult to extract automatically using the workflow implemented in the LiDAR Analyst, because of the high diversity of roof types and irregular shaped roofs. The LiDAR technology has the great advantage of enabling the production of 3D block models of LoD1 by extruding the building rooftops (or building polygons) using the attribute of building façade height estimated from LiDAR data.

Additionally, the automatic extraction of building height from LiDAR has revealed an acceptable accuracy regarding the height values obtained by topographic surveying. Finally, the quality of the extracted building parameters strongly depends on DSM and DTM positional quality (These products were generated over this automatic methodology).

b) *On the evaluation of the LiDAR point cloud for the extraction of building façade height parameter*

We have demonstrated that the magnitude of error for the building façade height acquired from LiDAR is strongly dependent on roof types and on whether there is any vegetation or any other objects around the base of the building.

The usage of LiDAR data for the extraction of building parameters, building façade height and building volume has revealed great potential for buildings whose rooftop is flat. The magnitude of vertical error of the building façade height parameter is lower than the height of a story. It is much lower for the flat rooftops than for the building roofs with railings or parapet wall. On the other hand, the magnitude of error acquired in the total volume estimated was not relevant and is acceptable at the urban planning level, namely for the usage in the characterization and analysis of the intervention area of an urban plan. However, the magnitude of this error might be significant when it comes to urban projects.

Analysing the sensitivity of LiDAR in the extraction of this type of data is important to adjust the methodology to larger built areas for a greater sample of buildings. The real extraction of these building parameters will be made without

accurate vector data in a context of urban planning to acquire or update 3D data.

c) *On the evaluation of the LiDAR point cloud for the characterization of building roof types*

This first approach to the use of a LiDAR point cloud for the characterization of building roof types has revealed potential use in a set of buildings that have similar characteristics in terms of slopes and material contrasts. There is a moderate relationship between slope and pulse intensity which should be explored for this type of applications. However, the proposed framework for the characterization of roofs from LiDAR data should be tested on larger built-up areas, in order to enable the identification of a standard behaviour under the heterogeneity of the materials on the building roofs, and also roof shape and composition.

d) *On testing and comparing the usability of LiDAR or UAV data for the extraction of building parameters using FOSS technologies*

This work introduced a methodology called 3DEBP (FOSS solution) for the semi-automatic extraction of building parameters from a 3D point cloud. Moreover, this study also compares and analyses the accuracy and performance of different point clouds (LiDAR or UAV) for the extraction of these building parameters.

The most useful characteristics when using the 3DEPB solution for this study area are: a) the capacity to process dense point clouds within a geographical spatial database; and b) the possibility of automating some of the procedures involved in the extraction of building parameters.

The results obtained in the extraction of building parameters from 3DEBP are very similar using either LiDAR or UAV. However, we can conclude that if the urban area has dense vegetation and tall trees near the buildings, UAV data can be more appropriate, because it has less 3D points recorded in these areas. However, this is only true if the building is not completely surrounded by trees, otherwise we would have gaps in the buildings.

The major difficulty in this study was the extraction of accurate building roof (or area) data with a regular shape from point clouds. Even facing a wide variety and complexity of building roofs (with various slopes), the results are acceptable for some of the stages of an urban plan.

e) *On the usability of LiDAR or UAV for urban planning*

LiDAR or UAV point clouds can be a great advantage for the generation of

LoD1 block models of buildings by the semi-automatic extraction of building height and rooftop. However, if there are any building rooftops (or building areas) that cannot be extracted from the methodology or data, then the building oultines (2D vector data) should be used for the creation of 3D building models.

The faster updating of 3D models on time can create a new paradigm in the geovisualization and monitoring of coastal urban areas for urban planning. This modelling process may represent an important step towards the operationalization of data processing methodologies for the virtual reconstruction of buildings based on LoD1 models.

We believe that UAV data together with a robust methodology using FOSS tools can be very useful for the production of 3D buildings models for urban planning. The results clearly show that UAV technologies are a valid alternative to LiDAR. These findings have significant consequences in terms of project management in urban planning, with important methodological and financial implications. The quality of the results shows that a UAV point cloud can be enough for: i) the process of discussion and public participation in the planning process; ii) the monitoring of the built-area, such as the detection of illegal changes in the height of buildings.

Both technologies will ensure the permanent updating of 3D geographic data for urban planning, supporting the monitoring of shoreline spatial plans and detailed plans for coastal urban areas. Moreover, the monitoring of plans can ensure the maintenance of an urban settlement policy that is sustainable over time.

In view of the results reported in this chapter, we can argue for the usage of the information acquired by LiDAR or UAV technology. In spite of its costs, we believe it is advisable to plan for its acquisition especially for urban areas that are under severe urban pressure and are consequently inclined to generate very strong dynamics – both formal and informal. Following this path, LiDAR technology – as well as the blossoming technology based on UAV acquisition – suggests the permanent updating of the information needed to monitor sustainability conditions for smart cities.

The next chapter will demonstrate the usage of very high resolution UAV imagery for the extraction of height and volume on urban morphology building blocks. The usability of these results will be demonstrated for high precision dasymetric mapping.

Chapter 3

Modelling 3D UAV Point Clouds for Urban Planning: The Case Study in the Urban Area of Amadora City

Nowadays, efficient technologies such as airborne systems with active or passive sensors require robust and optimized geoprocessing models to acquire geographical information of urban areas, as described in Chapter 2. The testing is also essential to understand their performance in the extraction of building parameters on different urban morphologies. Therefore, urban morphology can define the small spatial unit for the extraction of these parameters, such as a) building parameters from previously tested single-family dwellings; and b) block parameters (i.e. building blocks) from a residential building urban area or city block.

Building block parameters can support many studies and important urban planners' tasks that are currently hard to achieve because of the difficulty in acquiring low-cost updated 3D data. The definition of urban planning indicators based on 3D building spatial databases can optimize the urban morphology of a city, allowing for a better quality of life, improving namely pedestrian and thermal comfort within its boundaries.

Different studies performed by different authors have ascertained that the quantification of the morphological properties of an urban structure, such as the mean height and volume of building blocks, can be helpful. For instance, the re-

lationship between urban morphology and urban air ventilation environment performed in Ng et al. (2011), the definition of urban planning indicators, such as the green coverage ratio for the evaluation of urban thermal environment in a city (Zhao et al. 2011; Yahia & Johansson 2014), investigate the relationships between morphology and land use based on the volume of each block (Yoshida & Omae, 2005), as well as the characterization of urban typologies over time (Hermosilla et al., 2014).

This chapter addresses the usability of UAV data for the extraction of building block parameters in a small residential area in the Lisbon region. The usage of a UAV point cloud will be demonstrated for different urban typologies, whose smallest spatial unit is the block. This demonstration will be based on three studies: 1) the development of a methodology to evaluate UAV data for the extraction of building height parameter using FOSS tools, GRASS GIS and R software; 2) extraction of average (or median) building block height and volume using the **3DEBP** solution developed and presented in Chapter 2, followed by its evaluation; and 3) the demonstration of a new dasymetric mapping technique focused on building parameters extracted in a previous study. This latter study will demonstrate the usability and pertinence of UAV technology for urban planning.

3.1 *Study area and data acquisition*

The study area corresponds to a small neighbourhood in the outskirts of Lisbon. It belongs to the urban area of Amadora, located about 10 km from Lisbon. The selected geographic area has a total area of about 9 hectares, 150 metre-wide North to South and 600 metre long East to West (Figure 3.1). This neighbourhood features some steep slopes in the Northwest and all the streets have sidewalks on both sides. It is bounded South by the railway line. There are also some scattered trees near the building blocks and a street to the East lined with trees.

This small neighbourhood has around 2000 residents according to census data for 2011, and the total area of the building blocks is about 18200 m^2. This dwelling area has 88 buildings grouped into 7 residential building blocks with tiled roofs and heterogeneous shapes (Figures 3.1).

The characteristics of the chosen neighbourhood allowed the distinction between three types of building blocks: a) regular; b) irregular, and c) building islands (Figures 3.1). Afterwards, the study area was split into three areas A, B and C,

according to the urban morphology of the building blocks. These 3 areas allowed us to evaluate the behaviour of the point cloud when estimating building façade height from different morphologies.

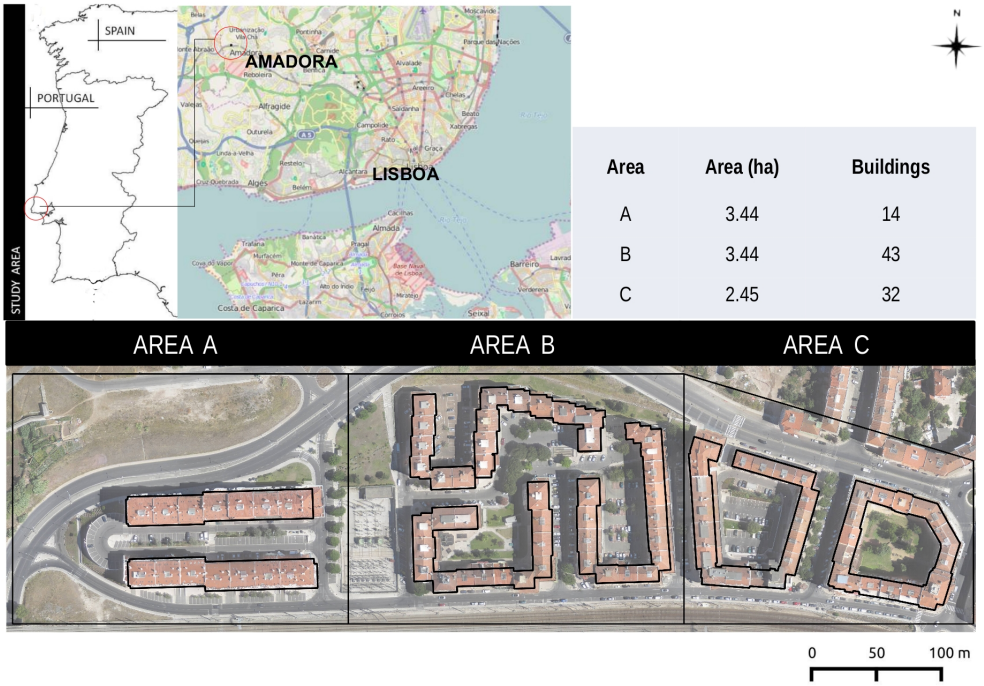

Figure 3.1: Study area of Amadora city, Portugal.

The building blocks in area A are six-story high in the northern block in the southern façade and five-story high in the northern façade of the southern block (Figure 3.2). However, the other building blocks of areas B and C have diversified building types (Figure 3.3). The number of stories of the buildings in area B varies between 4 and 6. In area C, the number of stories is between 4 and 7.

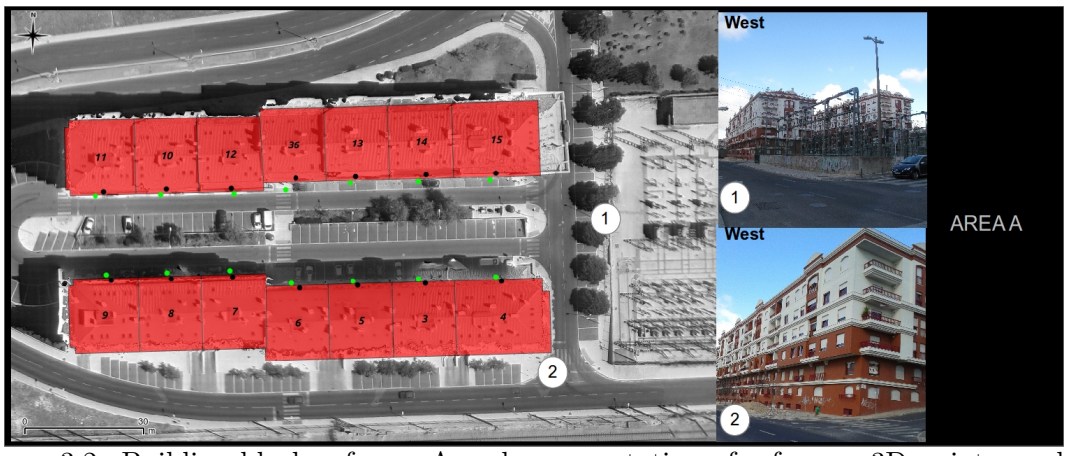

Figure 3.2: Building blocks of area A and representation of reference 3D points used in this case study (green points: elevation ground points; black points: elevation roof points).

Figure 3.3: Building blocks of areas B and C and representation of reference 3D points used along this case study (green points: elevation ground points; black points:elevation roof points).

3.1.1 UAV point cloud

At the end of the summer of 2012, a residential area of Amadora (about 90 hectares) was covered by 237 stereo aerial images (3000 by 4000 pixels each image) acquired from a swinglet CAM. This was the same UAV that was used to cover Praia de Faro (Figure 2.5 of Chapter 2).

The flight planning was performed with 10 flight lines during approximately 20 minutes. The stereo aerial images have a higher overlapping between them, which is about 80% along flight and 60% cross flight overlap. The GSD of these stereo images is about 6 cm.

The workflow of UAV imagery acquisition can be consulted in Figure 1.10 of Chapter 1. The UAV point cloud was obtained by an automatic processing workflow based on multiple stereo matching of a subset of stereo aerial images implemented in PIX4D. Along this procedure, 8 GCPs were used in order to obtain a more accurate point cloud. The report of this procedure can be found in Appendix H.

The 3D point cloud produced has 8.9 millions irregularly distributed points (Figure 3.4). However, the study area has little more than one million points (1.066.171 points).

The description of the point cloud data for each area A, B and C included in the study area can be seen in Table 3.1. The average density of the UAV point cloud of the study area is about 11 points per square metre, which means that the

average distance between points is about 30 centimetres.

Table 3.1: Characterization of point cloud areas

Areas	**Area (m^2)**	**No. of points**	**Point Density (points/m^2)**	**Average distance* between points**
A	34400	364811	10.6	0.31
B	34400	406185	11.8	0.29
C	29400	295175	10.0	0.32
A+B+C	93314	1066171	11.4	0.30

* The average distance between the two closest UAV points is the inverse of the square root of the point density.

Learning these point cloud parameters is important to know how the point cloud can be good at detecting object edges. Generally, the point density should be higher than 4pts/m^2 for these type of studies.

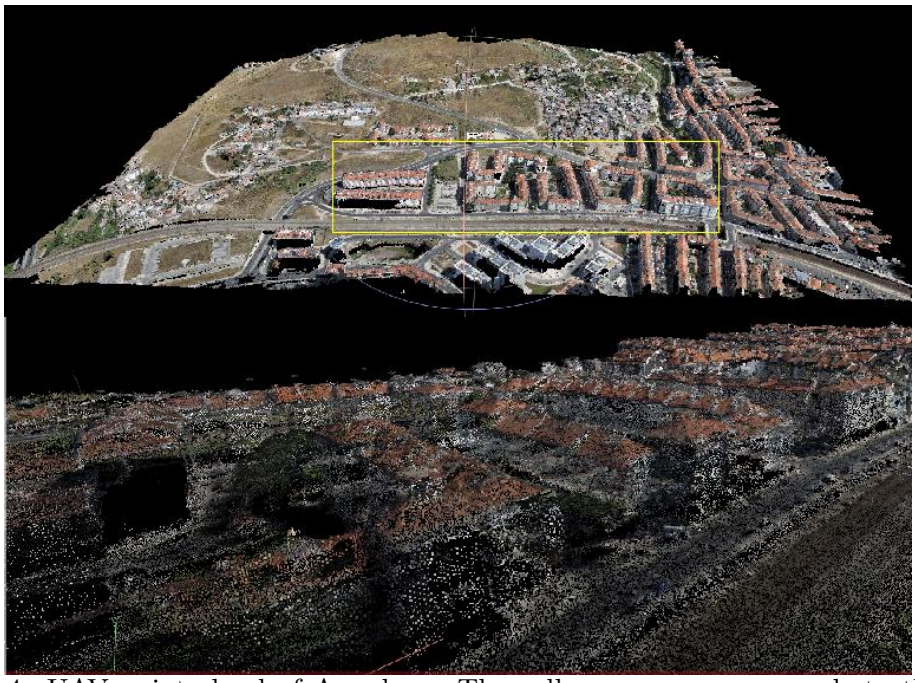

Figure 3.4: UAV point cloud of Amadora. The yellow square corresponds to the study area.

It is important to highlight that the UAV flight planning did not correspond to a traditional flight as established by the traditional photogrammetry regulations. In this type of acquisition the aerial images can achieve tilt values (angle of verticality) that would be unacceptable for traditional photogrammetry, where generally the tilt values should not be higher than 4°. In this case, most tilt image values in the study area range between 5 and 10 degrees and the maximum tilt value was 23° (Figure 3.5).

Figure 3.5: Trajectory flight lines performed by swinglet CAM on the area selected and the tilt values for each exposed image (adapted from Rebelo et al., 2013a).

The scale of these values is acceptable, because the objective is not to acquire 3D measurements through classical 3D stereoscopic vision. Besides, the dense image matching algorithms implemented for the processing of these aerial images can deal with these tilt values.

3.1.2 Reference dataset

The large-scale 2D/3D vector data was important for the development of methodologies and also for the evaluation of the results that will be detailed in this chapter. The vector data presented in Table 3.2 was kindly provided by SINFIC.

Table 3.2: Characterization of reference vector and raster data

Type of Data	**Year**	**Data**	**Technical acquisition**	**Details of data**
2D vector data	2003	Building outlines	Photogrammetric restitution	Large scale: 1:2000
3D vector data	2003	Elevations of roofs and terrain (near the buildings)	Photogrammetric restitution	Large scale: 1:2000
Raster data	2012	True Orthomosaic	Data source: DSM (produced from UAV point cloud) and aerial images from a CanonIXUS220HS_4.3 camera (12.1 MP)	GSD: 6 cm; For visual inspection of results.

The horizontal and vertical accuracy was evaluated by SINFIC company, which enabled this data to have higher positional quality.

The 3D vector points on the top of the building and building base elevation (Figures 3.2 and 3.3) were used to calculate the reference building façade height, which was used for the evaluation of the results obtained in this chapter. Moreover, this vector data was also used as reference in the extraction of building façade height performed in the first study.

3.2 *Evaluation of UAV point clouds for the extraction of building façade height from different block morphologies*

The main challenge of this study was the evaluation of average building height extracted from a UAV point cloud, whose spatial unit was the block. The spatial individualization of contiguous buildings with very similar heights in the same building block is a big challenge for filtering algorithms. Therefore, depending on the proposed target, the filtering of UAV data for the extraction of building height within a block was simplified by resorting to the usage of reference 3D data.

Furthermore, the demonstration of a UAV point cloud in different block morphologies is needed to understand the behaviour of this data for the estimation of this building parameter. This type of approach had already been made for the LiDAR data of a small coastal urban area shown in Chapter 2 (Section 2.3), but in that case the spatial unit was the building and not the block.

The methodology developed for the extraction of average building height within a block was based on spatial analysis functions implemented in free and open source GRASS GIS and R. Specific functions developed to filter LiDAR data were tested in this methodology to filter UAV data, which was also another challenge in this demonstration. Various authors, such as Sanchez & Brovelli (2007),Brovelli et al. (2002) and Barazzetti & Brovelli (2008), have tested the processing of LiDAR point clouds in GRASS GIS. More details about GRASS functions that were used to filter the UAV point cloud can be seen in Neteler & Mitasova (2008).

The methodology implemented for the evaluation of building height was based on reference vector data and performed in three main phases: *i)* the extraction

of UAV points (rooftop and ground) that will define the building façade height based on a geoprocessing model to filter data; *ii)* computation of average building façade height with R statistical; and *iii)* quality assessment of the extracted building parameters using R.

3.2.1 Building height from spatial unit block

The first part of the methodology included a set of operations that have been implemented in a geoprocessing model within a graphical modeller in GRASS GIS to select: 1) a 'set of UAV points' that defines the elevation of the top of the buildings or near the edge of roof; and 2) a 'set of UAV points' near the building base. The flowchart of this geoprocessing model was split according to these two types of selection (Figures 3.6 and 3.7) for a better understanding of the set of operations performed. Before the start of this set of operations, the UAV point cloud was split into three areas in GRASS according to the specified areas in Figure 3.1. The partition of the point cloud into three areas allowed us to optimize the processing time of this data in each of the schemes (Figures 3.6 and 3.7) that would be detailed.

3D Building rooftop edge points

The extraction of a set of UAV points on the top of the building (or edge points) was performed using the LiDAR analysis *v.outlier* and *v.lidar.edgedetection* functions. However, additional functions were included for this extraction, which are important when recording the results. The main sequential steps (Figure 3.6.) are described in detail in Appendix I (shows the GRASS commands used):

1. First, the 3D point cloud is cleaned by removing outliers using the *v.outlier* function. According to GRASS (2014) the outlier identification is performed by a bicubic spline interpolation of the observation using a regularization parameter and a low resolution parameter to the South-North (*son*) and East-West (*soe*). The parameter values chosen were the same values that have been chosen for the next step (Table 3.3). After this identification, the points above a given threshold value are considered outliers and they are removed. The threshold value considered was tested to 25 metres according to the height of the building blocks.

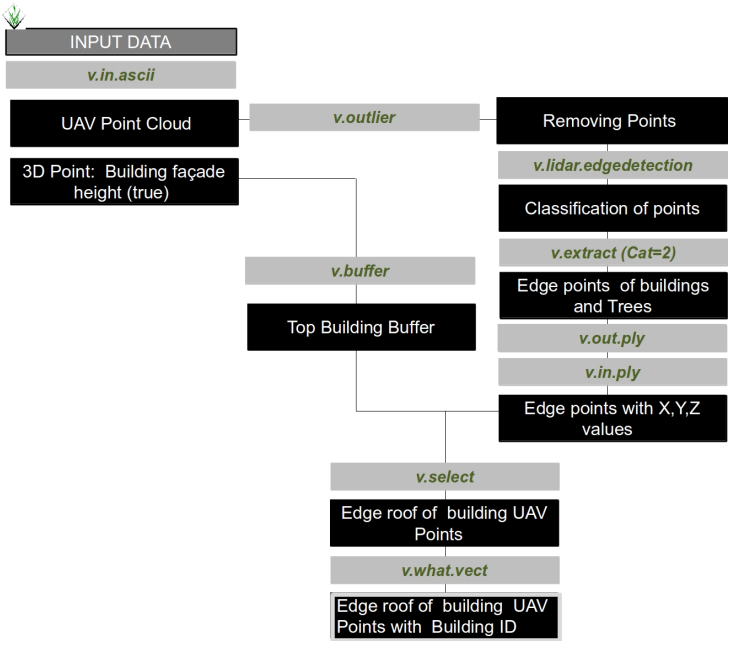

Figure 3.6: Flowchart of the selection of edge points on building roofs.

2. The *v.lidar.edge.detection* function of GRASS LiDAR analysis was used for the detection of the edge points of the buildings. This *v.lidar.edge.detection* function identifies the edges of buildings, trees and streetlamps along the street from a point cloud (Figure 3.6). The edge algorithm uses two interpolation spline parameters to the East (*see*) and North (*sen*) (Neteler & Mitasova, 2008). According to Brovelli et al. (2002), the values of these two parameters should be 3 up to 4 times of the planimetric resolution of the point cloud. In this methodology, we have considered these spline parameters: 2 and 4 times the reciprocal value of the point density value for Test 1 and Test 2, respectively (Table 3.3).

   The edge detection algorithm should be made with the best parameter values to minimize the selection of object points as not roof (points that do not belong to the building rooftop). Therefore, different parameter values were tested to understand the effect of different interpolation spline steps. After several tests, two parameter values were chosen for each area (Table 3.3). The processing time of *v.lidar.edge.detection* is inversely proportional to the parameter value for the same area, as can be seen in Table 3.3.

   The interpolated elevation values of each edge point will be classified by a category attribute value (cat), such as terrain (cat=1), edge (cat=2), and uncertain (cat=3). This classification was used for the extraction of edge points by the *v.extraction* function, where the edge points of a building block

are included.

Table 3.3: Parameter values of spline interpolation in edge detection

Tests	**Area**	**see**	**sen**	**Processing Time**
Test 1	A	0.19	0.19	75 min
	B	0.17	0.17	120 min
	C	0.20	0.20	30 min
Test 2	A	0.37	0.37	53 min
	B	0.34	0.34	50 min
	C	0.40	0.40	25 min

The results obtained in this step for each area using the highest values of spline interpolation are shown in Figure 3.7.

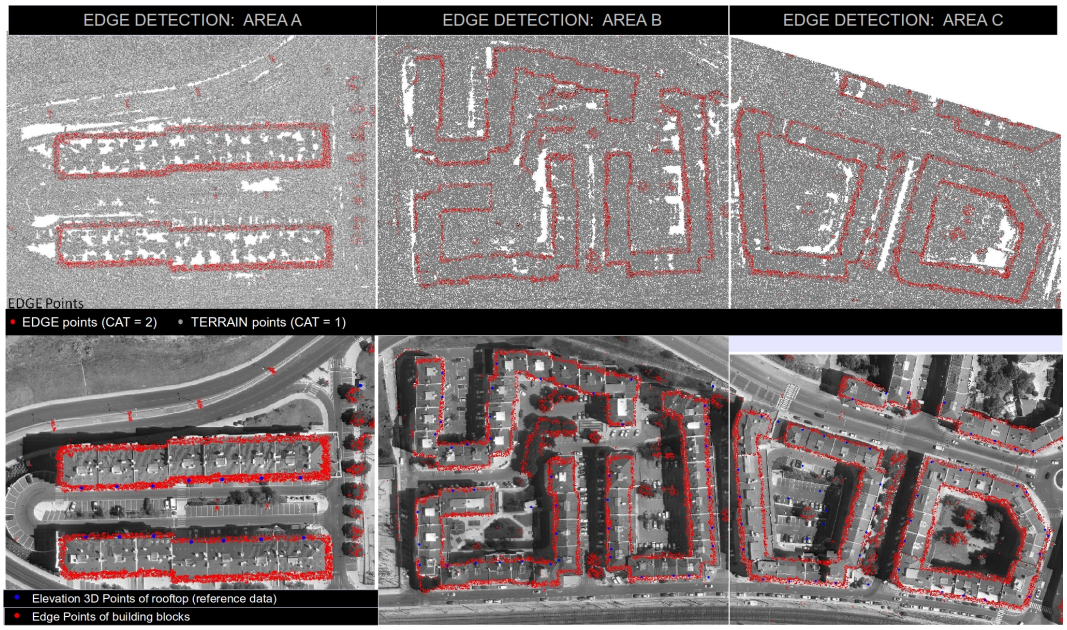

Figure 3.7: The classification of edge (red points) and non-edge points of the areas (grey points). The overlapping of these points in the orthoimage and the 3D points on the roof building edge (blue points) area is also shown.

3. After recording the coordinates X,Y and Z for the edge points, the building edge points (cat=2) that were within 0.8 m of the reference 3D point located on the edge of the roof were selected. This distance was chosen taking into account the average distance between points and the irregularity level of the point cloud in the edge of the roofs, ensuring the selection of a representative set of points. For this action, two functions were used: *v.buffer* and *v.select*. The 3D UAV points selected for each area at the end of this first part are shown in Figure 3.8.

4. Finally, the vector values of the building code in edge point positions were uploaded using the *v.what.vect* function.

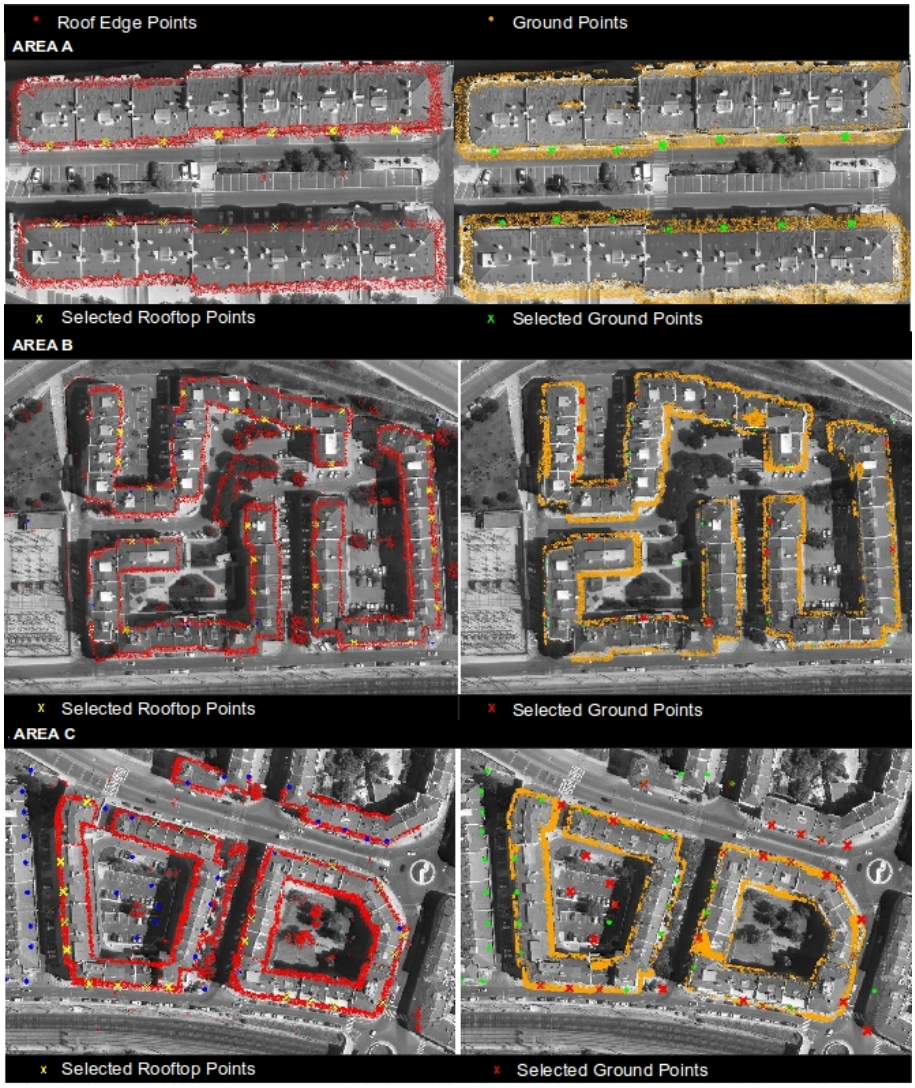

Figure 3.8: Results of the first part of the methodology. The green and blue points are the reference points used for the selection of ground and rooftop points, respectively.

3D ground points of the building base

The extraction of a set of points that defines the building base elevation was performed following these main steps (Figure 3.9):

1. The filtering of UAV data for the selection of 3D ground points near the building base was made from the results obtained at the end of the edge detection procedure (Figure 3.6). Then, the next step was the generation of DTM (or

selection of ground points), which was performed with the *v.lidar.growing* and *v.lidar.correction* functions.

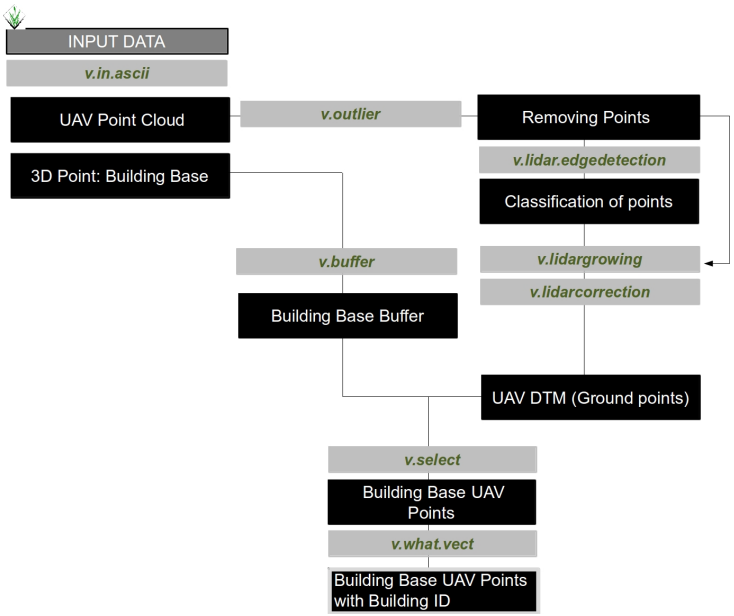

Figure 3.9: Flowchart of the selection of UAV ground points near the base of the building.

The *v.lidar.growing* function aims to fill the previously obtained edge lines, which implies the determination of the building contour and the internal area of every building using the Region Growing algorithm (Barazzetti & Brovelli, 2008). The result of *v.lidar.edge.detection* is rasterized and the convex hull is applied to cells classified as object. The other cells are used to create DTM. More details about this function in GRASS (2014).

Finally, *v.lidar.correction* the last of the three functions to filter data was executed to correct the points wrongly classified as ground. Barazzetti & Brovelli (2008) refer that it is 'based on a preliminary large step interpolation of the points classified as ground and a following analysis of the residuals between the new surface and the sparse points'.

2. UAV points that were within 0.8 m of the 3D reference point located on the sidewalk or near the building base (Figure 3.8) were selected from the DTM. The functions used for this selection were *v.buffer* and *v.select*. The results obtained at the end of this step are shown in Figure 3.8.

It is important to highlight that the buffer distance value for the selection of UAV points should not be less than the average distance between points (see Table 3.1). A reasonable value is required to avoid the selection of façade points or

objects that are not ground. The distance chosen was not enough for the selection of roof and ground points in some buildings of areas B and C (Figure 3.8, buildings that do not have red or yellow points selected), because there are no UAV points. However, if the distance value increases, the probability of selecting wrong points also increases. The difficulty is choosing a distance that ensures the selection of points without wrong ones from a higher irregularity distribution of UAV points.

Average building façade height

The second part of the methodology is the computation of building façade height by the trimmed mean of the elevation values of each of the previous points. The flowchart of this part is shown in Figure 3.10.

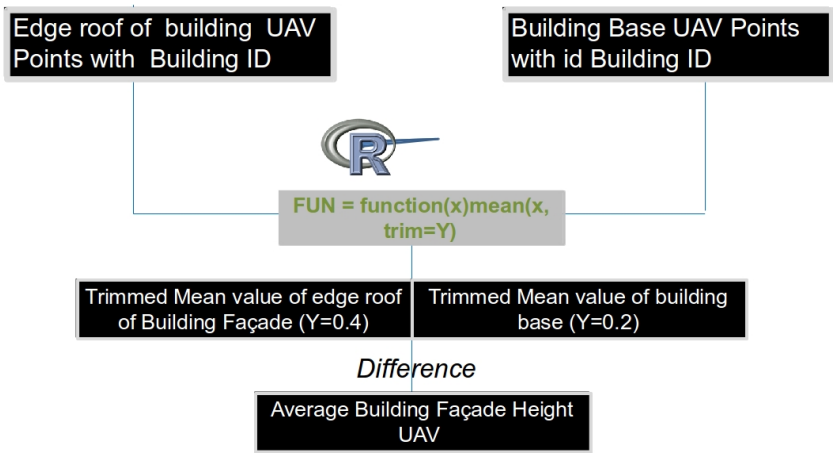

Figure 3.10: Second part of the methodology.

The building façade height was computed with the difference between the trimmed mean values calculated for the elevation points of the top of the building façade (trim =0.4) and the building base elevation (trim=0.2). The trimmed mean lies between the mean value and the median value. This statistical information is very useful to exclude outliers from dense point data with a high gradient of elevation values. The R script used for this step is shown in Listing J.1 of Appendix J.

3.2.2 Assessment of estimated building façade height values

The evaluation of the results achieved for each building regarding the building façade height (BH) parameter was based on the computation of positional vertical errors (Listing J.2 in Appendix J).

The absolute vertical error [VE] value of the estimated building façade height corresponds to the difference between the reference value of 3D vector data and the value estimated from the selected UAV points. This was given by the following equation:

$$VE = |BH_{true} - BH_{Estimated}| \tag{3.1}$$

The magnitude of vertical errors (errors above and below 1 metre) in the estimation of the building façade height for each edge detection process (Test 1 and Test 2) can be seen in Figure 3.11.

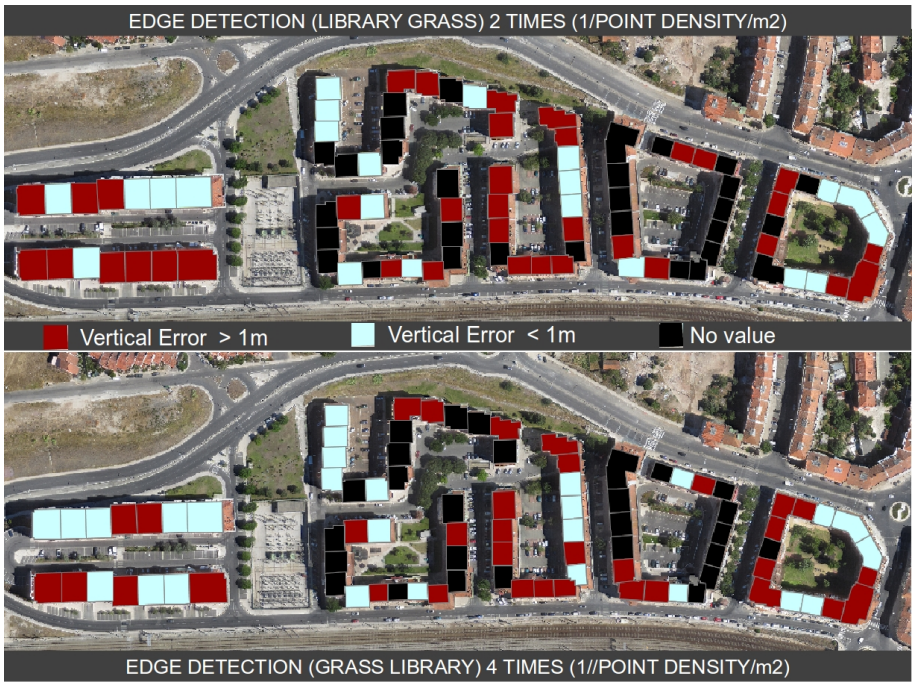

Figure 3.11: Distribution of the vertical error in each area, according to the edge detection process for different spline step values (Source: Rebelo et al., 2013a).

Test 2 of the edge detection processing procedure allowed us to achieve better results than the other edge detection process (Test 1), in which 8% more of the building façade heights were extracted and 5 more buildings were estimated with a vertical error below 1 m. The buildings that were not estimated are also represented in Figure 3.11 (black buildings). In this case, the extraction of the rooftop or ground elevations failed. The best Test is summarized in Table 3.4.

In around 30% of the buildings (Table 3.4), the selection of UAV points failed, mainly due to the presence of data gaps near the buildings (Figure 3.8), which in turn were due to the occlusion effect on aerial images. Furthermore, the

large proportion of buildings with an error above 1 m was due to the presence of wrong points in the DTM or edge detection, where most problems stem from the poor quality of the DTM.

Table 3.4: Results of the methodology applied (Test 2)

Areas	Total buildings	Estimated buildings (%)	% Buildings with vertical error ($< 1m$)
Area A	14	100.0	57.0
Area B	43	65.1	43.0
Area C	31	61.3	37.0
Total	88	69.3	45.0

The building façade height parameter was estimated for 61 buildings (Figure 3.11 and Table 3.4 for the remaining ones), around 45% of which have an error below one metre. On the other hand, about 67% of the vertical errors were below one story (approx. 3 m). The building façade height values estimated in each area and corresponding vertical errors (Test 2) are available in Appendix K.

Moreover, the distribution of vertical errors along the true height of the building façade (between 12 m and 21 m) for 55 buildings with a vertical error below 8 metres can be seen in Figure 3.12.

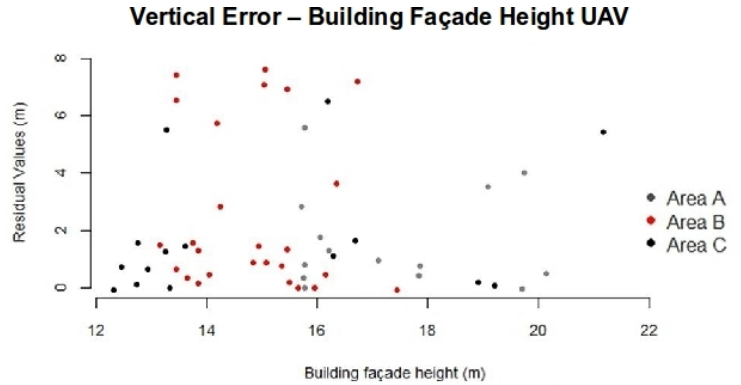

Areas	Min (m)	Max (m)	Average (m)	Median(m)	Standard Deviation (m)
Area A	0.01	5.60	1.64	0.89	1.71
Area B	0.01	7.61	2.58	1.31	2.83
Area C	0.01	6.51	1.76	1.13	2.19

In this analysis the building errors outliers were removed from each area

Figure 3.12: Distribution of vertical errors in the different areas A, B, and C for Test 2. Statistical analysis of vertical errors (Adapted from Rebelo et al., 2013a).

The representation of outliers in B and C areas was not considered in this

plot (building height outliers identified with a vertical error above 8 metres can be seen in Appendix K). Most residual values (or vertical errors) represented in Figure 3.12 were less than two metres, i.e. 45% of building heights estimated.

The statistical analysis of errors shows that area B has the worst results, with the highest variability. The average building façade errors for the areas A and C are below one story, while errors for area B are very similar to standard story height (it ranges between 2.5 and 2.8 m). The variability of the building façade height errors in areas B an C is higher due to the morphology of the building blocks.

The estimation of the building façade height is strongly dependent on the quality of the UAV points selected at the end of the geoprocessing model (Figures 3.7 and 3.8). The filtering action should be effective in the removal of wrong points (points that do not represent either the rooftop or the ground). These wrong points that were not removed effectively contributed to the incorrect estimation of the height of most buildings.

These wrong points in the edges of the buildings are generally identified as balconies or other elements of the façade. In area A, about 30% (Test 2) and 50% (Test 1) of the building rooftop elevations were estimated with an error above 1 m (or this means that the difference between the accurate point elevation and elevation estimated on the rooftop was above 1 m). However, the majority of the wrong points in other areas were provided by the DTM. These errors were due to objects located near the building façade, such as trees, streetlamps, and cars. Thus, the edge detection algorithm and the DTM process should be made with the best parameter values to minimize these wrong points.

The influence of urban morphology in the estimation of building façade height

The behaviour of the edge detection algorithm for different urban morphologies in the three areas was worse in areas B and C, where the building blocks are not regular. In general, the curve of estimated values of the building façade height did not approximate the true values for those areas (Figure 3.13).

Empirical density functions for area A with Test 2 show the best results (the estimated curve approximates the true values). The worst results are recorded for the heights estimated in areas B and C. These results provide evidence that

areas that are more homogeneous and with regular buildings can estimate a more accurate building height, unlike the areas with complex urban morphology (irregular in the case of area B and island building blocks in area C). There is strong evidence (Figure 3.13) that the estimation of building façade height from UAV depends on urban morphology.

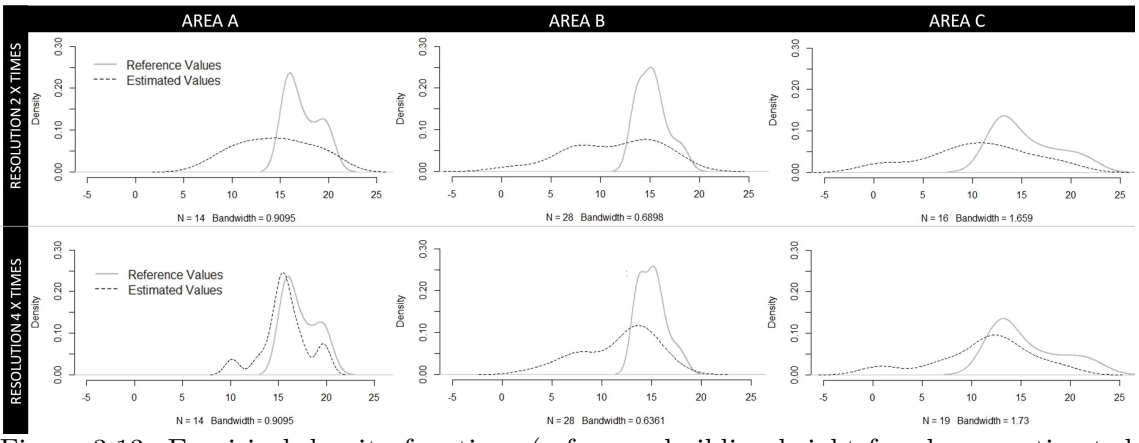

Figure 3.13: Empirical density functions (reference building height façade vs. estimated buildings façade for each area) for two different spline steps of the edge detection.(Source: Rebelo et al., 2013a)

In spite of the results we have achieved, we believe that the UAV technology for the acquisition of a low-cost 3D point cloud can be very useful for urban planning. The usage of the 3D point cloud data in this study demonstrated that there is a strong correlation between urban morphology and the accuracy of the height value of the building façade. To evaluate and understand more fully this result, further research would be necessary, particularly concerning the quality of UAV imagery processing, where some edges of the building blocks shown deep irregularities.

3.3 *Usability of UAV data for high precision dasymetric mapping*

The previous section was a simple testing of UAV data, where its potential and its difficulties in handing such data from a block spatial unit to a building unit was demonstrated. Currently, a new perspective for the usage of 3D data and FOSS tools is needed in urban planning. There are many studies that support the planning decisions in urban planning, where 3D data is crucial to adjust the analysis to the reality.

The main objective of this section is to demonstrate the usability of UAV data for the estimation of the resident population by the reallocation of 2001 census data according to a common geometry of 2011 census data (Rebelo et al., 2013c). The reallocation and aggregation of data according to a common geometry (Goodchild et al., 1993) is called dasymetric mapping technique. In this case, the high precision dasymetric mapping implies the usage of 3D control zones for the estimation of the resident population according to a common geometry, which is defined by the building block volume parameter.

The spatial problem of dasymetric mapping used as source geometry (zones) census tracts from 2001 and as target geometry census tracts from 2011 (Figure 3.14). In Portugal, census tracts' geometries are known as the Geographic Base for Information Referencing (BGRI). Moreover, census geometries have been used only to match building block footprints (Figure 3.14) that were used as control zones along the dasymetric mapping.

Figure 3.14: Study area with census tracts and building block footprints (Adapted from Rebelo et al., 2013c).

The pertinence of UAV point cloud data will be demonstrated in two ways: a) using a semi-automatic methodology that enables the extraction of building block parameters (area and height) from UAV data using the 3DEBP solution; and b) using building block volumes (computed from area and height) for the reallocation of census data via the high precision dasymetric mapping algorithm developed by Rodrigues & Tenedório (2015b); Rodrigues et al. (2013a); and Rodrigues & Tenedório

(2015a).

The usability of UAV data is also demonstrated in this section by: a) measuring the quality of the building block area, height, and volume estimated parameters to evaluate *'how this data is pertinent for urban planning'*; b) comparing high precision dasymetric mapping (using 3D data) with a spatial interpolation technique using uniform distribution along target areas, and with a dasymetric exercise based on 2D control datasets; and c) performing a sensitivity analysis using Monte-Carlo simulations showing the effect of changes in 3D data in the reallocation of the resident population.

3.3.1 Control zones: extraction and evaluation of building blocks estimated from UAV

Assuming that 2D and 3D data is not available, this means that 'low cost and faster data' is required for the extraction of control zones (block area and volume) – the use of UAV for the acquisition of this data might be the solution.

The methodology based on the 3DEBP solution (Figure 3.15) was applied to obtain the control zones – building block area and volume, which was also applied in Chapter 2 (Section 2.3) for the extraction of single family buildings of Praia de Faro. However, in this case the extraction was performed for the spatial unit of a building block, and therefore some procedures and processing parameters had to be adjusted to this new building morphology.

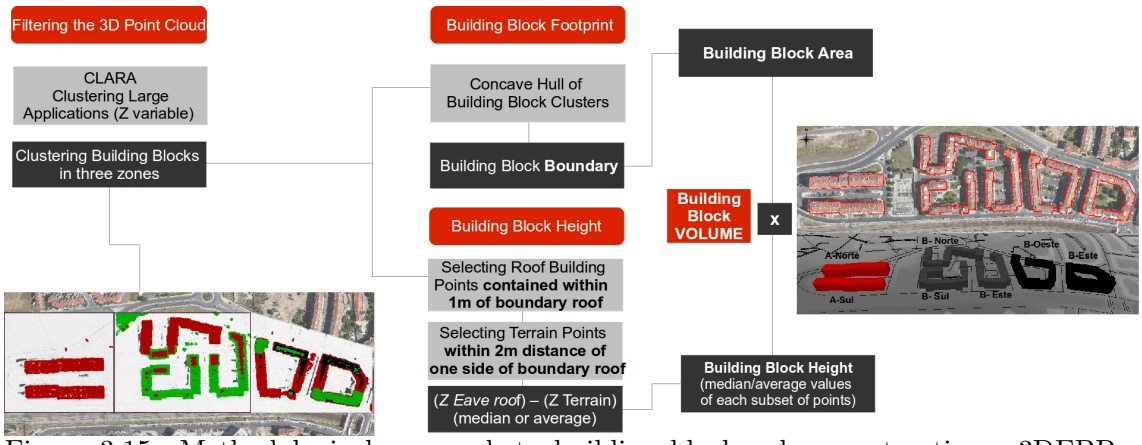

Figure 3.15: Methodological approach to building block volume extraction - 3DEBP - based on a 3D point cloud acquired from a neighbourhood of Amadora. Source: Rebelo et al., 2013b; Rebelo et al., 2013c.

As seen in Figure 3.15, the methodology was divided into three distinct steps for each area (Figure 3.14): a) Firstly, point cloud data was filtered in order to extract observations belonging to building rooftops, in order to obtain the footprint of each block; b) secondly, terrain and rooftop subsets (elevation points) were selected in order to obtain the estimated average (or median) height of each building block [1]; and c) building block volume was calculated using both estimated area and height.

Due to the morphological complexity, the clustering was performed separately for the three areas with distinct building block types. CLARA was applied to the orthometric elevation values (Figure 3.16b). For each area n observations were chosen and clustered into k sub-groups, allowing us to isolate each block.

The parameter values were selected for the clustering as shown in Table 3.5. The silhouette plots of the k-cluster for the entire dataset (intra-group homogeneity and average dissimilarity), allowed us to select the clusters that better represented the roofs of building blocks (Figure 3.16a). The algorithm used for the clustering of these areas is presented in Appendix L.

Table 3.5: Parameters of clustering and concave hull processing

Area	**Clustering**				**Concave-hull**
	k-cluster (dataset)	**Ave_Silhouette Width**	**Clustering structure**	**k-clusters selected**	**Threshold**
A	k=4	0.73	strong	k=3	9
B	k=5	0.69	reasonable	k=4,5	8
C	k=9	0.68	reasonable	k=7,8,9	8

The highest k-cluster (k=9) was selected for area C, due to the highest variation in the number of stories (between 4 and 7) of the building blocks, unlike the other morphologies.

The clustering structure given by average silhouette width was very similar between areas. Block footprints were made for a higher threshold *concave hull* (8 and 9), which implied a more convex hull polygon.

The clusters selected that better represent the building blocks for each area (Figure 3.16c) were coincident with the greatest elevation points represented in plot z of UAV point distribution (Figure 3.16b). The annotation for the corresponding UAV point clusters in each area is $A = C3$, $B = C4 \cup C5$ and $C = C7 \cup C8 \cup C9$.

[1] Here, the building block height is the same as the block façade height.

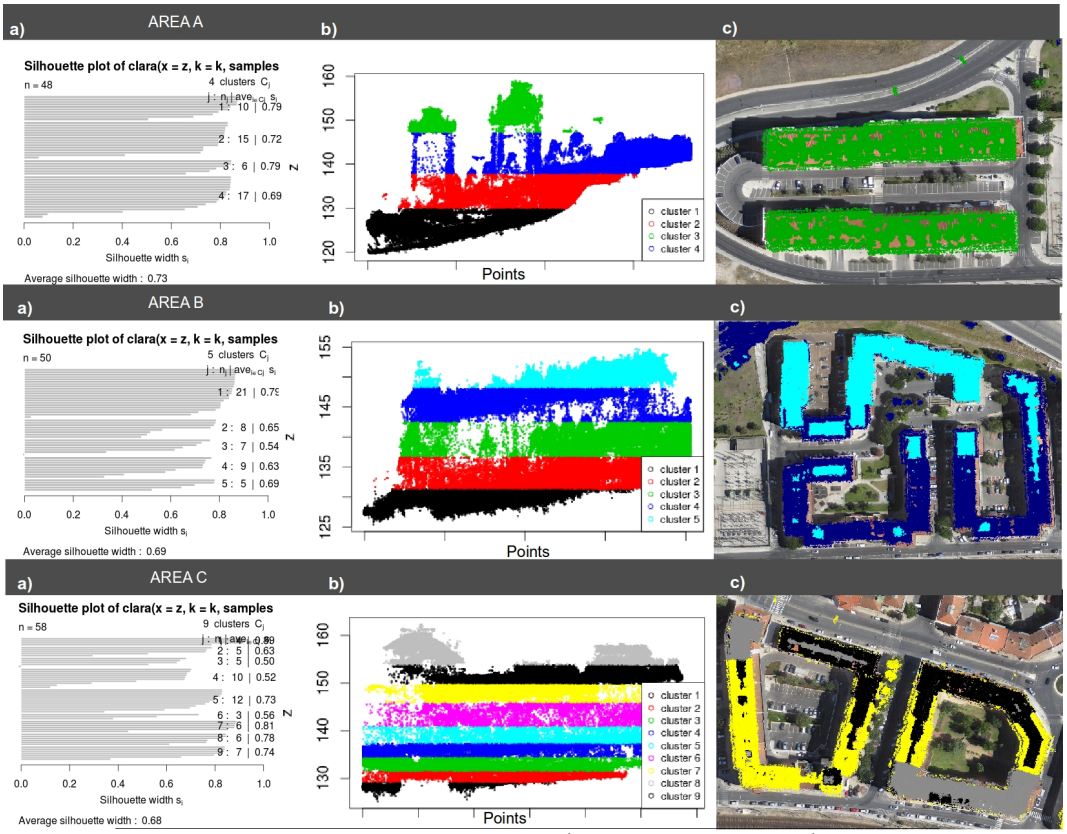

Figure 3.16: Clustering results for each area: a) Silhouette plot; b)Distribution of points in z; and c) Clusters selected for each building block.

To estimate building block height [BBH] (Figure 3.15), a set of spatial proximity functions were used (Subsection 2.3.1 of Chapter 2) in order to:

i) select sets of UAV points (r) that best define the eave of roof within a buffer of 1 m from block rooftop boundary (polygon obtained from *concave hull*) to the interior (Figure 3.17). This buffer distance was enough to filter the points that did not belong to the roof. The contribution of wrong points selected for the block may be mitigated by using the average or median statistical measures. The selection of points from corresponding UAV point clusters for each area can be represented by $R_{B_i} = \{r \in A : r \subset Eave\ block\ roof\ _i\}$, where i is the block i=1,2 and A is area.

ii) select ground points (g) of the block base located within a buffer of 2 m from the block rooftop boundary (Figure 3.17). This value was used given the average size of pedestrian sidewalks. These points were obtained by the intersection of two buffers: 2-metre buffer from block rooftop boundary and buffer (between 7-8 metres) along the central axis of streets that have accurate building base elevation points (yellow points in Figure 3.17). These ground points in area A can be represented by $G_{B_i} = \{g \in A : g \subset block\ base\ _i\}$, where i is the block i=1,2.

However, at the end of this process, the selected ground points should be filtered by a clustering process with CLARA to remove wrong points (cars, trees, streetlamps,...), based on the standard deviation of each cluster performed (*condition: if standard deviation > 1 then remove cluster*). In practice, the clustering was performed to k=3, where one cluster was removed for each area (Area A and B, k=3; Area C, k=2).

iii) for each block, calculate the estimated median ground and eave of roof elevation in order to take into account the existence of extreme elevation values (classified as 'wrong points'). Besides this, the average values of these two variables were also estimated. Both statistical measures were used to analyse the best measure for this case study. The difference between both statistics (ground and eave) for each block gives us the estimated median (or average) building block height, hence: $BBH_{med_i} = med(R_{B_i})–med(G_{B_i})$, i - block number.

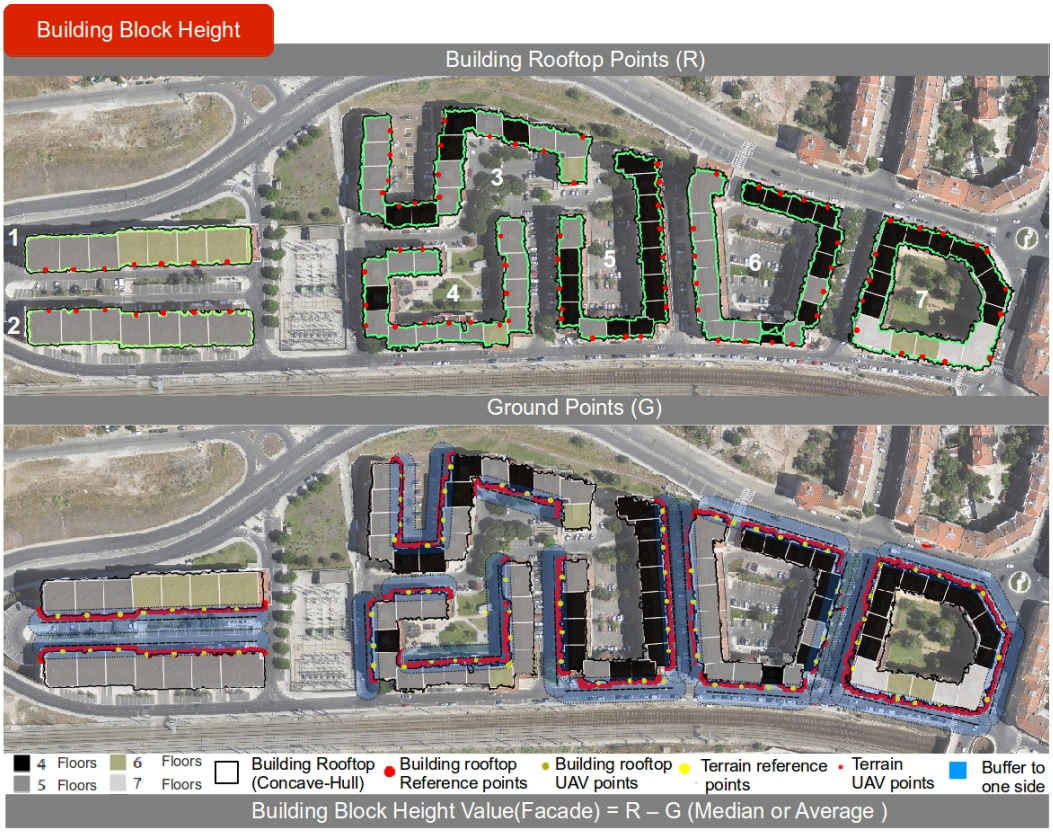

Figure 3.17: 3D points selected from the UAV point cloud: rooftop and ground (near the block base). A number is assigned to each building block.

Lastly, building block volume [BBV] was calculated using data from the previous stage, by multiplying estimated area and average/median block height for each block. The algorithm developed for the steps above and for the computation of

BBH and BBV for each area can be seen in Appendix M. Moreover, the average and median building height values estimated for each block are detailed in Appendix N. The average and median building height values obtained from accurate 3D data (i.e. stereo restitution) are also indicated.

The results achieved are presented in Table 3.6. For both methods, the building block located in the Northern section estimated for area A is the tallest, which is consistent with the existing data. The blocks with lowest' - estimated volume were building block 5 of area B (located to the East) and block 2 of area A (located to the South); this also agrees with the existing data.

Table 3.6: Building block volume [BBV] based on BBH and block area extracted from UAV point cloud.

Building Block	**Area** (m^2)	**Average**		**Median**	
		BBH (m)	**BBV** (m^3)	**BBH** (m)	**BBV** (m^3)
1	2473.924	18.65	**46139**	18.81	**46535**
2	2410.501	15.35	**37001**	15.48	**37315**
3	3206.119	14.51	**46521**	14.88	**47707**
4	2665.804	15.03	**40067**	16.10	**42919**
5	2614.843	13.78	**36033**	14.15	**37000**
6	3175.614	14.28	**45348**	13.60	**43188**
7	3175.020	15.75	**50007**	14.56	**46228**
Maximum	3206.12	18.65	50007	18.81	47707
Minimum	2410.50	13.78	360033	13.60	37000
Total	19722.00	-	301115	-	300892

Comparison between reference building rooftops (red line) and estimated building rooftops.

The total area of the building blocks was overestimated by around 1500 m^2 (Table 3.6). On the other hand, the total volume estimated by median or average has a difference of around 223 m^3. This building parameter was overestimated from point cloud by around 6% of the true total volume for both measures. The 3D block model (LoD1) generated from the results presented in Table 3.6 can be seen in Figure 3.18.

We can compare the resulting differences between volumes estimated for the blocks caused by the use of average (blue) and median (green) height values. The height differences between the two methods (average or median) imply different blocks volumes. An example of the difference between the two blocks' estimated height for block 6 is approximately more 0.7 m using average, which implies 2000 m^3 more in the average block volume (then the roof of block appeared 'Blue' in Figure 3.18).

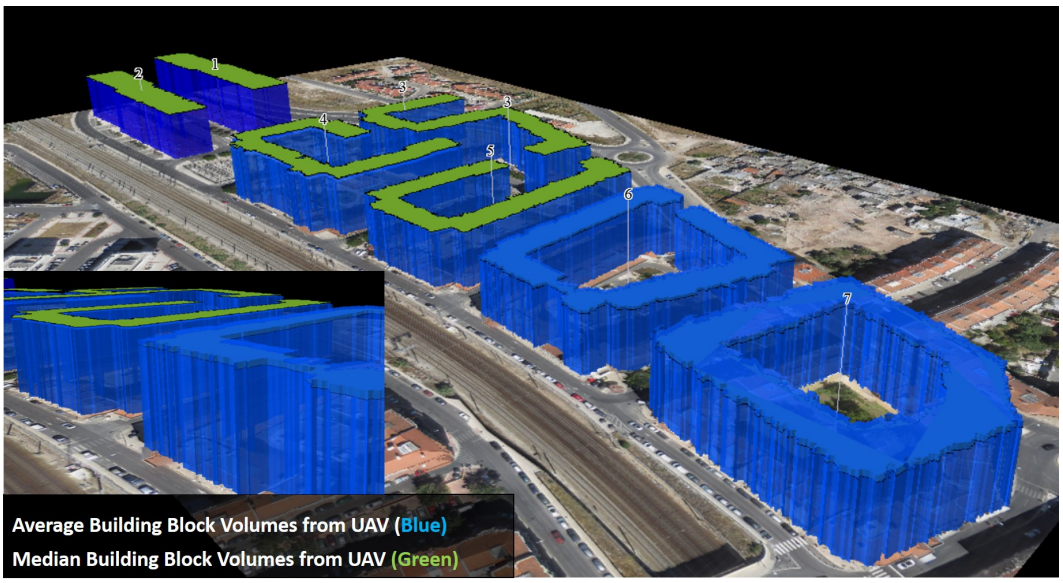

Figure 3.18: 3D block model (LoD1) with the representation of average and median block height values.

Most block volumes estimated with median block height are higher than if we use average block height, as represented by the green rooftops (Figure 3.18).

Evaluation of building block parameters estimated from UAV

Before the usage of area, height, and volume parameters of the building blocks in dasymetric mapping, it is important to evaluate the magnitude of error obtained for each parameter.

The extraction of accurate building block parameters (height and area) from UAV data strongly depends on the quality of the points selected along the eave of the roofs. The two keys issues for the successful extraction of building parameters are: i) the filtering method used to remove wrong points that do not belong to the roof; and ii) the own processing of point cloud from stereo aerial images to enable a good coverage of roof eaves. Furthermore, in this case study the probability of taking wrong points around the block is higher, because: a) the height of the buildings is variable within a block; and b) the block rooftops are not flat and they are very irregular.

The area, height and volume of building block parameter errors were computed, representing the difference between an accurate value given by the traditional photogrammetric for large scale mapping and estimated value from UAV. The evaluation was based on relative building block parameter error. This evaluation was

automatically obtained in the PostgreSQL/PostGIS database using the algorithm developed and presented in Appendix O.

The building block area error is represented in Table 3.7. This parameter extracted from UAV was overestimated for all the building blocks. Building block 7 was not well extracted, since it had a high error when compared with the average error of all the building blocks (217.13 m^2). The building blocks of area B had the lowest errors in the estimation of the area, with a relative error range of 4.1% to 6.1%.

Table 3.7: Evaluation of building blocks area [BBA] estimated from concave hull processing

Building Block	Reference BBA m^2	Area Error m^2	Relative Error %
1	2240.149	-233.77	10.4
2	2267.869	-142.63	6.3
3	3021.399	-184.72	6.1
4	2520.505	-145.30	5.8
5	2513.062	**-101.78**	**4.1**
6	2977.789	-197.82	6.6
7	2661.162	**-513.86**	**19.3**
Average*		217.13	
Median*		184.72	

Comparison between reference building rooftops (red line) and estimated building rooftops.

**Measured to the absolute error.

Nevertheless, some of the building block outlines of the reference data are not enough to measure the area values estimated from UAV data. In some cases, the building outlines of vector reference data do not represent the building roofs that were extracted from UAV points, which explains the large error of area values estimated for the building block on the study area C (Figure 3.19, building block 7).

Figure 3.19: Block footprints extracted from UAV.

On the other hand, the footprint of block 6 was not well extracted because

of the clustering process. The principle of decision-making in a clustering process depends on whether there are any trees (or vegetation) that are close to the buildings with the same height. Block 6 was an example of why this decision is so difficult to make, since the clustering (as k=6, selecting 4,5,6) that contained all the roof points had to be rejected, because there were trees in the Eastern side of the block that has the same roof height to the South, so it was included in this clustering as roof points.

The errors of estimated average (median) building block heights can be seen in Table 3.8. The average (median) building block heights were estimated with an average error below 0.45 m (Table 3.8). This means that the methodology applied was suitable for the extraction of these block morphologies.

Table 3.8: Evaluation of building block heights [BBH] estimated from selected UAV points, based on reference building block height average/median values [*BBHave/med*].

Building Block	BBHave (m)	BBHmed (m)	Error *BBHave* (m)	Rel_{Error} *BBHave* (%)	Error *BBHmed* (m)	Rel_{Error} *BBHmed* (%)
1	18.78	19.08	-0.13	0.7	-0.27	1.4
2	15.87	15.72	-0.52	3.3	-0.24	1.5
3	15.24	15.00	-0.73	4.8	-0.12	0.8
4	15.87	16.49	-0.84	5.3	-0.39	2.3
5	14.09	13.95	-0.31	2.2	0.20	1.4
6	14.59	15.28	-0.31	2.1	-1.68	11.0
7	15.59	14.37	0.16	1.0	0.19	1.3
Average*			0.43		0.44	
Median*			0.31		0.24	
St.Dev.*			**0.28**		**0.55**	

St.Dev.is Standard deviation; and (*) Measured to the absolute error.

The comparison between average and median BBH errors (statistical values) shows that they are closer. Most building block heights were overestimated by the UAV point cloud, except for building blocks 5 and 7. The vertical error range using the median varies between 0.12 m and 0.39 m (excluding the block 6) and for the average the range is between 0.13 m and 0.84 m. The lowest absolute building block height errors were obtained for blocks 1 (0.13 m) and 7 (0.16 m) using the average and blocks 3 (0.12 m) and 7 (0.19 m) using the median.

The BBH error of area A was slightly better estimated by the median, whose average of the two blocks height error was only 0.26 m. The block heights of area B (Blocks 3,4,5) estimated from the median had the lowest vertical error when

compared with those that were obtained from the average (Table 3.8). The average of block height errors in this area was 0.63 m using the average and 0.23 using the median. In area C, building block 7 was estimated with a relative error of about 1% for both measures. Furthermore, the block height of building 6 in area C, estimated by the median, registered the highest height error of all the blocks estimated (-1.68 m). However, this high error is acceptable because it is below one story.

If the maximum values of average or median block height error are removed from the sample, this implies a reduction to 0.36 m and 0.23 m of average height errors, respectively. There is evidence that the median measure would be the best choice for the estimation of building block height in order to mitigate the effect of the extreme values of the points selected.

The height errors registered for all the blocks (using average or median) provide evidence that the usability of this information for urban planning could be higher. The accuracy in centimetres enables the monitoring of the built-up area in terms of volume or height.

The evaluation of estimated volume for each building block (Table 3.9) was based on the calculation of the error, which corresponds to the difference between the volume value estimated from average (or median) building block height and area parameters estimated from UAV point data and the reference volume value from 2D/3D vector data (annotated by RefBVave for the average and RefBVmed for the median).

Table 3.9: Evaluation of building block volumes [BBV] (BBVave: average block volume and BBVmed: median block volume) computed from BBH and BBA.

Building Block	RefBVave m^3	RefBVmed m^3	Error BBVave m^3	Rel_{Error} BBVave (%)	Error BBVmed m^3	Rel_{Error} BBVmed (%)
1	42064	42742	-4075	**9.7**	-3792	**8.9**
2	35984	35651	-1017	2.8	-1664	4.7
3	46046	45321	-475	1.0	-2386	5.3
4	40008	41551	-59	**0.1**	-1369	**3.3**
5	35409	35057	-623	1.8	-1943	5.5
6	43440	45501	-1908	4.4	2312	5.1
7	41488	38241	-8519	**20.5**	-7987	**20.9**
Average*			2382	5.8	3065	7.7
Median*			1017		2312	
St. Dev.*			3021		2305	

St.Dev.is Standard deviation; and (*) Measured to the absolute error.

The BBVs computed from height and area values were overestimated from

UAV, except building block 6 using median for BBH. The error achieved for all the volumes estimated from only UAV data ranged approximately from 0.1% to 21%. About 85% of block volume errors estimated using average height values are lower than using median height values. Therefore, there is evidence that the calculation of building volume using average height allows us to obtain better results (because of a statistical compensation of area and height errors).

The magnitude of the volume of the errors is mainly due to the estimated block area parameter. The building block volumes estimated in area B achieved the best results using average block height, whose error volume range varies between 0.1% and 1.8%. Building block 7 had the worst relative error for both methods (about 21%), because the area error obtained for this block was extremely high (Table 3.7).

The 3D model of block volumes estimated using average or median height can be seen in Figure 3.20. The 3D visualization of block volumes extracted from UAV that were generated by extruded height value from the block footprint estimated have a 3D shape that is very close to the true reference volumes, except the South façade of block 6.

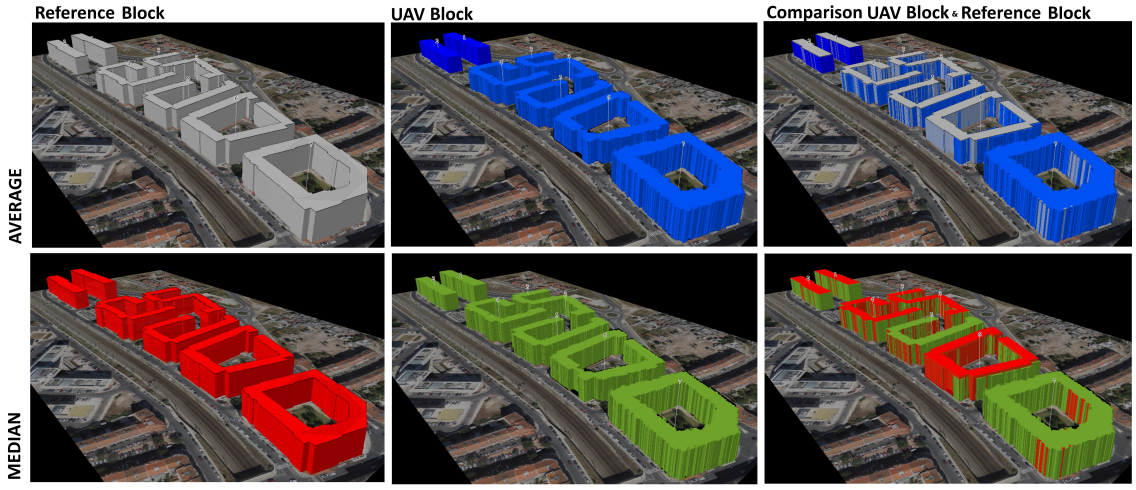

Figure 3.20: Comparison between 3D reference building models and 3D building models based on UAV data.

Additionally, it is important to highlight that the average error for the estimation of building block volume by using reference area value can be reduced approximately from 5.8% and 7.7% to 2.8% for both methods.

The methodology developed for the semi-automatic extraction of building block parameters (area and height) revealed a high potential for the spatial unit

block. The pertinence of point cloud data for the automatic extraction of building block units proved to achieve acceptable results for height and for a rough identification of the built-up area.

The next section will use the block area and the average block volume parameters (estimated with the average height) as control zones along the dasymetric mapping. The impact of volume errors in dasymetric mapping will be shown in section 3.3.3.

3.3.2 High precision dasymetric mapping using control zones

A common geometry for the census population regardless of the census year is very important to monitor plans. Without this spatial continuity between geometries, it is difficult to make analysis and take decisions in urban planning. Therefore, in case of any changes to census geometries, the continuity of statistical information - such as resident population - must be ensured. There are at least four situations that can happen during the reallocation of one variable to a common geometry: a) same geometry; b) aggregation of geometries; c) different geometries, which implies a reallocation of variables along the resulting polygons; and d) footprint not represented by control zones (Figure 3.21).

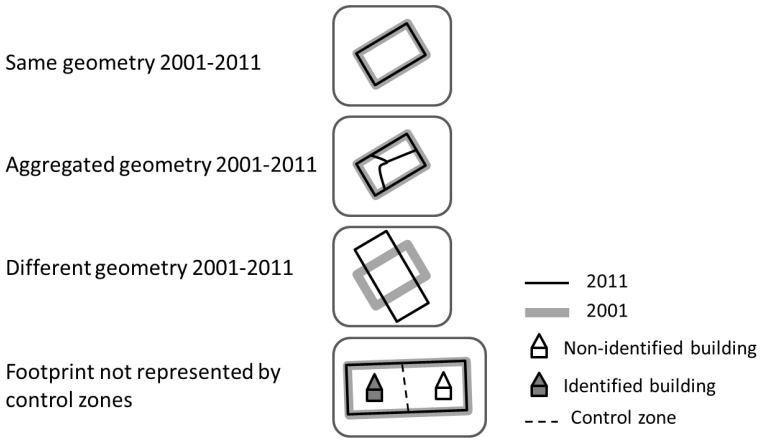

Figure 3.21: The approach of dasymetric mapping in these 4 situations. Source: Rodrigues et al. (2012).

The resident population is one of the statistical variables of census data. This variable is critical for the monitoring of mobility within cities, such as commuting and planning public services. Nowadays, a sustainable population density for cities is required: a) to ensure that the creation of good jobs and opportunities is a

priority; b) to check the infrastruture needs of a changing population, preserving and enhancing good accessibilities; c) to maintain a high quality living environment with public and green spaces; and d) to ensure a balanced distribution between residential neighbourhoods with the construction of new building blocks.

Furthermore, in Amadora city there is a municipal emergency plan that was drafted in 2013. This plan is a good example of the need for a common geometry in the analysis of the evolution of the resident population, because it is one of the variables that need to be taken into account when defining and monitoring some of the actions of the plan.

The approach to dasymetric mapping in the small neighbourhood that contains building blocks with heterogeneous forms was tested using different methodologies (Figure 3.22).

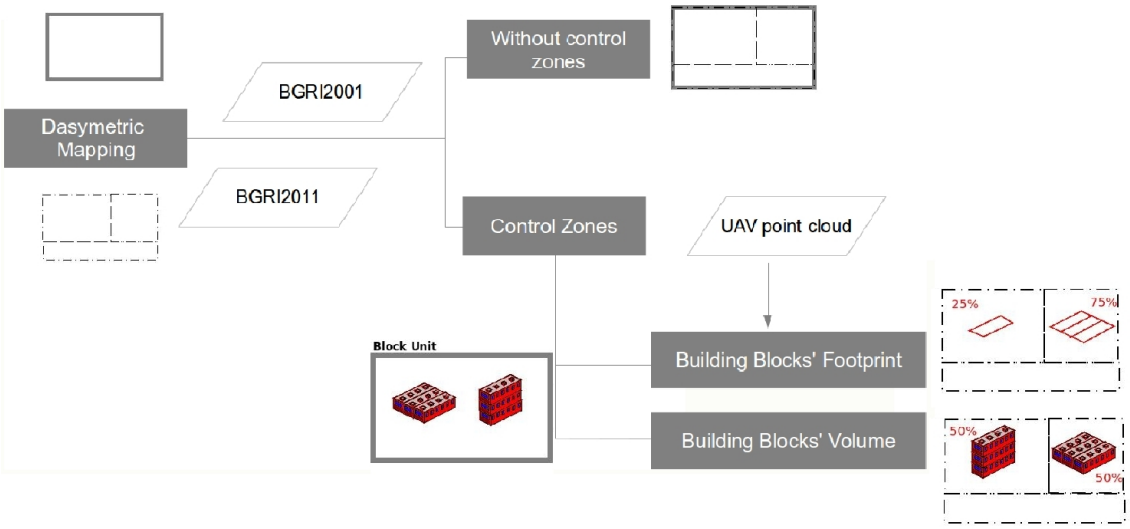

Figure 3.22: Summary flowchart with the main steps. Source: Rebelo et al. (2016).

This approach has been started in Rodrigues et al. (2013b) and Tenedório et al. (2013) in order to evaluate the added value of working with volumetric data. Three exercises were performed within dasymetric mapping (Rebelo et al., 2013c; Rebelo et al., 2016): a) The first assumed homogeneity within each zone (census tracts). In this exercise the resident population data was reallocated according to the area (size) of each small area resulting from the intersection of source and target schemes; b) The second exercise used as control data the building block rooftops estimated from the UAV point cloud data; and c) In the final exercise, the building block volume estimated from point cloud data was used. This last exercise attempts to approximate reality, as the level of abstraction given by the other exercises is

reduced. The algorithm used for these exercises was implemented in SQL using functions from PostGIS, a library which introduces spatial and geographic objects for PostgreSQL developed by Rodrigues & Tenedório (2015b).

After obtaining the control zones from the point cloud dataset, the resident population for 2001, distributed according to the 2011 geometrical zones (Figure 3.23), was estimated using the methodologies described – areal interpolation, and dasymetric mapping using 2D (building block rooftops) and 3D (building block volumes) control zones. Figure 3.23 shows the final results. The final column shows population estimates obtained from building point data. This final variable is understood as the one that is closer to reality, hence it was used to calculate the absolute statistical deviation shown in the last row.

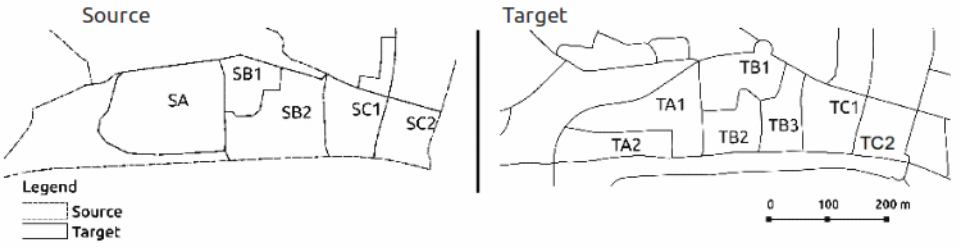

zone	Areal Interpolation	Control zones 2D	Control zones 3D	Benchmark*
TA1	4	0	0	0
TA2	14	0	0	0
TB1	374	379	380	367
TB2	327	342	356	348
TB3	312	336	321	343
TC1	486	498	498	498
TC2	350	384	384	384
Absolute deviation	*17.53*	*3.66*	*6.32*	

(*) Estimated from dwellings

Figure 3.23: Geometrical zones of 2001 and 2011 census tracts. Results estimated to 2001 population through dasymetric mapping using control zones (area and volume) Source: Rebelo et al. (2013c) and Rebelo et al. (2016).

As expected, the areal interpolation results are those with the highest absolute deviation; lower performance in this case is justified since distribution within zones is assumed to be homogeneous. When this stationary assumption is dropped, population estimates approximate the benchmark values. Moreover, the absolute deviation is lower when using 2D data when compared with the 3D control zones. Yet, given the small size of the dataset, differences are not significant. Only three zones are affected by the changing conditions – those whose boundaries intersect existing building blocks (Area B: TB1, TB2 and TB3).

3.3.3 Sensitivity analysis: The effect of building block volume accuracy in high precision dasymetric mapping

After comparing three methods of interpolating demographic data, the next exercise attempts to quantify the effect of overall UAV data accuracy - including omission and inclusion errors. Inclusion errors are mostly semantic (ex. Inclusion of non-residential buildings for population estimation), whilst omission errors are mostly producer and processing errors (blocks filtered out during processing).

In order to infer on the quality of 3D control data (volume) obtained through filtering UAV point cloud data, building block height was allowed to vary in order to study the impact on the resulting population distribution. The dasymetric mapping exercise was performed repeatedly with height varying according to a set of conditions. Eight tests were performed, covering a set of distinct possible condition-s/settings, as described in Figure 3.24.

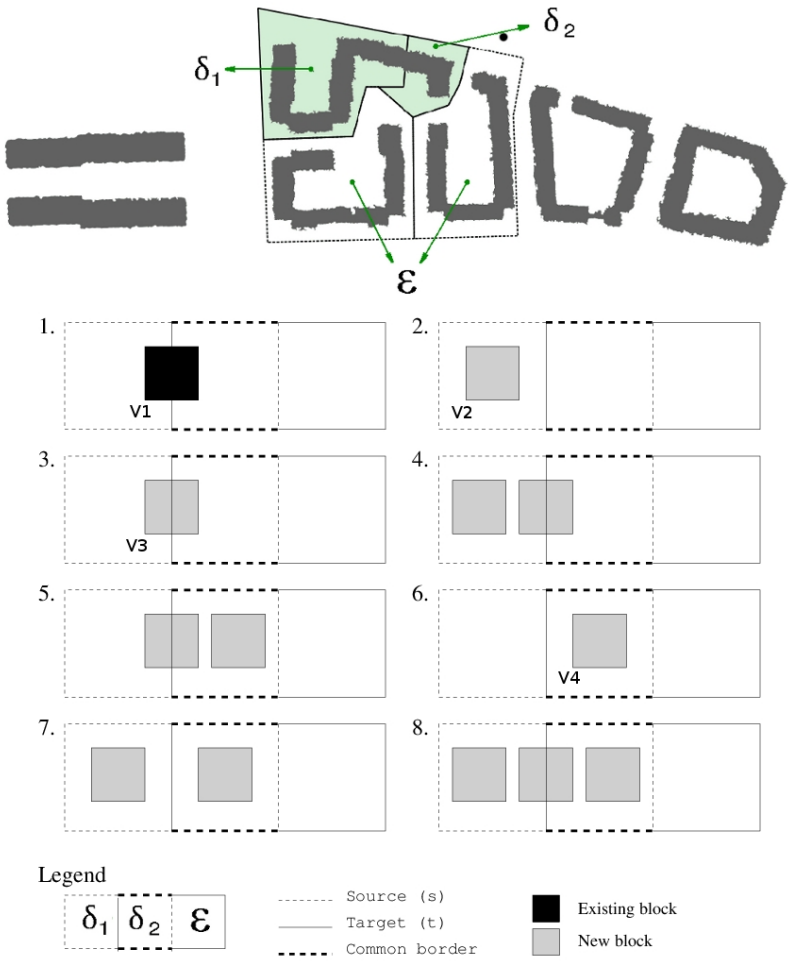

Figure 3.24: Sensitivity analysis: 8 situations. Source: Rebelo et al. (2016).

All the settings refer to situations where new buildings of varying heights are added to one or two particular source zones, in this case zones SB1 and SB2 (Figure 3.23). This is true with the exception of Test 1, where resident population estimations were subject to varying heights in one existing building block.

Figure 3.25 shows the results from running a number of Monte Carlo simulations according to conditions/rules one to eight. The values represent 2001 resident population according to 2011 census tracts for the geographical zone TB1 (T – target, B – type 'irregular', zone 1) – see Figure 3.23. This area results from the union of SB1 and part of SB2. SB2 was itself broken into three areas – TB1, TB2 and TB3. For the purposes of simplification these were generalized according to the following classification scheme: SB1 and TB1 $\rightarrow \delta_1$; SB2 and TB1 $\rightarrow \delta_2$; SB2, TB2 and TB3 $\rightarrow \varepsilon$ (Figure 3.24).

More precisely, the eight tests for these buildings were performed by the following rules:

Condition 1: $V1 \bigcap (\delta_2 \bigcup \delta_1)$
Condition 2: $V2 \bigcap \delta_1$
Condition 3: $V3 \bigcap (\delta_2 \bigcup \delta_1)$
Condition 4: $[V3 \bigcap (\delta_2 \bigcup \delta_1)] \bigcup (V2 \bigcap \delta_1)$
Condition 5: $[V3 \bigcap (\delta_2 \bigcup \delta_1)] \bigcup (V4 \bigcap \delta_2)$
Condition 6: $V4 \bigcap \delta_2$
Condition 7: $(V4 \bigcap \delta_2) \bigcup (V2 \bigcap \delta_1)$
Condition 8: $[V3 \bigcap (\delta_2 \bigcup \delta_1)] \bigcup (V2 \bigcap \delta_1) \bigcup (V4 \bigcap \delta_2)$

The Monte Carlo analysis was performed to analyse the effect of these tests for the estimation of the population. The Monte Carlo method allowed us to repeat various samples to obtain numerical results. In this case, the block height of the tests was increased by a scalar. Figure 3.25 shows the results from running a number of Monte Carlo simulations according to conditions/rules one to eight.

In these tests, population converges to the maximum population that lives in the affected areas. In other words, convergence represents the point when, as a result of increased building volume, all the population are transported from unaffected areas to those areas where construction is allowed to increase.

When a new building block is inserted in SB1 (rule 2), its relative weight in terms of volume increases, but the results do not change. This is simply explained

by the fact that no population from SB1 is reallocated to TB1 (both constitute δ_1). In fact, in all the tests that include changing conditions in δ_1, the results are the same as the proportional conditions (3&4, 6&7, 5&8). When a new building block is added to δ_2 (rules 6&7), population increases rapidly until convergence. When one of the simulation blocks is added between δ_1 and δ_2, convergence occurs but at a slower rate (rules 3&4 and 5&8). If existing volume was the same between SB1 and SB2 (δ_1 and δ_2), then results would not change. However, since the initial proportion in SB2 (δ_2) is lower, an equal increase in both represents a more rapid rate of change in δ_2 – which results in an increase in the estimates until convergence.

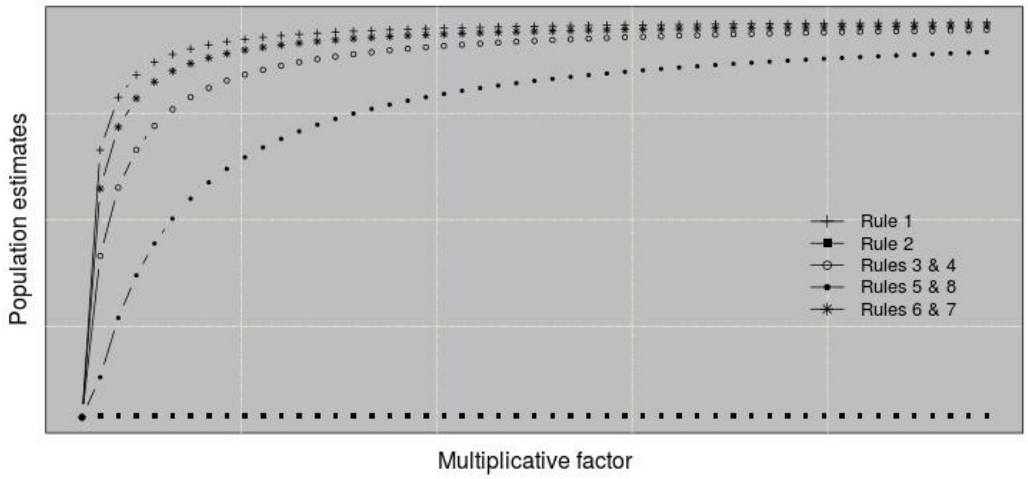

Figure 3.25: Sensitivity analysis using Monte Carlo results. Source: Rebelo et al., 2016.

The variation of block volume in dasymetric mapping is practically null since population estimates converges to a finite value (Figure 3.25). This means that the impact of volume errors obtained from UAV data for the estimation of population is null.

3.4 *Synthesis*

This section summarized the main conclusions resulting from the methodologies developed for the evaluation of building façade heights and the extraction of building block parameters in the neighbourhood of Amadora using a 3D UAV point cloud. They can be summarized as follows:

a) *On the evaluation of UAV point clouds for the extraction of building façade height from different block morphologies*

We have demonstrated the usage of a methodology to evaluate building façade height estimated from a 3D point cloud acquired by UAV imagery and reference 3D vector data, privileging the use of FOSS tools, GRASS GIS and R.

The most useful characteristics of GRASS GIS for this type of applications are:

- the capacity to process and to manipulate a dense point cloud with about 9 million points (original data), such as the creation of various tiles of the original data;

- higher suitability and more efficiency in the manipulation of this type of data (with higher density) when compared with usual proprietary desktop GIS;

- the edge detection algorithm used was very useful for the selection of top building points;

- and the use of a GRASS version optimized for larger datasets is essential for the manipulation of point clouds.

The use of the module LiDAR GRASS to filter points near buildings that are classified as ground (DTM) does not offer the expected results with the UAV point cloud data. The specific LiDAR algorithms used for this step are not adequated for the UAV point cloud, whose growing algorithm is based on first and last pulse LiDAR information. However, there is another function in GRASS GIS related with the generation of DSMs and DTMs that can be tested with a UAV point cloud.

Additionally, we have also demonstrated that there is a strong correlation between urban morphology and the quality of the height value of the building façade estimated. A set of regular building blocks enables more accurate building heights, since the filtering parameters can be more easily applied. The irregular and island block morphologies require an improvement of the methodology presented.

New developments in FOSS tools are needed to support the filtering and manipulation of dense 3D cloud points acquired by UAV, where different building block morphologies can be taken into account. In order to increase the performance of UAV point cloud processing, new algorithms which enable the use of RGB and infrared values to filter data need to be developed.

b) *On the usability of UAV data for high precision dasymetric mapping*

The second approach to the usage of UAV data for the extraction of building block parameters revealed potential use for the delimitation of building blocks. The 3DEBP solution based on a set of specific algorithms developed under FOSS tools was tested on building blocks, which allowed us to demonstrate that it is possible to obtain accurate low-cost block parameters (area, height and volume) from a UAV system.

The main key issues for the success of this methodology based on 3DEBP are the dense image matching processing of stereo aerial images and the filtering of point cloud. The presence of trees near building blocks may hinder the filtering of roof points, especially if the trees are the same height as the top of the building. One solution for the optimization of filtering these objects would be the combination of multispectral values with a point cloud for the detection of tree points. However, in this case study, the filtering of the point cloud for the removal of cars, streetlamps, trees or any other objects near the ground was solved with the CLARA algorithm, followed by the elimination of clusters that had a standard deviation value higher than one. This filtering process was fundamental to reduce the average error of base building block elevation from some metres to half a metre.

The evaluation of area, height, and volume of the extracted block shows the highest errors were achieved for the building blocks that had several buildings with a higher variation of height. The building blocks with a more regular morphology and without surrounding trees can achieve better results in the estimation of height. Furthermore, the differences between the building height parameter estimated with either statistical measure are not significant. The usage of the average highlights better results in the estimation of volume building blocks than the median, but its not conclusive due to compensation errors.

The usability of point cloud data for the extraction of a building block unit was demonstrated. Firstly, the results show a rough identification of the built-up area. Secondly, the estimated building block heights allow us to detect any illegal changes in a block, since the magnitude of vertical errors achieved was below one story. Thirdly, the semi-automatic methodology based on the 3DEBP solution developed revealed a high potential for the building block as a spatial unit.

On the other hand, this case study has revealed that the building parameters acquired from UAV data allow us to generate a 3D building block model that is very

similar to the 'real block model' (3D data acquired by traditional methods), where the magnitude of errors in the estimated building parameters is not significant for 3D geovisualization. Moreover, the use of the median or the average for the generation of 3D building block models does not have significant differences. Therefore, this type of 3D block models can be very useful for the public discussion of a plan, where smoothing of the extracted building footprints is essential.

The usability of the footprints and volume of building blocks extracted from a UAV point cloud was demonstrated in dasymetric mapping, which were used as control zones. As expected, the results for high precision dasymetric mapping (with 3D control zones) had a lower absolute deviation. However, the differences between footprint and volume in population estimates are not significant, due to: a) small size of the dataset; and b) only three zones are affected by the existing building blocks for the estimation of the population. The usage of 2D/3D control zones in dasymetric mapping is relevant for the estimation of population, where the contribution of UAV data is higher.

The sensitivity analysis based on the Monte Carlo simulation allowed us to conclude that the impact of building block volume errors (or block height errors) in dasymetric mapping is null.

Chapter 4

Discussion and Conclusion

Nowadays, the current geo-information technologies related to 3D point clouds have established a new vision for urban planning in the way urban analyses are conducted, decisions are made, and monitoring, evaluation and visualization are performed.

We have discussed the importance of 3D measurement for urban planning, and presented the 3D GIS and spatial databases to support them. The experiment results achieved for the 3D measurements of buildings along this thesis was described in three approaches. Additionally, we have also defined the conditions and procedures for the future implementation of 3D measurement into the planning process.

The pertinence and usability of the methodology developed for the extraction of building parameters was discussed as was also the future research in 3D measurement and 3D geovisualization for a 3D urban planning paradigm.

4.1 *3D measurement for urban planning*

The 3D measurement of building height and volume is very important to support many urban studies that are still being based on 2D maps. Some urban studies in the context of urban sustainability issues can be improved with 3D measurement through 3D modelling and 3D urban models, namely: *a) urban climate analysis* of thermal conditions (Peeters & Etzion, 2012) and thermal conditions and wind environment in a city (Zhao et al., 2011 and Ng et al., 2011). In both cases,

the urban structure related with building size (height and volume) and the spaces between the buildings, and street widths are crucial factors for urban climate analysis; *b) urban noise pollution*, mainly caused by industry and traffic levels, requires 3D urban noise models to identify the influence of noise in all directions at different levels of noise pollution and how many inhabitants can be affected in their homes by noise levels that are hazardous to health (Kurakula & Kuffer, 2008); *c) urban air pollution analysis*, where 3D urban models are important to understand changes in air pollution concentrations at and above the ground surface (Zahran et al., 2010 and Wang et al., 2008); *d) thermal comfort of the buildings*, Lorenz & Döllner (2010) show an example of residential quality assessement based on surface properties (noise pollution, light exposure and the visibility of vegetation), which vary along building façades; *e) outdoor thermal confort* for detached buildings in hot dry scenarios, analysing how the vegetation and landscape can be affected (Yahia & Johansson, 2014); and *f) solar energy potential:* it is important to ascertain the solar energy potential of buildings to improve the thermal and lighting comfort of homes. We also have to think about the deployment of photovoltaic systems in urban areas to convert energy from the Sun into electricity, which is an important issue for climate change. Brito et al. (2012) have estimated the photovoltaic potential from building footprints for the implementation of photovoltaic systems and Redweik et al. (2013) have estimated solar radiation on roofs and façades.

All these issues mentioned above must integrate 3D measurements for a better knowledge of the 'skeletal structure of the built form of the city' (urban structure) (Besussi et al., 2010). Thus, urban planners can better understand the effects of the urban structure in environmental conditions, which influences the way people live. Furthermore, 3D measurement can improve urban morphological analysis methods, such as the definition of 3D indicators that allow us to measure the physical form and morphology of urban land cover, as well as the compacteness level of urban settlements. Therefore, the introduction of 3D measurement into urban planning can improve all the issues mentioned above and ensure a better quality of life in our cities.

These urban planning issues require the development of methodologies within an efficient 2D-3D GIS solution that enables: 1) spatial modelling with topological models; and 2) their implementation in a spatial database management system that allows us to store and manage a large volume of 3D data, such as the 3D point clouds.

A 3D GIS framework includes 3D visualization, querying and 3D spatial analysis functions[1]. These 3D GIS issues must involve a 3D geometry and topological model[2] (vector-based 3D models) integrated into a spatial database.

3D GIS at the end of the last decade were focused on 2D functionalities and 3D visualization of cityscapes and landscapes, the navigation capability, and 3D visibility analysis (Kim et al., 2010 and Khuan et al., 2008). However, some authors have been showing interest in developing 3D functionalities for urban planning, namely in 3D geo-virtual environments to visualize plans and urban designs (Kibria, 2008) and in the development of a 3D topological model for municipal applications based on web-oriented query and visualization (Zlatanova, 2000). Furthermore, Koninger & Bartel (1998) address a 3D GIS framework for urban planning and Moser et al. (2010) show the potential of 3D GIS analysis (mainly 3D geometrical analysis) for 3D urban models, and even propose the development of 3D functions. The review and trends of 3D GIS for spatial analysis and topological models are presented in Kim et al. (2010).

The development of spatial databases[3] in these past few years has been fundamental for the support of 3D GIS. In fact, these spatial databases must have the ability to store big volume of 2D/3D georeferenced data, provide 2D/3D data modelling (using 3D analysis functions), and implement data handling techniques (querying and updating 3D spatial features) based on data structures with 3D geometry. Ledoux & Meijers (2013) tested the 3D modelling of buildings in a PostgreSQL/PostGIS spatial database comparing the performance of different database structures. Currently, PostGIS is able to deal with 3D geometries and 3D topology, where 3D functions were implemented, such as the calculation of 3D object volume, extrusion, and provision of 3D spatial analysis functions[4] between 3D objects.

The issue of spatial databases for 3D GIS has been reviewed and discussed by many authors, such as Breunig & Zlatanova (2011), Zlatanova & Prosperi (2006),

[1] According to Kim et al. (2010), spatial functions can be classified as geometrical (volume, aggregation), topological, and editing.

[2] Urban features are represented as a solid using a 3D topological structure, such as: *Formal Data Structure* model whose boundary is an envelope composed of surfaces, which includes the geometric primitives: arc, nodes, edge, and face; or *Tetrahedron Network* (TEN)(Pilouk, 1996) where the feature is represented by the tetrahedra model allowing us to represent complex structures, which includes the geometric primitives: arc, node, triangle, and tetrahedra (4 triangles).

[3] Oracle Spatial 12c and PostgreSQL/PostGIS integrate the 3D geometry and topologic models. Now, Oracle Spatial 12c can store point clouds, 3D city models and surfaces, and 3D spatial queries, such as volumetric analysis and 3D visibility queries.

[4] SFCGAL library provide 3D functions available from PostGIS2.2 (released October 2015), such as *ST_3Difference*, *ST_3DUnion*, *ST_volume*. It also, stores textures (Auer et al., 2014).

and Khuan et al. (2008).

Presently, all the issues regarding 3D GIS functionalities and spatial databases for 3D data are still in their early stages, and therefore have weaknesses that must be optimized and improved. 3D GIS to handle urban planning will remain an active research topic for a long time.

However, this thesis comprises the experimentation of 3D point clouds obtained from distinct technologies UAV and LiDAR for the semi-automatic extraction of building parameters – area, height, and volume – avoiding the time consuming photogrammetric stereo restitution. 3D point clouds are integrated into a PostgreSQL/PostGIS (FOSS) spatial database that can be connected with QGIS, which now incorporates 3D visualization. This 3D data was modelled using 2D spatial and statistical functions from PostGIS.

The fundamental aim of this experimentation was not to make the 3D modelling of buildings by exploring the 3D geometry model and 3D analysis functions in a 3D GIS environment. This experimentation was only focused on an accurate statistical 3D measurement of the roof eave and the base of the building. Consequently, the rationale behind this experimentation was the acquisition of 3D data, 2.5D modelling and statistical 3D measurement from a set of particular 3D points that better define the eave of building roof and the base of building, seeking accurate values (with the lowest error in terms of the difference between elevation estimated and 'true elevation') in these building locations.

4.2 *Implementation of 3D data for urban planning based on FOSS*

The implementation of 3D data for urban planning, particularly for the extraction of 3D building parameters[5] – height, volume, and total volume – was based on the experimentation of 3D point clouds acquired from two different technologies: LiDAR and UAV. It included the development of a methodology for the semi-automatic extraction of building parameters implemented in a FOSS solution.

Therefore, this experimentation involved the usage of three 3D point clouds, two of which were collected in the same urban area. The LiDAR and UAV point

[5]These definition also included building blocks.

clouds were acquired over a coastal urban area – Praia de Faro – where most buildings are single-family dwellings with a maximum of two stories. The building types in this urban area have a high diversity and complex typology mainly regarding roofs. Moreover, another UAV point cloud was acquired in a small neighbourhood of Amadora, in the outskirts of Lisbon, with residential building blocks that have tiled roofs and heterogeneous forms.

The mesh points and point density achieved in each point cloud partially reflect the acquisition technology. The point density of UAV point clouds collected from multiple stereo image matching was in the order of 61 points/m^2 with a very irregular distribution on the roofs and gaps (mainly in the coastal urban area). The LiDAR point cloud collected directly from a laser pulse had a point density of 6 points/m^2 with a more regular and more consistent mesh on the roofs and without gaps.

The beginning of this experimentation was based on the implementation of specific methodologies to test and evaluate the error in the building heights extracted from 3D point clouds: a) estimation of building height from LiDAR using spatial functions from the ArcGIS software; b) estimation of building height from the UAV point cloud using spatial and handling functions from the GRASS software. Accurate 2D/3D vector data obtained from photogrammetric stereo restitution was included in these methodologies. Furthermore, an automatic extraction of building area and height parameters from the LiDAR point cloud was tested under proprietary software: LiDAR Analyst ('black box').

All experiments were important to learn the difficulties in filtering point cloud data and the limitations of proprietary solutions for the extraction of building parameters, where the development of a robust methodology that can handle a big volume of data with million points is crucial.

Therefore, the implementation of a robust and semi-automatic methodology based on a FOSS solution for the extraction of building parameters, called 3DEBP was performed. The 3DEBP solution developed was based on a 2.5D-FOSS-GISDB solution[6] described in Section 1.4. The 3DEBP follows a set of statistical and spatial functions within specific scripts developed in R and SQL languages. The 3DEBP also allows us to make the evaluation of the estimated building parameters. The methodology and the tools developed were presented in Section 2.3 of Chapter 2.

[6] This FOSS solution did not cover the stereo image matching processing of UAV imagery for the acquisition of a point cloud. Both UAV point clouds were obtained from PIX4D software.

According to the three point clouds collected in two distinct urban morphologies and the automatic solution and the semi-automatic FOSS solution, the experiment of 3D point clouds for the extraction of building parameters – area, height, volume, and total volume – followed three approaches (Figure 4.1):

1. Testing two different solutions: LiDAR Analyst solution and the FOSS solution developed for the specific problem.
2. Testing UAV imagery and LiDAR system technologies on the same urban morphology using 3DEBP solution.
3. Testing UAV imagery on distinct urban morphologies using the 3DEBP solution.

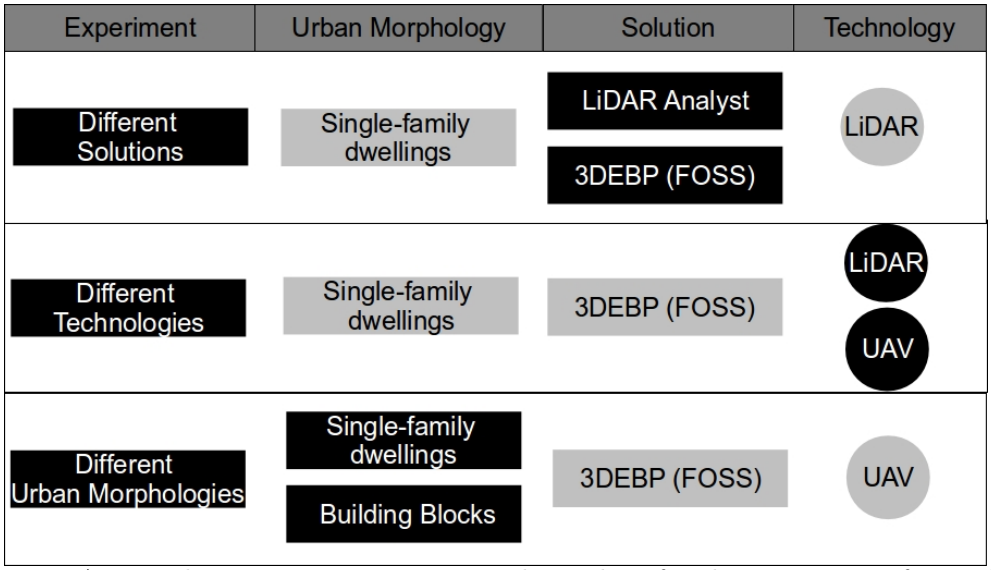

Figure 4.1: Approaches in experimentation with 3D data for the extraction of area, building height, and volume. Single-family dwellings in Praia de Faro and building blocks in Amadora.

The following discussion is centred on the results of the experiments carried out with these approaches, which also included the evaluation of errors for each building parameter estimated.

When we consider the solutions for an urban planner, we should ask: What is the most efficient type of solution for the extraction of building parameters?

- Both, LiDAR Analyst and 3DEBP solutions have the same difficulties in the extraction of the correct shape of roofs that defines the building area, because it is not easy to apply a filtering and a 3D modelling to cover the diversity of building types in an urban area such as Praia de Faro.

- Both solutions revealed potential use in the delimitation of built-up areas.
- The urban planner can extract buildings individually from 3DEBP, which is not possible with the LiDAR Analyst.'The individualization of buildings' was one of the motivations for the development of a FOSS solution, that would enable the extraction of height and volume parameters for each building.

Is it possible to extract accurate building parameters for single-family dwellings with a complex typology under a semi-automatic methodology using a FOSS solution?

Concerning the extraction of the **building area**[7] parameter, it is obtained from the selection of 3D points that represent the roof eave. An accurate building area depends on the filtering quality of 3D points selected which should represent only the roof eave as much as possible.

- Regarding the shape of the building areas extracted from LiDAR, they have a more regular boundary, unlike the areas extracted from the UAV point cloud. The reason for that is the fact that the LiDAR point cloud has fewer discontinuities along the roof eaves.
- The vegetation and tall trees near the buildings recorded by LiDAR constitute the greatest difficulty in the extraction of this parameter, requiring more efficient filtering methods that take these objects into consideration.
- Regarding UAV data, there are difficulties in the extraction of accurate building areas, because the point cloud acquired has many irregularities on the roofs, discontinuities along the roof eave and many gaps. These weaknesses are derived from the difficulty of the multiple stereo matching processing in dealing with very complex roofs that have a lot of untextured small surfaces, many small structures, and various terraces on the roof that can increase the existence of occlusions.
- Removing building points that do not belong to the roof eave, such as balconies in the façades is difficult in both point clouds. In these cases, this results in overestimated areas.
- However, we can conclude that LiDAR offers better results than UAV regarding the estimation of this parameter for a set of single-family buildings, since a low percentage of these buildings were rejected because of an unacceptable shape, which did not happen with UAV data.

[7]Building area also referred to as the area of building roof.

Regarding **building height parameter**[8] estimated from the roof eave and base points selected for each building, its calculation was made statistically for these points selected by using average or median measures. Therefore, the evaluation of error was performed in both measures.

- Concerning the building height errors obtained from both technologies, they are very similar[9]. The average building height errors are well below 1 m using the median statistical measure for LiDAR and the average measure for UAV for the estimation of building heights.
- Although the sample of buildings is small, there is strong evidence that these point clouds can ensure a vertical error well below 1 m in the estimation of this parameter.
- For urban areas with such great diversity and complexity in terms of building types, the solution developed can achieve for both point clouds a vertical error below 1 m for about 80% of the estimated building heights and below 50 cm for about 50% of the estimated building heights.

Regarding **building volume and total volume** calculated from the estimated building height and area, the evaluation of the building volume extracted was made analysing the error with a combination of the two issues: a) using estimated average and median building height; and b) using the area estimated from point clouds and accurate area obtained from photogrammetric stereo restitution.

- Regarding the magnitude of relative building volume error for both point clouds, it is similar, with an average relative error of about 10% using the accurate area value[10]. However, the average relative error using the area estimated from LiDAR and UAV was about 10%[11] and 17%, respectively.
- Considering a building type such as a single-family dwelling, we can say that if the vertical error in the extraction of building height[12] is: a) up to 7 cm, it ensures an error in volume below 1%; b) up to 50 cm, it ensures an error in volume below 8%; and c) up to 1 m, the error in building volume is below 15%.

[8] Also defined in this thesis as building façade height.

[9] One of the UAV point cloud cluster samples has an average error below 15 cm when compared with LiDAR.

[10] Building outline acquired using stereo restitution photogrammetry technique.

[11] Some buildings were rejected (incorrect shape), which allowed us to achieve this value.

[12] If the building height error is fixed, the volume error is inversely proportional to the area of building rooftop.

- Concerning the relative total volume error, a range varying between 2% and 6% for UAV and 3% and 10% for LiDAR is expected. In this building parameter, the use of average or median building height does not affect the results because there is a strong compensation of the errors obtained in each of the variables involved. There is also evidence that the UAV point cloud can be better to estimate the total volume in this urban area than LiDAR.

It is important to stress that the first stage of this semi-automatic methodology based on the 3DEBP solution related with the selection of 3D points using the clustering process is the key to the success of the estimation of accurate building parameters. It can have a strong influence in the quality of the results as demonstrated in Section 2.3 for two samples clustered from UAV.

What is the influence of urban morphology in the estimation of building parameters from UAV technology?

- Using UAV technology in an urban morphology that is structured into blocks makes it easier to extract block boundaries whose shape is closer to the real one, than in an urban area with higher complexity and diversity in terms of building roofs on single-family dwellings.
- The point cloud of building blocks is more consistent and has fewer gaps when compared with the ones obtained in an urban area with a higher diversity of single building types, which means that stricter conditions for the definition of flight planning in complex areas are needed.
- Statistically, the use of average or median measures in the estimation of building block heights has less impact than in single-family buildings. The average of building block height error for a block morphology is sligthy better: it is below 50 cm using either measure.
- The impact of building height errors on estimation of the volume is higher in an urban morphology of single-family dwellings than on building blocks.
- The average of relative volume error was around 6% using estimated average building height on a building block morphology. However, in single-family dwellings the average of relative volume error was higher, above 15%, because of the difficulties in estimating the area.
- Lastly, concerning the total volume extracted we expect an average of relative total volume error of about 3% in both urban morphologies using average

building height.

After this discussion, we can conclude that the methodology we have developed, coupled with low-cost and flexible UAV imagery technology, allows us to ensure the accuracy required for many studies in urban planning, with an error in terms of building height below one story. Additionally, in small urban areas the UAV can replace the LiDAR system. However, we need to ensure a higher point density for UAV point clouds from a high spatial resolution imagery and a high overlapping between images. Therefore, the flight planning should be adapted to the urban morphology to deal with these two issues and consequently ensure a good performance of the multiple stereo image matching algorithm.

The implementation of this FOSS-based semi-automatic methodology created conditions for:

- The *Quantification* of 3D building parameters (building height, volume, and total volume) in different urban morphologies using contemporary 3D data acquisition technologies.

- *High precision dasymetric mapping* for multi-temporal analysis of datasets, such as census population information. This spatial interpolation technique makes it possible to reallocate census population between two periods from different census tracts' geometries to a common geometry using 3D control zones (building volumes). These 3D control zones allow high precision in the estimation of the resident population for a target period.

- *Urban analysis* with the construction of 3D quantitative indicators that involve building height, volume, and total volume. Planners and decision-makers can more easily define accurate indicators to analyse and control urban development and the constraints established in the plans, and also to quantify the building density, urban physical structure, and urban morphological changes.

- *3D geovisualization* with the generation of 3D urban models. 3D urban models increased the spatial perception of the surroundings and the spatial disposition of the buildings due to the possibility of seeing the urban model from different perspectives, through the use of tools that enable the rotation of the model. For instance, this is an essential issue for urban planners and various stakeholders in the public discussion of a plan.

Currently, the new legal framework of the IGT[13] emphasizes the implementation of planning evaluation policies. Hence the need for a plan revision becomes more dependent on monitoring and evaluating the results. Thus, the law established that a plan must contain the definition of a set of qualitative and quantitative indicators to support their monitoring and evaluation. This implies regularly taking measurements and comparing these measurements with what is defined in the plan, which allows the identification of trends and changes for the adjustment of zoning regulations and the land use policy.

As a logical consequence, the need for a plan revision in case of land dynamics in the concerned area, such as constructive dynamics, will lead to the permanent monitoring of land use and land cover changes. Therefore, the updating of official and approved topographic and imagery mapping after ten years for the plan revision was replaced by a more frequent updating[14].

Furthermore, the 3D data must also be ensured in this updating process. 3D data will be needed for the construction of indicators that allows us to control some of the issues of the municipal plans, such as the monitoring of total building height in the consolidated planned urban areas and the calculation of total building volumes in the context of urban restructuring (including demolitions, conservation, and rehabilitation).

The methodology implemented in this work for the extraction of building parameters can support the monitoring and evaluation of 3D indicators in the planning process, but the conditions of their implementation for this process should be clearly defined.

4.3 *Is 3D a new paradigm?*

Throughout this thesis, we have demonstrated how 3D geo-information technologies can be used to measure building parameters based on the experimentation and the implementation of a specific methodology. We should now ask: *'Are the building parameters extracted by this methodology pertinent to the planning process? And, if so, what are the conditions for their implementation?'*. Both these questions will be answered simultaneously, if we are in fact facing a 3D paradigm for urban

[13] According to article Decree-Law No. 80/2015, of 14th May.

[14] Master plan: 3 years; urban plan: 2 years, and detailed plan: 1 year (article 15-A of Decree-Law No. 141/2014, of 19th September).

planning.

The first step is to combine the conceptual component with the operating character of the issues involved in the planning process based on their *relevance* and *pertinence*.

When we talk about the *relevance* we mean that the 3D measurements obtained from this methodology satisfy the needs of the planning process[15] and can compete with other methods. *Pertinence*, on the other hand, stresses a clear evidence of the relevance of the methodology used for 3D measurement, which can replace the 3D stereo-measurement of photogrammetric techniques.

Reflecting the results of the experimentation, Table 4.1 summarizes the relevance and pertinence of the building parameters estimated throughout this thesis for the planning process. Additionally, it also indicates the best combination of 3D technology and urban morphology to ensure the pertinence of an estimated building parameter and therefore its usability for the planning process.

Table 4.1: Relevance and pertinence of building parameters estimated from UAV and LiDAR technologies

Building parameter	**Error threshold**	**Relevance**	**Pertinence**	**Usability (according to the experimentation)**
Area	-	Elaboration (urban analysis)	Monitoring: detection and location of new buildings; Public discussion: 3D urban models	UAV blocks; LiDAR single-family dwellings
Building Height	Average error < 1m	Elaboration (urban analysis)	Monitoring: detection of changes and illegal issues in buildings, accurate 3D indicators dependent on the number of stories; Public discussion: 3D urban models	UAV and LiDAR single-family dwellings; UAV blocks
	Average error < 50cm	-	All the phases of the urban planning process	UAV Blocks
Volume	Relative average error < 10%	Elaboration (urban analysis)	Monitoring and evaluation: 3D indicators BH error should be less than 50cm; Public discussion: 3D urban models	LiDAR single-family dwellings; UAV blocks
Total Volume	Relative average error < 5%	-	All the phases of the urban planning process	UAV and LiDAR single-family dwellings; UAV blocks

Note: Point clouds should have a vertical accuracy of up to 10 cm.

We believe that the pertinence of the usage of 3D data obtained from UAV and LiDAR technologies was sufficiently demonstrated in this thesis for the extraction of building height and volume.

The usability of this 3D data coupled with a semi-automatic FOSS methodol-

[15]Evaluation, monitoring, evaluation and participation/public discussion.

ogy for the extraction of building parameters that support the planning process will be possible to implement in public administration under the following conditions:

Acquisition: Flights planned with UAV technology could be scheduled every year by public or private companies for the acquisition of 3D data, which is not feasible for LiDAR due to its higher costs. Some considerations should be taken into account when planning flights with these technologies:

- Size of the urban area: for a small urban area, UAV technology is recommended due to its low cost, flexibility and faster acquisition. Large areas imply various UAV flights, in this case, the usage of a LiDAR system or common digital airborne systems would be a better choice.
- Urban morphology and environment: the analysis of urban morphology is important for the definition of flight parameters, which is important to ensure a good overlapping imagery if we intend to use a UAV. For urban areas with a dense vegetation, the UAV is recommended, if the objective is only to extract the buildings.
- Flight conditions: the flight height and weather conditions (low wind and sunny day) are two important issues to ensure the good quality of the stereo images, which includes high overlapping and avoiding shadows in the case of UAV. LiDAR in classical airborne system is not dependent on weather conditions.

Quality control: the accurate assessment of this 3D data collected must be made before their usage to ensure the quality of the estimation of the parameters. Therefore, the 3D data must be controlled and approved by an entity that has responsibilities in the mapping production. This condition must be required only for the elaboration and monitoring of a plan. The regulation of 3D data and the creation of technical specifications for its acquisition is also an important task for the implementation of this data into the planning process.

Processing and modelling based on the developed FOSS solution: a) a dense point cloud that fully covers the buildings or at least the roof eaves is necessary to enable a good estimation of the building parameters; b) it is also crucial for a good estimation that the clustering process used in this methodology must identify the buildings correctly; and c) the average and median statistical measures should be used for the estimation of building heights (as from single-family dwellings) in UAV and LiDAR, respectively.

Human and technical resources: the creation of a technical team in the public administration composed of developers, experts, and researchers is necessary. This team should manage and develop new FOSS tools for the construction of 3D indicators for the plans from the building parameters extracted, thus supporting the new requirements of the legal framework – IGT. Moreover, strained and skilled technicians specializing in FOSS technologies should cooperate with the municipalities in this regard.

3D Open data: dissemination of 3D data via the implementation of a spatial database with point clouds available to every urban planners or other professionals that wish to work with this type of 3D data. This spatial database with metadata information should be checked and managed by a public administration body. This database should promote the usage of 3D data by urban planners, architects, and other professionals that deal with urban issues.

The implementation of the estimation of building parameters from 3D point clouds into the planning process should meet rigorous conditions that can preferably ensure a high positional quality (such as an error below one story for building height). The usability of this data for the planning process was demonstrated by the creation of conditions for its implementation based on the *pertinence* of the results of the experiments described in this thesis. Therefore, the 3D as a new paradigm is now a reality, since the interest in its usage and implementation is inevitable for the observation and monitoring of 3D changes over an urban area.

4.4 *Future developments*

3D measurement and 3D geovisualization are the future research issues for urban planning. Today, the growing constructive dynamics of the cities requires increased monitoring of the plans and so it needs 3D geographic information technologies that are able to meet this high monitoring frequency.

Therefore, the final discussion of this thesis will revolve around the research objectives based on the following three issues: the methodology developed for the extraction of building parameters, the needs of the new legal framework regarding the planning process for Portugal and the new vision of a 3D urban planning paradigm.

The usability of 3D data for the elaboration of plans by developing 3D com-

pactness indexes demands further demonstration. Therefore, the approach to 3D compactness should be a measure of '*volume and adjacency of a set of buildings*' which: i) is a combination of several metric attributes (height, volume, maximum and a minimum contact area between buildings); ii) comprises a set of several indexes that contribute to the measurement of density and urban contiguity; and iii) is as sum of multiple sets of buildings or blocks. The usability of 3D compactness indexes are expected to: i) contribute to the creation of a methodology to assess the relationships between 3D compactness, urban form, and density; and ii) define the way these indexes can contribute to the creation of urban rules that promote increased compactness, ensuring the sustainability of urban form, particularly through a balanced distribution of volume, alignment of buildings, and space void filling.

This thesis demonstrated the pertinence and usability of 3D point clouds acquired from UAV and ALS technologies for the 3D measurement of building parameters while simultaneously providing the solution for the monitoring and evaluation needs under the new legal framework that currently guide plan-makings in Portugal. Nevertheless, research to support this challenge must continue towards its implementation.

Improving and *optimizing* are the keywords for the future research on the extraction of building parameters derived from the 3DEBP methodology.

Firstly, the 3DEBP can be improved by testing it in other urban morphologies with the aim of refining how parameters are modelled and at the same time establishing a set of conditions to perform UAV flights in different urban morphologies. In addition, it is important to increase the urban area of experimentation, whilst ensuring greater spatial diversity in terms of the building roofs, which will simultaneously imply an increase in the spatial variability within the urban area through the diversity of the building roofs themselves.

Secondly, the set of algorithms developed to support the methodology need a robust *optimization* to increase the automation in the extraction building parameters. This implies reducing the FOSS solution to PostgreSQL/PostGIS and QGIS. This means including the clustering process in R and using the function *concave hull* (performed in GRASS) inside the SQL code as PostGIS function that runs in the PostgreSQL/PostPostGIS spatial database. Furthermore, the research on the integration of some 3D functions of the new SFCGAL library for the 3D measurement of building parameters could also be performed as the calculation of volume

in a 3D geometry model.

Still regarding the planning process, the *monitoring and evaluation* phases and the *participation/public discussion* phase need an active research. According to the legal framework – RJIGT, the development and implementation of a system of indicators that includes 3D data is needed for the plans. This implementation requires the development of FOSS tools for the quantification of indicators, which is a crucial research topic for the monitoring and evaluation process. Moreover, systems based on 3D measurement and 3D geovisualization are needed to support the monitoring and evaluation processes, through the detection and quantification of changes in built-up area, such as building volumes and heights in 3D geovisualization. Finally, the 3D geovisualization of the plans in the revision process is needed to increase the participation of stakeholders and citizens in the public discussion process.

The integration of 3D urban models (3D mapping) into the planning process will require a tight quality control in the future. The conceptual issues of 3D mapping are today an evolving discussion topic in the scientific community. The challenge will be to establish 3D mapping issues, as scale, accuracy, and level of detail, creating the conditions for the implementation of 3D quality control procedures in the production of 3D urban models.

Various research issues have contributed to the construction of the 3D urban planning paradigm, such as the 3D GIS framework and spatial databases with 3D modelling. However, these issues are bound to remain for a long time a research topic on the improvement of 3D data models (topology and geometry), the development of new 3D spatial functions, and the growth of data handling techniques inside spatial databases. Furthermore, the development and integration of better 3D geovisualization systems for 3D urban models into GIS FOSS is crucial.

When we think about the new issues in 3D urban planning, we consider the measurement of 3D compactness to be an important discussion topic in the years ahead. Until today, research has only addressed the issue of urban sprawl based on a 2D vision, but the challenge for the future will be planning '*vertical cities*' with denser and taller buildings, to ensure the quality of life by defining more sustainable urban indicators.

Bibliography

Aber, J. S., Marzolff, I., & Ries, J. B. (2010). *Small-Format Aerial Photography Applications*. Elsevier, 1 ed. ISBN: 978-0-444-53260-2.

Ackermann, F. (1999). Airborne laser scanning—present status and future expectations. *ISPRS Journal of Photogrammetry and Remote Sensing*, *54*(2-3), 64–67. DOI: 10.1016/S0924-2716(99)00009-X.

Ahokas, E., Kaartinen, H., & Hyyppä, J. (2003). A quality assessment of airborne laser scanner data. *International Archives of Photogrammetry, Remote Sensing and Spatial Information Sciences*, *34, Part 3/W13*, 1–7.

Alexander, C., Smith-Voysey, S., Jarvis, C., & Tansey, K. (2009). Integrating building footprints and LiDAR elevation data to classify roof structures and visualise buildings. *Computers, Environment and Urban Systems*, *33*(4), 285–292. DOI: 10.1016/j.compenvurbsys.2009.01.009.

Alves, R. (2007). *Políticas de Planeamento e Ordenamento do Território no Estado Português.*. Lisbon: Fundação Calouste Gulbenkian. ISBN: 9789723112108.

Alves, R., & Simões, C. (2015). INSPIRE and Land Use Planning System in Portugal. In *Geospatial World Forum*. Lisboa.

Auer, M., Agugiaro, G., Billen, N., Loos, L., & Zipf, A. (2014). Web-based Visualization and Query of semantically segmented multiresolution 3D Models in the Field of Cultural Heritage. *ISPRS Annals of Photogrammetry, Remote Sensing and Spatial Information Sciences*, *II-5*(June), 33–39. DOI: 10.5194/isprsannals-II-5-33-2014.

Baltsavias, E. P. (1999a). A comparison between photogrammetry and laser scanning. *ISPRS Journal of Photogrammetry and Remote Sensing*, *54*(2-3), 83–94. DOI: 10.1016/S0924-2716(99)00014-3.

Baltsavias, E. P. (1999b). Airborne laser scanning: basic relations and formulas. *ISPRS Journal of Photogrammetry and Remote Sensing*, *54*(2-3), 199–214. DOI: 10.1016/S0924-2716(99)00015-5.

Baltsavias, E. P. (1999c). Airborne laser scanning: existing systems and firms and other resources. *ISPRS Journal of Photogrammetry and Remote Sensing*, *54*(2-3), 164–198. DOI: 10.1016/S0924-2716(99)00016-7.

Barazzetti, L., & Brovelli, M. A. (2008). Lidar Filtering : Testing of an Automatic Procedure Developed in the Free Open Source GIS GRASS. *The International Archives of the Photogrammetry, Remote Sensing and Spatial Information Sciences.*, *XXXVII*(Part B4.), 359–366.

Bartoš, K., Pukanská, K., & Sabová, J. (2014). Overview of Available Open-Source Photogrammetric Software, its Use and Analysis. *International Journal for Innovation Education and Research www.ijier.net*, *2*, 62–70. Retrieved from http://www.ijier.net/assets/overview-of-available-open-source-photogrammetric-software,-its-use-and-analysis-ijier.net-vol-2-4_5.pdf.

Batista e Silva, J. M. (1998). *A função Monitorização em planeamento urbanístico ao nível municipal.*. Ph.D. thesis, Instituto Superior Técnico da Universidade técnica de Lisboa.

Bäumker, M., & Heimes, F. (2001). New Calibration and Computing Method for Direct Georeferencing of Image and Scanner Data Using the Position and Angular Data of an Hybrid Inertial Navigation System. In J. K. Heipke C., & W. H. (Eds.) *Integrated Sensor Orientation- Test Report and workshop proceedings 16 S.*, (pp. 1–17).

Bellavita, D., Ceccaroni, F., & Mazzitelli, A. (2013). Mapping a Landslide Using UAS. *GIM International*, *27*(2), 27–29. Retrieved from http://www.gim-international.com/content/article/mapping-a-landslide-using-uas.

Berg, M., Cheong, O., Kreveld, M. V., & Overmars, M. (2008). *Computational Geometry, algorithms and aplications*. Springer-Verlag Berlin Heidelberg, 3rd ed. ISBN: 978-3-540-77973-5.

Besussi, E., Chin, N., Batty, M., & Longley, P. (2010). The Structure and Form of Urban Settlements. In T. R. Jürgens, & Carsten (Eds.) *Remote Sensing of Urban*

and Suburban Areas, chap. 4, (pp. 13–31). London: Springer. DOI: 10.1007/978-1-4020-4385-7.

Bivand, R. S., Pebesma, E. J., & Gómez-Rubio, V. (2008). *Applied Spatial Data Analysis with R*. springer. DOI: 10.1007/978-0-387-78171-6.

Breunig, M., & Zlatanova, S. (2011). 3D geo-database research: Retrospective and future directions. *Computers & Geosciences*, *37*(7), 791–803. DOI: 10.1016/j.cageo.2010.04.016.

Brito, M. C., Gomes, N., Santos, T., & Tenedório, J. a. (2012). Photovoltaic potential in a Lisbon suburb using LiDAR data. *Solar Energy*, *86*(1), 283–288. DOI: 10.1016/j.solener.2011.09.031.

Brovelli, M. (2004). Digital terrain model reconstruction in urban areas from airborne laser scanning data: the method and an example for Pavia (northern Italy). *Computers & Geosciences*, *30*(4), 325–331. DOI: 10.1016/j.cageo.2003.07.004.

Brovelli, M. A., Cannata, M., & Longoni, U. M. (2002). Managing and processing LIDAR data within GRASS. (September), 11–13.

Brovelli, M. A., & Lucca, S. (2011). Filtering LiDAR with GRASS: overview of the method and comparisons with Terrascan. *Italian Journal of Remote Sensing*, *43*(2), 93–105. DOI: 10.5721/ItJRS20114327.

Campos, V., & Silva, M. A. (1997). Cartografia descritiva vs cartografia regulamentar. *Instituto Portugues Cartografia e Cadastro, IPCC*, (6), 16.

Carswell, A. I. (2011). Lidar Imagery – From Simple Snapshots to Mobile 3D Panoramas. In Dieter Fritsch (Ed.) *Photogrammetric Week '53,*, (pp. 3–14). Herbert Wichmann Verlag, Heidelberg. ISBN: 3879075077, 9783879075072.

Chiang, K.-w., Tsai, M.-l., & Chu, C.-h. (2012). The Development of an UAV Borne Direct Georeferenced Photogrammetric Platform for Ground Control Point Free Applications. *sensors*, (12), 9161–9180. DOI: 10.3390/s120709161.

Choi, K., & Lee, I. (2013). A Sequential Aerial Triangulation Algorithm for Real-time Georeferencing of Image Sequences Acquired by an Airborne. *Remote Sensing*, (5), 57–82. DOI: 10.3390/rs5010057.

Conway, J. (2012). PL/R User's Guide - R Procedural Language. Chapter 8. Aggregate Functions. Retrieved October 13, 2014 from the World Wide Web: http://www.joeconway.com/plr/doc/plr-aggregate-funcs.html.

Dandois, J. P., & Ellis, E. C. (2010). Remote Sensing of Vegetation Structure Using Computer Vision. *Remote Sensing*, *2*(4), 1157–1176. DOI: 10.3390/rs2041157.

Danese, M., Nolé, G., & Murgante, B. (2009). Visual Impact Assessment in Urban Planning. In B. Murgante, G. Borruso, & A. Lapucci (Eds.) *Geocomputation and Urban Planning Studies in Computational Intelligence*, vol. 176, (p. 280). Springer-Verlag Berlin Heidelberg. DOI: 10.1007/978-3-540-89930-3_8.

Deseilligny, P. M., & Clery, I. (2012). Apero, an Open Source Bundle Adjusment Software for Automatic Calibration and Orientation of Set of Images. *ISPRS Commision V Symposium, Image Engineering and Vision Metrology*, *XXXVIII-5/*, 269–276. DOI: 10.5194/isprsarchives-XXXVIII-5-W16-269-2011.

Deuber, M., Cavegn, S., & Nebiker, S. (2014). Dense Image Matching. *GIM International*, (September), 23–25. Retrieved from http://www.gim-international.com/content/article/dense-image-matching.

DGT (2013). O novo regime da Política de Solos de Ordenamento do Território e de Urbanismo. In *Palestra na Ordem dos Engenheiros*. Lisboa.

EASA (2015). Proposal to create common rules for operating drones in Europe. Retrieved October 25, 2015 from the World Wide Web: http://easa.europa.eu/system/files/dfu/209533-01-EASA_Summary of the ANPA.pdf.

Eisenbeiss, H. (2009). The Potential of Unmanned Aerial Vehicles for Mapping. In D. Fritsch (Ed.) *Photogrammetric Week '52*, (pp. 35–145). Herbert Verlag, Wichmann. ISBN: 9783879074839 3879074836.

Elberink, O., & Vosselman, G. (2011). Quality analysis on 3D building models reconstructed from airborne laser scanning data. *ISPRS Journal of Photogrammetry and Remote Sensing*, *66*(2), 157–165. DOI: 10.1016/j.isprsjprs.2010.09.009.

Espada, G. P. (2010). Existing Open Source Tools and Possibilities for Cadastre Systems Existing Open Source Tools and Possibilities for Cadastre Systems. (April), 11–16. ISBN: 978-92-5-106510-5.

Everaerts, J. (2008). Unmanned aerial vehicles for photogrammetry and remote sensing. In J. C. Zhilin Li, & E. Baltsavias (Eds.) *Advances in photogrammetry, remote sensing and spatial information sciences: 2008 ISPRS congress book*, (pp. 117–124). DOI: 10.1201/9780203888445.pt1.

Feifei, X., Zongjian, L., Dezhu, G., & Hua, L. (2012). Study on construction of 3D building based on UAV images. *International Archives of the Photogrammetry. Remote Sensing and Spatial Information Sciences.*, *XXXIX*(September), 469–473. DOI: 10.5194/isprsarchives-XXXIX-B1-469-2012.

Fernandes, E. G. (2001). Planos Municipais de OT. Continuidade e inovação em três gerações de planos. *Cadernos municipais –revista de acção regional e local, XV*, (75), 30–44.

Fernandes, E. G. (2002). Uma estória da carta militar de Portugal 1/25000. *Boletim do Instituto Geográfico do Exército*, (64), 80.

Forlani, G., Nardinocchi, C., Scaioni, M., & Zingaretti, P. (2006). Complete classification of raw LIDAR data and 3D reconstruction of buildings. *Pattern Analysis and Applications*, *8*(4), 357–374. DOI: 10.1007/s10044-005-0018-2.

FSF (2004). Free Software Foundation. Retrieved October 10, 2015 from the World Wide Web: http://www.fsf.org.

Furukawa, Y., & Ponce, J. (2010). Accurate, Dense, and Robust Multiview Stereopsis. *IEEE Transaction on pattern Analysis and Machine Intelligence*, *32*(8), 1362–1376. DOI: 10.1109/TPAMI.2009.161.

GNU, R. S. (2013). Free Software is even more important now. Retrieved October 10, 2015 from the World Wide Web: http://www.gnu.org/philosophy/free-software-even-more-important.html.

Gomes, T. P. (2011). A Cartografia Militar portuguesa no século XX : contributos do Instituto Geográfico do Exército. In *IV Simpósio LusoBrasileiro de Cartografia Histórica, 9 a 12 de Novembro de 2011*, (pp. 1–17). Porto. ISBN: 978-972-8932-88-6.

Goodchild, M., Anselin, L., & Deichmann, U. (1993). A framework for the areal interpolation of socioeconomic data. *Environment and Planning*, *25*(3), 383–397. DOI: 10.1068/a250383.

GRASS (2014). GRASS GIS 7.0.3svn Reference Manual. Retrieved October 23, 2014 from the World Wide Web: https://grass.osgeo.org/grass70/manuals/.

Haala, N. (2011). Multiray Photogrammetry and Dense Image Matching. *Multiray Photogrammetry and Dense Image Matching*, (pp. 185–195). Retrieved from http://www.ifp.uni-stuttgart.de/publications/phowo11/190Haala.pdf.

Haala, N., Hastedt, H., Wolff, K., Ressl, C., & Baltrusch, S. (2010). Digital Photogrammetric Camera Evaluation – Generation of Digital Elevation Models. *Photogrammetrie – Fernerkundung – Geoinformation (PFG)*, (2), 99–115. Retrieved from http://www.dgpf.de/neu/WWW-Projekt-Seite/PDF/03-PFG-02-2010-Hoehenmodelle-FinalVersion-20100112.pdf.

Haala, N., & Kada, M. (2010). An update on automatic 3D building reconstruction. *ISPRS Journal of Photogrammetry and Remote Sensing*, *65*(6), 570–580. DOI: 10.1016/j.isprsjprs.2010.09.006.

Haala, N., & Rothermel, M. (2012). Dense Multiple Stereo Matching of Highly Overlapping UAV Imagery. *XXXIX*(September), 387–392. DOI: 10.5194/isprsarchives-XXXIX-B1-387-2012.

Haarbrink, R., & Eisenbeiss, H. (2008). Accurate Dsm Production From Unmanned Helicopter Systems. *The International Archives of the Photogrammetry, Remote Sensing and Spatial Information Sciences. Vol. XXXVII. Beijing 2008 a*, *Vol. XXXVI*(Part B1.), 1259–1264. Retrieved from http://www.isprs.org/proceedings/XXXVII/congress/1_pdf/214.pdf.

Habib, A. F., Shin, S., Kim, C., & Ai-durgham, M. (2006). Integration of Photogrammetric and LIDAR Data in a Multi-Primitive Triangulation Environment. In V. Abdul-Rahman A., Zlatanova and Coors (Ed.) *Innovations in 3D Geo information systems*, (pp. 29–45). Springer Berlin Heidelberg. DOI: 10.1007/978-3-540-36998-1_3.

Hall, P. (2002). *Urban and Regional planning*. London: Taylor & Francis, 4th ed. ISBN: 0203995325.

Hartigan, J., & Wong, M. (1979). A k-means clustering algorithm. *Applied Statistics*, (28), 100–108. DOI: 10.2307/2346830.

Harwin, S., & Lucieer, A. (2012). An Accuracy Assessment Of Georeferenced Point Clouds Produced Via Multi-View Stereo Techniques Applied To Imagery Acquired Via Unmanned Aerial Vehicle. *International Archives of the Photogrammetry, Remote Sensing and Spatial Information Sciences, ISPRS Congress*, *XXXIX-B7*(September), 475–480. DOI: 10.5194/isprsarchives-XXXIX-B7-475-2012.

Hermosilla, T., Palomar-Vázquez, J., Balaguer-Beser, A., Balsa-Barreiro, J., & Ruiz, L. a. (2014). Using street based metrics to characterize urban typologies. *Computers, Environment and Urban Systems*, *44*, 68–79. DOI: 10.1016/j.compenvurbsys.2013.12.002.

Herold, M., & Roberts, D. A. (2010). The Spectral dimension in Urban Remote Sensing. In T. R. Jürgens, & Carsten (Eds.) *Remote Sensing of Urban and Suburban Areas*, chap. 4, (pp. 47–66). London: Springer. DOI: 10.1007/978-1-4020-4385-7.

Hirschmüller, H. (2008). Stereo Processing by Semiglobal Matching and Mutual Information. *IEEE Transactions on Pattern Analysis and Machine Intelligence*, *30*(2), 328–41. DOI: 10.1109/TPAMI.2007.1166.

Hirschmüller, H. (2011). Semi-Global Matching – Motivation, Developments and Applications. In D. Fritsch (Ed.) *Photogrammetric Week '53*, (pp. 173–184). Herbert Verlag, Wichmann. ISBN: 3879075077, 9783879075072. Retrieved from http://www.ifp.uni-stuttgart.de/publications/phowo11/180Hirschmueller.pdf.

Hirschmüller, H., & Bucher, T. (2010). Evaluation of Digital Surface Models by Semi-Global Matching. *Robotics*.

Hofmann, A., Maas, H.-g., & Streilein, A. (2009). Derivation of Roof Types by Cluster Analysis in Parameter Spaces of Airborne Laser scanner Point Clouds. (pp. 1–6). Retrieved from http://www.isprs.org/proceedings/XXXIV/3-W13/papers/Hofmann_ALSDD2003.pdf.

Holl, S. (2005). An introduction to the practical use of the Free Geographical Information System.

Hyyppä, J. (2011). State of the Art in Laser Scanning. In D. Fritsch (Ed.) *Photogrammetric Week '53*, (pp. 203–216). Stuttgart: Herbert Verlag, Wichmann. ISBN: 9783879075072.

Hyyppä, J., Jaakkola, A., Chen, Y., Kukko, A., Kaartinen, H., Zhu, L., Alho, P., & Hyyppä, H. (2015). Unconventional LIDAR Mapping from Air, Terrestrial and Mobile. In D. Fritsch (Ed.) *Photogrammetric Week '55*, (pp. 205–213). Stuttgart: Herbert Verlag, Wichmann. ISBN: 9783879075874.

Jahne, B. (2004). *Practical handbook on image processing for scientific and Technical applications*. CRC Press, 2 ed. ISBN: 0849319005.

Jancosek, M., & Padja, T. (2011). Multi-view reconstruction Preserving Weakly-Supported Surfaces. Colorado Springs, USA. DOI: 10.1109/CVPR.2011.5995693.

Kaartinen, H., & Hyyppä, J. (2006). Evaluation of Building Extraction. In *EuroSDR Projects*, 50, (p. 286). Frankfurt: Bundesamt für Kartographie und Geodäsie (BKG). ISBN: 9789051794748. Rtrieved from: http://www.eurosdr.net/2002/publications/publications.asp.

Kaartinen, H., Hyyppä, J., Gülch, E., Vosselman, G., Hyyppä, H., Matikainen, L., Hofmann, a. D., Mäder, U., & Persson, A. (2005). Accuracy of 3D city models : EuroSDR comparison. In *ISPRS Journal of Photogrammetry and Remote Sensing WGIII/3, V/3 Workshop "Laser scanning 2005"*, vol. 3, (pp. 227–232). Enschede, the Netherlands: Isprs. Http://www.isprs.org/proceedings/XXXVI/3-W19/papers/227.pdf.

Kada, M., Mckinley, L., & Systems, V. C. (2009). 3D Building Reconstruction from Lidar Based on a Cell Decomposition Approach. In U. Stilla, F. Rottensteiner, & N. Paparoditis (Eds.) *CMRT09*, vol. XXXVIII, (pp. 47–52). IAPRS. Http://www.pf.bgu.tum.de/isprs/cmrt09/pub/CMRT09_Kada_McKinley.pdf.

Kaufman, L., & Rousseeuw, P. J. (1986). Clustering large data sets (with discussion). In *Pattern Recognition in Practice II*, (pp. 425–437). Amsterdam: Elsevierflorth-Holland, e. s. gelsema and l. n. kanal ed. DOI: 10.1016/B978-0-444-87877-9.50039-X.

Kaufman, L., & Rousseeuw, P. J. (1990). *Finding Groups in Data: an introduction to cluster analysis*. John Wiley & Sons, Inc. ISBN: 0-471-73578-7.

Khuan, C. T., Abdul-Rahman, A., & Zlatanova, S. (2008). 3D Solids and Their Management In DBMS. In G. Gartner, L. Meng, & M. P. Peterson (Eds.) *Advances in 3D Geoinformation Systems*, chap. 16, (pp. 279–311). DOI: 10.1007/978-3-540-72135-2_16.

Kibria, M. (2008). *Functionalities of geo-virtual environments to visualize urban projects Functionalities of Geo-VE to visualize Urban Projects*. Ph.D. thesis. Http://www.gdmc.nl/publications/2008/Geo-virtual_environments.pdf.

Kim, T.-W., Lee, Y.-W., & Suh, Y.-C. (2010). A Literature Study on 3D Topology Models for the 3D Spatial Analysis. In *Asian Association Remote Sensing Overview*, (pp. 1–6). Http://www.a-a-r-s.org/aars/proceeding/ACRS2010/Papers/Oral

Kolbe, T., Gröger, G., & Plümer, L. (2005). CityGML - Interoperable Access to 3-D City Models. In *Van Oosterom, P., Zlatanova, S., Fendel, E. (Eds.):Proceedings of the Int. Symposium on Geoinformation for Disaster Management,21st–23rd March*. Delft, Netherlands, Springer.

Koninger, A., & Bartel, S. (1998). 3D-GIS for Urban Purposes. *Geoinformatica*, *2*(1), 79–103. DOI: 10.1023/A:1009797106866.

Küng, O., Strecha, C., Beyeler, A., Zufferey, J. C., Floreano, D., Fua, P., & Gervaix, F. (2011). The accuracy of Automatic Photogrammetric Techniques on Ultra-Light Uav Imagery. *International Archives of the Photogrammetry Remote Sensing and Spatial Information Sciences*, *XXXVIII*(1/C22 UAV-g), 1–6. DOI: 10.5194/isprsarchives-XXXVIII-1-C22-125-2011.

Kurakula, V. K., & Kuffer, M. (2008). 3D Noise Modeling for Urban Environmental Planning and Management Vinay Kumar KURAKULA and Monika KUFFER. *Real Corp 008*, *2*, 517–523.

Lafarge, F., & Mallet, C. (2012). Creating large-scale city models from 3D-point clouds: A robust approach with hybrid representation. *International Journal of Computer Vision*, *99*(1), 69–85. DOI: 10.1007/s11263-012-0517-8.

Leberl, F., Irschara, A., Pock, T., Meixner, P., Gruber, M., Scholz, S., & Wiechert, A. (2010). Point Clouds : Lidar versus 3D Vision. *Photogrammetric Engineering Remote Sensing*, *76*(10), 1123–1134. Https://www.cis.rit.edu/ cnspci/references/dip/urban_extraction/leberl2010.pdf.

Ledoux, H., & Meijers, M. (2013). A star-based data structure to store efficiently 3D topography in a database. *Geo-spatial Information Science*, *16*(4), 256–266. DOI: http://dx.doi.org/10.1080/10095020.2013.866618.

Lemmens, M. (2011). *Geo-Information, Technologies, applications and the environment*. Springer Heidelberg Dordrecht London New York. DOI: 10.1007/978-94-007-1667-4.

Li-Chee-Ming, J., & Armenakis, C. (2014). Feasibility study of using the RoboEarth cloud engine for rapid mapping and tracking with small unmanned aerial systems. *ISPRS - International Archives of the Photogrammetry, Remote Sensing and Spatial Information Sciences*, *XL-1*(November), 219–226. DOI: 10.5194/isprsarchives-XL-1-219-2014.

Lindenberger, J. (1993). *Laser-Profilmessung zur topographischen Gelandeaufnahme.*. Ph.D. thesis, Deutsche Geodatische Kommission bei der Bayerischen Akademie der Wis- senschaften.

Lorenz, H., & Döllner, J. (2010). 3D feature surface properties and their application in geovisualization. *Computers Environment and Urban Systems*, *34*(6), 476–483. DOI: 10.1016/j.compenvurbsys.2010.04.003.

Madden, M., Jordan, T., Cotten, D., Hare, N., Pascua, A., & Bernardes, S. (2015). The future of Unmanned Aerial Systems (UAS) for monitoring natural and culture resources. In D. Fritsch (Ed.) *55rd Photogrammetry WeeK*, (pp. 369–384). Stuttgart: Heidelberg, Germany: Herbert Wichmann Verlag. ISBN: 9783879075874.

Maechler, M. (2015). Package 'cluster'. Retrieved July 23, 2014 from the World Wide Web: https://cran.r-project.org/web/packages/cluster/cluster.pdf.

Mallet, C., & Bretar, F. (2009). Full-waveform topographic lidar: State-of-the-art. *ISPRS Journal of Photogrammetry and Remote Sensing*, *64*(1), 1–16. DOI: 10.1016/j.isprsjprs.2008.09.007.

Manyoky, M., Theiler, P., Steudler, D., & Eisenbeiss, H. (2011). Unmanned Aerial Vehicle in Cadastral Applications. *International Archives of the Photogrammetry Remote Sensing and Spatial Information Sciences*, *XXXVIII*, 1–6. DOI: 10.5194/isprsarchives-XXXVIII-1-C22-57-2011.

Mather, P. (2004). *Computer Processing of Remotely-Sensed Images*. Wiley, 3rd ed. ISBN: 0470849185.

Matos, J., Silva, J., Silva, M., & Campos, V. (1994). Aplicação dos Sistemas de informação Geográfica na elaboração e controlo de execução dos planos municipais de ordenamento de território. In *URBITEC94*, (p. 22). Lisbon.

Mayr, W. (2013). Unmanned Aerial Systems – for the Rest of Us. In D. Fritsch (Ed.) *Photogrammetric Week '54*, (pp. 151–163). Herbert Verlag, Wichmann. ISBN: 9783879075317.

Meng, X., Currit, N., & Zhao, K. (2010). Ground Filtering Algorithms for Airborne LiDAR Data: A Review of Critical Issues. *Remote Sensing*, *2*(3), 833–860. DOI: 10.3390/rs2030833.

Meng, X., Wang, L., & Currit, N. (2008). Morphology-based Building Detection from Airborne Lidar Data. *Photogrammetric Engineering Remote Sensing*, *75*(4), 437–442. DOI: http://dx.doi.org/10.14358/PERS.75.4.437.

Micmac (2013). Micmac. Retrieved October 10, 2015 from the World Wide Web: http://logiciels.ign.fr/?Micmac.

Moser, J., Albrecht, F., & Kosar, B. (2010). Beyond Visualisation 3D Gis Analyses for Virtual City Models. *International Archives of Photogrammetry Remote Sensing and Spatial Information Sciences*, *XXXVIII*, 143–146. Http://www.isprs.org/proceedings/XXXVIII/4-W15/Paper_ISPRS/Poster/14_3DGeoInfo2010_147_Moser_3D_GIS_Analyses.pdf.

Neteler, M., & Mitasova, H. (2008). *Open Source GIS: A GRASS GIS Approach*. Springer, 3rd ed. ISBN: -13: 978-0-387-35767-6.

Neumann, K. J. (2008). Trends for digital aerial mapping cameras. *Archives*, *37*, 551 – 553. Http://www.isprs.org/proceedings/XXXVII/congress/1_pdf/93.pdf.

Ng, E., Yuan, C., Chen, L., Ren, C., & Fung, J. C. (2011). Improving the wind environment in high-density cities by understanding urban morphology and surface roughness: A study in Hong Kong. *Landscape and Urban Planning*, *101*(1), 59–74. DOI: 10.1016/j.landurbplan.2011.01.004.

Obe, R., & Hsu, L. S. (2011). *PostGIS In action*. Manning. ISBN: 9781935182269.

Park, J.-S., & Oh, S.-J. (2012). A New Concave Hull Algorithm and Concaveness Measure for n-dimensional Datasets. *Journal of Information Science and Engineering*, (28), 587–600.

Patrício, P. (2006). Câmara Aérea Digital Ortofotomapas. *Forum Geográfico, Revista Cientifica e Técnica do IGP*, (1), 39–48.

Peeters, A., & Etzion, Y. (2012). Automated recognition of urban objects for morphological urban analysis. *Computers, Environment and Urban Systems*, *36*(6), 573–582. DOI: 10.1016/j.compenvurbsys.2012.05.002.

Pereira, M. (2003). Os próximos desafios do planeamento municipal. *GeoInova*, *1*(7).

Pilouk, M. (1996). *Integrated modeling for 3D GIS*. Ph.D. thesis, ITC Enschede, Netherlands.

PIX4D (2013). Menu Process. Retrieved July 10, 2015 from the World Wide Web: https://support.pix4d.com/hc/en-us/articles/202557799-Menu-Process-Options-2-Point-Cloud-and-Mesh-General.

Qin, R. (2014). An Object-based Hierarchical Method for Change Detection Using Unmanned Aerial Vehicle Images. *Remote Sensing*, *6*, 21. DOI: 10.3390/rs60x000x.

Ranzinger, M., & Gunther, G. (1998). GIS Datasets for 3D Urban Planning. *Computers Environment and Urban Systems*, *21*(2), 159–173. DOI: 10.1016/S0198-9715-97-10005-9.

Rebelo, C., Gonçalves, J., & Tenedório, J. (2012). Análise de dados LiDAR para a extração de parâmetros urbanísticos. In *Actas do XIII Congresso Ibérico de Geografia, "Respuestas de la Geografia Ibérica a la crisis actual"*, (pp. 940–951). Santiago de Compostela.

Rebelo, C., Rodrigues, A. M., Neves, B., Tenedório, J., & Gonçalves, J. (2013a). Extraction of urban parameters from 3D Point- Cloud within GRASS. In *VII Jornadas de SIG Libre. SIGTE - Servei de Sistemes d'informci´o Geográfica i Teledetecció, Girona*.

Rebelo, C., Rodrigues, A. M., Neves, B., Tenedório, J., & Gonçalves, J. (2013b). Dasymetric Mapping using volumetric information from UAV low-cost flights. In *18th European Colloquium on Theoretical and Quantitative Geography (ECTQG), 5-9 September*. Dourdan, France. Retrieved from http://s4.csregistry.org/tiki-index.php?page=Program

Rebelo, C., Rodrigues, A. M., & Tenedório, J. A. (2013c). Utilização de Dados UAV para Desenvolvimento de uma Metodologia de Mapeamento Dasimétrico de Alta Precisão Resumo. In *Actas do IX Congresso da Geografia Portuguesa Geografia: Espaço, Natureza, Sociedade e Ciência.*, (pp. 99–106). 28-30 Novembro, Évora.

Rebelo, C., Rodrigues, A. M., & Tenedório, J. A. (2016). Dasymetric Mapping using 3D information: Sensitivity Analysis of UAV high resolution data. Manuscript sumbitted for publication.

Rebelo, C., Rodrigues, A. M., Tenedório, J. A., Goncalves, J., & Marnoto, J. (2015). Building 3D City Models: Testing and Comparing Laser Scanning and Low-Cost UAV Data Using FOSS Technologies. In B. Gervasi, O., Murgante, B., Misra, S., Gavrilova , M., Rocha, A.,Torre, C., Taniar, D. and Apduhan (Ed.) *Computational Science and Its Applications – ICCSA 2015*, (pp. 367–379). Banff, Canada: Springer. DOI: 10.1007/978-3-319-21470-2.

Rebelo, C., & Tenedório, J. A. (2011a). Exploratory Analysis of LiDAR Data in Urban Areas: The Case of Faro Island in Southern Portugal. In *Proceedings of the 7th International Conference on Virtual Cities and Territories*, (pp. 447–453). Lisbon.

Rebelo, C., & Tenedório, J. A. (2011b). Avaliação de dados LiDAR para modelação 3D e caracterizçãao dos topos dos edifícios. In *VIII Congresso da Geografia Portuguesa Repensar a Geografia para Novos Desafios*, 1, (pp. 447–453). Lisbon.

Redweik, P., Catita, C., & Brito, M. (2013). Solar energy potential on roofs and facades in an urban landscape. *Solar Energy*, *97*, 332–341. DOI: 10.1016/j.solener.2013.08.036.

Rodrigues, A. M., Neves, B., & Rebelo, C. (2013a). Terra Communis (tComm): A free data provider for historical census micro-data. In *Proceedings of the VII Jornadas de SIG Libre*. Girona: SIGTE - Servei de Sistemes d'informció Geográfica i Teledetecció. ISBN: 978-84-694-9927-6.

Rodrigues, A. M., Rebelo, C., & Tenedório, J. (2013b). Dasymetric mapping using volumetric information from UAV low-cost flights. . In *CTQG 2013 - European Colloquium of Theoretical and Quantitative Geography, Dourdan*, (pp. 197–198).

Rodrigues, A. M., Santos, T., Deus, R. F., & Pimentel, D. (2012). Land-Use Dynamics at the Micro Level: Constructing and Analyzing Historical Datasets for

the Portuguese Census Tracts *. In B. Murgante, G. Borruso, & A. Lapucci (Eds.) *Computational Science and Its Applications, ICCSA 2012*, (pp. 565–577). Salvador da Bahia: Springer-Verlag. DOI: 10.1007/978-3-642-31075-1_42.

Rodrigues, A. M., & Tenedório, J. (2015a). Comuns: An Open-Data Provider, Explorer and Analytic Toolbox Based on FOSS. In M. B. M.-S. G. M. R. A. T. C. T. D. Gervasi, O., & B. Apduhan (Eds.) *Computational Science and Its Applications – ICCSA 2015*, vol. 9157, chap. 26, (pp. 356–366). Banff, Canada: Springer International Publishing. DOI: 10.1007/978-3-319-21470-2_25.

Rodrigues, A. M., & Tenedório, J. A. (2015b). Generalized Dasymetric Mapping Algorithm for Accessing Land-Use Change. In B. Gervasi, O., Murgante, B., Misra, S., Gavrilova , M., Rocha, A.,Torre, C., Taniar, D. and Apduhan (Ed.) *Computational Science and Its Applications – ICCSA 2015*, chap. 26, (pp. 345–355). Banff, Canada: Springer. DOI: 10.1007/978-3-319-21470-2.

Rosnell, T., Honkavaara, E., & Nurminen, K. (2011). On Geometric Processing of Multi-Temporal Image Data Collected By Light Uav Systems. *International Archives of the Photogrammetry Remote Sensing and Spatial Information Sciences*, *XXXVIII*(1/C22 UAV-g), 1–6. DOI: 10.5194/isprsarchives-XXXVIII-1-C22-63-2011.

Roth, R. (2011). Leica ALS70 – Point Density Multiplication for High Density Surface Acquisition. In D. Fritsch (Ed.) *Photogrammetric Week '53,*, (pp. 249–255). Stuttgart: Herbert Wichmann Verlag, Heidelberg. ISBN: 3879075077, 9783879075072.

Sampath, A., & Shan, J. (2007). Building boundary tracing and regularization from airborne lidar point clouds. *Photogrammetric Engineering and Remote Sensing*, *73*(7), 805–812. DOI: http://dx.doi.org/10.14358/PERS.73.7.805.

Sanchez, R. A., & Brovelli, M. A. (2007). LiDAR data filtering with GRASS GIS for the determination of digital terrain models. In *I Jornadas de SIG Libre*, 1. Girona, Spain. Retrieved from http://www.sigte.udg.edu/jornadassiglibre2007/comun/2pdf/4.pdf.

Scott, D. (2007). *GIS for Web Developers, Adding Where to Your Web Applications*. ISBN: 9780974514093.

Sensefly (2015). Fixed Wing vs Rotary Wing. Retrieved October 25, 2015 from the World Wide Web: http://waypoint.sensefly.com/buy-fixed-wing-drone-or-rotary/.

Setan, D. S., Halim, & Medical (2006). 3D Geo-database Implementation using Craniofacial Geometric Morphometries Database System. In A. Abdul-Rahman, S. Zlatanova, & V. Coors (Eds.) *Innovations in 3D Geo Information Systems*, (pp. 279–294). Springer Berlin Heidelberg. ISBN: 9783540369974.

Silva, C. N. (2010). The E-Planning Paradigm-Theory, Methods and Tools: An Overview. In C. N. Silva (Ed.) *Handbook of Research on E-Planning : ICTs for Urban Development and Monitoring*, chap. 1, (p. 546). Hersey, New York: IGI Global, 1 ed. DOI: 10.4018/978-1-61520-929-3.ch001.

Sithole, G., & Vosselman, G. (2004). Experimental comparison of filter algorithms for bare-Earth extraction from airborne laser scanning point clouds. *ISPRS Journal of Photogrammetry and Remote Sensing*, *59*(1-2), 85–101. DOI: 10.1016/j.isprsjprs.2004.05.004.

Skaloud, J., Schaer, P., Stebler, Y., & Tomé, P. (2010). Real-time registration of airborne laser data with sub-decimeter accuracy. *ISPRS Journal of Photogrammetry and Remote Sensing*, *65*(2), 208–217. DOI: 10.1016/j.isprsjprs.2009.12.003.

Snavely, N. (2012). Bundler: Structure from Motion for unordered image colections. Retrieved Setembro 23, 2015 from the World Wide Web: http://photoctour.cs.washingthon.edu/bundler#S3.

Snavely, N., Seitz, S. M., & Szeliski, R. (2008). Modeling the World from Internet Photo Collections. *International journal of computer vision*, *80*(2), 189–210. DOI: 10.1007/s11263-007-0107-3.

Sohn, G., & Dowman, I. (2007). Data Fusion of High-Resolution Satellite Imagery and LiDar Data for Automatic Building Extraction. *ISPRS Journal of Photogrammetry and Remote Sensing*, *62*(1), 43–63. DOI: 10.1016/j.isprsjprs.2007.01.001.

Steiniger, S., & Hay, G. J. (2009). Free and open source geographic information tools for landscape ecology. *Ecological Informatics*, *4*(4), 183–195. ISBN: 10.1016/j.ecoinf.2009.07.004.

Strecha, C. (2011). The accuracy of automatic photogrammetric techniques on ultra-light UAV imagery. In D. Fritsch (Ed.) *53rd Photogrammetry WeeK*, (pp. 289–294). Stuttgart: Heidelberg, Germany: Herbert Wichmann Verlag. ISBN: 3879075077, 9783879075072.

Tenedório, J. A., Rebelo, C., Estanqueiro, R., Henriques, C. D., Marques, L., & Gonçalves, J. A. (2013). New Developments in Geographical Information Technology for Urban and Spatial Planning. In *Technologies for Urban and Spatial Planning: Virtual Cities and Territories*, chap. 10, (pp. 196–227). IGI Global. DOI: 10.4018/978-1-4666-4349-9.ch010.

Toth, C. (2009). The State-of-the-Art in Airborne Data Collection Systens focused on LiDAR and Optical Imagery. In D. Fritsch (Ed.) *Photogrammetric Week '52,*, (pp. 147–161). Stuttgart: Herbert Wichmann Verlag, Heidelberg. ISBN: 9783879074839 3879074836.

Turner, D., Lucieer, A., & Wallace, L. (2013). Direct Georeferencing of Ultrahigh-Resolution UAV Imagery. *IEEE Transactions on Geoscience and Remote Sensing*, (pp. 1–8). DOI: 10.1109/TGRS.2013.2265295.

Vallet, J., Panissod, F., Strecha, C., & Tracol, M. (2011). Photogrammetric Performance of an Ultra Light Weight Swinglet "UAV". *ISPRS - International Archives of the Photogrammetry, Remote Sensing and Spatial Information Sciences*, *XXXVIII-1/*, 253–258. DOI: 10.5194/isprsarchives-XXXVIII-1-C22-253-2011.

Vosselman, G. (1999). Building reconstruction using planar faces in very high density height data. In *IAPRS VOL.XXXII/3-2W5*, (pp. 87–92). Retrieved from https://www.itc.nl/personal/vosselman/papers/vosselman1999.munich.pdf.

Vosselman, G., Kessels, P., & Gorte, B. (2005). The utilisation of airborne laser scanning for mapping. *International Journal of Applied Earth Observation and Geoinformation*, *6*(3-4), 177–186. DOI: 10.1016/j.jag.2004.10.005.

Wang, G., Bosch, F. V. D., & Kuffer, M. (2008). Modelling urban traffic air pollution dispersion. *The International Archives of the Photogrammetry, Remote Sensing and Spatial Information Sciences.*, *Vol. XXXVI*(Part B8), 153–158.

Wefelscheid, C., & Ronny, H. (2011). Three-Dimensional Building Reconstruction Using Images Obtained By Unmanned Aerial Vehicles. *International*

Archives of the Photogrammetry Remote Sensing and Spatial Information Sciences, *XXXVIII*(1/C22), 1–6. DOI: 10.5194/isprsarchives-XXXVIII-1-C22-183-2011.

Wehr, A., & Lohr, U. (1999). Airborne laser scanning—an introduction and overview. *ISPRS Journal of Photogrammetry and Remote Sensing*, *54*(2-3), 68–82. DOI: 10.1016/S0924-2716(99)00011-8.

Welch, R., Madden, M., & Doren, R. F. (1999). Mapping the Everglades. *Photogrammetric Engineering and remote Sensing*, *65*(2). Retrieved from http://info.asprs.org/publications/pers/99journal/february/1999_feb_163-170.pdf.

Welzheim, W. M. (2015). UAVS for production. In D. Fritsch (Ed.) *55rd Photogrammetry WeeK*, (pp. 51–56). Stuttgart: Heidelberg, Germany: Herbert Wichmann Verlag. ISBN: 9783879075874.

Wenzel, K., Rothermel, M., Haala, N., & Fritsch, D. (2013). SURE - The ifp Software for Dense Image Matching. *Photogrammetric Week ' 54th*, (pp. 59–70). ISBN: 9783879075317.

Wu, C., & et al. (2011). Multicore Bundle Adjustement. *IEEE Transaction Computer Vision and Pattern Recognition*, *32*. DOI: 10.1109/CVPR.2011.5995552.

Yahia, M. W., & Johansson, E. (2014). Landscape interventions in improving thermal comfort in the hot dry city of Damascus, Syria—The example of residential spaces with detached buildings. *Landscape and Urban Planning*, *125*, 1–16. DOI: 10.1016/j.landurbplan.2014.01.014.

Yan, W. Y., Shaker, A., & El-Ashmawy, N. (2015). Urban land cover classification using airborne LiDAR data: A review. *Remote Sensing of Environment*, *158*(November), 295–310. DOI: 10.1016/j.rse.2014.11.001.

Yoshida, H., & Omae, M. (2005). An approach for analysis of urban morphology: methods to derive morphological properties of city blocks by using an urban landscape model and their interpretations. *Computers Environment and Urban Systems*, *29*(2), 223–247. DOI: 10.1016/j.compenvurbsys.2004.05.008.

Zahran, E.-s. M., Bennett, L. D., & Smith, M. J. (2010). An approach to represent air quality in 3D digital city models for air quality-related transport planning

in urban areas. In Tizani (Ed.) *Proceedings of the International Conference on Computing in Civil and Building Engineering*, 2. Nottingham University Press. ISBN: 978-1-907284-60-1.

Zeng, Q., Lai, J., Li, X., Mao, J., & Liu, X. (2008). Simple building reconstruction from LIDAR point cloud. (pp. 1040–1044). IEEE. DOI: 10.1109/ICALIP.2008.4590062.

Zhang, K. Z. K., Yan, J. Y. J., & Chen, S.-C. C. S.-C. (2006). Automatic Construction of Building Footprints From Airborne LIDAR Data. *IEEE Transactions on Geoscience and Remote Sensing*, *44*(9), 2523–2533. DOI: 10.1109/TGRS.2006.874137.

Zhao, C., Fu, G., Liu, X., & Fu, F. (2011). Urban planning indicators, morphology and climate indicators: A case study for a north-south transect of Beijing, China. *Building and Environment*, *46*(5), 1174–1183. DOI: 10.1016/j.buildenv.2010.12.009.

Zhou, G., Song, C., Simmers, J., & Cheng, P. (2004). Urban 3D GIS From LiDAR and digital aerial images. *Computers & Geosciences*, *30*(4), 345–353. DOI: 10.1016/j.cageo.2003.08.012.

Zlatanova, S. (2000). *3D GIS for Urban Development.*. Ph.D. thesis, TU GRAZ, ITC Dissertation.

Zlatanova, S., & Prosperi, D. (2006). *Large-Scale 3D data integration*. Taylor and Francis. ISBN: 978-0-8493-9898-8.

List of Figures

List of Tables

Appendix A

Excerpt of Decree-Law No. 80/2015, of 14th May

n.º 140/2014, de 16 de setembro, passam a ter a seguinte redação:

«Artigo 30.º

[...]

1 — . . . . . .

a) *(Revogada.)*
b) *(Revogada.)*
c) . . . . . .
d) . . . . . .

2 — Os diplomatas com as categorias de embaixador e ministro plenipotenciário passam à disponibilidade na data em que perfizerem o limite de idade normal para a aposentação ordinária, nos termos legais.

3 — O disposto no número anterior não se aplica ao embaixador nomeado para as funções de secretário-geral.

Artigo 50.º

[...]

O limite de idade dos funcionários diplomáticos para o exercício de funções nos serviços periféricos externos corresponde ao da idade normal para a aposentação ordinária, nos termos legais.»

Artigo 3.º

Norma revogatória

São revogadas as alíneas *a*) e *b*) do n.º 1 do artigo 30.º do Decreto-Lei n.º 40-A/98, de 27 de fevereiro, alterado pelos Decretos-Leis n.os 153/2005, de 2 de setembro, e 10/2008, de 17 de janeiro, pela Lei n.º 55-A/2010, de 31 de dezembro, e pelo Decreto-Lei n.º 140/2014, de 16 de setembro.

Artigo 4.º

Entrada em vigor

O presente diploma entra em vigor no dia seguinte ao da sua publicação.

Visto e aprovado em Conselho de Ministros de 2 de abril de 2015. — *Pedro Passos Coelho — Maria Luís Casanova Morgado Dias de Albuquerque — Rui Manuel Parente Chancerelle de Machete.*

Promulgado em 8 de maio de 2015.

Publique-se.

O Presidente da República, Aníbal Cavaco Silva.

Referendado em 11 de maio de 2015.

O Primeiro-Ministro, *Pedro Passos Coelho.*

MINISTÉRIO DO AMBIENTE, ORDENAMENTO DO TERRITÓRIO E ENERGIA

Decreto-Lei n.º 80/2015

de 14 de maio

Estabelecidas as bases gerais de política pública de solos, do ordenamento do território e do urbanismo pela Lei n.º 31/2014, de 30 de maio, o presente decreto-lei procede, no cumprimento do estabelecido no artigo 81.º da referida lei, à revisão do Regime Jurídico dos Instrumentos de Gestão Territorial.

A lei de bases de política pública de solos, do ordenamento do território e do urbanismo procedeu a uma reforma estruturante, tanto do ponto de vista dos conteúdos, no sentido de definir um conjunto de normas relativas à disciplina do uso do solo, como do ponto do vista do seu sistema jurídico, com objetivo de traduzir uma visão conjunta do sistema de planeamento e dos instrumentos de política de solos, entendidos como os instrumentos por excelência de execução dos planos territoriais.

Constitui objetivo daquela lei o enriquecimento do sistema de gestão territorial através da distinção regimentar entre programas e planos, com fundamento na diferenciação material entre, por um lado, as intervenções de natureza estratégica da administração central e, por outro lado, as intervenções da administração local, de caráter dispositivo e vinculativo dos particulares. Assim, os instrumentos da administração central passam a designar-se programas, no sentido de reforçar o seu caráter de meio de intervenção do Governo na tutela de interesses públicos de âmbito nacional e regional.

Não obstante, o plano diretor municipal mantém-se como um instrumento de definição da estratégia municipal ou intermunicipal, estabelecendo o quadro estratégico de desenvolvimento territorial ao nível local ou sub-regional. Por outro lado, os planos territoriais passam a ser os únicos instrumentos passíveis de determinar a classificação e qualificação do uso do solo, bem como a respetiva execução e programação.

Desta forma, devem ser integradas no plano diretor municipal ou intermunicipal e aí adaptadas as orientações de desenvolvimento territorial decorrentes dos programas de âmbito nacional, regional e sub-regional.

Pretende-se, com esta opção, introduzir uma regulamentação que permita salvaguardar os interesses dos particulares e a sua confiança no ordenamento jurídico vigente, na medida em que todas as normas relativas à ocupação, uso e transformação dos solos, para poderem ser impostas aos particulares, devem estar previstas no mesmo regulamento.

Por outro lado, privilegiando-se a concretização da avaliação das políticas de planeamento, prevê-se a obrigatoriedade de fixação de indicadores destinados a sustentar a avaliação e a monitorização dos programas e dos planos territoriais no respetivo conteúdo documental, de cujos resultados passam a depender diretamente os processos de alteração e revisão dos planos.

Com o mesmo objetivo, clarifica-se o âmbito das relações entre os diversos níveis de planeamento, estabelecendo-se um princípio de prevalência cronológica uniforme, com obrigatoriedade de atualização e adaptação dos instrumentos anteriores.

Reconhecendo-se que a falta de agilidade na tramitação administrativa é incompatível com a urgência de iniciativas, é importante agilizar procedimentos, concertar posições e reforçar a contratualização e participação dos particulares nos processos de planeamento.

Deste modo, o novo regime, procurando superar as situações de impasse em fase final do acompanhamento da elaboração do plano diretor municipal, comete às comissões de coordenação e desenvolvimento regional a elaboração de um único parecer final que vincula toda a administração central, o qual é acompanhado pela ata da comissão consultiva.

Prevê-se, ainda, a disponibilização de uma plataforma eletrónica para efeitos de acompanhamento dos procedimentos de elaboração, alteração ou revisão dos planos diretores municipais. Garante-se, assim, maior eficiência dos serviços da Administração, impondo procedimentos desmaterializados e do conhecimento automático de todos os intervenientes.

Sendo certo que a uniformização de procedimentos e de normas técnicas constitui um fator essencial de simplificação é criada a Comissão Nacional do Território, que articula e avalia a política nacional do ordenamento do território, propõe a aprovação de normas técnicas no âmbito do planeamento e emite pareceres e recomendações sobre todas as questões relativas ao ordenamento do território e à articulação com os instrumentos de ordenamento do espaço marítimo, por sua iniciativa ou a solicitação de outras entidades. Esta Comissão vem, ainda, suceder à Comissão Nacional de Reserva Ecológica Nacional, nas suas atribuições.

O novo regime jurídico dos instrumentos de gestão territorial garante uma efetiva articulação e compatibilização dos programas e dos planos territoriais com os planos de ordenamento do espaço marítimo nacional, de modo a salvaguardar a interação mar-terra.

O presente decreto-lei prevê, no desenvolvimento da Lei n.º 31/2014, de 30 de maio, a possibilidade das entidades intermunicipais, por vontade conjunta dos municípios constituintes destas, e de municípios vizinhos, se associarem para definirem, de modo coordenado, a estratégia de desenvolvimento e o modelo territorial, as opções de localização e de gestão de equipamentos públicos e infraestruturas, aprovando conjuntamente programas intermunicipais de ordenamento e desenvolvimento, planos diretores, planos de urbanização ou planos de pormenor.

Um modelo coerente de ordenamento do território deve assegurar a coesão territorial e a correta classificação do solo, invertendo-se a tendência, predominante nas últimas décadas, de transformação excessiva e arbitrária do solo rural em solo urbano. Com efeito, pretende-se contrariar a especulação urbanística, o crescimento excessivo dos perímetros urbanos e o aumento incontrolado dos preços do imobiliário, designadamente através da alteração do estatuto jurídico do solo.

Institui-se um novo sistema de classificação do solo, em solo urbano e solo rústico, que opta por uma lógica de efetiva e adequada afetação do solo urbano ao solo parcial ou totalmente urbanizado ou edificado, eliminando-se a categoria operativa de solo urbanizável. Em nome do princípio da sustentabilidade territorial, a reclassificação do solo como urbano é limitada ao indispensável, sustentável dos pontos de vista económico e financeiro, e traduz uma opção de planeamento necessária, devidamente programada, que deve ser objeto de contratualização. Assim, institui-se a obrigatoriedade da demonstração da sustentabilidade económica e financeira da transformação do solo rústico em urbano, através de indicadores demográficos e dos níveis de oferta e procura do solo urbano.

Por forma a assegurar a execução da operação urbanística, o plano deve definir um prazo para a execução da operação urbanística, findo o qual a classificação pode caducar, no caso de a mesma não ser realizada. A reclassificação do solo como urbano implica a fixação, por via contratual, dos encargos urbanísticos da operação e do respetivo prazo de execução e a redistribuição de benefícios e encargos, considerando todos os custos urbanísticos envolvidos na operação. Uma vez demonstrada a viabilidade económica na transformação do solo rústico em solo urbano, o direito de construir apenas se adquire com a aprovação da programação e com o cumprimento dos ónus urbanísticos fixados no contrato.

Em resumo, os programas e os planos territoriais integram orientações para a sua execução, nomeadamente no que respeita à identificação e à programação das intervenções consideradas estratégicas, com a estimativa dos custos individuais e dos respetivos prazos de execução, à ponderação da viabilidade jurídico-fundiária e da sustentabilidade económico-financeira das propostas, à definição dos meios e dos sujeitos responsáveis pelo financiamento e à estimativa da capacidade de investimento público.

Com a revisão dos instrumentos de gestão territorial a Administração ganha novos meios de intervenção pública no solo, destacando-se a reserva de solo, a venda e o arrendamento forçado de prédios urbanos, cujos proprietários não cumpram os ónus e os deveres a que estão obrigados por um plano territorial.

As políticas públicas devem ser direcionadas para a disponibilização de um ambiente sustentável e adequadamente infraestruturado, exigindo-se uma correta programação pública das intervenções a efetuar pelos municípios, assente em dois princípios fundamentais: o princípio da sustentabilidade financeira e o princípio da incorporação dos custos. Deste modo, os municípios devem elaborar um plano de sustentabilidade urbanística, que integra o programa plurianual de investimentos municipais na execução, na manutenção e no reforço das infraestruturas gerais e na previsão de custos gerais de gestão urbana.

Pretende-se, assim, iniciar um novo conceito e uma nova forma de gestão territorial, mais coerente, consequente e responsável, e dotando-a da racionalidade coletiva que o ordenamento do território lhe confere, enquadrando as dinâmicas económicas e sociais com efeitos espacializados.

Foram ouvidos os órgãos de governo próprio das Regiões Autónomas e a Associação Nacional de Municípios Portugueses.

Assim:

No desenvolvimento do regime jurídico estabelecido pela Lei n.º 31/2014, de 30 de maio, e nos termos das alíneas *a*) e *c*) do n.º 1 do artigo 198.º da Constituição, o Governo decreta o seguinte:

CAPÍTULO I

Disposições gerais

SECÇÃO I

Disposições gerais relativas ao planeamento territorial

Artigo 1.º

Objeto

O presente decreto-lei desenvolve as bases da política pública de solos, de ordenamento do território e de urbanismo, definindo o regime de coordenação dos âmbitos nacional, regional, intermunicipal e municipal do sistema de gestão territorial, o regime geral de uso do solo e o regime de elaboração, aprovação, execução e avaliação dos instrumentos de gestão territorial.

Artigo 2.º

Sistema de gestão territorial

1 — A política de ordenamento do território e de urbanismo assenta no sistema de gestão territorial, que se

3 — A câmara municipal pondera as reclamações, as observações, as sugestões e os pedidos de esclarecimento, apresentados pelos particulares, ficando obrigada a resposta fundamentada perante aqueles que invoquem, designadamente:

a) A desconformidade ou a incompatibilidade com programas e planos territoriais e com projetos que devem ser ponderados em fase de elaboração;
b) A desconformidade com disposições legais e regulamentares aplicáveis;
c) A lesão de direitos subjetivos.

4 — A resposta referida no número anterior é comunicada por escrito aos interessados, sem prejuízo do disposto no n.º 4 do artigo 10.º da Lei n.º 83/95, de 31 de agosto.
5 — Sempre que necessário ou conveniente, a câmara municipal promove o esclarecimento direto dos interessados, quer através dos seus próprios técnicos, quer através do recurso a técnicos da administração direta ou indireta do Estado e das regiões autónomas.
6 — Findo o período de discussão pública, a câmara municipal pondera e divulga os resultados, designadamente, através da comunicação social, da plataforma colaborativa de gestão territorial e do respetivo sítio na Internet, e elabora a versão final da proposta de plano para aprovação.
7 — São obrigatoriamente públicas, todas as reuniões da câmara municipal e da assembleia municipal que respeitem à elaboração ou aprovação de qualquer plano municipal.

Artigo 90.º

Aprovação

1 — Os planos municipais são aprovados pela assembleia municipal, mediante proposta apresentada pela câmara municipal.
2 — Quando o plano diretor municipal aprovado contiver disposições desconformes ou incompatíveis com programas setoriais, especiais ou regionais, o órgão responsável pela sua aprovação solicita a ratificação nos termos do artigo seguinte.

Artigo 91.º

Ratificação

1 — A ratificação de plano diretor municipal implica a revogação ou a alteração das disposições constantes do programa setorial, especial ou regional em causa e dos respetivos elementos documentais, de modo a que traduzam a atualização da disciplina vigente.
2 — A ratificação pelo Governo de plano diretor municipal é excecional e ocorre, por solicitação do órgão responsável pela respetiva elaboração, quando no âmbito do procedimento de elaboração e aprovação tiver sido suscitada, por si ou pelos serviços ou entidades com competências consultivas, a incompatibilidade referida no número anterior.
3 — Recebida a proposta de ratificação, o membro do Governo responsável pela área do ordenamento do território solicita, à comissão de coordenação e de desenvolvimento regional territorialmente competente e à entidade competente pela elaboração do programa territorial, parecer fundamentado, a emitir no prazo de 15 dias, que inclui a identificação das disposições inerentes a cada programa, a publicar no ato de aprovação referido no número seguinte.
4 — A ratificação do plano diretor municipal pode ser total ou parcial, devendo adotar a forma prevista para a aprovação do programa setorial, especial ou regional.

Artigo 92.º

Conclusão da elaboração e prazo de publicação

1 — A elaboração dos planos municipais considera-se concluída com a aprovação da respetiva proposta pela assembleia municipal, salvo quando careça de ratificação.
2 — Os procedimentos administrativos subsequentes à conclusão da elaboração dos planos municipais devem ser concretizados de modo a que, entre a respetiva aprovação e a publicação no *Diário da República,* medeiem os seguintes prazos máximos:

a) Plano diretor municipal — 60 dias;
b) Plano de urbanização — 30 dias;
c) Plano de pormenor — 30 dias.

3 — Os prazos fixados no número anterior suspendem-se nos casos previstos no n.º 2 do artigo anterior.

Artigo 93.º

Vigência

1 — Os planos municipais podem ter um prazo de vigência máximo previamente fixado, permanecendo, no entanto, eficazes até à entrada em vigor da respetiva revisão ou alteração.
2 — Os planos municipais devem ser obrigatoriamente revistos quando a respetiva monitorização e avaliação, consubstanciada nos relatórios de estado do ordenamento do território, identificarem níveis de execução e uma evolução das condições ambientais, económicas, sociais e culturais que lhes estão subjacentes, suscetível de determinar uma modificação do modelo territorial definido.

Artigo 94.º

Disponibilização da informação

1 — Os planos municipais são disponibilizados, com caráter de permanência e na versão atualizada, no sítio eletrónico do município a que respeitam, bem como no sítio eletrónico do Sistema Nacional de Informação Territorial (SNIT), através de ligação eletrónica a este sistema nacional.
2 — Para efeitos do número anterior, os municípios devem proceder à transcrição digital vetorial e georreferenciada das peças gráficas dos planos municipais, disponibilizando-as nos respetivos sítios eletrónicos, de acordo com modelo de dados a aprovar pela Direção-Geral do Território.
3 — As plantas e o respetivo acesso devem estar disponíveis em modelo a aprovar pela Direção-Geral do Território.

SUBDIVISÃO II

Plano diretor municipal

Artigo 95.º

Objeto

1 — O plano diretor municipal é o instrumento que estabelece a estratégia de desenvolvimento territorial municipal, a política municipal de solos, de ordenamento do território e de urbanismo, o modelo territorial municipal, as opções de localização e de gestão de equipamentos de

utilização coletiva e as relações de interdependência com os municípios vizinhos, integrando e articulando as orientações estabelecidas pelos programas de âmbito nacional, regional e intermunicipal.

2 — O plano diretor municipal é um instrumento de referência para a elaboração dos demais planos municipais, bem como para o desenvolvimento das intervenções setoriais da administração do Estado no território do município, em concretização do princípio da coordenação das respetivas estratégias de ordenamento territorial.

3 — O modelo territorial municipal tem por base a classificação e a qualificação do solo.

4 — O plano diretor municipal é de elaboração obrigatória, salvo nos casos em que os municípios optem pela elaboração de plano diretor intermunicipal.

Artigo 96.º

Conteúdo material

1 — O plano diretor municipal define o quadro estratégico de desenvolvimento territorial do município e o correspondente modelo de organização territorial, estabelecendo nomeadamente:

a) A caracterização, ou a sua atualização, económica, social e biofísica, incluindo a identificação dos valores culturais, do sistema urbano e das redes de transportes e de equipamentos, de educação, de saúde e de segurança, bem como os sistemas de telecomunicações, de abastecimento de energia, de gás, de captação, de tratamento e abastecimento de água, de drenagem e tratamento de efluentes e de recolha, depósito e tratamento de resíduos;

b) Os objetivos de desenvolvimento económico local e as medidas de intervenção municipal no mercado de solos;

c) Os critérios de sustentabilidade a adotar, bem como os meios disponíveis e as ações propostas, que sejam necessários à proteção dos valores e dos recursos naturais, recursos hídricos, culturais, agrícolas e florestais, e a identificação da estrutura ecológica municipal;

d) A referenciação espacial dos usos e das atividades, nomeadamente através da definição das classes e das categorias de espaços;

e) A definição de estratégias e dos critérios de localização, de distribuição e de desenvolvimento das atividades industriais, turísticas, comerciais e de serviços;

f) A identificação e a qualificação do solo rústico, garantindo a adequada execução dos programas e das políticas de desenvolvimento agrícola e florestal, bem como de recursos geológicos e energéticos;

g) A identificação e a delimitação das áreas urbanas, com a definição do sistema urbano municipal e os correspondentes programas na área habitacional, bem como as condições de promoção da regeneração e da reabilitação urbanas e as condições de reconversão das áreas urbanas de génese ilegal;

h) A identificação das áreas de interesse público para efeitos de expropriação, bem como a definição das respetivas regras de gestão;

i) Os critérios para a definição das áreas de cedência e a definição das respetivas regras de gestão, assim como a cedência média para efeitos de perequação;

j) Os critérios de compensação e de redistribuição de benefícios e encargos decorrentes da gestão urbanística, a concretizar nos planos previstos para as unidades operativas de planeamento e gestão;

k) A especificação qualitativa e quantitativa dos índices, dos indicadores e dos parâmetros de referência, urbanísticos ou de ordenamento, a estabelecer em plano de urbanização e em plano de pormenor, bem como os de natureza supletiva aplicáveis na ausência destes;

l) A programação da execução das opções de ordenamento estabelecidas e a definição de unidades operativas de planeamento e gestão do plano, identificando, para cada uma destas, os respetivos objetivos e os termos de referência para a necessária elaboração de planos de urbanização e de pormenor;

m) A identificação de condicionantes de caráter permanente, designadamente reservas e zonas de proteção, bem como as necessárias à concretização dos planos de emergência de proteção civil de âmbito municipal;

n) A identificação e a delimitação das áreas com vista à salvaguarda de informação arqueológica contida no solo e no subsolo;

o) As condições de atuação sobre áreas de reabilitação urbana, situações de emergência ou de exceção, bem como sobre áreas degradadas em geral;

p) A articulação do modelo de organização municipal do território com a disciplina consagrada nos demais planos municipais aplicáveis;

q) A proteção e a salvaguarda de recursos e de valores naturais que condicionem a ocupação, uso e transformação do solo;

r) O prazo de vigência, o sistema de monitorização e as condições de revisão.

2 — Não obstante a existência dos índices, parâmetros e indicadores de natureza supletiva a que alude a alínea *k*) do número anterior, são diretamente aplicáveis às operações urbanísticas a realizar em zona urbana consolidada, como tal identificada no plano, os índices, os parâmetros e os indicadores de referência, para elaboração de plano de urbanização ou de plano de pormenor, nas seguintes condições:

a) Tenha decorrido o prazo de cinco anos sobre a data da entrada em vigor do plano diretor municipal, sem que haja sido aprovado o plano de urbanização ou o plano de pormenor;

b) Os índices e os parâmetros de referência estabelecidos no plano diretor municipal definam os usos e a altura total das edificações ou a altura das fachadas, bem como os indicadores relativos à definição da rede viária e do estacionamento.

Artigo 97.º

Conteúdo documental

1 — O plano diretor municipal é constituído por:

a) Regulamento;

b) Planta de ordenamento, que representa o modelo de organização espacial do território municipal, de acordo com os sistemas estruturantes e a classificação e qualificação dos solos, as unidades operativas de planeamento e gestão definidas e, ainda, a delimitação das zonas de proteção e de salvaguarda dos recursos e valores naturais;

c) Planta de condicionantes que identifica as servidões administrativas e as restrições de utilidade pública em vigor que possam constituir limitações ou impedimentos a qualquer forma específica de aproveitamento.

2 — O plano diretor municipal é acompanhado por:

a) Relatório, que explicita a estratégia e modelo de desenvolvimento local, nomeadamente os objetivos es-

tratégicos e as opções de base territorial adotadas para o modelo de organização espacial, bem como a respetiva fundamentação técnica, suportada na avaliação das condições ambientais, económicas, sociais e culturais para a sua execução;

b) Relatório ambiental, no qual se identificam, descrevem e avaliam os eventuais efeitos significativos no ambiente resultantes da aplicação do plano e as alternativas razoáveis, tendo em conta os objetivos e o âmbito de aplicação territorial respetivos;

c) Programa de execução, contendo, designadamente, as disposições sobre a execução das intervenções prioritárias do Estado e do município, previstas a curto e médio prazo, e o enquadramento das intervenções do Estado e as intervenções municipais previstas a longo prazo;

d) Plano de financiamento e fundamentação da sustentabilidade económica e financeira.

3 — O plano diretor municipal é, ainda, acompanhado pelos seguintes elementos complementares:

a) Planta de enquadramento regional, elaborada a escala inferior à do plano diretor municipal, com indicação dos centros urbanos mais importantes, principais vias de comunicação, infraestruturas relevantes e grandes equipamentos que sirvam o município e indicação dos demais programas e planos territoriais em vigor para a área do município;

b) Planta da situação existente com a ocupação do solo à data da deliberação que determina a elaboração do plano;

c) Planta e relatório com a indicação dos alvarás de licença e dos títulos de comunicação prévia de operações urbanísticas emitidos, bem como das informações prévias favoráveis em vigor ou declaração comprovativa da inexistência dos referidos compromissos urbanísticos na área do plano;

d) Mapa de ruído;

e) Participações recebidas em sede de discussão pública e respetivo relatório de ponderação;

f) Ficha dos dados estatísticos em modelo a disponibilizar pela Direção-Geral do Território.

4 — O plano diretor municipal inclui indicadores qualitativos e quantitativos que suportem a avaliação prevista no capítulo VIII.

SUBDIVISÃO III

Plano de urbanização

Artigo 98.º

Objeto

1 — O plano de urbanização desenvolve e concretiza o plano diretor municipal e estrutura a ocupação do solo e o seu aproveitamento, fornecendo o quadro de referência para a aplicação das políticas urbanas e definindo a localização das infraestruturas e dos equipamentos coletivos principais.

2 — O plano de urbanização pode abranger:

a) Qualquer área do território do município incluída em perímetro urbano por plano diretor municipal eficaz e, ainda, os solos rústicos complementares de um ou mais perímetros urbanos, que se revelem necessários para estabelecer uma intervenção integrada de planeamento;

b) Outras áreas do território municipal que possam ser destinadas a usos e a funções urbanas, designadamente à localização de instalações ou parques industriais, logísticos ou de serviços ou à localização de empreendimentos turísticos e equipamentos e infraestruturas associados.

3 — Nas sedes de concelho e nas áreas urbanas com mais de 25.000 mil habitantes, o regime do uso do solo deve ser previsto, preferencialmente, em plano de urbanização municipal.

Artigo 99.º

Conteúdo material

O plano de urbanização adota o conteúdo material apropriado às condições da área territorial a que respeita, aos objetivos das políticas urbanas e às transformações previstas nos termos de referência e na deliberação municipal que determinou a sua elaboração, dispondo nomeadamente, sobre:

a) A definição e a caracterização da área de intervenção, identificando e delimitando os valores culturais e naturais a proteger e a informação arqueológica contida no solo e subsolo;

b) A conceção geral da organização urbana, a partir da qualificação do solo, definindo a rede viária estruturante, a localização de equipamentos de uso e interesse coletivo, a estrutura ecológica, bem como o sistema urbano de circulação, de transporte público e privado e de estacionamento;

c) A definição do zonamento para localização das diversas funções urbanas, designadamente habitacionais, comerciais, turísticas, de serviços, industriais e de gestão de resíduos, bem como a identificação das áreas a recuperar, a regenerar ou a reconverter;

d) A adequação do perímetro urbano definido no plano diretor municipal ou no plano diretor intermunicipal, em função do zonamento e da conceção geral da organização urbana definidos, incluindo, nomeadamente, o traçado e o dimensionamento das redes de infraestruturas gerais que estruturam o território, fixando os respetivos espaços-canal, os critérios de localização e de inserção urbanística e o dimensionamento dos equipamentos de utilização coletiva;

e) As condições de aplicação dos instrumentos da política de solos e de política urbana previstos na lei, em particular os que respeitam à reabilitação e regeneração urbanas de áreas urbanas degradadas;

f) Os indicadores e os parâmetros urbanísticos aplicáveis a cada uma das categorias e subcategorias de espaços;

g) A delimitação e os objetivos das unidades ou subunidades operativas de planeamento e gestão, a estruturação das ações de compensação e redistribuição de benefícios e encargos e a identificação dos sistemas de execução do plano.

Artigo 100.º

Conteúdo documental

1 — O plano de urbanização é constituído por:

a) Regulamento;

b) Planta de zonamento, que representa a estrutura territorial e o regime de uso do solo da área a que respeita;

c) Planta de condicionantes, que identifica as servidões administrativas e as restrições de utilidade pública em vigor que possam constituir limitações ou impedimentos a qualquer forma específica de aproveitamento.

2 — O plano de urbanização é acompanhado por:

a) Relatório, que explicita os objetivos estratégicos do plano e a respetiva fundamentação técnica, suportada na avaliação das condições ambientais, económicas, sociais e culturais para a sua execução;

b) Relatório ambiental, no qual se identificam, descrevem e avaliam os eventuais efeitos significativos no ambiente que possam decorrer da aplicação do plano e as alternativas razoáveis, tendo em conta os objetivos e o âmbito de aplicação territorial respetivos;

c) Programa de execução, contendo, designadamente, disposições indicativas sobre a execução das intervenções municipais previstas;

d) Modelo de redistribuição de benefícios e encargos;

e) Plano de financiamento e fundamentação da sua sustentabilidade económica e financeira.

3 — O plano de urbanização é, ainda, acompanhado pelos seguintes elementos complementares:

a) Planta de enquadramento, elaborada a escala inferior à do plano de urbanização, com indicação das principais vias de comunicação, outras infraestruturas relevantes e grandes equipamentos, bem como outros elementos considerados pertinentes;

b) Planta da situação existente, com a ocupação do solo à data da deliberação que determina a elaboração do plano;

c) Planta e relatório, com a indicação dos alvarás de licença e dos títulos de comunicação prévia de operações urbanísticas emitidos, bem como das informações prévias favoráveis em vigor ou declaração comprovativa da inexistência dos referidos compromissos urbanísticos na área do plano;

d) Plantas de identificação do traçado de infraestruturas viárias, de abastecimento de água, de saneamento, de energia elétrica, de recolha de resíduos de gás e de condutas destinadas à instalação de infraestruturas de telecomunicações e demais infraestruturas relevantes existentes e previstas na área do plano;

e) Mapa de ruído, nos termos do n.º 1 do artigo 7.º do Regulamento Geral do Ruído;

f) Participações recebidas em sede de discussão pública e respetivo relatório de ponderação;

g) Ficha dos dados estatísticos, em modelo a disponibilizar pela Direção-Geral do Território.

4 — O conteúdo documental do plano de urbanização é adaptado ao seu conteúdo material.

5 — O plano de urbanização inclui indicadores qualitativos e quantitativos que suportem a avaliação prevista no capítulo VIII.

SUBDIVISÃO IV

Plano de pormenor

Artigo 101.º

Objeto

1 — O plano de pormenor desenvolve e concretiza em detalhe as propostas de ocupação de qualquer área do território municipal, estabelecendo regras sobre a implantação das infraestruturas e o desenho dos espaços de utilização coletiva, a implantação, a volumetria e as regras para a edificação e a disciplina da sua integração na paisagem, a localização e a inserção urbanística dos equipamentos de utilização coletiva e a organização espacial das demais atividades de interesse geral.

2 — O plano de pormenor abrange áreas contínuas do território municipal, que podem corresponder a uma unidade ou subunidade operativa de planeamento e gestão ou a parte delas.

Artigo 102.º

Conteúdo material

1 — O plano de pormenor adota o conteúdo material apropriado às condições da área territorial a que respeita, aos objetivos e aos fundamentos técnicos previstos nos termos de referência e na deliberação municipal que determinou a sua elaboração, estabelecendo, nomeadamente:

a) A definição e a caracterização da área de intervenção, identificando e delimitando os valores culturais e a informação arqueológica contida no solo e no subsolo, os valores paisagísticos e naturais a proteger, bem como todas as infraestruturas relevantes para o seu desenvolvimento;

b) As operações de transformação fundiária preconizadas e a definição das regras relativas às obras de urbanização;

c) O desenho urbano, exprimindo a definição dos espaços públicos, incluindo os espaços de circulação viária e pedonal e de estacionamento, bem como o respetivo tratamento, a localização de equipamentos e zonas verdes, os alinhamentos, as implantações, a modelação do terreno e a distribuição volumétrica;

d) A distribuição de funções, conjugações de utilizações de áreas de construção e a definição de parâmetros urbanísticos, designadamente, densidade máxima de fogos, número de pisos e altura total das edificações ou altura das fachadas;

e) As operações de demolição, conservação e reabilitação das construções existentes;

f) As regras para a ocupação e para a gestão dos espaços públicos;

g) A implantação das redes de infraestruturas, com delimitação objetiva das áreas que lhe são afetas;

h) Regulamentação da edificação, incluindo os critérios de inserção urbanística e o dimensionamento dos equipamentos de utilização coletiva, bem como a respetiva localização no caso dos equipamentos públicos;

i) A identificação dos sistemas de execução do plano, do respetivo prazo e da programação dos investimentos públicos associados, bem como a sua articulação com os investimentos privados;

j) A estruturação das ações de compensação e de redistribuição de benefícios e encargos.

2 — O plano de pormenor relativo a área não abrangida por plano de urbanização, incluindo as intervenções em solo rústico, procede à prévia explicitação do zonamento, dos fundamentos e dos efeitos da alteração do zonamento, com base na disciplina consagrada no plano diretor municipal ou plano diretor intermunicipal.

Artigo 103.º

Modalidades específicas

1 — O plano de pormenor pode adotar modalidades específicas com conteúdo material adaptado a finalidades particulares de intervenção.

2 — São modalidades específicas de plano de pormenor:

a) O plano de intervenção no espaço rústico;
b) O plano de pormenor de reabilitação urbana;
c) O plano de pormenor de salvaguarda.

Artigo 104.º

Plano de intervenção no espaço rústico

1 — O plano de intervenção no espaço rústico abrange o solo rústico e estabelece as regras relativas a:

a) Construção de novas edificações e a reconstrução, alteração, ampliação ou demolição das edificações existentes, quando tal se revele necessário ao exercício das atividades autorizadas no solo rústico;
b) Implantação de novas infraestruturas de circulação de veículos, de animais e de pessoas, e de novos equipamentos, públicos ou privados, de utilização coletiva, e a remodelação, ampliação ou alteração dos existentes;
c) Criação ou beneficiação de espaços de utilização coletiva, públicos ou privados, e respetivos acessos e áreas de estacionamento;
d) Criação de condições para a prestação de serviços complementares das atividades autorizadas no solo rústico;
e) Operações de proteção, valorização e requalificação da paisagem natural e cultural.

2 — O plano de intervenção no espaço rústico não pode promover a reclassificação do solo rústico em urbano.

Artigo 105.º

Plano de pormenor de reabilitação urbana

1 — O plano de pormenor de reabilitação urbana abrange solo urbano correspondente à totalidade ou a parte de:

a) Centro histórico delimitado em plano diretor ou plano de urbanização eficaz;
b) Área de reabilitação urbana constituída nos termos da lei.

2 — O conteúdo e as finalidades do plano de pormenor de reabilitação urbana são definidos no regime jurídico da reabilitação urbana.

Artigo 106.º

Plano de pormenor de salvaguarda

O conteúdo e as finalidades do plano de pormenor de salvaguarda são definidos nos termos previstos na lei de bases do património cultural e demais legislação complementar.

Artigo 107.º

Conteúdo documental

1 — O plano de pormenor é constituído por:

a) Regulamento;
b) Planta de implantação, que estabelece, designadamente, o desenho urbano e as parcelas, os alinhamentos e o polígono base para a implantação de edificações, a altura total das edificações ou a altura das fachadas, o número de pisos, o número máximo de fogos, a área de construção e respetivos usos, a demolição e manutenção ou reabilitação das edificações existentes e a natureza e localização dos equipamentos, dos espaços verdes e de outros espaços de utilização coletiva;
c) Planta de condicionantes, que identifica as servidões administrativas e as restrições de utilidade pública em vigor, que possam constituir limitações ou impedimentos a qualquer forma específica de aproveitamento.

2 — O plano de pormenor é acompanhado por:

a) Relatório, contendo a fundamentação técnica das soluções propostas no plano, suportada na identificação e caracterização objetiva dos recursos territoriais da sua área de intervenção e na avaliação das condições ambientais, económicas, sociais, e culturais para a sua execução;
b) Relatório ambiental, sempre que seja necessário proceder à avaliação ambiental, no qual se identificam, descrevem e avaliam os eventuais efeitos significativos no ambiente resultantes da aplicação do plano e as alternativas razoáveis, tendo em conta os objetivos e o âmbito de aplicação territorial respetivos;
c) Peças escritas e desenhadas que suportem as operações de transformação fundiária previstas, nomeadamente para efeitos de registo predial e de elaboração ou conservação do cadastro geométrico da propriedade rústica ou do cadastro predial;
d) Programa de execução das ações previstas;
e) Modelo de redistribuição de benefícios e encargos;
f) Plano de financiamento e fundamentação da sustentabilidade económica e financeira.

3 — Para efeitos de registo predial e, quando aplicável, para a execução ou conservação do cadastro geométrico da propriedade rústica ou do cadastro predial, as peças escritas e desenhadas previstas na alínea *c*) do número anterior consistem em:

a) Planta cadastral ou ficha cadastral original, quando existente;
b) Quadro com a identificação dos prédios, natureza, descrição predial, inscrição matricial, áreas e confrontações;
c) Planta da operação de transformação fundiária, com a identificação dos novos prédios e dos bens de domínio público;
d) Quadro com a identificação dos novos prédios ou fichas individuais, com a indicação da respetiva área, da área destinada à implantação dos edifícios e das construções anexas, da área de construção, da volumetria, da altura total da edificação ou da altura da fachada e do número de pisos acima e abaixo da cota de soleira para cada um dos edifícios, do número máximo de fogos e da utilização de edifícios e fogos;
e) Planta com as áreas de cedência para o domínio municipal;
f) Quadro com a descrição das parcelas a ceder, sua finalidade e área de implantação, bem como das áreas de construção e implantação dos equipamentos de utilização coletiva;
g) Quadro de transformação fundiária, explicitando a relação entre os prédios originários e os prédios resultantes da operação de transformação fundiária.

4 — O plano de pormenor é, ainda, acompanhado pelos seguintes elementos complementares:

a) Planta de localização, contendo o enquadramento do plano no território municipal envolvente, com indicação

das principais vias de comunicação e demais infraestruturas relevantes, da estrutura ecológica e dos grandes equipamentos, existentes e previstos na área do plano e demais elementos considerados relevantes;

b) Planta da situação existente, com a ocupação do solo e a topografia à data da deliberação que determina a elaboração do plano;

c) Planta ou relatório, com a indicação dos alvarás de licença e dos títulos de comunicação prévia de operações urbanísticas emitidos, bem como das informações prévias favoráveis em vigor ou declaração comprovativa da inexistência dos referidos compromissos urbanísticos na área do plano;

d) Plantas contendo os elementos técnicos definidores da modelação do terreno, cotas mestras, volumetrias, perfis longitudinais e transversais dos arruamentos e traçados das infraestruturas;

e) Relatório sobre recolha de dados acústicos ou mapa de ruído, nos termos do n.º 2 do artigo 7.º do Regulamento Geral do Ruído;

f) Participações recebidas em sede de discussão pública e respetivo relatório de ponderação;

g) Ficha dos dados estatísticos, em modelo a disponibilizar pela Direção-Geral do Território.

5 — O conteúdo documental do plano de pormenor é adaptado, de forma fundamentada, ao seu conteúdo material.

6 — Nas modalidades específicas de plano de pormenor previstas no n.º 2 do artigo 103.º, o conteúdo documental do plano é ajustado, de forma fundamentada, devendo ser garantida a correta fundamentação técnica e caracterização urbanística, face à especificidade do conteúdo de cada plano.

7 — O plano de pormenor inclui indicadores qualitativos e quantitativos que suportem a avaliação prevista no capítulo VIII.

Artigo 108.º

Efeitos registais

1 — A certidão do plano de pormenor que contenha as menções constantes das alíneas *a*) a *d*), *g*) a *i*) do n.º 1 do artigo 102.º, e que seja acompanhada das peças escritas e desenhadas enunciadas no n.º 3 do artigo anterior, constitui título bastante para a individualização no registo predial dos prédios resultantes das operações de transformação fundiária previstas no plano.

2 — O registo previsto no número anterior incide apenas sobre as inscrições prediais em que o requerente surja como titular.

3 — Nas situações de reestruturação da compropriedade ou de reparcelamento, o registo referido no n.º 1 depende da apresentação, respetivamente, do acordo de reestruturação da compropriedade ou do contrato previsto no n.º 2 do artigo 165.º

4 — O acordo e os contratos referidos no número anterior são oponíveis ao proprietário ou ao comproprietário que tenha inscrito o seu direito após a data da respetiva celebração.

5 — É dispensada a menção do sujeito passivo nas aquisições por reestruturação da compropriedade ou por reparcelamento.

6 — As parcelas de terreno cedidas ao município integram-se no domínio municipal no ato de individualização no registo predial dos lotes respetivos e estão sujeitas a cadastro predial.

7 — Nas situações previstas no presente artigo não é aplicável o disposto no n.º 1 do artigo 49.º do regime jurídico da urbanização e da edificação.

Artigo 109.º

Taxas e obras de urbanização

1 — Sempre que outra solução não resulte do plano de pormenor, a emissão da certidão referida no n.º 1 do artigo anterior depende do prévio pagamento:

a) Da taxa pela realização, manutenção e reforço de infraestruturas, sem prejuízo do disposto no artigo no n.º 3 do artigo 175.º;

b) Das compensações em numerário devidas nos termos do n.º 4 do artigo 44.º do regime jurídico da urbanização e da edificação.

2 — A certidão do plano de pormenor identifica a forma e o montante da caução de boa execução das obras de urbanização referentes às parcelas a individualizar, nos termos do artigo anterior.

3 — Na falta de indicação e fixação de caução nos termos do número anterior, a caução é prestada por primeira hipoteca legal sobre as parcelas a individualizar, calculada de acordo com a respetiva comparticipação nos custos de urbanização.

4 — Cada prédio responde apenas pela parte do montante da garantia que lhe cabe nos termos da parte final do número anterior, sendo lícito ao seu titular requerer a substituição da hipoteca legal por outro meio de caução admissível, valendo a deliberação camarária de aceitação, como título bastante para cancelamento da inscrição da hipoteca legal.

DIVISÃO III

Planos intermunicipais

Artigo 110.º

Regime geral

1 — Os planos intermunicipais são instrumentos de natureza regulamentar que prosseguem os objetivos previstos no artigo 75.º relativamente ao território de dois ou mais municípios vizinhos.

2 — Aos planos intermunicipais aplicam-se as disposições relativas aos planos municipais correspondentes com as necessárias adaptações, sem prejuízo do disposto nos artigos seguintes.

3 — Nas áreas metropolitanas, quando promovido por todos os municípios que as integram, o plano diretor intermunicipal tem a designação de plano metropolitano de ordenamento do território.

Artigo 111.º

Elaboração

1 — A elaboração dos planos intermunicipais compete a uma comissão constituída para o efeito, cuja composição é definida conjuntamente pelas câmaras municipais dos municípios associados para a elaboração do plano, sem prejuízo do número seguinte.

2 — Quando promovido por todos os municípios que integram uma entidade intermunicipal, a elaboração do plano intermunicipal compete à comissão executiva me-

Appendix B

Planning of the topographic survey – Praia de Faro

Surveying Area

The topograhic survey in Praia de Faro was made on 19th March 2012.

Below, we can see an excerpt of the topographic planning for the building ED6 and the draft before the surveying. In the plan, the location of roof points that should be surveyed was made in orthophotos.

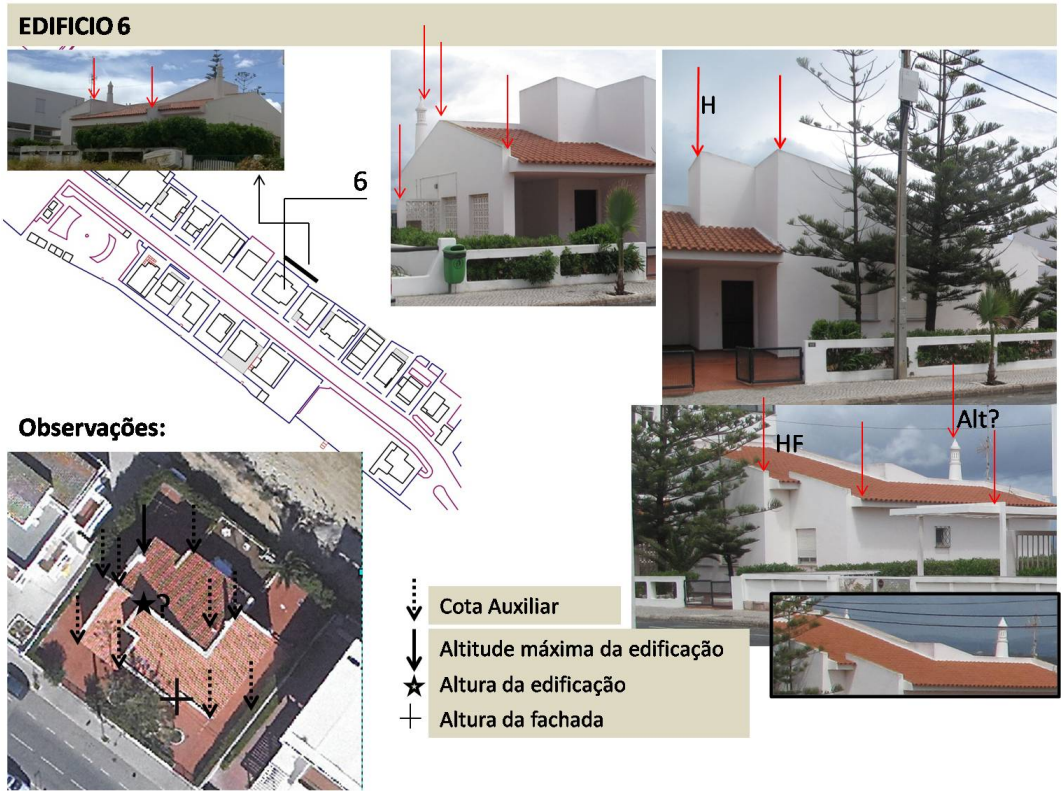

Notes of next draft:

- Maximum of Building Height (Altitude maxima da edificaçao);
- Building Height (Altura da edificaçao)
- Building Façade Height (Altura da fachada)

19 de Março 2012

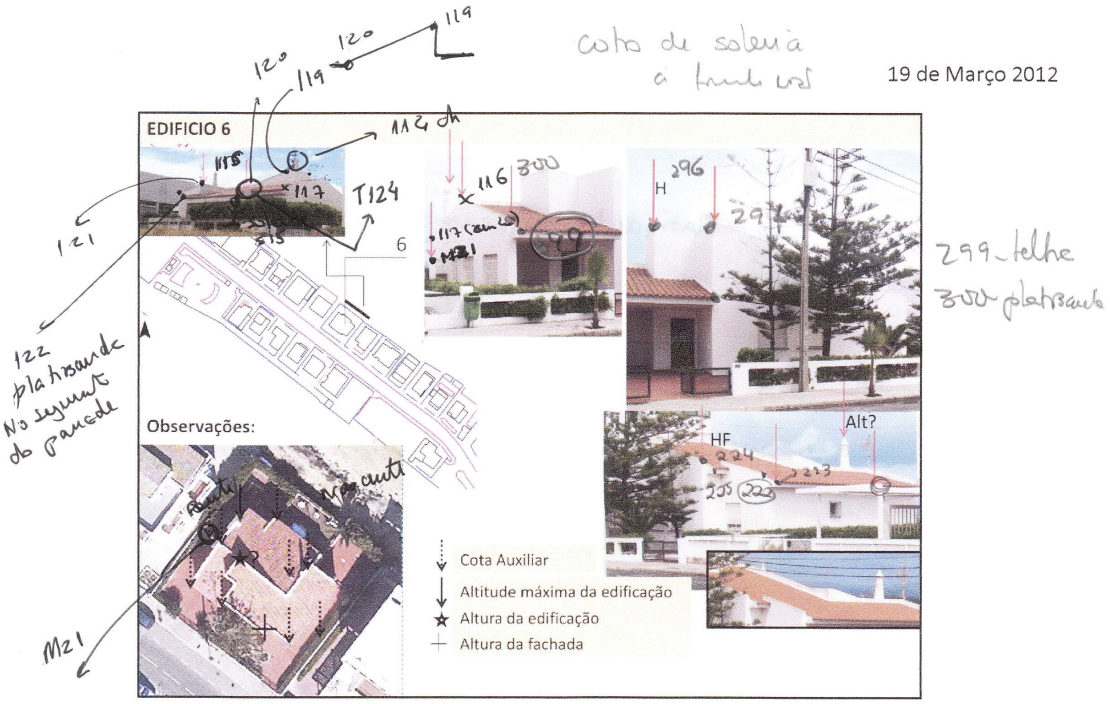

Cota de soleira a confirmar

299 - telha
300 - platibanda

122 platibanda No seguimento da parede

M21

PTEst.

E11

Dois pontos laterais da moradia não estão no ortofoto ("telheiros").

T119 - chaminé

T115 - chaminé (ponta a ferro) → 2009 ou se já estiver

T116 - cumeeira

T117 - ~~beiral~~ beirado (platibanda)

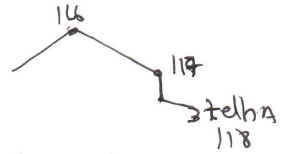

ALÇADO FRENTE

T118 - Beirado telha

T119 - ponto mais alto é a ~~altitude~~ altura da edif.

T120 - fim da pendente

T121 - Ponta parede

T122 - platibanda

T123 - telha ponta

S15 - soleira

M21 - Muro junto à casa ~~lado~~ frente

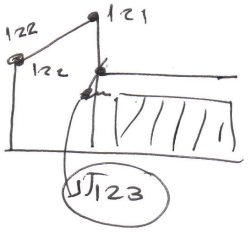

15

Appendix C

Report: UAV imagery processing – Praia de Faro

Quality Report

See *Quality Report Help* for detailed explanations. Generated with version 2.2.6 (build 2.2.20)

Summary

Project:	faropraia_20140116_5cm_compfs
Camera name:	CanonPowerShotELPH300HS_4.3_3000x4000
Average Ground Sampling Distance (GSD):	4.94 cm
Area covered:	0.07 sq. km / 6.73 ha / 0.03 sq. mi.
Image coordinate system:	WGS84
Ground Control Point (GCP) coordinate system:	Datum 73 / Modified Portuguese Grid
Output coordinate system:	Datum 73 / Modified Portuguese Grid
Processing type:	full (scale 1)
Time for Initial Processing (without report):	04m:18s:

Quality Check

Images:	median of 19430 keypoints per image	✓
Dataset:	46 out of 47 images calibrated (97%)	✓
Camera optimization quality:	1.36% relative difference between initial and final focal length	✓
Matching quality:	median of 2818 matches per calibrated image	✓
Georeferencing:	6 GCPs, 0.084 [m]	✓

Preview

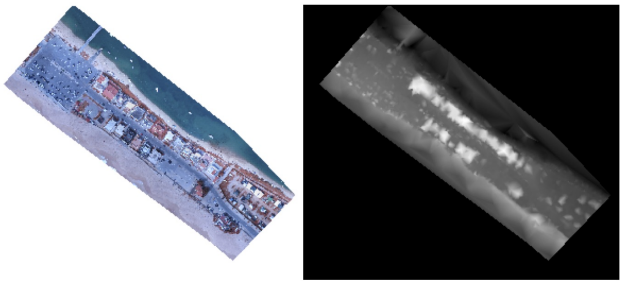

Figure 1: Ortho mosaic and the corresponding sparse digital surface model (DSM) before densification.

Calibration details

Number of calibrated images:	46 out of 47
Number of geotagged images:	47 out of 47

Geotag position

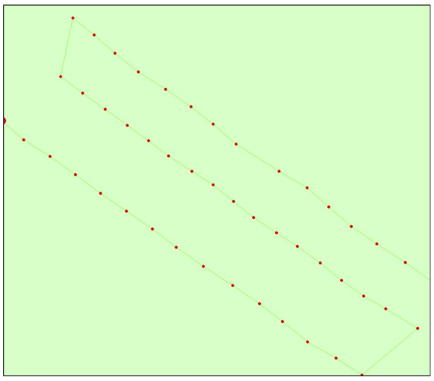

Figure 2: Top view of the geotags. The green line follows the geotag in time starting from the large red dot.

Optimized camera position

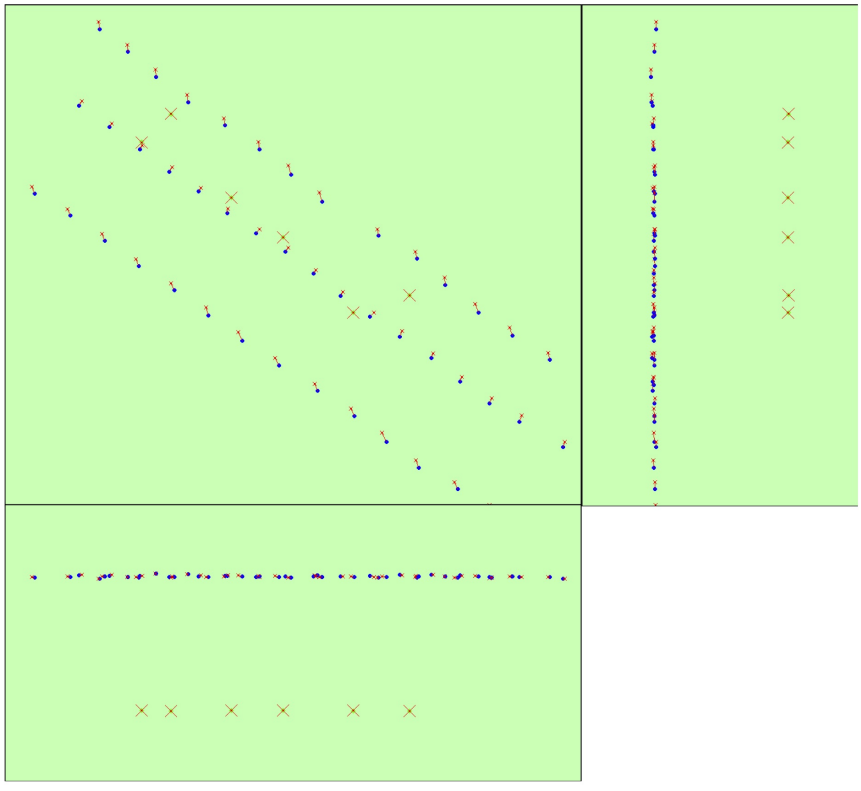

Figure 3: Offset between image geotags (small red crosses) and optimized positions (small blue dots) as well as the offset between the GCPs (large red crosses) and their optimized positions (large green dots) in the top-view (XY plane), front-view (XZ plane) and side-view (YZ plane).

Geotag variance

Geotag localisation variance	sigma [m]
Longitude direction (x)	2.34238
Latitude direction (y)	1.58717
Altitude direction (z)	0.416886

Table 1: Relative camera localisation accuracy of the geotags. Please note that this does not correspond to the accuracy on the ground.

Overlap

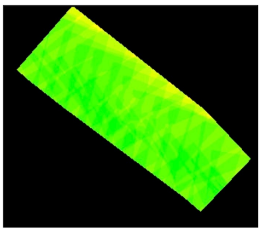

Number of overlapping images: 1 2 3 4 5+

**Figure 4: Overlapping score computed for each pixel of the orthomosaic.
Red indicates areas where the overlap between the images is too low and could lead to poor results. For good quality results, the overlap should be over 5 images (green) for every pixel of the mosaic.**

Bundle Block Adjustment details

number total keypoint observations for bundle block adjustment	115657
number total 3D points for bundle block adjustment	39798
mean reprojection error	0.133062 [pixels]

Internal Camera Parameters CanonPowerShotELPH300HS_4.3_3000x4000 sensor dimension: 6.2 4.65 [mm]

	Focal length	Principal point X	Principal point Y	RD 1	RD 2	RD 3	TD 1	TD 2
initial values	2839.640 [pix] 4.400 [mm]	2019.760 [pix] 3.068 [mm]	1547.000 [pix] 2.251 [mm]	-0.043	0.026	-0.006	0.001	0.002
optimized values	2800.803 [pix] 4.340 [mm]	2004.630 [pix] 3.092 [mm]	1513.463 [pix] 2.303 [mm]	-0.043	0.029	-0.012	0.001	0.001

2D Keypoints Table

	Number of 2D keypoints per image	Number of matched 2D keypoints per image
Median	19430.000	2818.000
Min	8798.000	262.000
Max	25750.000	5932.000
Mean	17889.543	2514.283

3D points from 2D keypoints matches

	Number of 3D points observed
In 2 images	22479
In 3 images	8715
In 4 images	3701
In 5 images	1965
In 6 images	1392
In 7 images	964
In 8 images	434
In 9 images	129
In 10 images	17
In 11 images	2

2D Keypoints Graph

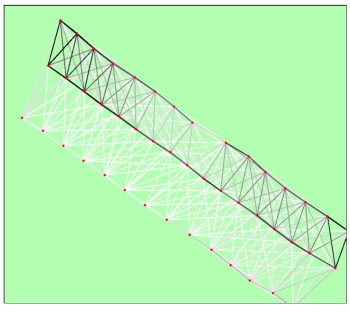

Number of matches

25 222 444 666 888 1111 1333 1555 1777 2000

Figure 5: Top view of the geotags with a link between matching images. The darkness of the links indicates the number of matched 2D keypoints between the images. Bright links indicate low confidence and would require more overlap between the images or better quality images.

Most visible 2D keypoints

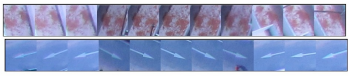

Figure 6: Cropped area of 2 3D points arising from 11 2D keypoints. Each cropped area should represent the same object on the ground.

Geo-location and Ground Control Points

GCP name	tolerance [m]	error X [m]	error Y [m]	error Z [m]	projection error [pixel]	verified/ measured
3D GCP: PARQ5	0.020	0.112	0.244	0.140	0.963	7 / 7
3D GCP: PARQ8	0.020	0.211	0.174	0.110	0.547	7 / 7
3D GCP: ED18_3	0.020	0.010	0.032	0.077	0.704	6 / 6
3D GCP: PARQ2_3	0.020	0.021	0.008	0.054	0.645	7 / 7
3D GCP: ED13_4	0.020	0.027	0.083	0.056	0.773	7 / 7
3D GCP: ED1_10	0.020	0.094	0.020	0.048	0.962	7 / 7
Mean		0.079	0.093	0.081		
Sigma		0.070	0.087	0.034		

Localisation accuracy of the individual GCP, their mean error distance and the mean errors in the three coordinate directions.The last column counts the number of images where the GCP has been measured (clicked on the images) and on how many of them have been automatically verified.
0 out of 6 GCPs have been labeled as inaccurate (see Figure below).

Ground control points

GCP name: PARQ5 (12305.765,-295247.057,3.214)

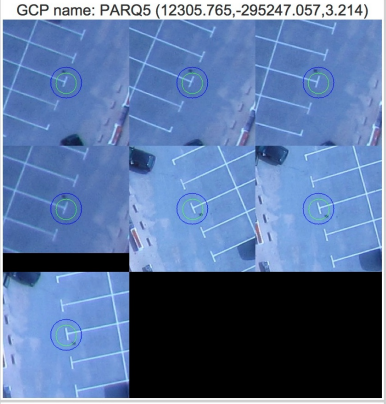

IMG_0948.JPG
IMG_0949.JPG
IMG_0950.JPG
IMG_0951.JPG
IMG_0955.JPG
IMG_0956.JPG
IMG_0957.JPG

GCP PARQ5 was not measured in the following images. If the circle is too far away from the real GCP position, this indicates that the GCP should be also measured (clicked) in this image to improve the accuracy.

IMG_0947.JPG
IMG_0954.JPG

GCP name: PARQ8 (12277.075,-295275.115,4.197)

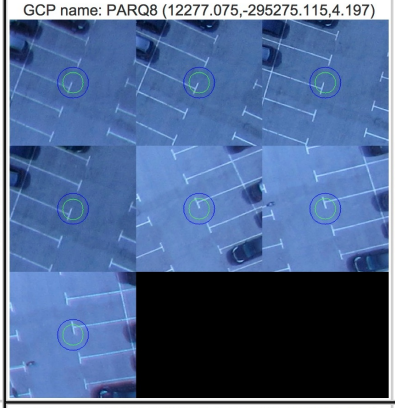

IMG_0948.JPG
IMG_0949.JPG
IMG_0950.JPG
IMG_0951.JPG
IMG_0955.JPG
IMG_0956.JPG
IMG_0957.JPG

GCP name: ED18_3 (12541.277,-295426.263,3.640)

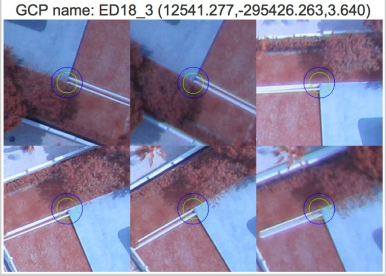

IMG_0941.JPG
IMG_0942.JPG
IMG_0961.JPG
IMG_0962.JPG
IMG_0963.JPG
IMG_0964.JPG

GCP ED18_3 was not measured in the following images. If the circle is too far away from the real GCP position, this indicates that the GCP should be also measured (clicked) in this image to improve the accuracy.

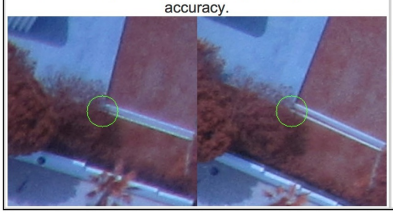

IMG_0939.JPG
IMG_0940.JPG

Figure 7: Images in which GCPs have been measured (blue circle) and in which the 3D point have been projected (green circle). A green circle outside of the blue one indicates either an accuracy issue or a GCP issue.

Appendix D

PostgreSQL/PostGIS Algorithm (*building_top_base.sql*): selection of roof eave and ground points of each building (Praia de Faro)

Listing D.1: *building_top_base.sql* for the extraction of top and ground building 3D points

```
Objective: Code developed for extract
top and ground base points of each building
Author: Carla Rebelo, 2014

-- First Part: Extraction of building rooftop points that
--represents eave roof from clustering Point-Cloud
-- Input: Boundary of buildings - out concavehull
-- Point-cloud clustered -LiDAR."k10s100LIDAR"
-- Output: Building rooftop 3D points

UPDATE LiDAR."outconcavehull_LiDARk10s100"
SET the_geom = ST_SetSRID(the_geom, 27493);

drop TABLE if exists A;
create table A AS
select st_union(st_buffer(the_geom,-1)) as the_geom
from LiDAR."outconcavehull_LiDARk10s100";

alter table A
add column gid serial primary key;

CREATE INDEX A_idx
  ON A
  USING gist
  (the_geom);
  ALTER TABLE A CLUSTER ON A_idx;
-------------------------
drop TABLE if exists B;
create table B AS
select st_union(st_buffer(the_geom,-0.5)) as the_geom
from LiDAR."outconcavehull_LiDARk10s100";

alter table B
add column gid serial primary key;

CREATE INDEX B_idx
  ON B
  USING gist
  (the_geom);
  ALTER TABLE B CLUSTER ON B_idx;
```

```
-------------------------------------------------------------
-- Intersection of buffers obtained above. Produce a buffer
-- of 0.5m at a distance of 0.5m of boundary.
-------------------------------------------------------------
drop TABLE if exists C;
CREATE Table C AS
select ST_Difference(B.the_geom, A.the_geom)
as the_geom
from A, B;

alter table C
add column gid serial primary key;

CREATE INDEX C_idx
  ON C
  USING gist
  (the_geom);
ALTER TABLE C  CLUSTER ON C_idx;

-------------------------------------------------------------
--update reference system of C
-------------------------------------------------------------
UPDATE C SET the_geom = ST_SetSRID(the_geom, 27493);
-------------------------------------------------------------
--Intersection of buffer 0.5m and point-cloud clustered
-------------------------------------------------------------
select * from LiDAR."k10s100LIDAR"; /* deve conter x, y, z */
-------------------------------------------------
drop TABLE if exists toppoints;
create table toppoints as
SELECT
    LiDAR."k10s100LIDAR".gid as idnuvem,
    LiDAR."k10s100LIDAR".the_geom, C.gid as idpol
    from  LiDAR."k10s100LIDAR", C
WHERE
     LiDAR."k10s100LIDAR".the_geom && C.the_geom
     /* Uses GiST index with the polygon's bounding box */
AND
    ST_Contains(C.the_geom,  LiDAR."k10s100LIDAR".the_geom);
     /* Uses exact matching */

select * from toppoints;
```

```
--output: building rooftop points (with x,y,z)

drop TABLE if exists LiDAR.topo_lidark10s100;
create table LiDAR.topo_lidark10s100 as
select toppoints.idnuvem, LiDAR."k10s100LIDAR".*
from toppoints, LiDAR."k10s100LIDAR"
where toppoints.idnuvem = LiDAR."k10s100LIDAR".gid;

alter table LiDAR.topo_lidark10s100
add column gid1 serial primary key;

CREATE INDEX topo_lidark10s100_idx
  ON LiDAR.topo_lidark10s100
  USING gist
  (the_geom);
ALTER TABLE LiDAR.topo_lidark10s100
CLUSTER ON topo_lidark10s100_idx;



-------------------------------------------------------------
-- Second Part: Extraction of building ground points that
-- represents base of building from Point-Cloud
-- Input:  Boundary of buildings - out concavehull
--         Original Point-cloud
--         Buffer of 11m along the public street
-- Output: Building base - 3D points
-------------------------------------------------------------

--Create Buffers
-------------------------------------
--Buffer 2m from building rooftop
-------------------------------------
drop TABLE if exists D CASCADE;
create table D AS
select st_union(st_buffer(the_geom,2)) as the_geom
from LiDAR."outconcavehull_LiDARk10s100";

alter table D
add column gid serial primary key;

CREATE INDEX D_idx
  ON D
  USING gist
```

```
  (the_geom);
ALTER TABLE D CLUSTER ON D_idx;
-------------------------------------
--Buffer 0.5m from building rooftop
-------------------------------------
drop TABLE if exists E CASCADE;
create table E AS
select st_union(st_buffer(the_geom,0.5)) as the_geom
from LiDAR."outconcavehull_LiDARk10s100";

alter table E
add column gid serial primary key;

CREATE INDEX E_idx
  ON E
  USING gist
  (the_geom);
ALTER TABLE E CLUSTER ON E_idx;
-----------------------------------------------------
--Buffer 1.5m obtained from the difference between D and E
-----------------------------------------------------
drop TABLE if exists F;
CREATE Table F AS
select ST_Difference(D.the_geom,E.the_geom)
as the_geom
from D, E;

alter table F
add column gid serial primary key;

CREATE INDEX F_idx
  ON F
  USING gist
  (the_geom);
ALTER TABLE F  CLUSTER ON F_idx;

-----------------------------------------
--Multipolygon F to single polygon
-----------------------------------------
drop TABLE if exists G;
create table G  as
select (st_dump(the_geom)).geom as the_geom
from  F;
```

```
alter table G
add column gid serial primary key;

CREATE INDEX G_idx
  ON G
  USING gist
  (the_geom);
ALTER TABLE G CLUSTER ON G_idx;

alter table G
add column area double precision;

update G
set area = st_area(the_geom);

------------------------------------------------------------
--update reference system of G
------------------------------------------------------------
UPDATE G SET the_geom = ST_SetSRID(the_geom, 27493);

------------------------------------------------------------------
---Buffer around public street
------------------------------------------------------------------
drop TABLE if exists LiDAR.H;
CREATE Table LiDAR.H AS
select st_union(st_buffer(the_geom,11)) as the_geom
from "Cartografia".estrada;

alter table LiDAR.H
add column gid serial primary key;

CREATE INDEX H_idx
  ON LiDAR.H
  USING gist
  (the_geom);
ALTER TABLE LiDAR.H CLUSTER ON H_idx;
UPDATE LiDAR.H
SET the_geom = ST_SetSRID(the_geom, 27493);
------------------------------------------------------------
---I: area around buildings intersection between H and G
drop TABLE if exists LiDAR.I;
```

```
CREATE Table LiDAR.I AS
select ST_intersection(G.the_geom,LiDAR.H.the_geom)
as the_geom
from G,LiDAR.H;

alter table LiDAR.I
add column gid serial primary key;

CREATE INDEX I_idx
  ON LiDAR.I
  USING gist
  (the_geom);
ALTER TABLE LiDAR.I CLUSTER ON I_idx;

------------------------------------------------------------------
--Intersection of buffer I and point-cloud
------------------------------------------------------------------
UPDATE lidar.lidar_8485sel2m
SET the_geom = ST_SetSRID(the_geom, 27493);

drop TABLE if exists tmp4;

create table tmp4 as
SELECT
      lidar_8485sel2m.gid as idnuvem, I.gid as idpol
      from lidar.lidar_8485sel2m, LiDAR.I
WHERE
      lidar_8485sel2m.the_geom  && I.the_geom
      /* Uses GiST index with the polygon's bounding box */
AND
     ST_Contains(I.the_geom,lidar_8485sel2m.the_geom);
      /* Uses exact matching */

---output:Ground 3D points

drop TABLE if exists
LiDAR.pavimento_k10s100;
create table LiDAR.pavimento_k10s100 as
select tmp4.idnuvem, lidar_8485sel2m.*
from tmp4, lidar.lidar_8485sel2m
where tmp4.idnuvem = lidar.lidar_8485sel2m.gid;

alter table LiDAR.pavimento_k10s100
```

```
add constraint ih9 primary key(idnuvem);

CREATE INDEX LiDAR.pavimento_k10s100_idx
  ON LiDAR.pavimento_k10s100
  USING gist
  (the_geom);
ALTER TABLE LiDAR.pavimento_k10s100
CLUSTER ON LiDAR.pavimento_k10s100_idx;
-------------------------------------------------------------
--Create a table csv to filtering the output
select * from  LiDAR.pavimento_k10s100;
-------------------------------------------------------------
copy LiDAR.pavimento_k10s100
from '/home/xxx.csv'
with delimiter ',' csv header;
```

Appendix E

R Algorithm: filtering of selected ground points

Listing E.1: Filtering Ground Points (Step 2 - Figure 2.33 of Subsection 2.3.1 of Chapter 2)

```
-----------------------------------------------
Carla Rebelo, February 2013
objectivo: Filter the ground points for the
removal of residual points ("wrong points: which
not are ground points ")
-----------------------------------------------

-----------------------------------------------
1. Input: Ground Points (format csv) in R
-----------------------------------------------
setwd("/home/.../Desktop")
data1 <- read.table("ground_k10Lidar.csv",
          header=TRUE, sep=",",encoding="latin1")
names(data1)

-----------------------------------------------
2. Analyse: Empirical density curve of ground
points
-----------------------------------------------
d<-plot(density(data1$z), main="Elevation Z UAV:
base of buildings")

-----------------------------------------------
3. How many spikes there are in curve?
ked=spikes number +1
-----------------------------------------------
library(cluster)
cz<- cbind(data1$x,data1$y,data1$z)

k=ked
claraclusCp <- clara(data1$z,k,samples=10)

-----------------------------------------------
4.Create the plot of k-clusters defined by k
-----------------------------------------------
plot(cz, col = claraclusCp$cluster, cex=0.2,
       xlab="coordinate X(m)",
       ylab="coordinate Y (m)")
legend("bottomleft", legend = paste("cluster", 1:k),
```

```
      pch=1, col=1:k, cex=0.7)

-------------------------------------------------
5. Preparation of data to analyze the standard
deviation of each cluster; Create table
with clusters chosen
-------------------------------------------------
library(sqldf)
library(tcltk)

x <- data.frame(cz, claraclusCp$cluster)
colnames(x) <- c("x","y","z","cluster")
sqlclus <- head(x)

-------------------------------------------------
6. Selection of each cluster
Ak's, k=1,2,...n by this line code
sqlclusAk <- sqldf("select * from x where cluster=k",
           row.names=TRUE)
-------------------------------------------------
sqlclusA1 <- sqldf("select * from x where cluster=1",
           row.names=TRUE)
sqlclusAn <- sqldf("select * from x where cluster=n",
           row.names=TRUE

-------------------------------------------------
7. Analyze the standard deviation of each cluster
sdk, k=1,2,...n
-------------------------------------------------
sd1 <-sd(sqlclusA1$z)
sdn <-sd(sqlclusAn$z)

-------------------------------------------------
8. If value is higher than value 1 remove the
cluster of ground points; create the output
-------------------------------------------------
sqlcluster <- rbind(sqlclusA1, sqlclusA2)
sqlcluster1 <-rbind(sqlcluster, sqlclusAn)
write.csv(sqlcluster1, file="filt_ground_k10_lidar.csv"
          ,row.names=FALSE)
```

Appendix F

Total building volumes estimated in Praia de Faro

The next table shows the total volume errors obtained for every sample (LiDAR, UAVk2 and UAVk10) considering all the buildings of Praia Faro (in section 2.3.2, of Chapter 2).

Table shows the relative total volume (Tvol) errors of all estimated building volumes using accurate building area (reference) and building heights estimated from point cloud.

BV	**Point Cloud**	**Tvol Reference** m^3	**Tvol Estimated** m^3	**Tvol Error** m^3	**Relative Tvol error %**
BHave*BAref	UAVk2	23953	23099	854	3.6
	UAVk10	22426	21218	1208	5.4
	LiDAR	23953	21729	2224	9.3
BHmed*BAref	UAVk2	24453	24035	418	1.7
	UAVk10	22926	23319	-394	-1.7
	LiDAR	24453	22027	2426	9.9

The next table shows the total volume errors obtained for every sample (LiDAR, UAVk2 and UAVk10), but only considering the buildings which have an acceptable area (in section 2.3.2, of Chapter 2).

Table shows the relative total volume (Tvol) errors of estimated building volumes (accepted) using area and height buildings estimated from point cloud.

BV	**Point Cloud**	**Tvol Reference** m^3	**Tvol Estimated** m^3	**Tvol Error** m^3	**Relative Tvol error %**
BHave*BA	UAVk2	12685	12235	451	3.6
	UAVk10	13442	14065	-623	-4.6
	LiDAR	18666	18140	526	2.8
BHmed*BA	UAVk2	12422	13341	-919	-7.4
	UAVk10	13223	15595	-2372	-17.9
	LiDAR	19488	18607	881	4.5

Appendix G

Excerpt of RCM No. 103/2005, of 27th May

PRESIDÊNCIA DO CONSELHO DE MINISTROS

Resolução do Conselho de Ministros n.º 103/2005

O troço de costa compreendido entre Vilamoura e Vila Real de Santo António, numa extensão total de cerca de 75 km, apresenta notável diversidade paisagística e ambiental, alternando zonas de mar e sapal com extensos areais, zonas densamente humanizadas com troços de paisagem que mantém praticamente inalteradas as suas características naturais. A diversidade dos valores naturais tem vindo a ser preservada, tanto quanto possível, através da delimitação concelhia dos espaços afectos à Reserva Ecológica Nacional, bem como por meio dos regimes contidos nos instrumentos de gestão territorial, o Plano Regional de Ordenamento do Território do Algarve, o Plano de Ordenamento do Parque Natural da Ria Formosa e os diversos planos municipais de ordenamento do território.

Aliás, a existência neste troço da costa de uma extensa área territorial sujeita a um especial estatuto de protecção e gestão indicia, desde logo, a presença de valores muito significativos do património natural, o que, por si só, justificaria o reforço dos níveis de protecção. Neste caso, atendendo às reconhecidas pressões de utilização urbanística desta estreita faixa litoral, razões acrescidas concorrem para que se aperfeiçoem as medidas de salvaguarda, gestão, recuperação e valorização dos recursos e valores naturais constantes dos instrumentos de planeamento em vigor.

Por outro lado, neste troço da orla costeira assume especial significado a necessidade de prever, desde já, um conjunto de intervenções que assegurem o retardamento do processo de erosão costeira, responsável por situações preocupantes de construções e núcleos edificados em situação de risco, quer em zonas sensíveis do sistema costeiro, quer nas designadas ilhas barreira, quer no espaço lagunar. Por isso, caracterizados os processos costeiros relevantes, foram definidas áreas de salvaguarda da evolução natural da linha da costa, designadas por faixas de protecção.

Aos mencionados objectivos de compatibilização da ocupação urbana e turística com os valores naturais, culturais e paisagísticos e de salvaguarda do factor risco que ameaça a linha da costa acresce a necessidade de correcção de disfunções territoriais graves, não só as já citadas ocupações urbanísticas em zonas sensíveis como também em zonas degradadas no domínio público hídrico ou em zonas adjacentes directamente relacionadas com a fruição pública da orla costeira. Por esta razão justifica-se proceder ao reordenamento balnear, articulando a procura com as restrições e potencialidades biofísicas, sem prejuízo da necessária requalificação deste troço da costa sob a vertente económica do turismo e da actividade piscatória.

Conclui-se, assim, com a aprovação do Plano de Ordenamento da Orla Costeira (POOC) Vilamoura-Vila Real de Santo António o ciclo do planeamento do Litoral de Portugal continental.

A elaboração do Plano decorreu ao abrigo do disposto no Decreto-Lei n.º 309/93, de 2 de Setembro, e no artigo 2.º do Decreto-Lei n.º 151/95, de 24 de Junho. Porém, a aprovação do presente POOC é efectuada ao abrigo do Decreto-Lei n.º 380/99, de 22 de Setembro, na redacção que lhe foi conferida pelo Decreto-Lei n.º 310/2003, de 10 de Dezembro, que estabeleceu o novo regime jurídico dos instrumentos de gestão territorial.

Atento o parecer final da comissão técnica de acompanhamento da elaboração do Plano, na qual se encontraram representados os municípios de Loulé, Faro, Olhão, Tavira, Vila Real de Santo António e Castro Marim, bem como os competentes serviços da administração central directa e indirecta que asseguram a prossecução de interesses públicos sectoriais com relevância na área de intervenção do Plano;

Atento o teor do parecer da ex-Direcção Regional do Ambiente e do Ordenamento do Território do Algarve no que se refere à articulação do Plano com os objectivos, princípios e regras definidos pelos demais instrumentos de gestão territorial aplicáveis na respectiva área de intervenção;

Ponderados os resultados da discussão pública que decorreu entre 15 de Novembro e 31 de Dezembro de 2002:

Assim:

Ao abrigo do disposto no artigo 49.º do Decreto-Lei n.º 380/99, de 22 de Setembro, na redacção que lhe foi conferida pelo Decreto-Lei n.º 310/2003, de 10 de Dezembro, e nos termos da alínea *g*) do artigo 199.º da Constituição, o Conselho de Ministros resolve:

1 — Aprovar o Plano de Ordenamento da Orla Costeira (POOC) Vilamoura-Vila Real de Santo António, cujo Regulamento e respectivas plantas de síntese e de condicionantes são publicados em anexo à presente resolução, dela fazendo parte integrante.

2 — Nas situações em que os planos municipais de ordenamento do território não se conformem com as disposições do POOC devem os mesmos ser objecto de alteração sujeita a regime procedimental simplificado, nos termos do artigo 97.º do Decreto-Lei n.º 380/99, de 22 de Setembro, e no prazo constante do n.º 3 do mesmo artigo.

3 — Na área de intervenção do presente Plano são alterados os artigos 2.º, 3.º, 4.º, 5.º, 7.º, 8.º, 9.º, 10.º, 12.º, 13.º, 14.º, 17.º, 18.º, 23.º, 24.º, 27.º, 28.º, 29.º e 30.º do Regulamento do Plano de Ordenamento do Parque Natural da Ria Formosa, aprovado pelo Decreto Regulamentar n.º 2/91, de 24 de Janeiro.

4 — Na área de intervenção do presente Plano são revogados os artigos 6.º, 15.º e 16.º do Regulamento do Plano de Ordenamento do Parque Natural da Ria Formosa, aprovado pelo Decreto Regulamentar n.º 2/91, de 24 de Janeiro.

5 — As áreas de jurisdição portuária deverão ser definidas de acordo com a portaria prevista no n.º 3 do artigo 6.º do Decreto-Lei n.º 257/2002, de 22 de Novembro.

6 — Os originais das plantas referidas no n.º 1, bem como os elementos a que se refere o n.º 2 do artigo 3.º do Regulamento do POOC, encontram-se disponíveis para consulta no Instituto da Conservação da Natureza e na Comissão de Coordenação e Desenvolvimento Regional do Algarve.

Presidência do Conselho de Ministros, 5 de Junho de 2005. — O Primeiro-Ministro, *José Sócrates Carvalho Pinto de Sousa.*

REGULAMENTO DO PLANO DE ORDENAMENTO DA ORLA COSTEIRA VILAMOURA-VILA REAL DE SANTO ANTÓNIO

TÍTULO I

Disposições gerais

Artigo 1.º

Natureza jurídica e âmbito

1 — O Plano de Ordenamento da Orla Costeira Vilamoura-Vila Real de Santo António, adiante abreviadamente designado por POOC,

tem a natureza de regulamento administrativo e com ele se devem conformar os planos municipais e intermunicipais de ordenamento do território, bem como os programas e projectos, de iniciativa pública ou privada, a realizar na sua área de intervenção.

2 — O POOC aplica-se à área identificada na respectiva planta de síntese, abrangendo parte dos concelhos de Loulé, Faro, Olhão, Tavira, Vila Real de Santo António e Castro Marim.

3 — Excluem-se da área de intervenção do POOC as áreas sob jurisdição portuária, nos termos da lei.

Artigo 2.º

Objectivos

O POOC estabelece regimes de salvaguarda de recursos e valores naturais e fixa os usos e o regime de gestão a observar na execução do Plano com vista a assegurar a permanência dos sistemas indispensáveis à utilização sustentável da sua área de intervenção, visando, em especial, a prossecução dos seguintes objectivos:

a) O ordenamento dos diferentes usos e actividades específicas da orla costeira;
b) A classificação das praias e a regulamentação do uso balnear;
c) A valorização e qualificação das praias consideradas estratégicas por motivos ambientais ou turísticos;
d) A orientação do desenvolvimento de actividades específicas da orla costeira;
e) A defesa e valorização dos recursos naturais e do património histórico e cultural.

Artigo 3.º

Composição

1 — O POOC é constituído por:

a) Regulamento;
b) Planta de síntese, à escala de 1:25 000;
c) Plantas dos planos de praia, à escala de 1:2000, e respectivas fichas de intervenção.

2 — O POOC é acompanhado por:

a) Relatório;
b) Programa de execução;
c) Plano de financiamento;
d) Planta de enquadramento, à escala de 1:100 000;
e) Planta de condicionantes, à escala de 1:25 000;
f) Planta de conflitos, à escala de 1:25 000;
g) Estudos de caracterização.

Artigo 4.º

Definições

Para efeitos da aplicação do presente Regulamento, são adoptadas as seguintes definições e abreviaturas:

a) «Acções de consolidação» — acções tendentes a evitar a degradação ou o colapso de sistemas naturais, de edifícios ou de infra-estruturas;
b) «Acesso pedonal consolidado» — espaço delimitado e regularizado com recurso a elementos naturais ou obstáculos adequados à minimização dos impactes sobre o meio, que permite o acesso dos utentes ao areal em condições de segurança e conforto de utilização, podendo ser constituído por caminhos regularizados, rampas, escadas ou passadeiras amovíveis em madeira;
c) «Acesso pedonal construído» — espaço delimitado, pressupondo obras de construção civil, que permite o acesso dos utentes ao areal em condições de segurança e conforto de utilização, podendo incluir caminhos pavimentados ou sobrelevados, escadas, rampas ou passadeiras, bem como os passeios marítimos associados a frentes urbanas consolidadas delimitados nos planos de praia;
d) «Acesso pedonal informal» — espaço delimitado que permite o acesso dos utentes ao areal, oferecendo condições de segurança de utilização, e que não é regularizado, pavimentado ou constituído por estruturas permanentes;
e) «Acesso viário pavimentado» — acesso delimitado com drenagem de águas pluviais e revestimento com materiais semipermeáveis ou impermeáveis, desde que sejam estáveis e resistentes às cargas e aos agentes atmosféricos;
f) «Acesso viário regularizado» — acesso delimitado, regularizado, com materiais permeáveis ou semipermeáveis e com sistema de drenagem de águas pluviais;
g) «Acesso viário não regularizado» — acesso delimitado com recurso a elementos naturais ou outros obstáculos adequados à minimização dos impactes sobre o meio;
h) «Actividades de motonáutica» — abrangem quaisquer actividades desportivas formais ou informais, incluindo demonstrações de perícia em manobras ou evoluções com os diferentes modos náuticos motorizados;
i) «Altura da arriba» — dimensão correspondente à diferença de cota entre a linha de encontro do areal ou do leito do mar com a arriba e a linha de crista, podendo ser definida localmente ou por troços onde não se verifiquem diferenças superiores a 10 % do valor médio;
j) «Antepraia» — zona costeira contígua à praia para o interior;
l) «Apoio balnear (AB)» — conjunto de instalações amovíveis sazonais destinadas a melhorar a fruição da praia pelos utentes, situado no areal, e que compreende, nomeadamente, barracas, toldos, chapéus-de-sol, passadeiras para peões e arrecadação de material, integrando a informação e o serviço de assistência e salvamento a banhistas, podendo, complementarmente, associar venda de gelados e alimentos pré-embalados;
m) «Apoio com equipamento associado (A/E)» — núcleo de funções e serviços idêntico ao previsto para o apoio de praia completo ou para o apoio de praia simples, mas integrando funções e serviços de equipamento;
n) «Apoio de praia completo (AC)» — núcleo básico de funções e serviços infra-estruturados que integra instalações sanitárias, balneários e vestiários, com acesso independente e exterior, posto de socorros, comunicações de emergência, informação e serviço de assistência e salvamento a banhistas, limpeza da praia e recolha de lixo; complementarmente pode assegurar outras funções e serviços, nomeadamente comerciais, com excepção dos serviços de equipamento;
o) «Apoio de praia mínimo (AM)» — núcleo básico de funções e serviços, amovível e sazonal, não infra-estruturado, com excepção da infra-estrutura eléctrica, que integra comunicações de emergência, informação e serviço de assistência e salvamento a banhistas, recolha de lixo e pequeno armazém para o material de praia, podendo eventualmente assegurar outras funções e serviços comerciais, nomeadamente comércio de gelados, de refrigerantes e de alimentos pré-embalados, bóias, revistas, artigos de praia e tabacaria;
p) «Apoio de praia simples (AS)» — núcleo básico de funções e serviços, infra-estruturado, que integra instalações sanitárias, com acesso independente e exterior, posto de socorros, comunicações de emergência, informação e serviço de assistência e salvamento, limpeza da praia e recolha de lixo, podendo assegurar outras funções e serviços, nomeadamente comerciais e de armazenamento de material de praia, semelhantes aos previstos para o apoio de praia mínimo;
q) «Apoio de pesca» — instalação destinada a arrecadação de utensílios e apetrechos de pesca;
r) «Apoio recreativo (AR)» — conjunto de instalações amovíveis sazonais destinadas à prática desportiva e lúdica dos utentes da praia, incluindo, nomeadamente, pranchas flutuadoras, instalações para desportos náuticos e diversões aquáticas, instalações para pequenos jogos de ar livre e recreio infantil;
s) «Área de estacionamento» — área definida para estacionamento e servida por acesso viário, com as características exigidas em função da classificação da praia e das características do meio onde se insere;
t) «Área bruta de construção» — somatório das áreas brutas de pavimento edificadas, ou susceptíveis de edificação, medidas pelo exterior das paredes, acima e abaixo da cota de soleira, em cada lote ou parcela, excluindo a área das caves, sótãos, terraços descobertos, galerias exteriores públicas e arruamentos ou espaços livres de uso público cobertos pela edificação;
u) «Área impermeabilizada» — área do terreno ocupada por edifícios, vias, passeios, estacionamentos, piscinas e demais obras que não permitam a infiltração da água da chuva no local em que ocorre a precipitação;
v) «Área de lazer equipada» — espaço complementar ao usufruto da orla costeira, decorrente dos planos de praia ou das UOPG, podendo conter áreas de estada, parques de merenda, áreas de sombra, áreas desportivas ou recreativas, áreas polivalentes destinadas a esplanadas, concertos ou outras actividades afins, áreas para instalação de equipamento de interpretação do meio, de miradouros ou de estruturas afins, o qual, em função da respectiva localização, apresenta programas diferenciados definidos no plano de praia

ou no projecto, de acordo com a classificação da praia ou com as características do meio onde se insere;

x) «Área de jurisdição portuária» — áreas do domínio hídrico situadas entre as faixas da costa, delimitadas nos termos da legislação em vigor;

z) «Área licenciada ou concessionada de uma praia» — praia ou parte dela, devidamente identificada, que seja objecto de utilização privativa do domínio público titulada por meio de licença ou de concessão;

aa) «Área *non aedificandi*» — área delimitada geograficamente onde é interdita qualquer edificação.

bb) «Areal» — zona de fraco declive, constituída por depósitos de sedimentos, tais como areias e calhaus, sem ou com pouca vegetação e formada pela acção das águas, ventos e outros agentes naturais ou artificiais;

cc) «Artificialização de arribas» — intervenções que impliquem consolidação de arribas e que envolvam estruturas de suporte ou de revestimento de qualquer natureza, associadas ou não a inclusões de reforço ou a qualquer outro impacte paisagístico relevante;

dd) «Arriba» — vertente costeira abrupta ou com declive forte, em regra talhada em material consolidado pela acção conjunta dos agentes morfogenéticos, marinhos, continentais e biológicos;

ee) Canal de navegação» — parte de uma via de água destinada à circulação de embarcações, devidamente assinalada e definida por uma largura, ou rasto, e uma profundidade ou cota de serviço;

ff) «Capacidade de carga da praia» — número máximo de utentes em simultâneo no areal, estimado de acordo com os critérios constantes dos elementos do POOC, a seguir enunciados:

i) Área útil da praia;
ii) Capacidade física da sua ocupação em situação de conforto;
iii) Capacidade de suporte do meio natural;
iv) Restrições relacionadas com o factor risco e ou com fragilidades ambientais;
v) Possibilidades e potencialidades balneares;
vi) Estratégia global de ordenamento da orla costeira;

gg) «Cais» — estrutura de acostagem de embarcações, de carga e descarga de mercadorias ou de embarque e desembarque de passageiros, que está aderente à margem na sua maior dimensão;

hh) «Cércea» — dimensão vertical da construção, medida a partir da cota média do terreno ou da plataforma de implantação, no alinhamento da fachada, até à linha superior do beirado, platibanda ou guarda do terraço;

ii) «Construção» — resultado da realização de qualquer tipo de obras, independentemente da sua natureza, designadamente edificações, muros, vedações, aterros ou escavações, incorporado ou não no solo e com carácter permanente ou temporário;

jj) «Construção de apoio à actividade agrícola» — construção de apoio às actividades inerentes à produção agrícola, podendo assumir funções complementares de armazenamento dos produtos agrícolas;

kk) «Construção ligeira» — estrutura construída com materiais ligeiros, designadamente prefabricados, que permitam a sua fácil desmontagem e remoção;

ll) «Construção sobrelevada» — estrutura construída com materiais ligeiros que permitam a sua fácil desmontagem e remoção, sobrelevada em relação ao meio em que se insere, mediante a colocação de estacas, permitindo a migração das areias;

mm) «Construção mista» — estrutura construída com materiais ligeiros, integrando elementos ou partes de construção em alvenaria ou de betão armado;

nn) «Construção pesada» — estrutura construída por recurso predominante a elementos de alvenaria ou de betão;

oo) «Corredor afecto à actividade piscatória» — varadouro destinado a embarcações de pesca artesanal e faixa adjacente do plano de água que lhe dá acesso;

pp) Corredor afecto às actividades náuticas recreativas» — varadouro destinado a modos náuticos de desporto e lazer e faixa adjacente do plano de água que lhe dá acesso;

qq) «Demolição» — obras de destruição, total ou parcial, de uma edificação ou estrutura existente, compreendendo também trabalhos de reposição de terrenos, designadamente para efeito de encerramento ou de interdição de circulação nos caminhos existentes;

rr) «Doca de recreio» — conjunto de infra-estruturas marítimas e terrestres localizadas num plano de água abrigado destinadas exclusivamente à náutica de recreio e dispondo em terra dos apoios necessários às tripulações e à manutenção das embarcações;

ss) «Domínio hídrico (DH)» — abrange os terrenos das faixas do litoral, os leitos e águas do mar e demais águas sujeitas à influência das marés, as correntes de água, lagos ou lagoas, com os seus leitos, margens e áreas adjacentes, delimitado nos termos da lei, com o respectivo subsolo e espaço aéreo correspondente, bem como as águas subterrâneas;

tt) «Drenagem» — conjunto de operações necessárias para eliminar o excesso de água do solo;

uu) «Duna litoral» — formações geomorfológicas resultantes de transporte eólico e acumulação de material sedimentar de origem marinha;

vv) «Edificação» — a actividade ou o resultado da construção, reconstrução, ampliação, alteração ou conservação de um imóvel destinado a utilização humana, bem como de qualquer outra construção que se incorpore no solo com carácter de permanência;

ww) «Equipamentos (E)» — núcleo de funções e serviços infra-estruturado, habitualmente considerado estabelecimento de restauração e bebidas, nos termos da legislação aplicável;

xx) «Erosão» — processo de degradação da superfície do solo, das margens ou leitos das águas, sob acção de agentes físico-químicos e biológicos, designadamente agitação marítima, águas superficiais e vento, podendo ser potenciada por acção antrópica;

zz) «Espécies não indígenas» — qualquer espécie da flora ou da fauna, não originária de uma determinada área biogeográfica e nunca aí registada como ocorrendo naturalmente, e com populações auto-sustentadas e integradas no contexto fito-sociológico da região;

aaa) «Estacada-cais» — designação normalmente associada a pequenos cais ou pontes cais cuja plataforma da estrutura está assente sobre estacas;

bbb) «Estacionamento pavimentado» — área destinada a parqueamento, devidamente delimitada, com drenagem de águas pluviais, revestida com materiais estáveis e resistentes às cargas e aos agentes atmosféricos, e com vias de circulação e lugares de estacionamento devidamente assinalados;

ccc) «Estacionamento regularizado» — área destinada a parqueamento, devidamente delimitada, com superfície regularizada, revestimento permeável ou semipermeável e com sistema de drenagem de águas pluviais, onde as vias de circulação e os lugares de estacionamento estão devidamente assinalados;

ddd) «Estaleiros navais» — instalações industriais destinadas à construção, beneficiação e reparação de navios e embarcações;

eee) «Faixa de protecção» — zona costeira sujeita a medidas de salvaguarda decorrentes da existência de risco para os utilizadores e para a manutenção do sistema costeiro ou lagunar ou decorrentes da necessidade de conservação dos valores naturais;

fff) «Fundeadouro» — área do plano de água destinada ao estacionamento esporádico de embarcações, fixadas ao fundo por meios próprios;

ggg) «Frente de praia» — comprimento da faixa de areal sujeita a ocupação balnear;

hhh) «*Habitat*» — conjunto dos elementos físicos e biológicos que uma determinada espécie utiliza para desenvolver o seu ciclo de vida;

iii) «Índice de construção (IC)» — quociente entre a área total de construção e a área total do terreno, no caso do índice de construção bruto, ou a área do terreno com exclusão das áreas afectas a equipamentos públicos, no caso do índice de construção líquido;

jjj) «Índice de utilização da praia» — área de utilização confortável de uma praia, por utente, definido em função da tipologia da praia e da sua vocação;

lll) «Licença ou concessão balnear» — autorização de utilização privativa de uma praia ou parte dela destinada à instalação dos respectivos apoios de praia, apoios balneares ou apoios recreativos, com uma delimitação e prazo determinados, com o objectivo de assegurar as funções e serviços de apoio ao uso balnear;

mmm) «Linha de máxima baixa-mar de águas vivas (LMBMAV)» — linha definida em função do espraiamento das vagas em condições médias de agitação do mar na baixa-mar de águas vivas;

nnn) «Linha de máxima preia-mar de águas vivas equinociais (LMPMAVE)» — linha definida em função do espraiamento das vagas em condições médias de agitação do mar

na preia-mar de águas vivas equinociais; para efeitos de aplicação do POOC, deve ser adoptado o valor utilizado como referência pelas entidades com jurisdição na área para a gestão corrente. Na área de aplicação do POOC, nas áreas sujeitas a acção directa da ondulação, o valor adoptado é de + 5,5 ZH; em áreas lagunares e estuarinas, sem influência directa da ondulação, o valor de referência é de + 4 ZH, podendo variar localmente em função da deformação da maré durante a sua propagação;

ooo) «Linha de média preia-mar no período balnear (LMPMPB)» — linha de cota do espraiamento médio das vagas na preia-mar durante o período balnear. Na área de aplicação do POOC, nas áreas sujeitas a acção directa da ondulação, o valor adoptado é de + 3,6 ZH em praias de declive suave (1:80 entre os 3,5 ZH e o ZH), podendo ser maior em praias de declive mais acentuado; em áreas lagunares e estuarinas, sem influência directa da ondulação, o valor de referência é de + 3 ZH, podendo variar localmente em função da deformação da maré durante a sua propagação;

ppp) «Margem das águas do mar» — faixa de terreno contígua ou sobranceira à LMPMAVE, com uma largura mínima de 50 m, que se estende até onde o terreno apresentar natureza de praia, correspondendo, no presente POOC, às subcategorias de espaço praias e dunas;

qqq) «Marina» — conjunto de infra-estruturas localizadas em plano de água abrigado, exclusivamente destinadas ao turismo, desporto e lazer, dispondo em terra dos apoios necessários às embarcações e tripulações, e enquadrado por complexo hoteleiro e residencial;

rrr) «Medidas correctivas da erosão superficial» — conjunto de acções previsto nos planos de praia que pretende corrigir formas de erosão, como ravinamentos, queda de blocos ou deslizamento de materiais, sendo as medidas concretas definidas em projecto, por recurso a técnicas de estabilização e recuperação biofísica sem utilização de materiais pesados;

sss) «Modos náuticos» — todos os veículos flutuantes autónomos, motorizados ou não, com funções de transporte de um ou mais passageiros em meio aquático;

ttt) «Navegação costeira» — navegação efectuada até 6 milhas da costa com apoio de detecção de referências em terra;

uuu) «Navegação local» — navegação em áreas de fraca agitação marítima, junto à costa e em águas interiores;

vvv) «Núcleo de pesca» — conjunto de pequenas infra-estruturas marítimas e ou terrestres, podendo ou não estar inserido num plano de água abrigado, integrando dispositivos de apoio à actividade pesqueira e instalações de pesca que servem a frota de embarcações de pesca local ou costeira;

xxx) «Núcleo de recreio náutico» — conjunto de pequenas infra-estruturas marítimas e ou terrestres, localizado num plano de água abrigado, de apoio à náutica de recreio, podendo, na sua expressão mais simples, ser constituído apenas por um fundeadouro;

zzz) «Obras de conservação» — obras destinadas a manter uma edificação nas condições existentes à data da sua construção, reconstrução, ampliação ou alteração, designadamente as obras de restauro, reparação ou limpeza;

aaaa) «Obras de reconstrução» — obras de construção subsequentes à demolição total ou parcial de uma edificação existente, das quais resulte a manutenção ou a reconstituição da estrutura das fachadas, da cércea e do número de pisos;

bbbb) «Obras de requalificação da frente urbana» — processo de transformação urbana, compreendendo a execução de obras de conservação, reconstrução ou readaptação, com o objectivo de garantir a coerência e qualidade do conjunto, assim como a melhoria das condições de uso e habitabilidade dos edifícios que o integram;

cccc) «Parcela» — área de território jurídica e ou fisicamente autonomizada não resultante de uma operação de loteamento;

dddd) «Passadiços flutuantes» — estruturas flutuantes fixas aos fundos por estacas ou amarras que têm como objectivo a costagem de pequenas embarcações e protecção da pequena agitação marítima;

eeee) «Pavimento» — materiais inertes de revestimento da superfície do solo, de natureza permeável, semipermeável ou impermeável, resultante de uma acção de construção;

ffff) «Plano de água associado» — massa de água e respectivo leito afectos à utilização específica de uma praia, considerando-se o leito do mar com o comprimento correspondente ao areal e a largura de 300 m para além da LMBMAVE;

gggg) «Plano de praia» — instrumento de planeamento territorial que disciplina os usos de praias especialmente vocacionadas para utilização balnear;

hhhh) «Projecto de intervenção e requalificação» — projecto a elaborar pelo ministério responsável pela área do ambiente assumindo características semelhantes aos planos de pormenor;

iiii) «Ponte-cais» — estrutura de acostagem de embarcações, de carga e descarga de mercadorias ou de embarque e desembarque de passageiros, perpendicular ou oblíqua em relação à margem;

jjjj) «Porto comercial» — conjunto de infra-estruturas marítimas e terrestres num plano de água abrigado destinado à carga, descarga, armazenagem e transferência modal de granéis sólidos, líquidos e carga geral, unitizada ou não;

llll) «Porto de pesca» — conjunto de infra-estruturas marítimas e terrestres localizadas num plano de água abrigado destinado à descarga, acondicionamento, armazenamento e comercialização do pescado, que permite o estacionamento das embarcações de pesca e possui meios de apoio logístico e operacional às mesmas;

mmmm) «Recuperação dunar» — acção que visa recuperar ou repor o equilíbrio do sistema dunar na íntegra ou em parte, efectuada através da instalação de paliçadas, ou outros meios atenuantes da migração das areias, e associada à plantação de espécies características desses sistemas, podendo implicar a reposição artificial de areias;

nnnn) «Rede pública de abastecimento de água» — rede de distribuição de água explorada e gerida, directa ou indirectamente, por uma entidade pública;

oooo) «Rede pública de esgotos» — rede de drenagem de águas residuais explorada e gerida, directa ou indirectamente, por uma entidade pública;

pppp) «Remodelação» — execução de obras que, por qualquer forma, modifiquem o plano primitivo da construção existente; poderá também corresponder a situações de adequabilidade a um novo uso ou, apenas, à melhoria das condições actuais de utilização;

qqqq) «Renaturalização de áreas degradadas» — acção prevista nos planos de praia com o objectivo de repor a situação natural de áreas degradadas, consistindo em soluções específicas para cada situação a determinar com base no controlo das acessibilidades, descompactação do solo, plantação de espécies vegetais características das formações costeiras e ou outras técnicas adequadas;

rrrr) «Sítio» — área geográfica claramente delimitada, constante da Lista Nacional de Sítios incluídos na Rede Natura 2000, nos termos da legislação em vigor;

ssss) «Unidade balnear» — base de ordenamento do areal, nas praias dos tipos I, II e III, ao qual está associado um apoio de praia mínimo, simples ou completo;

tttt) «Unidade operativa de planeamento e gestão (UOPG)» — área que pela sua dimensão, localização e especificidade justifica o planeamento e gestão integrada a submeter a planos de pormenor, projectos de intervenções ou estudos específicos;

uuuu) «Uso balnear» — conjunto de funções e actividades destinadas ao recreio físico e psíquico do homem, satisfazendo necessidades colectivas que se traduzem em actividades multiformes e modalidades múltiplas, conexas com o meio aquático;

vvvv) «Valorização de linhas de água» — acção de valorização, recuperação e estabilização biofísica do leito, margens e zona adjacente de linhas de água, através de técnicas de engenharia biofísica e constituição de matas ou orlas arbustivas de carácter ribeirinho;

xxxx) «Varadouro» — frente de águas do mar e faixa terrestre adjacente, natural ou construída, cuja geometria permite colocar embarcações em seco e se destina ao seu estacionamento;

zzzz) «Vegetação autóctone» — vegetação originária de uma determinada área biogeográfica, incluindo vegetação endémica, e que forma associações vegetais características dessa região;

aaaaa) «Zero hidrográfico (ZH)» — superfície em relação à qual são referidas as sondas e as linhas isobatimétricas das cartas náuticas, bem como as previsões de alturas de maré publicadas nas tabelas de maré do Instituto Hidrográfico; nas cartas portuguesas, o ZH fica situado abaixo do nível da maré astronómica mais baixa, sendo situado aproximadamente 2 m abaixo do nível médio do mar;

bbbbb) «Zona dunar» — área constituída pelo conjunto de dunas e depressões interdunares, cordões ou sistemas dunares existentes ou passíveis de se formarem através de acções de revestimento e ou reposição dunar;

ccccc) «Zona de uso balnear» — área de praia destinada ao uso balnear, submetida a um zonamento com base nas unidades balneares, e incluindo áreas não concessionadas.

SECÇÃO VI

Outras intervenções

Artigo 79.º

Outras intervenções

1 — As outras intervenções previstas pelo POOC para as praias e que constam dos planos de praia são as seguintes:

a) Recuperação dunar;
b) Áreas de lazer equipadas;
c) Renaturalização de áreas degradadas;
d) Medidas correctivas de erosão superficial.

2 — A recuperação dunar é efectuada através da instalação de paliçadas ou outros meios atenuantes da migração das areias, plantação de espécies características desses sistemas e, em certos casos, reposição artificial de areias.

3 — As áreas de lazer equipadas são infra-estruturas complementares ao uso balnear e alternativa de uso da orla costeira.

4 — A renaturalização de áreas degradadas implica o controlo das acessibilidades, a descompactação do solo, a plantação com espécies vegetais características das formações costeiras e a adopção de outras medidas que permitam uma reposição da situação natural das formações costeiras.

5 — As medidas correctivas de erosão superficial, definidas na execução dos projectos de cada plano de praia, aplicam-se, designadamente, em caso de ravinamentos, queda de blocos ou deslizamento de materiais.

CAPÍTULO VI

Unidades operativas de planeamento e gestão

Artigo 80.º

Âmbito e objectivo

1 — As unidades operativas de planeamento e gestão (UOPG) correspondem a unidades territoriais que podem integrar uma ou mais classes de espaço e que, pelas suas características próprias, se individualizam da restante orla costeira.

2 — As UOPG constituem unidades indicativas para a elaboração de planos de pormenor e projectos de intervenção e requalificação, os quais se encontram sujeitos às disposições constantes do artigo 80.º ao artigo 90.º do presente Regulamento.

3 — As UOPG, assinaladas na planta de síntese, são as seguintes:

a) UOPG I — Quarteira;
b) UOPG II — Litoral de Vale de Lobo;
c) UOPG III — ilha de Faro;
d) UOPG IV — núcleo da Culatra;
e) UOPG V — núcleo da Armona;
f) UOPG VI — Quatro Águas;
g) UOPG VII — Cacela/Fábrica;
h) UOPG VIII — Verde Lago;
i) UOPG IX — faixa litoral de Monte Gordo;
j) UOPG X — faixa nascente de Monte Gordo.

Artigo 81.º

UOPG I — Quarteira

1 — Esta UOPG contempla a realização de um projecto de intervenção e requalificação a elaborar pelo ministério responsável pela área do ambiente, com a colaboração das entidades com tutela sobre as áreas de jurisdição portuária.

2 — Para esta UOPG definem-se os seguintes objectivos:

a) Requalificação dos acessos viários;
b) Implementação de um espaço de lazer, sujeito à elaboração de um projecto de enquadramento paisagístico, que compreenda, designadamente, parques de recreio, áreas verdes, percursos pedonais e pistas para velocípedes;
c) Articulação com o porto de pesca existente e com a respectiva área envolvente, tendo em conta a necessidade de virem a ser construídas infra-estruturas de apoio ao porto.

Artigo 82.º

UOPG II — Litoral de Vale de Lobo

1 — Esta UOPG contempla:

a) A realização de um projecto de intervenção e requalificação para a praia de Vale de Lobo e área adjacente, a elaborar pelo ministério responsável pela área do ambiente;
b) A realização de plano de pormenor para a área de Vale de Lobo integrada na faixa de protecção, a elaborar pela Câmara Municipal de Loulé.

2 — Para a frente urbana adjacente à praia de Vale de Lobo e praia de Vale de Lobo determina-se:

a) No âmbito de um projecto de intervenção e requalificação, uma análise do custo/benefício que equacionará as soluções adequadas face aos riscos de erosão existentes e cujas conclusões constituirão fundamento para as decisões a tomar;
b) A adopção de medidas urgentes para a salvaguarda dos utentes da praia, nomeadamente as seguintes:
i) Demolição das estruturas implantadas à face da arriba em risco eminente de desmoronamento;
ii) Reformulação de acessos pedonais e viários;
iii) Ordenamento e valorização dos estacionamentos existentes;
iv) Criação de espaços de lazer directamente relacionados com a área de uso balnear.

3 — Para a área urbana e espaços turísticos de Vale de Lobo integrados na faixa de protecção determina-se, no âmbito de um plano de pormenor, a elaboração de uma análise custo/benefício que equacionará as soluções adequadas face aos riscos de erosão existentes e cujas conclusões constituirão fundamento para as decisões a tomar relativamente à segurança da área de toda a área turística.

4 — O programa desta UOPG é articulado com o protocolo celebrado em 16 de Abril de 1998 entre o Ministério do Ambiente e do Ordenamento do Território e a empresa Vale do Lobo para esta área.

Artigo 83.º

UOPG III — Ilha de Faro

1 — Esta UOPG contempla:

a) A realização de um projecto de intervenção e requalificação para a área do domínio hídrico, a elaborar pelo ministério responsável pela área do ambiente;
b) A realização de plano de pormenor para a área desafectada do domínio hídrico a elaborar pela Câmara Municipal de Faro.

2 — O programa desta UOPG resultará da articulação entre o projecto de intervenção e requalificação e o plano de pormenor, os quais devem conter as seguintes medidas:

a) Elaboração de uma análise do custo/benefício que equacionará a remoção programada das edificações existentes na área desafectada do domínio hídrico em alternativa a soluções a adoptar para salvaguarda das edificações localizadas em faixa de risco;
b) Realojamento dos residentes em primeiras habitações que se encontram no domínio hídrico na área desafectada do domínio hídrico;
c) Na área de domínio hídrico, demolição e remoção das edificações;
d) Condicionamento ao acesso de veículos particulares e de fornecedores durante a época balnear;
e) Promoção de alternativas de acesso através de transportes públicos;
f) Criação de estacionamento na margem terrestre;
g) Ordenamento dos acessos pedonais ao longo da área edificada a reestruturar;
h) Reestruturação do caminho de acesso à ilha com restabelecimento da circulação de água nos esteiros;
i) Renaturalização de áreas degradadas e das áreas que resultem não ocupadas.

Artigo 84.º

UOPG IV — Núcleo da Culatra

1 — Esta UOPG contempla a realização de um projecto de intervenção e requalificação e de um plano de praia, a elaborar pelo ministério responsável pela área do ambiente.

2 — Para esta UOPG estabelecem-se os seguintes objectivos:

a) Manutenção do carácter de dominialidade do domínio hídrico;
b) Regularização da situação das edificações existentes;
c) Requalificação das edificações que correspondem a primeira habitação;
d) Demolição das construções que correspondam a segunda habitação;

Appendix H

Report: UAV imagery processing – Amadora

Automatic Reconstruction Report (version 1.22291)

pdf

Figure 1: Ortho mosaic (left) and (right) the corresponding digital elevation model (DEM).

Overall Quality

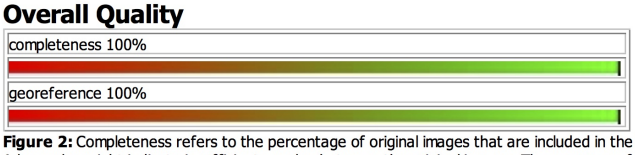

Figure 2: Completeness refers to the percentage of original images that are included in the final ortho image.
A low value might indicate insufficient overlap between the original images. The accuracy of the geotags relates to the quality of the geotags that are associated with each original image (see Figure 6).

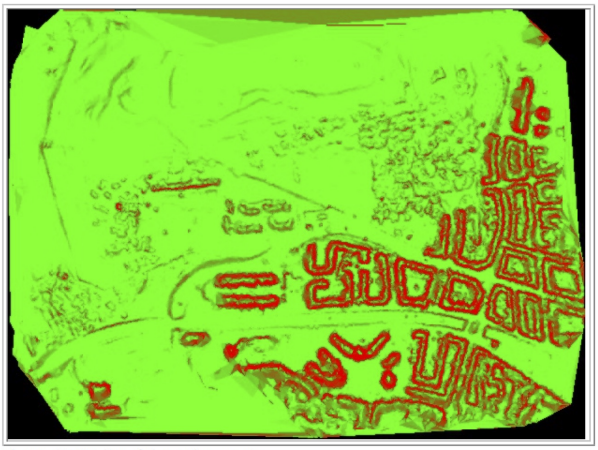

Figure 3: Quality of the ortho mosaic.
Red indicates areas where the ortho mosaic and the digital elevation model could contain artefacts, e.g. non-linear building edges.

Original Image Dataset

1

The dataset contains 238 original images.

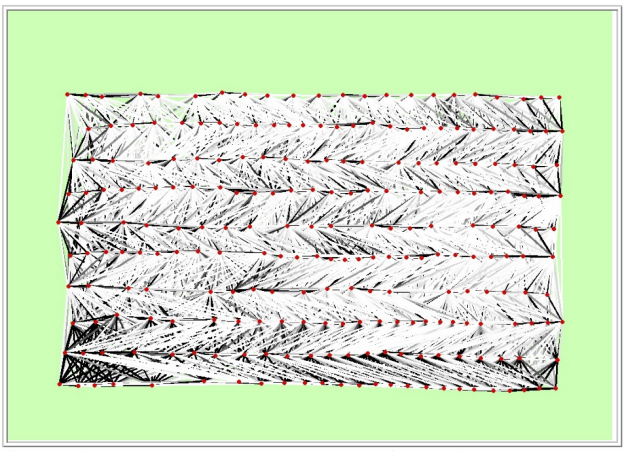

Figure 4: This connectivity graph displays the number of potential keypoint matches (color coded in gray values) between the original images. A high quality result can be obtained if each orginal image is connected with sufficient matches to the neighbouring images along all directions. The large red dot corresponds to the starting original image. The green line follows the original image geotags over time. Keypoint matches consist of distinct images keypoints that are visible in two images and for which a correspondence could be established.

Result

The ortho mosaic is composed from 238 out of 238 original images.
The ortho mosaic covers an area of 0.94 sq. km / 93.77ha / 0.36 sq. mi.
The mean GSD (size of a pixel on the ground) of the original images is computed at 5.80126 cm.

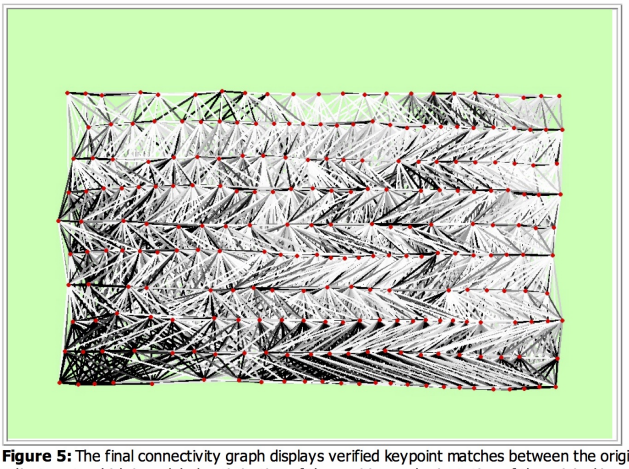

Figure 5: The final connectivity graph displays verified keypoint matches between the original images after bundle block adjustment, which is a global optimisation of the position and orientation of the original images and the digital elevation model.

	number of keypoint observations per original image
median	5537
min	379
max	17934
mean	7901.54

	number of 3D points observed
in 2 - 3 images	550926
in 4 - 5 images	62831
in 6 - 7 images	21672
in 8 - 9 images	10918
in 10 - 11 images	6241
in 12 - 13 images	3686
in 14 - 15 images	1816
in 16 - 17 images	966
in 18 - 19 images	406
in 20 - 21 images	95
in 22 - 23 images	13

Table 1: Matching statistics for the bundle block adjustment.

number total keypoint observations for bundle block adjustment	1880566
number total 3D points for bundle block adjustment	659570
mean reprojection error	0.247005 [pixels]

Table 2: Characteristics of bundle block adjustment.

Georeference

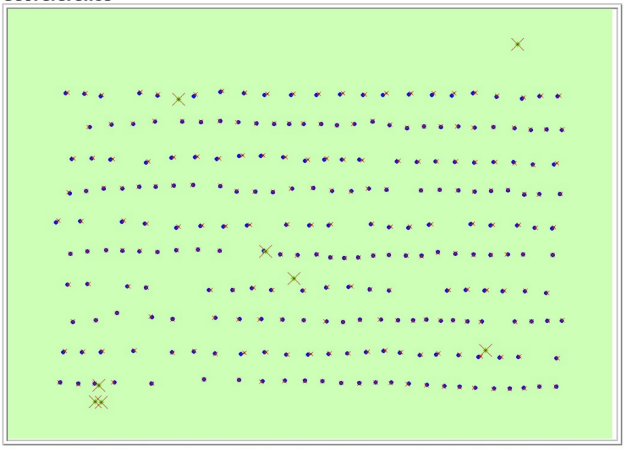

Figure 6: Offset between image GPS tags (small red crosses) and estimated positions of the original images (small blue dots) as well as the offset between the GCP's (large red crosses) and their estimated positions (large green dots) in the horizontal plane.

GCP name	error X [m]	error Y [m]	error Z [m]
GCP: 1	0.0903412	0.00969952	0.144737
GCP: 2	0.0279888	0.0172704	0.0986652
GCP: 3	0.09075	0.00969728	0.00903047
GCP: 4	0.0537006	0.0158433	0.112338
GCP: 5	0.0290029	0.0756771	0.158016
GCP: 6	0.00879389	0.0198316	0.0179626
GCP: 7	0.0197579	0.0112533	0.0156044
GCP: 11	5.16782e-005	0.013666	0.006979
mean	0.0400484	0.0216173	0.0704166
sigma	0.0326767	0.0207142	0.0605197

Table 3: Localisation accuracy of the individual Ground Control Points (GCP) in meters, their mean error distance and the mean errors in the three coordinate directions.
0 out of 8 GCP's have been labeled as inaccurate (see Figure 6).

geotag localisation variance	sigma [m]

longitude direction (x)	2.21923
latitude direction (y)	0.789232
altitude direction (z)	0.827126

Table 4: Localisation accuracy of the geotags in meters. 28 out of 238 original image geotags have been labeled as inaccurate (see Figure 6).

Appendix I

GRASS GIS commands for the selection of UAV points on roof eave

The methodology developed for the evaluation of the building height parameter extracted from the UAV point cloud was made in GRASS 6.4.2 and GRASS 7 (lasted version of GRASS for Linux). In GRASS 7, the overall performance of the functions was much higher, with a significantly reduced processing time. As an example, importing a point cloud to GRASS (around 8 million points) only takes about 5 minutes (1 hour in GRASS 6.4.2.). Therefore, this lastest version of GRASS GIS should be used for this type of applications. Next, we shall provide details on the commands used in the first part of methodology for the selection of 3D building rooftop edge points:

Listing I.1: Selection of UAV points of eave roof for Area A (for the other areas B or C it's the same)

```
#Importing of ASCII file to GRASS vector format
v.in.ascii -z input="/media/user/pointcloud.txt"
output="pointcloud@proc_TileUAVamadora"
format="point" fs="space" skip=0 x=1 y=2 z=3 cat=0
-----------------------------------------------------
#Repeat this comand for each Tile (Area)
v.select ainput="pointcloud@proc_TileUAVamadora"
atype="point,line,boundary,centroid,area" alayer=1
binput="Area@proc_TileUAVamadora"
btype="point,line,boundary,centroid,area" blayer=1
output="pointcloudarea@proc_TileUAVamadora"
operator="overlap"
-----------------------------------------------------------
v.db.addcol "--q" "map=pointcloudarea@proc_TileUAVamadora"
"layer=1" "columns=x double precision"
v.db.addcol "--q" "map=pointcloudarea@proc_TileUAVamadora"
"layer=1" "columns=y double precision"
v.db.addcol "--q" "map=pointcloudarea@proc_TileUAVamadora"
"layer=1" "columns=z double precision"
-------------------------------------------------------------------
v.outlier input="pointcloudarea@proc_TileUAVamadora"
output="T1out037cl"
outlier="T1out037otl" qgis="T1037cl"
soe=0.37 son=0.37 lambda_i=0.1 thres_o=35
-----------------------------------------------------------------
v.lidar.edgedetection input="T1out037cl@proc_TileUAVamadora"
output="T1edge037"
see=0.37 sen=0.37 lambda_g=0.01 tgh=6 tgl=3
```

```
theta_g=0.26 lambda_r=2
-------------------------------------------------------------------
v.extract input=T1edge037cl@proc_TileUAVamadora
output=T1edge037cat2 type=point list=2
-------------------------------------------------------------------
#The next two commands are importante to obtain the coordinates
x,y,z of edge points: a) exporting a vector map to a PLY file
(\textit{v.out.ply}; and b) creating of vector points from a
PLY file (\textit{v.in.ply}).

v.out.ply vect=T1edge037cat2@proc_TileUAVamadora
file=T1edge037cat2.ply
v.in.ply file=/home/crebelo/T1edge037cat2.ply vect=T1edge037xyz

#The optimization of this crucial procedure was achieved with these
two functions, where in few minutes this step is concluded. Using the
old way (\textit{v.to.db} function) the processing time to do this
operation would have been about half day for each area (in GRASS GIS 6.4.
-------------------------------------------------------------------
v.buffer input=a_roofref@proc_TileUAVamadora
output=buffbeirado
type=point distance=0.80
-------------------------------------------------------------------
v.select ainput=T1edge037xyz@proc_TileUAVamadora
binput=buffbeirado output=selectpts
-------------------------------------------------------------------
v.what.vect vector=selectpts@proc_TileUAVamadora column=idpt
qvector=a_roofref@proc_TileUAVamadora qcolumn=predioid
dmax=15
-------------------------------------------------------------------
```

The optimization of coordinates registry for each 3D point is crucial and it was achieved with PLY functions, since this was concluded in few minutes. Using the old way (*v.to.db* function), the processing time to perform this operation would have been about half day for each area (in GRASS GIS 6.4.2).

Appendix J

R algorithm for the calculation and evaluation of estimated building façade height

The R algorithm developed for the calculation of building façade height is presented in listing J.1.

Listing J.1: Compute Building Façade Height for area X using trim mean

```
#####################################################
#PART 1: Edges of roof
#Input: UAV points of edges building roof "file.csv"
#####################################################
data <- read.table("AreaA.csv", header=TRUE, sep=",",
        encoding="latin1")

#Conversion to numeric values
cce <- as.numeric(tapply(data$z,data$idpt,FUN =
       function(x)mean(x, trim=.4)))
outputE <- data.frame(cce)
colnames(outputE) <- c("edif","mediae_t0.4")

#Export results
write.csv(outputE, file="resultsAreaA.csv")
#####################################################
#PART 2: Ground
#Input: UAV Ground points "file.csv"
#####################################################
datag <- read.table("AreaAG.csv", header=TRUE, sep=",",
         encoding="latin1")
ccg <- as.numeric(tapply(datagp$z,datag$idpav,
       FUN = function(x)mean(x, trim=.2)))
outputG <- data.frame(ccg)
colnames(outputG) <- c("edif","mediag_t0.2")

# Merge the two tables (rows) and compute building
#Facade Height
resultsM <- merge(outputE,outputG, by.x = "edif",
            by.y = "edif")
resultsM$HfachadaUAV <- resultsM$mediae_t0.4 -
                        resultsM$mediag_t0.2

#Export results
write.csv(resultsM, file="resultsArea_AG.csv")
```

The R algorithm developed for the evaluation of building façade height results achieved for each building based on the calculation of vertical error is presented

in listing J.2.

Listing J.2: Compute Building Façade Height using trim mean

```
# Import table of reference building height values
datref <- read.table("abuildsreference.csv",
                     header=TRUE, sep=";",
                     encoding="latin1")
# Merge the two tables (rows) by identical attribute
Tile <- merge(datref,resultsM, by.x = "predioid",by.y = "edif")
# Compute residuals of Building Height
Tile$residuoHF <- Tile$HFacade -
                  Tile$HFacadeUAV
```

Appendix K

Building façade height values estimated from UAV point cloud within GRASS

RESULTS OF SUBSECTION 3.2.2

This appendix presents the results achieved for all the building façade heights estimated from different block morphologies in Amadora city.

AREA A Building blocks of area A. Blue: selected UAV points; Black: Reference elevation point on the ground; Green: Reference elevation point on the rooftop. The UAV points selected for *building 4* are presented in the figure below.

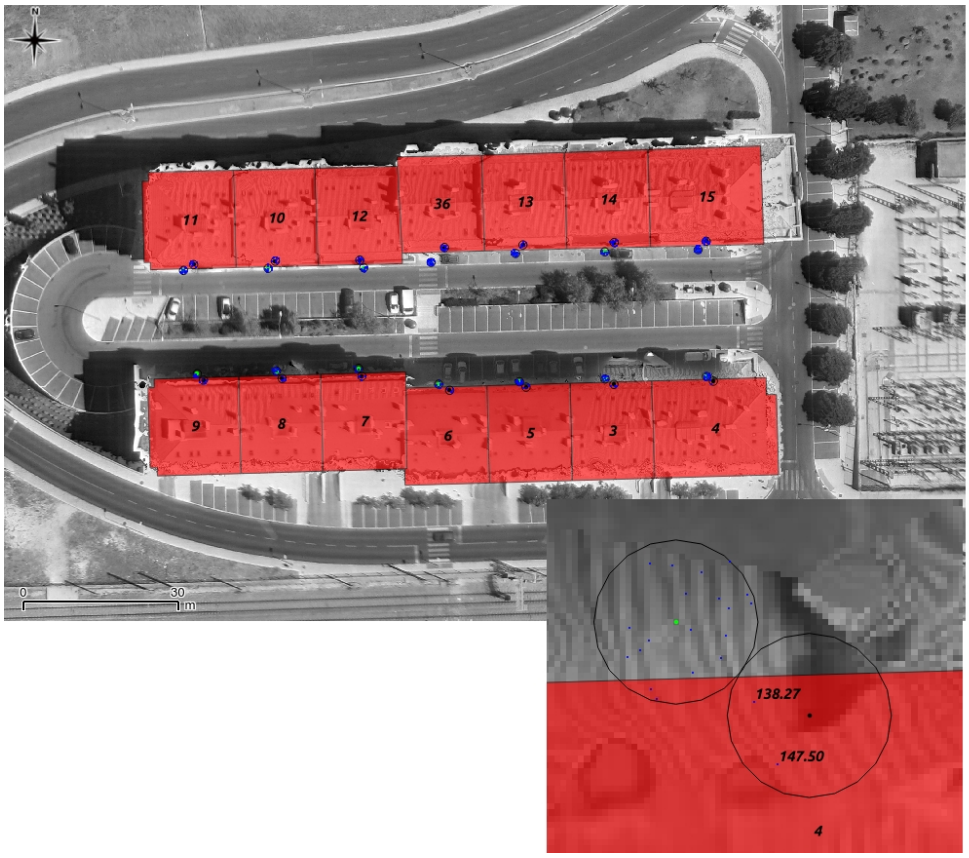

The results presented are related with the best processing [(1/point density)x 4]. The building façade heights that have not been well estimated are highlighted in blue in the next table. These values correspond to the difficulty of filtering points on the rooftop on the ground.

The maximum error in area A was 5.60 m for *building 4*, whose the elevation at the top has 'wrong points' (Figure above). The higher vertical errors obtained for all buildings are due to the estimated elevation rooftops.

Area A: estimated building façade height estimated and vertical errors

Building Code	Rooftop Elevation (exact)	Base Elevation (exact)	BFH True (m)	Rooftop Elevation* (UAV)	Base Elevation* (UAV)	BFH UAV (m)	Residual (Vertical Error)
3	148.00	132.23	15.77	147.93	132.99	14.95	0.82
4	148.00	132.23	15.77	142.89	132.71	10.17	5.60
5	148.00	132.24	15.76	148.64	133.23	15.40	0.36
6	148.00	132.28	15.72	147.29	134.40	12.89	2.83
7	148.16	132.39	15.77	147.99	132.23	15.76	0.01
8	148.38	132.32	16.06	147.85	133.55	14.30	1.76
9	148.50	132.28	16.22	147.49	132.57	14.92	1.30
10	151.19	133.36	17.83	150.52	133.13	17.39	0.44
11	150.43	133.33	17.10	149.53	133.37	16.15	0.95
12	151.21	133.36	17.85	150.24	133.17	17.07	0.78
13	153.30	133.56	19.74	149.00	133.26	15.74	4.00
14	153.30	133.59	19.71	152.93	133.19	19.74	-0.03
15	153.72	133.59	20.13	152.91	133.29	19.61	0.52
36	152.47	133.39	19.08	148.72	133.17	15.56	3.52

*Elevation Base based on 0.4 trimmed mean; Elevation Rooftop based on 0.2 trimmed mean

AREA B Building blocks of area B. Blue: selected UAV points; Black: Reference elevation point on the ground; Green: Reference elevation point on the rooftop. The UAV points selected for *buildings 73 and 80* are shown in the figure below.

Analysing the table of errors for area C, we can see that the maximum error was about 15 m for *building 80*. The higher vertical errors are due estimated ground elevations, which means that the DTM does not have good quality along these areas (points that do not belong to the ground were not completely removed).

Area B: Estimated building façade height and vertical errors. (NB: the wrong points are identified in red.)

Building Code	Rooftop Elevation (exact)	Base Elevation (exact)	BFH True (m)	Rooftop Elevation* (UAV)	Base Elevation* (UAV)	BFH UAV (m)	Residual (Vertical Error)
17	147.3	132.45	14.85	147.08	133.1	13.97	0.88
18	146.84	131.75	15.09	146.12	131.94	14.19	0.90
19	146.88	131.82	15.06	140.50	133.05	7.45	7.61
23	144.2	130.45	13.75	144.44	132.26	12.18	1.57
24	143.8	130.35	13.45	144.26	138.21	6.05	7.40
34	148.4	133.05	15.35	148.14	133.56	14.58	0.77
38	149.2	134.15	15.05	148.61	140.64	7.98	7.07
39	149.9	134.95	14.95	149.76	136.25	13.51	1.44
43	143.7	128.25	15.45	144.24	135.71	8.53	6.92
45	144	130.35	13.65	144.05	130.76	13.29	0.36
46	144.4	130.55	13.85	144.77	132.21	12.56	1.29
47	145.2	131.75	13.45	145.38	132.61	12.78	0.67
48	146	131.95	14.05	145.82	132.23	13.59	0.46
49	146.2	132.35	13.85	146.44	132.73	13.71	0.14
50	146.6	133.15	13.45	146.07	139.16	6.91	6.54
52	147.4	131.05	16.35	147.67	134.96	12.71	3.64
53	146.7	133.55	13.15	146.82	135.18	11.65	1.50
59	149.4	133.45	15.95	149.42	133.48	15.94	0.01
60	150.1	134.45	15.65	150.22	134.58	15.64	0.01
61	151.6	135.45	16.15	151.26	135.57	15.69	0.46
73	149.7	132.05	17.65	145.52	140.43	5.09	12.56
76	145.7	128.25	17.45	145.81	128.29	17.52	-0.07
77	143.2	127.75	15.45	142.15	128.02	14.12	1.33
79	142.7	127.2	15.5 0	142.61	127.30	15.31	0.19
80	145.8	127.45	18.35	146.01	143.18	2.83	15.52
81	146.28	129.55	16.73	146.49	136.94	9.54	7.19
82	143.4	129.15	14.25	143.46	132.06	11.41	2.84
87	143.75	129.56	14.19	143.39	134.95	8.44	5.75

*Elevation Base based on 0.4 trimmed mean; Elevation Rooftop based on 0.2 trimmed mean

The highest building façade height errors of area B were due to UAV imagery processing, which showed great discontinuities along the boundaries of the buildings.

AREA C Building blocks of area C. Blue: selected UAV points; Black: Reference elevation point on the ground; Green: Reference elevation point on the rooftop. The UAV points selected for *buildings 66 and 75* are shown.

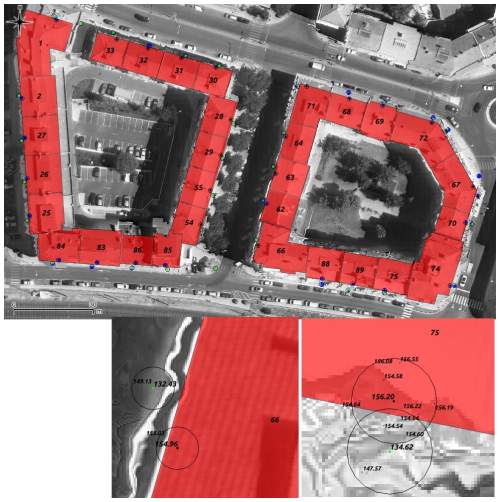

The highest building façade height errors in area C are due to a wrong estimated ground elevation. The maximum error was about 17 m for *building 66* (next table and figure above).

Area C: Estimated Building façade height and vertical errors. The wrong points are identified in red.

Building Code	Rooftop Elevation (exact)	Base Elevation (exact)	BFH True (m)	Rooftop Elevation* (UAV)	Base Elevation* (UAV)	BFH UAV (m)	Residual (Vertical Error)
25	147.17	130.98	16.19	147.06	137.39	9.68	6.51
31	151.55	138.30	13.25	151.24	139.27	11.98	1.27
32	151.55	138.62	12.93	150.99	138.73	12.26	0.67
62	147.51	133.67	13.84	147.68	147.04	0.64	13.20
64	149.42	136.15	13.27	149.37	141.6	7.77	5.50
66	154.96	132.43	22.53	155.03	149.13	5.91	16.62
67	148.72	136.4	12.32	148.82	136.44	12.38	-0.06
68	150.57	137.8	12.77	150.72	139.5	11.22	1.55
69	150.07	137.6	12.47	149.64	137.91	11.73	0.74
70	149.12	136.4	12.72	149.07	148.22	0.85	11.87
71	150.62	137.01	13.61	150.93	138.79	12.14	1.47
72	150.17	137.42	12.75	149.79	137.18	12.62	0.13
74	157.37	136.2	21.17	151.57	135.83	15.74	5.43
75	156.2	134.62	21.58	155.11	147.57	7.54	14.04
83	147.17	130.87	16.3	145.93	130.76	15.17	1.13
84	147.17	130.49	16.68	145.53	130.51	15.02	1.66
86	144.61	131.28	13.33	144.25	130.93	13.32	0.01
88	152.28	133.38	18.9	152.64	133.94	18.71	0.19
89	153.53	134.32	19.21	154.26	135.12	19.14	0.07

*Elevation Base based on 0.4 trimmed mean; Elevation Rooftop based on 0.2 trimmed mean

Appendix L

Clustering blocks with an algorithm implemented in R

Listing L.1: Algorithm implemented in R language for clustering point cloud

```
-------------------------------------------------------------
--Developed on July 2013, Carla rebelo
--objetive: Clustering point cloud by z value and aggregate
--the clusters that represent the buildings
-------------------------------------------------------------
--Libraries: cluster,sqldf, tcltk
-------------------------------------------------------------
--PART 1
-------------------------------------------------------------
-- Work directory of files (input .csv files with point
--cloud areas)
setwd("/home/User/files.csv")
-- 1) read all files csv
filenames <- list.files(path="/home/user/..", pattern="pcl+.*csv")
-- filelist
filelist <- lapply(filenames, read.csv, sep=",")
--if necessary, assign names to data.frames
names(filelist) <- c("pclA","pclB","pclC")

-- 2) Extract the column z of files from each dataframe in R
--(by loop) support: http://stackoverflow.com/questions/13861296/
how-do-i-make-a-loop-to-extract-a-column-from-multiple-lists-
and-then-bind-them

n <- length(filelist)
xx<-filelist
for(i in 1:n){
  assign(paste("z", i,sep = ""), as.matrix(xx[[i]]$z))
}

-- 3) Change the name of column to z
for(i in 1:n){
  names <-(get(paste("z", i, sep = "")))
  colnames (names) <- "z"
  assign(paste("z", i,sep = ""), names)
}

rm(names)

-------------------------------------------------------------
```

```
-- PART 2: Clustering with CLARA for large data sets
-------------------------------------------------------------------
-- INPUT: parameters k-cluster, s-sample, and z data
--with variable z. According the nature of data and the
--objectives: The minimum of k value is 2 for separate ground
--and non ground points.However, the maximum k value is depends
--of number of classes objects that we want to extract. If the
--terrain is flat (ideal situation) k will be: 2-non ground points
--and ground points, 3- buildings, non ground point and ground
--points, 4- 3+trees (with different heights of buildings),
--5-4+streetlamps, ..)
-- Then, kmin=2 e kmax=10 is the best choice

library(cluster)

-------------------------------------------------------------------
-- Note: Run the next lines for each area (dataframe),
--z1- area A, z2-area Bm, z3 area C
-------------------------------------------------------------------
-- Choice the best k based in silhoette plots, by default s=10.
-- input "z<- input file"
z<-z2 --area
-- Define s samples and range for k
kmin <- 2
kmax <-10
s<-10 --samples

c10 <- c("tomato", "forest green", "dark blue", "purple2",
"goldenrod4","gray20", "red","yellow","blue","green")
for(k in kmin:kmax){
  plot(silhouette(clara(z, k=k, samples=s)),
  main = paste("k = ",k),
  do.n.k=FALSE,
       col = c10[1:k])
}

--2. Optional
--Verify if the sample s=10 is the best choice for k selected.
--If for k the clustering doesn't change between s and sc values,
--then s it's ok. If change, you have to choose another value of
-- sample (which the average silhoette converge)

k <-10  --input value integer [2,10]
```

```
s <-10  --input value integer [2,10]
sc<- 100  --input value integer 50,100,150,200,300
(clx10 <- clara(z, k, samples=s))
---- "better" number of samples
cl.10 <- clara(z, k, samples=sc)
-- but that did not change the result here:
stopifnot(cl.10$clustering == clx10$clustering)


--3. Run the next code for the k selected in 1), which the
--average silhoette value should be at least higher than 0.5

k <-10 --input integer value betwween (1-10).
s<-10 --samples
claraz <- clara(z,k,samples=s)
plot(claraz,ask=TRUE)
summary(claraz)

--4.optional: plots for visualize the position of clusters in z

library(fpc)
plotcluster(ol, claraz$cluster, cex=0.3)
save.image("~/Documents/")

--or
plot(zi, col = claraz$cluster, cex=0.2, pch=16, cex=0.3,
main="Title",xlab="name", ylab="name")
legend("bottomleft", legend = paste("cluster", 1:k), pch=1,
col=1:k,cex=0.7)

--5 Append cluster assignment,
--http://stackoverflow.com/questions/12937250/legend
-not-showing-from-k-means-clustering

p<-zi --point cloud pclA (z=z1) or pclB(z=z2) or pclC(z=z3)
clusterz<- data.frame(p,claraz$cluster)
colnames(clusterz) <- c("cat","x", "y","z","cluster")
head(clusterz)
--analysis in desktop GIS (QGIS)
write.csv(clusterz,file="/home/...", row.names=FALSE)

-------------------------------------------------------
-- PART 3:selection of clusters ci= ki,
```

```
---that represent buildings
-------------------------------------------------------------
library(sqldf)
library(tcltk)

--clusters selected if 3 then c1=k1,c2=k3,c3=k3.
-- Example: c1=3,c2=9,c3=8

c1 <- k1 -- cluster integer
c2 <- k2-- cluster integer
c3 <- k3 -- cluster integer
sqlclus1 <- sqldf("select * from clusterz where cluster=k1",
row.names=TRUE)
sqlclus2 <- sqldf("select * from clusterz where cluster=k2",
row.names=TRUE)
sqlclus3 <-sqldf("select * from clusterz where cluster=k3",
row.names=TRUE)
sqlcluster <- rbind(sqlclus1,sqlclus2)
sqlcluster1 <- rbind(sqlcluster,sqlclus3)

--write.table(sqlcluster1, "name.txt",sep=",")
write.csv(sqlcluster1,file="/home/user/../name.csv",
row.names=FALSE)

--support:
-- http://manuals.bioinformatics.ucr.edu/home/R_BioCondManual--
TOC-Basics-on-Functions-and-Packages
-- http://blog.snap.uaf.edu/2012/06/08/matrix-rotation-for-image-
and-contour-plots-in-r/
```

Appendix M

Computing building blocks (height and volume) from UAV data using an algorithm in PostgreSQL/PostGIS

Listing M.1: Extraction of Eave Roof and Base Points of each building block and compute average/median building block height

```
--Author: Carla Rebelo, 2013
--OBJECTIVE: Compute average/median building block height
--and block volumes from a sets of UAV points selected
--that represent the eave of rooftop and base building

--Description:
--First part: Import original point cloud and clustering of
--one area
--Second part: Selection of roof eave points for each block
-- and compute the median/average elevation of these points
--selected;
--Third part: Selection of block base points (ground)
--for each block and compute the median/average elevation
of these points selected;
--Fourth part: Compute average and median blocks' height and
-- blocks'volume

--Input data: original point-cloud (pcl);
--clustering result with the identification of building
--blocks (points);
--reference lines based on reference points elevation of
--building block;
--concave-hull result (building block boundary).
--These last data can be imported to database from QGIS
--(command spit)

--Output results: roof_points and ground_points;
--blocks' height, blocks' volume

-------------------------------------------------------------
--PART 1: Import data
-------------------------------------------------------------
--Create tables of point cloud data original and clustering data
CREATE TABLE pcl_area
(cat integer, x double precision, y double precision,
z double precision, constraint ck primary key(cat));

copy pcl_area FROM '/home/crebelo/Desktop/pcl_C.csv'
```

```
 with delimiter ',' csv header;

CREATE TABLE pcl_cluster
(cat integer, x double precision, y double precision,
z double precision,constraint ck primary key(cat));

copy pcl_cluster FROM '/home/crebelo/Desktop/pcl_ClusterC.csv'
 with delimiter ',' csv header;

--Add geometry for the previous tables
ALTER TABLE pcl_area
 ADD column the_geom geometry;
UPDATE pcl_area
 SET the_geom = ST_SetSRID(ST_MakePoint(x,y,z),3763);
ALTER TABLE pcl_cluster
 ADD column the_geom geometry;
UPDATE pcl_cluster
 SET the_geom = ST_SetSRID(ST_MakePoint(x,y,z),3763);

-----------------------------------------
--PART 2: Selection of block roof points and compute
--the median/average elevation
-----------------------------------------

--1) Buffer -1m from block boundary
--Input: building boundary extract from concave-hull (GRASS)
"bchull" with attribute code building (idblock).
--Parameter can be change is the value of buffer

UPDATE bchull
 SET geom = ST_SetSRID(geom, 3763);

DROP TABLE if exists bchull_buffer CASCADE;
CREATE TABLE bchull_buffer AS
SELECT st_union(st_buffer(geom,-1)) as the_geom
 FROM bchull;

ALTER TABLE bchull_buffer
 ADD column gid serial primary key;
CREATE INDEX bchull_buffer_idx
  ON bchull_buffer
 USING gist
 (the_geom);
```

```
  ALTER TABLE bchull_buffer
   CLUSTER ON bchull_buffer_idx;

--2) Difference between buffer -1m and polygon of
--concave-hull(building block boundary)
DROP TABLE if exists buff_roof CASCADE;
CREATE Table buff_roof AS
 SELECT ST_Difference(bchull.geom, bchull_buffer.the_geom)
 as the_geom, bchull.idblock
  FROM bchull_buffer, bchull;

ALTER TABLE buff_roof
 ADD column gid serial primary key;
CREATE INDEX buff_roof_idx
  ON buff_roof
  USING gist
  (the_geom);
ALTER TABLE buff_roof
  CLUSTER ON buff_roof_idx;
--definition of coordinate system
UPDATE buff_roof
 SET the_geom = ST_SetSRID(the_geom, 3763);

--3) Selection of points that belongs the eave roof
--or the buffer generated (buff_roof)
DROP TABLE if exists tmp2 CASCADE;
CREATE TABLE tmp2 as
SELECT pclcluster.cat as idnuvem, buff_roof.gid as idpol,
buff_roof.idblock
  FROM  pclcluster, buff_roof
    WHERE
      pclcluster.the_geom  && buff_roof .the_geom
     AND
      ST_Contains(buff_roof.the_geom, pclcluster.the_geom);

--4) Output Results - Eave roof points of buildings'
--block(Roof_area)

DROP TABLE if exists Roof_points CASCADE;
CREATE TABLE Roof_points as
SELECT tmp2.idnuvem,tmp2.idblock, pclcluster.*
 FROM tmp2, pclcluster
  WHERE tmp2.idnuvem = pclcluster.cat;
```

```
ALTER TABLE Roof_points
ADD constraint id7s primary key(idnuvem);
CREATE INDEX Roof_points_idx
  ON Roof_points
  USING gist
  (the_geom);
ALTER TABLE Roof_points
  CLUSTER ON Roof_points_idx;

--5) Compute median/average elevation of block roof
--Source code for median by using plr function median provided by
--Joe conway,
--http://www.joeconway.com/plr/doc/plr-aggregate-funcs.html

CREATE or replace function r_median(_float8)
 returns float as 'median(arg1)' language 'plr';

CREATE AGGREGATE median (
  sfunc = plr_array_accum,
  basetype = float8,
  stype = _float8,
  finalfunc = r_median
);

DROP table if exists Roof_measure;
 create table Roof_measure as
  SELECT
          idblock,
          st_union(the_geom) as the_geom,
          avg(z)as mean_znb,
          median(z) as med_znb
  from Roof_points group by idblock;

--see the results
SELECT * from Roof_measure;

-------------------------------------------------------------
--PART 3: Selection of block base points and compute
--the median/average elevation
-------------------------------------------------------------

--1) Buffer 2 m from block boundary
```

```
--Input: building block boundary extract from concave-hull
--(GRASS) bchull
--Parameter can be change is the value of buffer

DROP TABLE if exists tmp1_buff2m CASCADE;
CREATE TABLE tmp1_buff2m AS
 SELECT st_union(st_buffer(geom,2)) as the_geom
  FROM bchull;

ALTER TABLE tmp1_buff2m
  ADD column gid serial primary key;
CREATE INDEX tmp1_buff2m_idx
  ON tmp1_buff2m
  USING gist
  (the_geom);
ALTER TABLE tmp1_buff2m
  CLUSTER ON tmp1_buff2m_idx;

--2) BUFFER Multipolygon to singlepolygon

DROP TABLE if exists bchull_buffer2m CASCADE;
CREATE TABLE  bchull_buffer2m  as
 SELECT (st_dump(the_geom)).geom as the_geom
  FROM  tmp1_buff2m;

ALTER TABLE bchull_buffer2m
 ADD column gid serial primary key;
CREATE INDEX bchull_buffer2m_idx
  ON bchull_buffer2m
  USING gist
  (the_geom);
ALTER TABLE bchull_buffer2m
  CLUSTER ON bchull_buffer2m_idx;

UPDATE bchull_buffer2m
 SET the_geom = ST_SetSRID(the_geom, 3763);

--add area to bchull_buffer2m
ALTER TABLE bchull_buffer2m
 ADD column area double precision;
UPDATE bchull_buffer2m
 SET area = st_area(the_geom);
```

```
--3) Difference between buffer 2 m and polygon of
--concave-hull (buffer of building block base)

DROP TABLE if exists buff_ground CASCADE;
CREATE Table  buff_ground AS
SELECT ST_Difference(bchull_buffer2m.the_geom, bchull.geom)
as the_geom, bchull.idblock
 FROM bchull_buffer2m
 JOIN bchull
   ON ST_Intersects(bchull_buffer2m.the_geom, bchull.geom);

ALTER TABLE  buff_ground
 ADD column gid serial primary key;
CREATE INDEX  buff_ground_idx
  ON  buff_ground
  USING gist
  (the_geom);
ALTER TABLE  buff_ground
 CLUSTER ON  buff_ground_idx;

--Add reference system
UPDATE pinterspav
 SET the_geom = ST_SetSRID(the_geom, 3763);

--4) Intersect buffer_ground with buffer of reference
--side of building block (this last buffer is based on
--streets lines of sides of building block)
--Parameter can be change is the value of buffer

--Buffer 7m to the reference lines
DROP TABLE if exists linesreference;
CREATE Table linesreference AS
 SELECT st_union(st_buffer(the_geom,7)) as the_geom
  FROM lines;

ALTER TABLE linesreference
 ADD column gid serial primary key;
CREATE INDEX linesreference_idx
  ON linesreference
   USING gist
  (the_geom);
ALTER TABLE linesreference
 CLUSTER ON linesreference_idx;
```

```
--Intersection between buffer reference lines with
--buffer buff_ground
DROP TABLE if exists buff_groundside;
CREATE Table buff_groundside AS
 SELECT ST_intersection(buff_ground.the_geom,
 linesreference.the_geom) as the_geom, buff_ground.idblock
  FROM buff_ground,linesreference;

ALTER TABLE buff_groundside
 ADD column gid serial primary key;

CREATE INDEX buff_groundside_idx
  ON buff_groundside
  USING gist
  (the_geom);
ALTER TABLE buff_groundside
 CLUSTER ON buff_groundside_idx;

--5) Selection of ground points that belongs the
--buffer that represents building block base
--(buff_groundside).

DROP TABLE if exists tmp4 CASCADE;
CREATE TABLE tmp4 as
SELECT pcl_area.cat as idnuvem, buff_groundside.gid as idpol,
buff_groundside.idblock
 FROM pcl_area, buff_groundside
   WHERE
      pcl_area.the_geom  && buff_groundside.the_geom
/* Uses GiST index with the polygon's bounding box */
    AND
      ST_Contains(buff_groundside.the_geom,pcl_area.the_geom);
 /* Uses exact matching */

--6) Output Results - Base points of buildings'
--block (ground_points)

DROP TABLE if exists  CASCADE;
CREATE TABLE ground_points as
 SELECT tmp4.idnuvem, tmp4.idblock, pcl_area.*
  FROM tmp4, pcl_area
   WHERE tmp4.idnuvem = pcl_area.cat;
```

```
ALTER TABLE ground_points
 ADD constraint idg primary key(idnuvem);
CREATE INDEX ground_points_idx
  ON ground_points
  USING gist
  (the_geom);
ALTER TABLE ground_points
  CLUSTER ON ground_points_idx;

--7)Compute median/average elevation of
--block base

DROP TABLE if exists ground_measure;
 CREATE TABLE ground_measure as
  SELECT
         idblock,
         st_union(the_geom) as the_geom,
         avg(z)as mean_zpav,
         median(z) as med_zpav
  FROM ground_points group by idblock;

--see the results
SELECT * from ground_measure;

-----------------------------------------------
PART 4: Compute average and median blocks'_height
--and_blocks' volume
-----------------------------------------------

DROP TABLE if exists output_tmp;
CREATE TABLE output_tmp AS
SELECT
Roof_measure.*,ground_measure.mean_zpav,
ground_measure.med_zpav
FROM ground_measure,Roof_measure
where Roof_measure.idblock = ground_measure.idblock

--1) add area to results, the name of table should be
--renamed to area A,B or C

DROP TABLE if exists output_areai;
CREATE TABLE output AS
```

```
SELECT
output_tmp.*, bchull.area
FROM output_tmp, bchull
where output_tmp.idblock = bchull.idblock

--2) Compute block height and volume

ALTER TABLE output_areai
ADD column ave_hfuav double precision,
ADD column med_hfuav double precision,
ADD column ave_voluav double precision,
ADD column med_voluav double precision;

UPDATE output_areai
SET ave_hfuav = mean_znb-mean_zpav,
med_hfuav = med_znb-med_zpav;

UPDATE output-areai
SET ave_voluav = ave_hfuav*area,
med_voluav = med_hfuav*area;

--3) See results
SELECT * from output_areai;
```

Appendix N

Control zones: detailed average and median block height values

RESULTS OF SECTION 3.3: ROOF AND BASE BUILDING BLOCK ELEVATIONS

Building Block Heights [BBH] computed from 3D reference points*

Building Block	Average Z_{Roof}	Average Z_{Base}	**Average BBH**	Median Z_{Roof}	median Z_{Base}	**Median BBH**
1	152.23	133.45	18.78	152.47	133.39	19.08
2	148.15	132.28	15.87	148.00	132.28	15.72
3	149.11	133.87	15.24	149.20	134.20	15.00
4	144.78	128.91	15.87	144.74	128.25	16.49
5	145.00	130.91	14.09	144.40	130.45	13.95
6	149.11	134.52	14.59	148.72	133.44	15.28
7	151.35	135.77	15.59	150.57	136.20	14.37

*- All these values are in metres

Building Block Heights [BBH] Estimated from UAV points selected*

Building Block	Average Z_{Roof}	Average Z_{Base}	**Average BBH**	Median Z_{Roof}	median Z_{Base}	**Median BBH**
1	151.87	133.22	18.65	151.99	133.18	18.81
2	148.08	132.73	15.35	148.01	132.53	15.48
3	148.89	134.38	14.51	149.22	134.34	14.88
4	144.82	129.79	15.03	144.94	128.84	16.1
5	145.37	131.59	13.78	145.38	131.23	14.15
6	149.21	134.93	14.28	148.35	134.75	13.6
7	151.87	136.12	15.75	150.71	136.15	14.56

*- All these values are in meters unit

Appendix O

Evaluation of building block height and volume extracted from UAV data using an algorithm in PostgreSQL/PostGIS

Listing O.1: Evaluation of Building blocks' height and volume extracted from UAV point cloud.

```
--Author: Carla Rebelo, 2013
--OBJECTIVE: Compute average/median reference building
--blocks' height and blocks' volume from a sets of elevation
--points, which are using to calculated the errors of
--parameters extracted from point cloud

--Description:
--First part: Compute reference blocks'height and volume
--from reference elevation points of each building
--Second part: Compute absolute errors and relative error
--of blocks'height and volume estimated from UAV point cloud;

--Input data: table of reference buildings' block (buildings);
--blocks' height and volume estimated from point cloud;

--Output results: refblocks and errors

-------------------------------------------------------------
--PART 1:Compute reference blocks'height and volume from
--reference elevation points of each building
-------------------------------------------------------------

--1) Agregate attributes by block

SELECT *
FROM buildings order by block;

DROP TABLE if exists tmprefblocks;
 CREATE TABLE tmprefblocks as
  SELECT
          block,
          st_union(the_geom) as the_geom,
          count(*) as nbuildings,
          sum(area) as sum_area,
          sum(nfloors) as sum_nfloors,
          avg(elevationb)as ave_refznb,
          avg(elevationp) as ave_refznp,
          median(elevationb) as med_refznb,
          median(elevationp) as med_refznp
```

```
  FROM buildings group by block;

SELECT * FROM tmprefblocks order by block;

--2) Compute the average of floors for each block

ALTER TABLE tmprefblocks
ADD column ave_nfloors double precision;
UPDATE tmprefblocks
SET  ave_nfloors = sum_floors/nbuildings;

ALTER TABLE tmprefblocks
ADD column ave_refhf double precision,
ADD column ave_refvol double precision,
ADD column med_refhf double precision,
ADD column med_refvol double precision;

--3) Compute the average/median block height and volume

--Height
UPDATE tmprefblocks
SET ave_refhf = ave_refznb-ave_refznp,
med_refhf = med_refznb-med_refznp;

--volume
UPDATE tmprefblocks
SET ave_refvol = ave_refhf*sum_area,
med_refvol = med_refhf*sum_area;

DROP TABLE if exists refblocks;
CREATE TABLE refblocks as
 SELECT
    block,nbuildings,med_nfloors as mean_npisos,
    sum_area as area_ref,ave_refhf,
    med_refhf, ave_refvol as volrefave_block,
    med_refvol as volrefmed_block,the_geom
 FROM tmprefblocks;

-----------------------------------------------
-PART 2: Compute absolute errors and relative
--error of blocks' height and volume estimated
--from UAV point cloud;
-----------------------------------------------
```

```
--1) Add all information of each areas of study
--In this case 3 areas A,B,C

INSERT INTO output_areaA
SELECT * FROM output_areaB, output_areaC;

CREATE TABLE uavblocks as
SELECT *
FROM output_areaA;

--2)MERGE the two tables UAV and Reference

DROP TABLE if exists refblocksuav;
CREATE TABLE refblocksuav
as SELECT refblocks.*,uavblocks.area as areauav,
    uavblocks.ave_hfuav, uavblocks.med_hfuav,
    uavblocks.ave_voluav,uavblocks.med_voluav
     FROM refblocks, uavblocks
        where refblocks.block = uavblocks.idblock;

SELECT *
FROM refblocksuav order by block asc;

--3) Errors or residuals between UAV and reference
-- parameters

CREATE TABLE errors as SELECT *
FROM refblocksuav;

ALTER TABLE errors
ADD column resHf_ave double precision,
ADD column resHf_med double precision,
ADD column Error_area double precision;

UPDATE errors
SET Error_area=area_ref-areauav,
resHf_ave= ave_refhf- ave_hfuav,
resHf_med=med_refhf- med_hfuav;

--4) Errors of volumes estimated by UAV

ALTER TABLE errors
```

```
ADD column Erro_Volhfuav_med double precision ,
ADD column Erro_Volhfuav_ave double precision ,
ADD column RELError_Volhfuav_med double precision ,
ADD column RELError_Volhfuav_ave double precision;

UPDATE errors
SET Error_Volhfuav_med = volrefmed_block-med_voluav ,
RELErro_Volhfuav_med=(abs(volrefmed_block-med_voluav)
/volrefmed_block)*100;
UPDATE errors
SET Error_Volhfuav_ave = volrefave_block-ave_voluav ,
RELErro_Volhfuav_ave=(abs(volrefave_block-ave_voluav)
/volrefave_block)*100;

--5) CREATE table  of all errors achieved for the study

DROP TABLE if exists evaluation;
CREATE TABLE evaluation as
SELECT block, Error_area ,
resHf_ave ,resHf_med ,
Error_Volhfuav_med , RELErro_Volhfuav_med ,
Error_Volhfuav_ave , RELErro_Volhfuav_ave ,the_geom
 FROM errors
  ORDER BY bloco ASc;

SELECT *
FROM erros_volumesuav_arearef
ORDER BY bloco ASc;
```